CHARACTERIZATION OF CdS BASED MULTILAYER THIN FILMS USEFUL FOR PHOTOVOLTAIC DEVICE FABRICATION USING DIFFERENT TECHNIQUES WITH EMPHASIS ON ELLIPSOMETRY

THESIS SUBMITTED
IN PARTIAL FULFILMENT OF THE REQUIREMENTS
FOR THE AWARD OF THE DEGREE OF

DOCTOR OF PHILOSOPHY

SUNNY MATHEW

G5645

DEPARTMENT OF PHYSICS
COCHIN UNIVERSITY OF SCIENCE AND TECHNOLOGY
COCHIN - 682 022
INDIA

1994

CERTIFICATE

Certified that the work presented in this thesis entitled **"Characterization of CdS based multilayer thin films useful for photovoltaic device fabrication using different techniques with emphasis on ellipsometry"** is based on the bonafide research work done by Mr.Sunny Mathew under my guidance, at the Department of Physics, Cochin University of Science and Technology, and has not been included in any other thesis submitted previously for the award of any degree.

Cochin -22
28.06.1994

Dr.K P Vijayakumar
Reader in Industrial-Physics

DECLARATION

Certified that the work presented in this thesis entitled **"Characterization of CdS based multilayer thin films useful for photovoltaic device fabrication using different techniques with emphasis on ellipsometry"** is based on the original research work done by me under the guidance of Dr.K.P.Vijayakumar, Department of Physics, Cochin University of Science and Technology, and has not been included in any other thesis submitted previously for the award of any degree.

Cochin -22
28.06.1994

Sunny Mathew

PREFACE

Wide band gap polycrystalline CdS (E_g=2.42eV) thin films are extensively used as a window material in heterojunction solar cells together with several narrow band gap semiconductors (Cu_2S, CdTe, $CuInSe_2$ etc.). Recently very thin CdS films, prepared by chemical technique are found to be extremely useful as the window material in thin film solar cells with efficiency >12%. In the present work the analysis of chemically prepared single layer CdS as well as CdS based bilayer films are done using different techniques. The major tool used for this work is a home made Variable Angle Spectroscopic Ellipsometer (VASE).

Ellipsometry is a non destructive optical technique for the surface analysis of thin films and crystals. It belongs to a class of optical instruments in which polarization represents the fundamental property of the light. Ellipsometry is the optical characterization technique in which the change in polarization state of light that occurs due to reflection from the surface of a sample is measured and interpreted to determine the physical properties of the sample. In spectroscopic ellipsometry the measurement and analysis are done as a function of wavelength. Since ellipsometry is highly sensitive to the surface imperfections, inter diffusion, interlayer formation in multilayer thin film system, etc.; this technique gives the information about the surface roughness, structural changes and layer structure of the thin films under investigation. Here Bruggeman's effective medium theory is used for the volume fraction analysis of mixed layers with the help of ellipsometry. Photometric ellipsometer calculate the parameters ψ and Δ using the measured values of intensity of reflected light from the sample surface. The values of these two parameters are used for the calculation of optical parameters of thin film system.

In the VASE system fabricated for the present work the azimuth of analyser and polariser can be measured with an accuracy of 1 minute while the angle of incidence can be measured at an accuracy of 20 secs. The accuracy of intensity measurement is ±0.5% of full scale reading of 4 1/2 DMM. The possible wave length range is 400-750 nm. The angle of incidence can vary from 20 to 80°

In this thesis we describe the details of the construction of VASE (photometric type) and the methods and application of this sensitive equipment to study surface, interlayer structure and material properties of thin films. We have also used the other characterization techniques like X-ray Photoelectron Spectroscopy (XPS), X-ray Diffractometer (XRD), Scanning Electron Microscope (SEM), Spectro Photometer and in some cases electrical conductivity measurement for corroborating the results. The materials selected for these studies are CdS, SnO_2 and $CuInSe_2$ which find large application in thin film solar cells. The single and bilayer thin film systems used for the study are CdS, CdS/Cu, CdS/SnO_2 and CdS/$CuInSe_2$. These films are prepared by different techniques like spray pyrolysis, vacuum evaporation and chemical bath deposition (CBD).

The chapter 1 gives an introduction to the works presented in this thesis with emphasis on thin films. A brief description of different preparation techniques of thin films and methods of thickness measurements are given. The bilayer structure of thin films is also discussed in this section which has applications in thin film solar cells. A detailed account of optical reflection and transmission by an ambient-film-substrate system is given along with a brief introduction to ellipsometer. Towards the end of this chapter, a brief description of the techniques used for the optical studies of thin films is added. The other experimental techniques used in the present study for the characterization

of the samples like XRD, XPS, SEM are also described in this chapter after dealing with the optical techniques.

The chapter 2 contains the detailed description of theory of ellipsometry and the variation of polarization due to different optical components used in ellipsometry. Jones matrix is used for this analysis. It also contains an account of photometric ellipsometer and a brief description of other ellipsometric systems. Next part of this chapter describes the VASE set up (Polarizer-System-Analyzer) fabricated as a part of this work and different components used for this such as light source, polarizing elements, monochromator, light detection and signal processing etc. It also describes the measurement of ψ and Δ spectra of glass surface.

The chapter 3 contains the calculation techniques of photometric ellipsometer. This chapter also includes the computer programming techniques used in the forward and reverse problems. Ellipsometer measures only the parameters ψ and Δ and not the material parameter. These material parameters (like thickness, refractive indices surface/interface roughness etc) have to be inferred from the ellipsometric parameters by selecting the correct optical model. The parameter values of the best fit model is attributed to the film system. This section describes the techniques for selecting the best model by minimizing the error values. In order to get the best results using VASE, the angle of incidence and wavelength should be in the most sensitive region of the system. Here the sensitive regions of ψ and Δ of the CdS single layer film, and two CdS based bilayer films (viz. CdS/SnO_2 , $CdS/CuInSe_2$) which are studied in the present work are given. The analysis of rough surface/interface using the Bruggeman's effective medium theory (EMT) is also included in this chapter. This chapter comes to an end with the flow chart of the FORTRAN computer programme used for the analysis of various parameters of the

multilayer thin film systems analysed in the present work.

Chapter 4 describes the details of spray pyrolysis technique and the setup of spray coating. The CdS thin films are widely used as a window material in several thin film solar cells. The ellipsometric analysis of CdS film prepared at different temperatures are given. The results of ellipsometric analysis of variation of surface and structural properties of these films with preparation temperature are given along with the supporting results using SEM and XRD spectrum. The variation of surface roughness of the film is explained using the growth rate at different substrate temperature. The refractive index spectra (in the visible region) of CdS film (both real and imaginary) is calculated taking into account of surface roughness. The effect of annealing on surface roughness of the CdS films prepared by spray pyrolysis technique is also included in this chapter.

Chapter 5 describes the variation taking place on the CdS/Cu bilayer thin film systems due to annealing. The CdS film is prepared by spray pyrolysis and Cu is coated over this CdS film by vacuum evaporation. The ellipsometer is used for the studies of diffusion of Cu into CdS due to annealing. Bruggeman's EMT is used for the analysis of mixture layers (CdS:Cu). It is observed that the doping of Cu into CdS changes CdS at first into intrinsic,and on increasing the percentage of Cu in CdS, the latter is converted into p-type. It has wide application in thin film solar cells because these films can form CdS homojunctions. The results of the analysis of CdS:Cu film using XRD, XPS and optical absorption studies are also given in this chapter along with the electrical properties of the films.

SnO_2 and $CuInSe_2$ are widely used in thin film solar cells. SnO_2 film is often used as transparent conducting electrode material for thin film solar cell. SnO_2 films with very low resistivity and high percentage transmission are

prepared by spray pyrolysis technique as a part of the present work. $CuInSe_2$ is p-type material and it is widely used with CdS film to form p-n junctions. In the present study we have prepared SnO_2/CdS bilayer thin film by spray coating technique and the interface of SnO_2 and CdS is analyzed using ellipsometry and the results are given in chapter 6. $CuInSe_2$ film are prepared by CBD technique. The main attraction of CBD is that it can reduce cost of preparation of thin film and is very much important in developing low cost photovoltaic devices. Optical constants of $CuInSe_2$ film are also calculated in wavelength range 470 to 650 nm and this result is much useful for solar cell fabrication work. CdS/$CuInSe_2$ films are prepared by CBD technique. The interface of these layers are also studied using ellipsometer after annealing at different temperatures.

The last chapter contains the conclusion of all the results given in the previous sections and also the scope of this type of work for the single and multilayer semiconductor analysis.

The following papers have been published/ communicated for publication in different journals during the course of the work.

List of publications.

1. Multiple wavelength ellipsometry technique for the studies of superficial and interior properties of CdS thin films.
   Sunny Mathew and K.P.Vijayakumar. National Seminar on Instrumentation, CUSAT, Cochin, Nov.7-9, 1989.
2. Application of spectroscopic ellipsometry to study the effect of annealing of CdS thin films.
   Sunny Mathew and K.P.Vijayakumar. J. Optics (A) 19 (1989) 22.

3. Photoconductive and ellipsometric studies of spray pyrolysed CdS thin films.
   A. G. Valyomana, Sunny Mathew, K. P. Vijayakumar, and C. Purishothaman. Bull. Mater. Sci. 16 (1993) 55

4. Microscopic surface roughness analysis of CdS thin films by ellipsometry.
   Sunny Mathew and K. P. Vijayakumar. Proc. N. Symp. of Vacuum Sci. and Tech., NPL, New Delhi, Oct 7-9 (1993) p C156

5. Ellipsometric studies of structural properties of CdS thin films.
   Sunny Mathew and K. P. Vijayakumar. Proc. of DAE solid state symp. BARC, Bombay, C36 (1993) p 159.

6. Spectroscopic ellipsometric studies of CdS Thin films prepared by spray pyrolysis.
   Sunny Mathew and K. P. Vijayakumar. (Communicated to J. Phys. Soc. Japan.)

7. Optical constants of Spray coated CdS thin films.
   Sunny Mathew and K. P. Vijayakumar. (Bull. Mater. Sci. in press) (1994).

8. Ellipsometric studies of microscopic surface roughness of CdS thin films.
   Sunny Mathew and K. P. Vijayakumar. (Accepted for publication in Bull. Mater. Sci.)

9. Optical and Surface properties of spray pyrolysed CdS thin films.
   Sunny Mathew, P. S. Mukerjee and K. P. Vijayakumar. (Accepted for publication in Thin Solid Films)

10. Ellipsometric studies of CdS/SnO_2 interface.
    Sunny Mathew and K. P. Vijayakumar (XXI Nat. symp on Optics, IIT, Madras Feb. 10-12, (1994))

11. Characterization of spray pyrolysed CdS film doped with Cu.
    Sunny Mathew, P. S. Mukerjee and K. P. Vijayakumar. (Accepted for publication in Jpn. J. Appl. Phys).

12. Interdiffusion studies of CdS/SnO_2 thin films prepared by spray pyrolysis technique.
Sunny Mathew and K.P. Vijayakumar. (Communicated Solid State Commun.)
13. Interdiffusion studies of $CdS/CuInSe_2$ thin films system prepared by chemical bath technique.
Sunny Mathew, P.K. Vidyadharan Pillai and K.P. Vijayakumar. (Communicated to Thin solid Films)

CONTENTS

Page No.

PREFACE

CHAPTER-1 GENERAL INTRODUCTION TO BILAYER THIN FILMS

1.1 Introduction 1

1.2 Techniques for preparation of thin films. a brief description 3

1.3 Measurement of film thickness 8

1.4 Bilayer thin films 10

1.5 Optics of thin films 19

1.6 Other thin film characterization techniques used 39

References 42

CHAPTER-2 ELLIPSOMETRY: THEORY AND INSTRUMENTATION

2.1 Introduction 49

2.2 Theory of Ellipsometry 53

2.3 Experimental setup of the ellipsometer fabricated 65

2.4 Conclusion 76

References 77

CHAPTER-3 ELLIPSOMETRIC CALCULATION TECHNIQUE AND APPLICATIONS

3.1 Introduction 81

3.2 Ellipsometric data analysis 83

3.3 Surface and interface analysis 92

3.4 Sensitivity analysis 96

3.5 Conclusion 116

References 117

CHAPTER-4 ANALYSIS OF SPRAY PYROLYSED CdS THIN FILMS

4.1 Introduction 119
4.2 Experiment 121
4.3 Results and discussion 126
4.4 Conclusion 155
References 158

CHAPTER-5 ANALYSIS OF Cu/CdS BILAYER THIN FILMS AND PREPARATION OF p-TYPE CdS FILMS

5.1 Introduction 162
5.2 Experiment 163
5.3 Results 167
5.4 Discussion 189
5.5 conclusion 191
References 192

CHAPTER-6 STUDIES OF BILAYER THIN FILMS IMPORTANT IN SOLAR CELL APPLICATIONS

PART-I CdS/SnO_2 BILAYER THIN FILM

6.1 Introduction 195
6.2 Experiment 196
6.3 Results and discussion 198
6.4 Conclusion 204

PART-II CdS/$CuInSe_2$ BILAYER THIN FILM

6.5 Introduction 205
6.6 Chemical bath deposition 206
6.7 Measurements 208
6.8 Results and discussion 208
6.9 Conclusion 212
References 213

CHAPTER-7 CONCLUSION OF RESULTS 216

Chapter 1

GENERAL INTRODUCTION TO BILAYER THIN FILMS.

1.1 Introduction.

Today, thin film pervades over every day life as transparent conductors in LCD, watches and computer displays, as antireflection coating for cameras, on planar waveguides for communication, as coating to improve both the colour and energy efficiency of glass, as highly reflecting mirror coating, on solar cells and on most of other electronic, optical and optoelectronic devices. Thin films of metals, semiconductors and dielectrics have become of increasing importance for fundamental studies in many fields of physics, electronics and chemistry. Many workers use such films to obtain information about the properties of solids in general, since certain measurements can be made more conveniently using thin films. Others are more interested in fundamental properties in thin film form, since they may differ considerably from those of the bulk materials.

Recently thin films got very high application in the field of thin film solar cells. The 1970's have brought the end of the thought of unlimited source of conventional cheap energy. The major problem facing the technologists now is thus how can one use the solar energy to provide preferably high grade energy in a useful form which is also economically competitive. In spite of the other major constraints in this research work the materials one use must also be readily available and abundant. The direct conversion of solar energy into electricity by photovoltaic is more efficient than other indirect techniques like photothermal, photochemical etc.

If we analyse the structure of a simple device like thin film solar cell it can be seen that intensive research is required for solving the different problems coming up even in

this case. In the case of solar cells, one should prepare multilayer structure for forming pn junction and also to have upper and lower electrodes. A large number of materials that form homo or heterojunctions are used for the fabrication of photovoltaic devices. Generally the thin film heterojunction solar cells fabricated using materials having good photon absorption capacity will have thickness in the range 3-10 μm, while the bulk devices are about 200-400μm thick. The lower thickness of thin film devices reduces the production coast of the cell as well as the quantity of the required materials. A large variety of semiconducting materials are used for the fabrication of such cells. The important materials are CdS, Cu_2S, CdTe, FeS_2, InP, $CuInSe_2$, Cu_2Se, αSi:H etc. and detailed review of the materials are given by Chopra et al [1]. Now in the depletion region of the junction there can be interdiffusion of different layers and cause the formation of an interlayer and these process will be more predominant in the case of heterojunction.

In solar cells also just like in any other electronic device there should be electrodes. But this should be transparent and conducting and hence the use of metals as electrode materials is restricted because they are opaque to light. Chopra et al, [2] have reviewed about non-stoichiometric and doped thin films of oxides of metals like Sn, In, Cd, Zn, and other various alloys that exhibit simultaneous optical transparency and electrical conductivity are used as electrode material in solar cells. In some other design of the thin film cells other layers are required. The best examples are metallic and dielectric films. Metal films provide barrier electrodes for Schottky barrier solar cells and also widely used as the base electrodes for various types of solar cells. The dielectric films like MgO_2, SiO_2...etc. are used as protective layer as well as antireflection coating over the thin film solar cells.

Thus the cell contain different layers of different types of materials and these layers can be prepared using entirely different techniques. The preparation technique used for one layer should not affect the other layers which are already deposited. Again as the cell has to function in a high temperature ambients, there are several other important problems (like interdiffusion between junctions layers, between semiconductor and electrode layers, corrosion of the electrode layer etc) which is to be solved through intensive research. So the studies leading to the characterization of multilayer films are of great practical importance.

In the present study we analyse a few bilayer thin films which find great application in the fabrication of terrestrial solar cells. Here we mainly use an optical technique viz., ellipsometry. The experimental setup required for this has been fabricated. The necessary theory as well as the experimental details are included in the following chapters.

In the next section we give a brief review of different techniques for the fabrication of thin films with due importance to chemical deposition. In the subsequent section a review of different techniques used for the analysis of multilayer thin film is included.

1.2 Techniques for Preparation of Thin Films - a brief description.

Two dimensional materials of thickness ranging from few angstroms to few microns can be prepared by various techniques. Several aspects are to be considered before selecting a particular technique for thin film preparation and this mainly depends upon application of the film. For example large area thin films are to be deposited by using some low cost process for the fabrication terrestrial solar cells while microelectronics requires multilayers over an area of few

square microns. In some cases like heterojunction lasers thin films of high crystalline quality are required and these are deposited using techniques like molecular beam epitaxy (MBE). The different processes used for the deposition of thin films have been extensively reviewed in many publications [1,3-8]. Generally thin film deposition process involves the following steps.

1. Creation of atomic/molecular/ionic species.
2. Transport of these species through a medium.
3. Nucleation of these species on a substrate.

Depending upon the nature of creation of these species the deposition process can be classified into different groups mainly physical methods and chemical methods.

1.21 Physical methods.

1.211 Vacuum evaporation.

Deposition of thin films by evaporation is very simple, convenient and most widely used technique. One merely has to produce a vacuum environment (usually of the order of 10^{-6} Torr) in which sufficient amount of heat is given to the evaporant to attain the vapour pressure necessary for evaporation. The evaporated material is allowed to condense on a substrate kept at suitable temperature and at convenient distance from the evaporant. Different techniques are employed to supply heat of vaporization of materials and the important ones are the following.

1.211(a) Resistive heating.

Resistive heating is the technique in which the material is evaporated by electrical resistive heating. Details of this is given in section 5.21. This technique is used for the preparation of metallic films [4-6] and also semiconducting films like CdS [9,10], CdSe [11,12], CdTe [13,14] CuSe [15,16] Cu_2S [17,18], InP [19] etc.

1.211(b) Flash evaporation

Flash evaporation is used for the preparation of thin film of multicomponent alloys or compounds containing constituents having a low melting point and high vapour pressure. Here a small quantity of material to be evaporated is dropped on a flat heater that results in instantaneous evaporation of the material. $CuInSe_2$ [20,21] films can be prepared by this technique.

1.211(c) Electron beam evaporation.

In this technique a stream of electron is accelerated through field of typically 5-10 kV and focused onto the surface of material for evaporation. Dielectric films like MgF_2, SiO_2 [22], etc., are prepared by this technique.

1.211(d) Laser evaporation.

In laser evaporation laser is used as the thermal source to vaporize the evaporant material and preparation of thin film. Smith et al [23] have made preliminary studies and showed that many materials can be vaporized in a vacuum by direct laser beam. High power CO_2 laser [24] and pulsed Nd:YAG laser [25] are commonly used for evaporation.

1.212 Sputtering.

It has long been known that when a surface is bombarded with high velocity positive ions, [illegible] results in the ejection to the surface atoms. This process of ejection of atoms from the surface by the bombardment of positive ions of (usually) inert gases is commonly known as sputtering. The ejected atoms can be made to condense on a substrate to form a thin film. Sputtering is used for the preparation of different films CdSe [26], CdTe [27], CdS [28,29], $CuInSe_2$ [30], SiO_2 [31], ZnO_2 [32,33], SnO_2 [34] etc. Several systems have been

employed for the deposition of the thin films by this technique. The names of important types of sputtering are mentioned below. (1). Glow discharge arc sputtering. (2). Triode sputtering. (3). Getter sputtering (4). Radio frequency sputtering. (5). Magnetron sputtering. (6). Facing target sputtering. (7). Ion beam sputtering. (8). AC sputtering.

1.213 Ion assisted deposition.

Ion related technique of thin film preparation have been in use for more than two decades. In ion deposition the desired film material is ionized, and the slightly accelerated ions of film material are directed to a high vacuum region and then decelerated before striking the substrate for direct deposition at low energy. An Ion Assisted Deposition (IAD) process is a cross between evaporation and sputtering. The details of film deposition using IAD are given by George [3]. IAD is categorized as follows: (1). Ion plating. (2) Cathode arc plasma deposition. (3). Hot hollow cathode gun evaporation (4). Concurrent ion bombardment deposition. (5). Ion Beam deposition.

1.22 Chemical Methods.

Chemical deposition techniques are the most important methods for the growth of films useful for thin film solar cells. Generally these techniques do not require complicated and costly technology or equipment. The various deposition processes are described in the following section.

1.221 Chemical Vapour deposition.

A simple definition of Chemical Vapour deposition (CVD) is the condensation of a compound or compounds from the gas phase onto a substrate where reaction occurs to produce a solid deposit. The gaseous compound, bearing the deposit material, if not already in the vapour state, is formed by

volatilization from either a liquid or a solid feed. This is then made to flow either by gas pressure difference or by the action of a carrier gas, to the substrates. The chemical reaction is initiated at or near the substrate surface which produces the desired material in the form of a deposit on the substrate. This is activated by the application of an external agency such as heating, rf field, light or X-rays, an electric arc or glow discharge, electron bombardment etc. a:SiH [35,36] InP [37], CdTe [38], CdS [39,40], SiO_2 [41,42], Sn [43] etc., are some of the films prepared using this technique.

1.222 Electrodeposition.

Electrodeposition is a process of depositing a substance upon an electrode by electrolysis. The phenomenon of electrolysis is governed by Faraday's law. Various metals, alloys and semiconducting materials have been deposited by this technique. For example metals like Cu, Ag, Au, Cr etc., [44] and semiconducting materials like CdS [45,46], CdSe [47,48], $CuInSe_2$ [49,50], CdTe [51,52], etc., are also deposited by this technique.

1.223 Spray Pyrolysis.

Spray Pyrolysis is essentially a thermally stimulated reaction between clusters of liquid/vapour atoms of different chemical species. The main attractions of this technique are the low cost and easiness to operation. The detailed description of spray pyrolysis is given in section 4.21. It is widely used for the preparation of thin films used in thin film solar cells. CdS [53-55], $CuInSe_2$ [56,57], FeS_2 [58,59], SnO_2 [60,51], In_2O_3 [62,63], ZnO [64] etc are prepared by this technique.

1.224 Chemical Bath deposition.

Film can be grown on either metallic or nonmetallic

substrates by dipping them in appropriate solutions containing the required ions without the application of any electric field. The details of chemical bath deposition (CBD) is included in section 6.6. Recently this technique has gained importance in the fabrication of large area and low cost thin film solar cells. This is used for the fabrication of thin film CdS [65-67], ZnO [68], $CuInSe_2$ [69-71], In_2O_3 [72], SnO_2 [73] etc.

1.225 Screen Printing.

Screen Printing is essentially a thick film process in which pastes containing the desired material are screen printed onto a suitable substrate and subsequently the substrate is fixed under appropriate conditions of time and temperature to yield components bonded to the substrate. This technique is used for the preparation of active semiconductor layers and devices [74,75].

1.3 Measurement of film thickness.

Film thickness is an important parameter and in many case this has to be measured with an accuracy of few angstroms. Several techniques are devised for the measurement of thin film thickness. This may be measured either by *insitu* monitoring of the rate of the deposition or after the film deposition is completed. In the present investigation the thickness of the films was measured using multiple beam interferometer, microbalance, ellipsometer and quartz crystal monitor. Among these first three techniques are used after the completion of the film deposition. A brief description of these technique is included in the following section.

1.31 Multiple Beam Interferometry.

The basic principle involved in this technique is the interference of light reflected from two surfaces which

are slightly inclined to each other, thus forming an air wedge [76]. These fringes are known as Fizeau fringes of equal thickness. During the film deposition, part of the substrate is masked. After the film deposition the mask is removed and a good reflecting film is deposited onto the film surface resulting in a step. A parallel monochromatic beam illuminates the wedge shaped air film formed between the top Fizeau plate and the step film, giving rise to a fringe pattern. By measuring the fringe shift (l) and fringe spacing (L), the thickness of the film (t) can be calculated using the equation.

$$t = \frac{l}{L} \lambda \qquad (1.1)$$

where λ is the wavelength of the light used.

1.32 Microbalance.

The technique is employed for thickness determination of films with thickness (t) t> 250nm. The substrate was weighed after film deposition, Then the film was carefully removed using dilute acid and again weighed. The difference between the two weights give the weight of the film. By knowing the dimension of the film and assuming the bulk density, the film thickness can be estimated. But this is not an accurate techniques for the determination of very thin film samples.

1.33 Ellipsometry.

Ellipsometry is a non-destructive technique for thin film studies. It is widely used for the thickness measurements for thin films [77]. The details of theory and experimental technique of ellipsometry is given in chapter 2 and 3. This is a very sensitive and accurate technique and can be used for the measurement of thickness of few tens angstroms.

1.34 Quartz thickness monitor.

Quartz crystal thickness monitor is used for *insitu* monitoring of thickness of the film as well as for the determination of deposition rate. The principle involved in this technique is that the natural frequency of quartz crystal changes when the material gets deposited on the crystal surface. So the crystal is kept along with the substrate during the film deposition process. The change in frequency of the crystal which depends on the thickness of film deposited on the crystal is measured.

1.4 Bilayer Thin Films.

Bilayer or multilayer structures are required in many different areas of science and technology. Computer disks, reflectors, antireflection coatings, optical filters, active electronic devices, solar cells etc., are some of the important examples where we find the multilayerfilms essential. These films form different types of interfaces like, insulator-semiconductor, semiconductor-metal, semiconductor-semiconductor, etc. The two types of interfaces that are commonly required in active devices are metal-semiconductor and semiconductor-semiconductor interfaces. These multilayer thin films are deposited using the techniques for thin film deposition described earlier. Here the second layer is deposited over the first one using the same technique or a different one. For example we have fabricated Cu/CdS bilayer system by using two different techniques. The CdS layer is deposited over glass substrate by spray pyrolysis technique and the next Cu layer by vacuum evaporation inside a high vacuum coating unit. In the case of CdS/SnO_2 bilayer film systems same technique is used for the preparation of both the layers. At first SnO_2 layer is deposited over glass substrate by spray pyrolysis at 450°C and then CdS film is deposited by the same technique over SnO_2

layer at 300°C. Similarly $CdS/CuInSe_2$ bilayer films are prepared by using the CBD technique for both the layers. At first $CuInSe_2$ films are deposited on glass and then the CdS films are deposited on the $CuInSe_2$ film. The following sections give a brief discussion on metal-semiconductor and semiconductor-semiconductor interfaces.

1.41 Metal-Semiconductor Interfaces.

Four different types of interfaces between metals and semiconductors can be delineated.

1. A metal is only physisorbed on the surface of a semiconductor without making any chemical bond.

2. A non-reactive metal forms a week chemical bond with a highly polarizable semiconductor but does not form any compound with it.

3 A highly polarizable semiconductor reacts with a metal to form one or more chemical compounds.

4. A thin insulating film of native oxide prevents intimate contact between the metal and semiconductor .

Type 1 interface represents an ideal Schottky barrier, while type 2 interface approximates to the Bardeen barrier. The following section contains small description of two types metal-semiconductor interfaces that forming ohmic contact and Schottky barrier.

The Schottky barrier is a metal-semiconductor (m-s)contact that possesses rectifying properties. The rectification of metal-semiconductor was first observed in 1874 by Braun [78]. Schottky effect is the image force induced lowering of the potential energy for charge carrier emission, when an electric field is applied. The detailed treatment of the barrier is given in several text books [79-84]. Here a small description of m-s barrier formation theory is given. The work function ϕ_m of the metal is assumed to be larger than that of the semiconductor work function ϕ_{sc1} (as shown in

Figs. 1.1(a) and 1.1(b)). The semiconductor is assumed to be n type. χ_1 is the electron affinity of the semiconductor. When the metal is bought into contact with the semiconductor, electrons from the semiconductor conduction band flow into metal till the Fermi level in the two substances are aligned. The band bending in the semiconductor is equal to the difference between the work functions. The barrier height is given by Schottky [85] and Mott [86] independently. A metallic contact on the n-type semiconductor is rectifying when $\phi_m > \phi_{sc1}$ and is non rectifying when $\phi_m < \phi_{sc1}$. The opposite is true for a metal p-type semiconductor contact [79].

Bardeen [87] pointed out the deviation of m-s contact due to the surface states in a covalently bonded crystal. The surface states are characterized by a neutral level of ϕ_o. If a metal is now brought into contact with the semiconductor the exchange of electrons takes place largely between the metal and semiconductor surface states and the depletion region charge remains practically unaffected.

A metal-semiconductor contact is defined as ohmic if its resistance is negligibly small compared with the resistance of the semiconductor specimen to which the contact is applied. A satisfactory ohmic contact should not significantly perturb the device performance, and it can supply the required current with a voltage drop across the active region of the device. It should be possible to create an ohmic contact by choosing a metal within the case of n type semiconductor and for p type. A low resistance contact to a semiconductor is obtained when the depletion region of the contact barrier is reduced in thickness by heavy doping of the semiconductor. The contact barrier is very thin and is essentially transparent to electrons in both directions. The specific contact resistance R_c is an important figure of merit for ohmic contact [88]. A good ohmic contact should have a specific contact resistance less than 10^{-4} Ω cm [79].

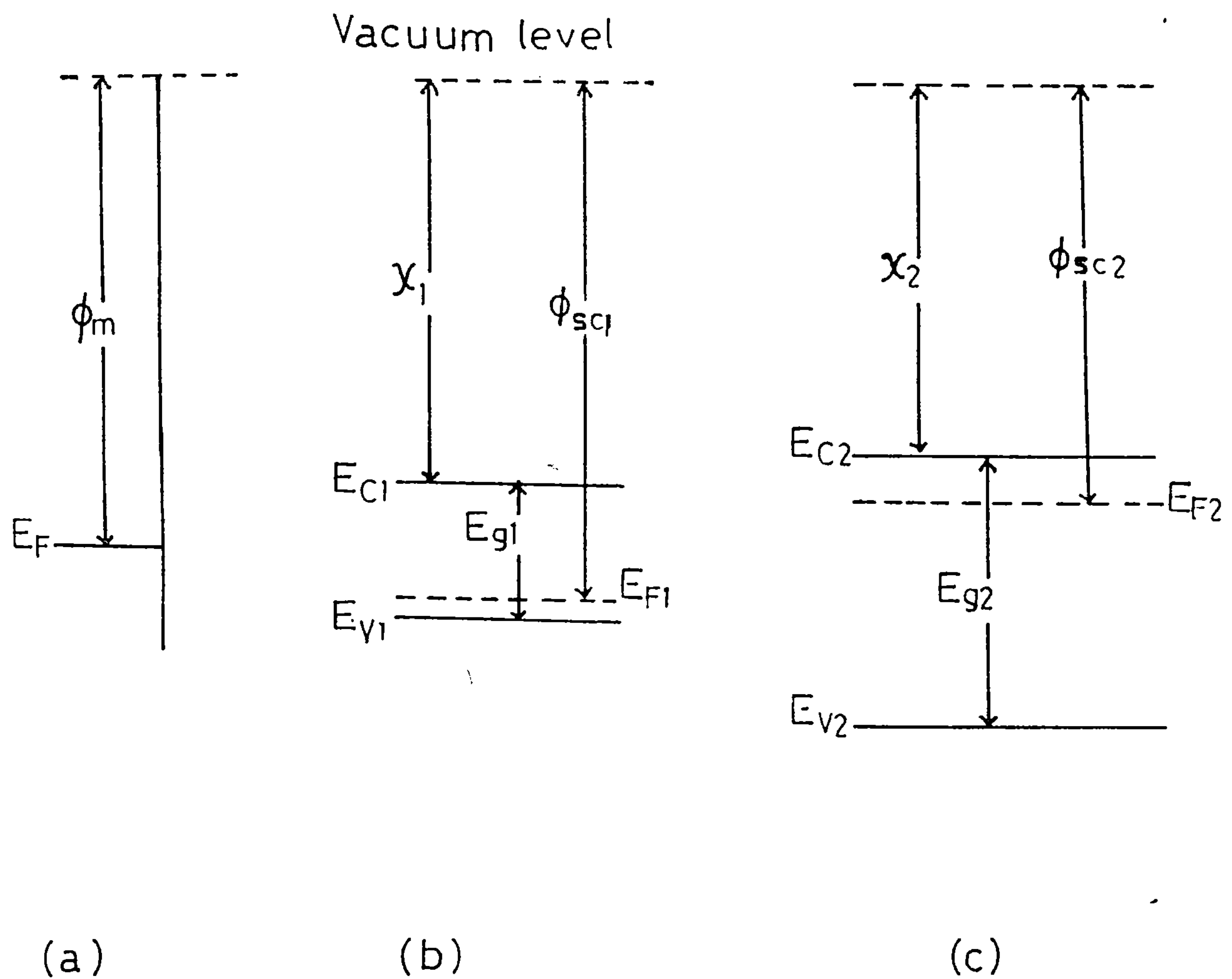

Fig.1.1 Energy band diagram of the metal and semiconductor. (a) Metal with work function ϕ_m, (b) n-type semiconductor with band gap E_{g1}, work function ϕ_{sc1} and electron affinity χ_1 and (c) p-type semiconductor with band gap E_{g2}, work function ϕ_{sc2} and electron affinity χ_2

1.42 Semiconductor-Semiconductor interface.

One of the most important interface between the materials is semiconductor-semiconductor contact. The pn junctions are formed by these interfaces and are of great importance both in modern electronics applications and in the understanding of other semiconductor devices. It is the metallurgical bonding between the n and p regions of a semiconductor. These junctions can be classified into two groups homojunctions and heterojunctions. Interface between the same semiconductor materials with different types of conductivity is known as homojunction and that of different types of materials is known as heterojunction. Details of s-s junctions are given elsewhere [79-84].

The basic theory of pn homojunction was established by Shockley [89]. This theory was extended by Schokley et al [90] and Moll [91]. When the initially separated n and p-type semiconductors are brought into contact, majority carriers flow across the junction down the concentration gradients until the Fermi levels on the two sides are aligned. At thermal equilibrium condition, (that is, with no applied voltage) the current flow is zero.

The energy band model of an ideal abrupt heterojunction without traps was proposed by Anderson [92]. We will consider an ideal heterojunction that has no interfacial layer of any kind between the two semiconductors as well as no interface states. The semiconductors are assumed to have different band gap E_{g1} and E_{g2}, different permittivities ε_1 and ε_2, different work functions ϕ_{sc1} and ϕ_{sc2} and different electron affinities χ_1 and χ_2 (as shown in Figs. 1.1(b) and 1.1(c)). When these two materials are brought into intimate contact, electron hole flow occurs across the junction until thermal equilibrium is reached.

1.43 Necessity of bilayer thin film in solar cells.

Since the present work mainly deals with semiconductor materials and multilayer thin film structures which finds extensive application in the area of solar cells, we will give due importance to these devices in our descriptions. Optoelectronic devices convert optical energy into electrical energy and vice-versa. The mechanism of converting optical radiation into electrical energy is known as the photovoltaic effect. In a solar cell, electron hole pairs are produced by absorption of light. The essential electric field inside the cell is produced due to the presence of the junction or contact between two different layers. If it is between a p-type and n-type layer then it is called a pn junction and if it is between a semiconductor and a metal then it is called a Schottky barrier. But the important aspect to be noticed here is that in both these cases a bilayer film structure is essential for the formation of a solar cell. Generally in thin film pn junction solar cells, the active semiconductor layers are polycrystalline or amorphous films and these are deposited on electrically active or passive substrate, such as glasses, plastics, ceramics, metals etc. This is true for both homojunction and heterojunction.

The solar cells require another contact other than the junction which creates the build-in-field, and that is the contact between the electrode and the semiconductor layer itself. In fact there are two electrodes- the upper electrode and the lower electrode. In this the lower electrode will be usually a thick metal layer (if the front side of the cell is exposed to light) or a layer of transparent conducting material (if the back side of the cell is exposed to light) like tin oxide, indium tin oxide, zinc oxide etc. But the top electrode will be a thin film of good metallic conductor and this will have a either a grid or a comb structure, so as to allow the maximum light to fall on the semiconductor.

This structure of solar cell described gives the picture of a very conventional and old one. At present the same has much complicated structure containing more layers [93,94]. However this description makes it clear that a solar cell will contain at least one semiconductor-semiconductor contact and two metal-semiconductor contacts; in other words, one rectifying contact and two ohmic contacts. So it is clear that the material study as well as the design aspects of solar cells will be mainly based on the preparation and the characterization of multilayer films which can form these necessary junctions/ contacts.

1.44 Problems and characterization of bilayer thin films.

In earlier sections we have seen the fabrication techniques and applications of bilayer thin films. We have also seen that the different types of interfaces in thin film solar cells are semiconductor-electrode (optically transparent and electrically conducting material), semiconductor-metal and semiconductor-semiconductor. The quality of these thin film interfaces affect the efficiency of the cells. One of the main resons for the degradation of thin film solar cells is due to the interface phenomenon between the layers, like diffusion, chemical reaction etc. These processes usually cause the formation of an interlayer between the thin films that form the devices. Details of interface diffusion and reaction are given in several text books [1,95-97]. In the world of bulk or large-scale structures, interdiffusion or reaction taking place on a ~10 nm scale can generally be ignored. This is not the case of thin film structures, whose total thickness is of the order of few hundred nm and the reaction on an interface leading to the formation of interlayer of thickness of the order of few ten nm can be totally detrimenental to the thin film devices.

In the present study we have analysed the interlayer

diffusion of different layers that are usually formed in thin film solar cells. For example as described earlier usually metals are used as back electrodes in thin film solar cell and the stability of the interface has very important role in the performance of the device. A small account of metal-semiconductor interface is given in section 1.41. Similarly another important interface is the semiconductor-semiconductor type and details of this is given in section 1.42.

The polycrystalline nature of thin film increase the interlayer diffusion of materials and the degradation of the cell [98]. For example Chopra et al [1] have given a detailed account of interlayer degradation of Cu_2S/CdS bilayer structure due to the grain boundary diffusion of Cu_2S into CdS layer. In fact this results in the formation of a path, short circuiting the junction and this leads to the total destruction of Cu_2S /CdS cell. Another case of the degradation of this cell is the diffusion of Cu from Cu_2S into CdS after fabrication. This really leads to the formation of a Cu-deficit phase. Similarly Kazmerski et al [99] have studied the degradation of CdS/$CuInSe_2$ thin films junction. They observed the diffusion of S and Se across the junction and this results in the widening of the depletion layer. The high temperature heat treatment causes the diffusion of Cd into $CuInSe_2$ and this results in the catastrophic degradation of the cell.

All these results point out that the study of interlayer formation and interface diffusion are very important for the characterization of solar cell as well as to increase it's life time and efficiency. Different techniques like Auger Electron Spectroscopy (AES), X-ray Photoelectron Spectroscopy (XPS), Rutherford Back Scattering (RBS), X-ray diffraction (XRD), Secondary Ion Mass Spectroscopy (SIMS), Ellipsometry etc are used for the surface and interface

analysis. But it should be noticed that any one of these techniques alone is not sufficient to characterize the multilayer film completely.

AES is one of the most powerful and widely used technique for surface and interface analysis. In AES the emitted Auger electron is analysed for the characterization of the thin film [100]. The mass analysis of the secondary ions by an ion mass analyser forms the basis of SIMS and it is used for the depth profiling of samples [100]. In Rutherford Back Scattering (RBS) ions of different particles (usually He ions) in the range of 100 keV-5 MeV bombard the sample and the back scattered ions are detected. RBS provides a nondestructive way to distinguish the atomic masses of elements and their distribution as a function of depth [100]. In the present study we have used XRD, SEM and XPS along with optical technique to characterize the surface and interface of the single and multilayer films prepared in our laboratory and a brief description of these are given in section 1.6.

Among these experimental techniques listed here the optical techniques viz, optical absorption and spectroscopic ellipsometry require special mentioning. Eventhough these are simple techniques, these can reveal much about the superficial as well as interior aspects of thin films. This has become much relevant after the advent of high speed personal computers as these can be used for theoretical modelling along with the optical experiments. However in the case of semiconductor thin films the selection of wavelengths is also very important. This is because semiconductor materials will absorb light waves having energy grater than the band gap of the material. So one can not use such wavelength for probing the interior of semiconducting thin films. If one really wants to know about the interior details of semiconductors, light wave having energy lower than that of the band gap should be selected for the study. In the next section the details of the

theory dealing with the interaction of electromagnetic radiation with multilayer thin films is given.

1.5 Optics of thin films.

The Optical constants and thickness of thin films are important parameters for predicting the performance of an the films. The optical constants are sensitive to the microstructure which is affected by the deposition condition [101-104]. A good knowledge of the film parameters is necessary for the design and manufacture of new optical coatings and devices, such as multilayer coatings, filters, optoelectronic devices like thin film solar cells etc.

1.51(a) Multilayer film

In order to interpret the data from an ellipsometer or other optical techniques one has to derive the necessary expressions governing the interaction of electromagnetic wave with optical system (thin film system). A detailed description of this is given in several publications [77,105-107]. In this section we will consider the reflection and transmission of polarised light from a multilayer thin film system with an example of single layer thin film system. In this analysis equations for calculating the reflected as well as transmitted amplitudes are derived and hence these are later used for a detailed explanation of the theory behind ellipsometry (in chapter 2).

The propagation of a plane wave in an isotropic absorbing medium is described by the complex refractive index N.

$$N = n - ik \tag{1.2}$$

where n is called index of refraction and k the extinction coefficient of the medium. The expression for the electric vector of an optical plane wave travelling in the positive direction of the Z-axes in an isotropic absorbing

medium such that the planes of constant phase and those of constant amplitude of the wave are parallel is given by

$$E = E_o e^{i(\omega t + \delta)} e^{-i\omega Nz/c} \qquad (1.3)$$

where δ is a constant phase angle, c is the free space velocity, and E_o, which is in general complex defines both the amplitude and polarisation of the wave.

Consider a stratified structure (shown in Fig. 1.2) that consists of a stack of 1,2,...j...m parallel layers sandwiched between two semi infinite ambient (0) and substrate (m+1) media. All the layers are linear homogeneous and isotropic. Also the complex index of refraction of jth layer be N_j and its thickness is t_j. N_o and N_{m+1} be the complex indices of refraction of the ambient and substrate media respectively. The interface between j^{th} layer and $(j+1)^{th}$ layer will be denoted as j(j+1). An incident monochromatic plane wave in medium '0' generates a resultant reflected plane wave in the same medium and a resultant transmitted plane wave in medium (m+1). The total field inside the jth layer, consist of two plane waves; a forward travelling plane wave denoted by (+) and a backward travelling plane wave denoted by (-). The wave vectors of all plane waves lie on the same plane (the plane of incidence) and the wave vectors of the two plane waves in the jth layer make equal angles with z-axis which is perpendicular to the plane boundaries directed towards the substrate. When the incident wave in the ambient is linearly polarised with its electric vector vibrating parallel (p) or perpendicular(s) to the plane of incidence, all plane waves excited by that incident wave in the various layers of the stratified structure will be similarly polarised, parallel or perpendicular to the plane of incidence as the case may be. In the following discussions it will be assumed that all waves are either p or s polarised.

Let $E^+(z)$ and $E^-(z)$ denote the complex amplitudes of the

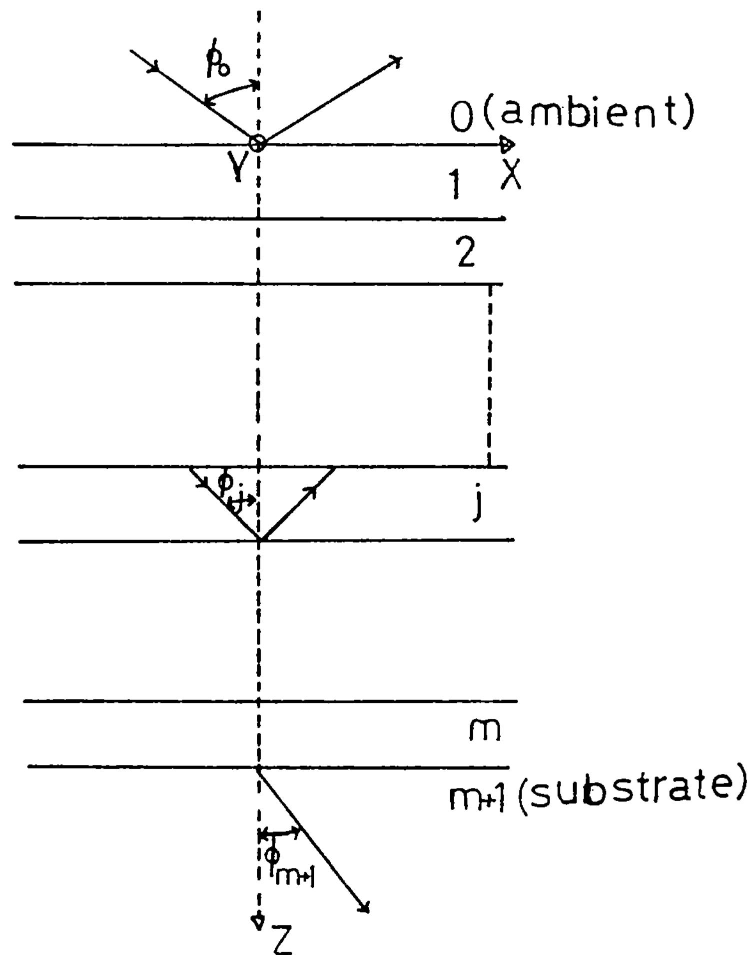

Fig.1.2 Reflection and transmission of a plane wave by a multilayer-film structure (films 1,2,...j,...m) sandwiched between semi-infinite ambient (0) and substrate (m+1) media. ϕ_0 is the angle of incidence, ϕ_j and ϕ_{m+1} is the angle of refraction in the *jth* film and substrate respectively.

forward and backward travelling plane waves at an arbitrary plane z. The total field at z can be described by a 2x1 column vector.

$$E(z) = \begin{bmatrix} E^{+}(z) \\ E^{-}(z) \end{bmatrix} \quad (1.4)$$

The fields at two different plane z' and z" (ie., E(z') and E(z")) are related by a 2x2 matrix transformation

$$\begin{bmatrix} E^{+}(z') \\ E^{-}(z') \end{bmatrix} = \begin{bmatrix} S_{11} & S_{12} \\ S_{21} & S_{22} \end{bmatrix} \begin{bmatrix} E^{+}(z'') \\ E^{-}(z'') \end{bmatrix} \quad (1.5)$$

In a more simplified way the above equation can be written as

$$E(z') = S\, E(z'') \quad (1.6)$$

Here the matrix S characterizes that part of the stratified structure confined between the two parallel planes at z'and z".

Let z' and z" lie immediately on opposite sides of the (j-1)j interface located at z_j between the layers (j-1) and j. Then Eq.1.6 becomes

$$E(z_j) = I_{(j-1)j}\, E(z_j) \quad (1.7)$$

where $I_{(j-1)j}$ is a 2x2 matrix characteristic of the (j-1)j interface. If z' and z" are selected inside the jth layer at its boundaries, then

$$E(z_j) = L_j\, E(z_j + t_j) \quad (1.8)$$

where L_j is a 2x2 matrix characteristic of the jth layer, whose layer thickness is t_j. Here the only measurable quantities are the intensities (and hence the amplitudes) of the reflected wave to the ambient side and transmitted wave on the substrate side. So it is necessary to relate their fields to those of the incident wave. Let z' and z" are in the

ambient and substrate media immediately adjacent to the 01 and m(m+1) interfaces. Then

$$E(z_1) = S\, E(z_{m+1}) \qquad (1.9)$$

where S is scattering matrix governing the overall reflection and transmission properties of the stratified structure. S can be expressed as the product of the interface and layer matrices, I and L which describe the effects of individual interfaces and layer of the entire stratified structure.

$$S = I_{01} L_1 I_{12} L_2 \ldots\ldots I_{(j-1)} L_j \ldots\ldots L_m I_{m(m+1)} \qquad 1.10$$

It is evident that the determination of the scattering matrix S, is possible only if the individual interface and layer matrices I and L are known.

The matrix I of an interface between two media 'a' and 'b' relates the field on its both sides as

$$\begin{bmatrix} E_a^+ \\ E_a^- \end{bmatrix} = \begin{bmatrix} I_{11} & I_{12} \\ I_{21} & I_{22} \end{bmatrix} \begin{bmatrix} E_b^+ \\ E_b^- \end{bmatrix} \qquad (1.11)$$

Consider Fig. 1.3(a) in which a plane wave is incident on the 'ab' interface from medium 'a'. The complex amplitude of the transmitted and reflected plane waves in media 'b' and 'a' can be expressed in terms of the complex amplitude of the incident wave in the medium 'a' as

$$E_b^+ = t_{ab} E_a^+ \qquad (1.12(a))$$

$$E_a^- = r_{ab} E_a^+ \qquad (1.12(b))$$

and $E_b^- = 0$,

where r_{ab} and t_{ab} are the Fresnel reflection and transmission coefficients of the interface 'ab'. Eq. 1.11 can be now modified as

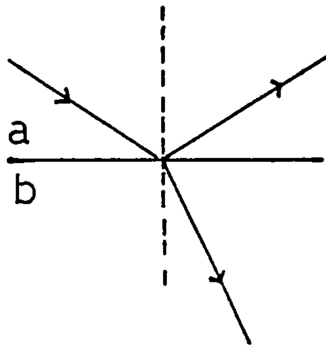

(a)

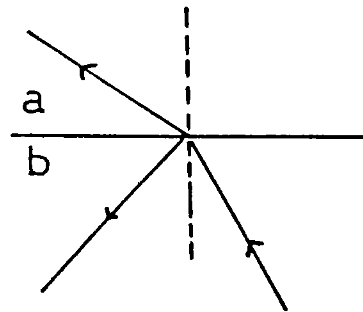

(b)

Fig.1.3 Interaction of plane wave at an interface. (a) when incident of the on the 'ab' interface from medium 'a' and (b) when incident on the 'ba' interface from medium 'b' at an angle of incidence equal to the angle of refraction in the case (a).

$$\begin{bmatrix} E_a^+ \\ E_a^- \end{bmatrix} = \begin{bmatrix} I_{11} & I_{12} \\ I_{21} & I_{22} \end{bmatrix} \begin{bmatrix} E_b^+ \\ 0 \end{bmatrix} \qquad (1.13)$$

which can be expressed as

$$E_a^+ = I_{11}\, E_b^+ \qquad (1.14(a))$$

$$E_a^- = I_{21}\, E_b^+ \qquad (1.14(b))$$

Comparing Eqs.1.12(a) and 1.12(b) with Eqs.1.14(a) and 1.14(b),

$$I_{11} = 1/t_{ab} \qquad (1.15(a))$$

$$I_{21} = r_{ab}/t_{ab} \qquad (1.15(b))$$

Next let us consider that the beam is incident from medium 'b' (Fig. 1.3(b)) at an angle of incidence equal to the angle of refraction in the above case depicted in Fig.1.3(a). Now the path of the light beam is to be exactly reversed on comparison with that in Fig.1.3(a). The fields immediately adjacent to the ba interface are

$$E_b^+ = r_{ab}\, E_b^- \qquad (1.16(a))$$

$$E_a^- = t_{ba}\, E_b^- \qquad (1.16(b))$$

and $E_a^+ = 0$,

Where r_{ba} and t_{ba} are the Fresnel reflection and transmission coefficient of the ba interface respectively. In this case Eq. 1.11 can be written as

$$\begin{bmatrix} 0 \\ E_a^- \end{bmatrix} = \begin{bmatrix} I_{11} & I_{12} \\ I_{21} & I_{22} \end{bmatrix} \begin{bmatrix} E_b^+ \\ E_b^- \end{bmatrix} \qquad (1.17)$$

$$0 = I_{11}\, E_b^+ + I_{12}\, E_b^- \qquad (1.18(a))$$

$$E_a^- = I_{21}\, E_b^+ + I_{22}\, E_b^- \qquad (1.18(b))$$

Substituting the value of I_{11} and I_{21} from Eqs.1.15(a) and 1.15(b) into Eqs.1.18(a) and 1.18(b) one gets

$$E_b^{+} = -I_{12}\, t_{ab}\, E_b^{-} \tag{1.19(a)}$$

$$E_a^{-} = \left[\frac{r_{ab} r_{ba}}{t_{ab}} + I_{22} \right] E_b^{-} \tag{1.19(b)}$$

Comparing Eqs.1.16(a) and 1.16(b) and Eqs. 1.19(a) and 1.19(b), we get

$$I_{12} = - r_{ba} \,/\, t_{ab} \tag{1.20(a)}$$

$$I_{22} = \left(t_{ab}\, t_{ba} - r_{ab}\, r_{ba} \right) / \, t_{ab} \tag{1.20(b)}$$

Using the following relations between the Fresnel's coefficients

$$r_{ab} = -r_{ab} \tag{1.21(a)}$$

$$t_{ba} = \left(1 - r_{ab}^{2} \right) / \, t_{ab} \tag{1.21(b)}$$

one can rewrite the interface matrix as

$$I_{ab} = \begin{bmatrix} 1/t_{ab} & r_{ab}/t_{ab} \\ r_{ab}/t_{ab} & 1/t_{ab} \end{bmatrix}$$

$$I_{ab} = \frac{1}{t_{ab}} \begin{bmatrix} 1 & r_{ab} \\ r_{ab} & 1 \end{bmatrix} \tag{1.22}$$

Using Snell's law one can write

$$N_o \sin\phi_o = N_1 \sin\phi_1 = \ldots\ldots = N_j \sin\phi_j = \ldots\ldots = N_{m+1} \sin\phi_{m+1} \tag{1.23}$$

The effect of propagation through a homogeneous layer of index of refraction N and thickness t can be found out by getting the relationship between the fields inside the layer at both ends. As the only change occurring to the wave due to such a travel is the phase shift (ignoring the amplitude attenuation) one can denote the change by the following equation.

$$\begin{bmatrix} E_o^+ \\ E_o^- \end{bmatrix} = \begin{bmatrix} e^{i\beta} & 0 \\ 0 & e^{-i\beta} \end{bmatrix} \begin{bmatrix} E_t^+ \\ E_t^- \end{bmatrix} \qquad (1.24)$$

The subscript 0 and d identify the beginning and end of the jth (t_j is the thickness of the jth layer) layer along the direction of the forward travelling wave, and phase shift β is given by

$$\beta = \frac{2\pi t_j N}{\lambda} \cos\phi \qquad (1.25)$$

where ϕ is the angle between the direction of propagation in the layer and the perpendicular to the boundaries (z-axis) (see Fig. 1.2). The layer matrix L can be therefore written as

$$L = \begin{bmatrix} e^{i\beta} & 0 \\ 0 & e^{-i\beta} \end{bmatrix} \qquad (1.26)$$

Thus from the interface and layer matrices I and L (ie., from Eqs. 1.22 and 1.26), the overall scattering matrix S of the structure substrate is obtained by direct multiplication. Now Eq. 1.9 becomes

$$\begin{bmatrix} Ea^+ \\ Ea^- \end{bmatrix} = \begin{bmatrix} S_{11} & S_{12} \\ S_{21} & S_{22} \end{bmatrix} \begin{bmatrix} Es^+ \\ 0 \end{bmatrix} \qquad (1.27)$$

where the subscripts a and s refer to the ambient and substrate media respectively and $E_s^- = 0$. From Eq. 1.27 the overall reflection and transmission coefficients of the stratified structures can be written as:

$$R = \frac{E_a^-}{E_a^+} = \frac{S_{21}}{S_{11}} \qquad (1.28)$$

$$T = \frac{E_s^+}{E_a^+} = \frac{1}{S_{21}} \qquad (1.29)$$

In the case of ellipsometry the scattering matrix S has to be calculated for both the linear polarizations, parallel (p) and perpendicular (s) to the plane of incidence. Let the subscripts 'p' and 's' represent the scattering matrices for the p and s polarisations. Then,

$$R_p = \frac{S_{21p}}{S_{11p}} \qquad (1.30(a))$$

$$R_s = \frac{S_{21s}}{S_{11s}} \qquad (1.30(b))$$

$$T_p = \frac{1}{S_{21p}} \qquad (1.31(a))$$

$$T_s = \frac{1}{S_{21s}} \qquad (1.31(b))$$

Considering the case of reflection ellipsometry, the ellipsometric parameter ρ is given by

$$\rho = \frac{R_p}{R_s} = \frac{S_{21p}}{S_{11p}} \text{ X } \frac{S_{11s}}{S_{21s}} \qquad (1.32)$$

The importance as well as the method of calculation of ρ are included in section 1.52 which descriebs the theory of ellipsometry.

1.51(b) Single layer film

Consider the case of a single layer film over a substrate as shown in Fig. 1.4. The thickness of the film is given by t1. N_o, N_1 and N_s are the complex refractive indices of air, film and substrate respectively. Let ϕ_0 is the angle of incidence and ϕ_1 and ϕ_2 are angles of refraction in the film and substrate respectively. The scattering matrix is given by

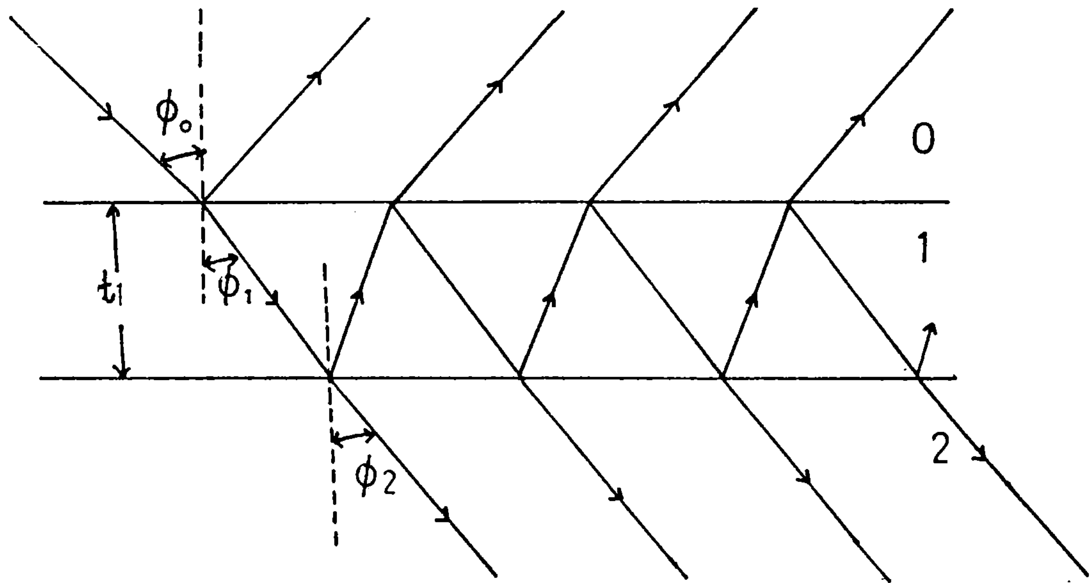

Fig.1.4 Oblique reflection and transmission of a plane wave by an ambient (0)-film (1)- substrate (2) system with parallel plane boundaries. 't' is the thickness of the film. ϕ_o is the angle of incidence in the ambient and ϕ_1 and ϕ_2 are the angle of refraction in the film and substrate respectively.

$$S = I_{01} L_1 I_{12} \tag{1.33}$$

Substituting from Eqs.1.22 and 1.26, the above equation becomes

$$S = \frac{e^{i\beta}}{t_{01} t_{12}} \begin{bmatrix} (1 + r_{01} r_{12} e^{-i2\beta}) & (r_{12} + r_{01} e^{-i2\beta}) \\ (r_{01} + r_{12} e^{-i2\beta}) & (r_{01} r_{02} + r_{12}\, e^{-i2\beta}) \end{bmatrix} \tag{1.34}$$

where r_{01} and r_{12} is the Fresnel reflection coefficient of interface 01 and 12 respectively. Similarly t_{01} and t_{12} are the Fresnel transmission coefficient at 01 and 12 interface respectively. Then the above equation gives

$$S_{11} = \frac{e^{i\beta}}{t_{01} t_{12}} (1 + r_{01} r_{12} e^{-i2\beta}) \tag{1.35(a)}$$

$$S_{12} = \frac{e^{i\beta}}{t_{01} t_{12}} (r_{01} + r_{01} r_{12} e^{-i2\beta}) \tag{1.35(b)}$$

Using these Eqs.1.28 and 1.29 the complex reflection and transmission coefficients are written in terms of Fresnel coefficients as follows

$$R = \frac{r_{01} + r_{12} e^{-i2\beta}}{1 + r_{01} r_{12} e^{-i2\beta}} \tag{1.36(a)}$$

$$T = \frac{t_{01}\, t_{12} e^{-i2\beta}}{r_{01} + r_{12} e^{-i2\beta}} \tag{1.36(b)}$$

Reflection/ transmission coefficients corresponding to the perpendicular (s) and parallel (p) components of polarisation are obtained from Eqs.1.36(a) and 1.36(b) as follows. Here also the subscripts p and s denote the

respective polarisation under consideration.

$$R_s = \frac{r_{01s} + r_{12s} e^{-i2\beta}}{1 + r_{01s} r_{12s} e^{-i2\beta}} \qquad (1.37(a))$$

$$R_p = \frac{r_{01p} + r_{12p} e^{-i2\beta}}{1 + r_{01p} r_{12p} e^{-i2\beta}} \qquad (1.37(a))$$

$$T_s = \frac{t_{01s} t_{12s} e^{-i\beta}}{1 + r_{01s}\ r_{12s} e^{-i2\beta}} \qquad (1.38(a))$$

$$T_p = \frac{t_{01p} t_{12p} e^{-i\beta}}{1 + r_{01p}\ r_{12p} e^{-i2\beta}} \qquad (1.38(b))$$

Where the phase angle β (film phase thickness) is given by

$$\beta = \frac{2\ \pi\ t_1}{\lambda} N_1 \cos\phi_1$$

$$\text{Or, } \beta = \frac{2\ \pi\ t_1}{\lambda} \left(N_1^2 - N_0^2 \sin^2\phi_0 \right)^{1/2} \qquad (1.39)$$

The Fresnel's reflection/ transmission coefficients for the air-film-substrate system is given by [77]

$$r_{01p} = \frac{N_1\ \cos\phi_0\ -\ N_0\ \cos\phi_1}{N_1\ \cos\phi_0\ +\ N_0\ \cos\phi_1} \qquad (1.40(a))$$

$$r_{12p} = \frac{N_s\ \cos\phi_1\ -\ N_1\ \cos\phi_2}{N_s\ \cos\phi_1\ +\ N_1\ \cos\phi_2} \qquad (1.40(b))$$

$$r_{01s} = \frac{N_0 \cos\phi_0 - N_1 \cos\phi_1}{N_0 \cos\phi_0 + N_1 \cos\phi_1} \qquad (1.40(c))$$

$$r_{12s} = \frac{N_1 \cos\phi_1 - N_s \cos\phi_2}{N_1 \cos\phi_1 + N_s \cos\phi_2} \qquad (1.40(d))$$

$$t_{01p} = \frac{2N_0 \cos\phi_0}{N_1 \cos\phi_0 + N_0 \cos\phi_1} \qquad (1.41(a))$$

$$t_{12p} = \frac{2N_1 \cos\phi_1}{N_s \cos\phi_1 + N_1 \cos\phi_2} \qquad (1.41(b))$$

$$t_{01s} = \frac{2N_0 \cos\phi_0}{N_0 \cos\phi_0 + N_1 \cos\phi_1} \qquad (1.41(c))$$

$$t_{12p} = \frac{2N_1 \cos\phi_1}{N_1 \cos\phi_1 + N_s \cos\phi_2} \qquad (1.41(d))$$

With the help of above theory almost all the optical experiments performed on thin films can be explained. For example in the case of spectrophotometry one measures the reflection as well as transmission of the film at different wavelengths. These data can be the theoretically calculated using Eqs.1.36(a) and 1.36(b), provided one has the values of Fresnel's coefficients. As these coefficients are functions of refractive indices (as shown by Eqs. 1.40(a)-1.41(d)) one can compute the unknown refractive index from a curve fitting method. This type of analysis can be extended further to see whether the given film contains any surface layer (like oxides, nitrides etc.) or has surface roughness [77]. Similarly this set of analysis can give information about the presence of any interlayer or to some extend the percentage composition of the film. The details of the analysis is not given here as it is not directly related to the present work.

This sort of analysis can be done using ellipsometry

with better accuracy and its description is included in the following chapter. In the next section we give a very brief review of different optical techniques used for thin film analysis. Even though this description just indicates the measurement of refractive index of the material of thin film using these technique one can clearly go deeper into the material analysis also.

1.52 Different optical techniques for thin film characterization.

1.521 Spectrophotometric Technique.

A Spectrophotometer is defined as a spectrometer with associated equipment so that it furnishes the ratio or a function of the ratio of the radiant power of the two beams as a function of spectral wavelength. These two beams may be separated in time, space or both [100]. Spectrophotometer can operate both in reflection mode and transmission mode. The total intensity (I) of light is given by [100]

$$I = R + T + A \tag{1.42}$$

where R, T and A are reflection, transmission and absorption respectively. There are different techniques for the determination of optical constants of thin films using spectrophotometer reflectance and transmission data. One usually assumes, when calculating the transmittance and reflectance of a film, that the distribution of n is homogeneous throughout the volume of the film. More detailed studies indicate that there may be random spatial variations of n with a significant index gradient normal to the surface of the film. In such a case layered structure may be assumed for the film to do the theoretical calculation.

1.521(a) Transmission.

Many researchers obtain the optical constants of

dielectric thin films from the transmittance measurements of a light beam which penetrates through the film and supporting substrate [108-110]. In this section we describe the method suggested by Farabugh et al [110]. They have used a multiparameter curve fitting method to determine the optical constants (refractive index n and extinction coefficient k) and thickness (t) of thin film from transmittance spectra. In this method, the transmittance of a weakly absorbing film can be expressed by the following equations.

$$T = \frac{16\, n_0\, n^2\, n_s\, A}{C_1^2 + C_2^2 A^2 + 2C_1 C_2 A \cos(4\pi n t/\lambda)} \qquad (1.43)$$

$$\text{where } C_1 = (n + n_0)\ (n_s + n) \qquad (1.44(a))$$

$$C_2 = (n - n_0)\ (n_s - n) \qquad (1.44(b))$$

$$A = \exp(-4\pi k t/\lambda) = \exp(-\alpha t) \qquad (1.45)$$

and α is the absorption coefficient of the film.

Here n_s and n_0 are the refractive indices of the substrate and ambient respectively. The form of n is given by Cauchy's formula

$$n^2 = a_1 + (a_2/\lambda^2) + (a_3/\lambda^4) \qquad (1.46)$$

The form for α is given by

$$\alpha = a_4 \exp(-a_5\lambda) + a_6 \qquad 1.47$$

The thickness is taken as $t = a_7$. The transmittance curve of each spectrum is fitted to Eq. 1.43 with the parameters given above (a_1 to a_7) and hence the optical constants are calculated.

1.521(b) Transmittance envelope method.

In this method refractive index is calculated from the envelope of the interference pattern of transmission spectrum as suggested by Manifacier et al [111]. This technique is widely used for the determination of n, k and

thickness t [111,112]. According to the Manifacier T_{max} and T_{min} of the interference pattern of the transmission spectrum is a function of λ is given by

$$\alpha = \frac{C_1 \left[1 - \left(T_{max}/T_{min}\right)^{1/2} \right]}{C_2 \left[1 + \left(T_{max}/T_{min}\right)^{1/2} \right]} \qquad (1.48)$$

Then n is, $n = \left[N + \left(N^2 - n_0^2\, n_s^2 \right)^{1/2} \right]^{1/2}$ (1.49)

$$\text{where } N = \frac{n_0^2 + n_s^2}{2} + 2n_0 n_s \frac{T_{max} - T_{min}}{T_{max}\ \ T_{min}} \qquad (1.50)$$

This shows that n is explicitly determined from T_{max}, T_{min}, n_s and n_o at the same wavelength (λ).

Knowing n one can determine t (thickness of the film) using the equation that relate two maxima and minima

$$t = \frac{m\, \lambda_1\, \lambda_2}{2\, \left(n(\lambda_1)\lambda_2 - n(\lambda_2)\lambda_1 \right)} \qquad (1.51)$$

where m is the number of oscillation between two extrema. λ_1, $n(\lambda_1)$ and λ_2, $n(\lambda_2)$ are the wavelengths and corresponding refractive indices of the film. Knowing t and α it is now possible to calculate the extinction coefficient k using Eq.1.45

1.521(c) Reflection spectra.

Films which are highly absorbing ($k > 1.5$) in some part of spectral range may transmit so little light that only the reflectance can be measured in this case. Hence the reflectivity measurement is used for the determination of optical constants of such films [113-115]. Tomlin [115] has suggested a technique, in which the reflectance from the specimen itself and from the specimen coated with a transparent film are measured. If the specimen does not

transmit, its reflection is given by

$$R = \frac{(n_o - n_2)^2 + k_2^2}{(n_o + n_2)^2 + k_2^2} \qquad (1.52)$$

where n_o is the refractive index of air and $N=(n_2-ik_2)$ is the complex refractive index of the film.

The reflectance R_1 from the transparent film of refractive index n_1 deposited on the specimen film, (now assuming that the film as substrate since it does not transmit) is given by

$$\frac{1 + R_1}{1 - R_1} = \frac{1}{4\pi n_o n_2 n_1^2}\Big[\left(n_o^2 + n_1^2\right)\left(n_1^2 + n_2^2 + k_2^2\right) + \left(n_o^2 - n_1^2\right)$$

$$\Big\{\left(n_1^2 - n_2^2 - k_2^2\right)\cos(2\gamma_1) + 2n_1k_2\sin(2\gamma_1)\Big\}\Big] \qquad (1.53)$$

where $\gamma_1 = 2\pi n_1 t_1/\lambda$, t_1 is the thickness of the transparent film and λ is the wavelength.

Using this equation n_2 and k_2 of the film can be calculated.

1.521(d) Reflectance and Transmittance at normal incidence.

If t is the thickness of a film and its reflectance R as well as and transmittance T measured at normal incidence are known, it is possible, in principle, to derive the components n and k of the complex refractive index (n-ik). Tomlin's expression given below [116] is used for the determination of n and k [117-118]. The expression given here for a single layer film coated over a substrate.

$$\frac{1+R}{T} = \frac{1}{4n_o n_s\left(n_1^2 + k_1^2\right)}\Big[\left(n_o^2+n_1^2+k_1^2\right)\Big\{\left(n_1^2+n_s^2+k_1^2+k_s^2\right)\cos(h2\alpha_1)$$

$$2\left(n_1n_s + k_1k_s\right)\sin(h2\alpha_1)\Big\} + \left(n_o^2-n_1^2-k_1^2\right) \times$$

$$\left\{\left(n_1^2-n_s^2+k_1^2-k_s^2\right)\cos(h2\gamma_1) + 2\left(n_1k_s - n_sk_1\right)\sin(h2\gamma_1)\right\}\Bigg] \quad (1.54)$$

$$\frac{1-R}{T} = \frac{1}{2n_s\left(n_1^2 + k_1^2\right)}\Bigg[n_1 \left\{\left(n_1^2+n_s^2+k_1^2+k_s^2\right)\sin(h2\alpha_1) + 2\left(n_1n_s + k_1k_s\right)\cos(h2\alpha_1)\right\} + k_1\left\{\left(n_1^2-n_s^2+k_1^2-k_s^2\right)\sin(h2\gamma_1) - 2\left(n_1k_s - n_sk_1\right)\cos(h2\gamma_1)\right\} \quad (1.55)$$

where $\gamma_1 = 2\pi n_1 t_1/\lambda_1$ and $\alpha_1 = 2\pi k_1 t_1/\lambda_1$

These expressions are simpler than the expression for R and T separately [105]. Where (n_1-ik_1) is complex refractive index of the film and (n_s-ik_s) is that of substrate. Using the given experimental values for $(1\pm R)/T$, t, n_0, n_s and k_s these equations can be readily solved using a computer after rearranging the Eqs. 1.54 and 1.55 in the form $f_1(n_1,k_1)=0$ and $f_2(n_s,k_s)=0$ respectively.

1.53 Ellipsometry.

Ellipsometry deals with the measurement and interpretation of changes in the polarization state of light upon reflection from the surface. Depending upon the mode of operation it can be classified into two groups viz., reflection and transmission ellipsometer. Theory of reflection ellipsometry is given here. The ellipsometric parameter ρ, the ratio of complex amplitude of reflection R_s and R_p is given by

$$\rho = R_p / R_s \quad (1.56)$$

The complex amplitude reflection (R_p, R_s) can be written in terms of their absolute values and phase angles

$$R_p = |R_p| e^{i\Delta_{rp}} \quad (1.57(a))$$

$$R_s = |R_s| e^{i\Delta_{rs}} \qquad (1.57(b))$$

where $|R_p|$ and Δ_{rp} represent the amplitude attenuation and phase shift respectively as p-polarised light is reflected by the film covering the substrate. $|R_s|$ and Δ_{rs} have the similar meaning in the case of s polarisation. Here incident wave is assumed of unit amplitude. Thus one can define Eq.1.56 as

$$\rho = \frac{R_p}{R_s} = \frac{|R_p|}{|R_s|} e^{i(\Delta_{rp} - \Delta_{rs})}$$

$$\text{ie., } \rho = \tan\psi \; e^{i\Delta} \qquad (1.58)$$

Now the ellipsometric parameter ψ and Δ can be defined as

$$\tan\psi = \frac{|R_p|}{|R_s|} \qquad (1.59(a))$$

$$\Delta = \Delta_{rp} - \Delta_{rs} \qquad (1.59(b))$$

The ψ and Δ are the differential changes in amplitude and phase respectively, due to the reflection by the components of electric vector parallel and perpendicular to the plane of incidence.

Using Eqs.1.37(a) and 1.37(b) one gets

$$\tan\psi \; e^{i\Delta} = \frac{r_{01p} + r_{12p} e^{-i2\beta}}{1 + r_{01p} r_{12p} e^{-i2\beta}} \times \frac{1 + r_{01s} r_{12s} e^{-i2\beta}}{r_{01s} + r_{12s} e^{-i2\beta}} \qquad (1.60)$$

Or the functional dependence of ψ and Δ on the system parameters is given by

$$\tan\psi \; e^{i\Delta} = \rho\left(N_0, N_1, N_2, t_1, \phi, \lambda\right) \qquad (1.61)$$

These parameters ψ and Δ are used for the ellipsometric calculation by relating it to the experimentally calculated ψ

and Δ by ellipsometer as described in chapter 2.

1.6 Other thin film characterization techniques used.

The other properties of thin films like structural, surface and chemical composition were characterized using the techniques X-ray Diffractometer (XRD), X-ray Photoelectron Spectroscopy (XPS) and Scanning Electron Microscope (SEM).

1.61 X-ray Diffractometer.

X-ray diffraction is one of the most precise method for determining the crystal structure and identification of the samples (thin film). It requires no elaborate sample preparation and is essentially non-destructive. It gives a whole range of information like lattice constants, crystalline size, composition (with the help of standard data files), defects, and stresses in thin films. Analysis of the diffraction patterns obtained and comparison with standard JCPDS data cards can reveal the existence of different crystallographic phases in the film, their relative abundance and preferred orientations. From the width of the diffraction line, the average grain size in the film can also be estimated.

The interplanar spacing (d) was calculated from the X-ray diffraction profiles using the formula [100]

$$2\, d \sin\theta = n\, \lambda \qquad (1.62)$$

where θ is the Bragg's angle, n the order of diffraction, λ the wavelength of X-rays. Using the d value, the set of lattice planes [hkl] are identified from the standard data cards.

If the sample contains a mixture, each component has to be identified individually. This is done by treating the list of d values as if they belong to a single component. After a suitable match for one component is obtained, all the lines of the identified components are avoided from further analysis.

The intensities of the remaining lines are rescaled by setting the strongest intensity equal to 100 and the entire process of identification is repeated.

1.62 X-ray Photoelectron Spectroscopy.

When a molecule or atom is bombarded with high energy X-ray, the emission of inner electrons from atoms takes place. The kinetic energies of these photoelectrons (E_k) are then measured by an energy analyser. The core electron binding energy (E_b) relative to Fermi level can be computed from the relation [100]

$$E_b = h\nu - E_k - \phi_v \qquad (1.63)$$

where $h\nu$ is the energy of exciting photon. ϕ_v is the spectrophotometer work function (a constant). Most XPS measurements of solid generates useful information from only the surface layer of thickness 2 nm.

The binding energies of core electrons are affected by the valence electrons and therefore by the chemical environment of the atom. When the atomic arrangement surrounding the atom ejecting a photoelectron changes, it alters the local charge environment at that atomic site. This change, in turn, reflects itself as a variation in the binding energy of all the electrons of that atom. Thus, not only the valence electrons, but also the binding energies of the core electrons experience a characteristic shift. Such a shift is inherent to the chemical species producing the results and thus provides the capability of chemical analysis. Hence one can use this technique to find out whether an element is present in a sample in pure form or in the form of a compound. In a simple sense, the shifts of the photoelectron line in an XPS spectra reflects the variation in binding energy as the oxidation state of the atom changes. The magnitudes of chemical shifts will vary from element to element, and the sensitivity for a particular element will vary with the

photoelectron cross-section.

1.63 Scanning Electron Microscope.

The scanning electron microscope is the most widely used instrument for obtaining microstructural and surface features of the film. A finely focused electron beam is scanned over the surface of the specimen and the secondary electrons emanating from the specimen are used for the imaging of the surface. Since these electrons emanate only from surface layer of thickness about 1nm the picture obtained is a faithful reproduction of the surface features. To avoid charging problem a thin layer of gold is deposited over the specimen surface without altering the surface features.

References.

1. K.L.Chopra and S.R.Das. "*Thin film solar cells*", Plenum press, New york. (1983)
2. K.L.Chopra, S.Major and D.K.Pandya. *Thin Solid films.* **102**, (1983) 1.
3. Joy George. "*Preparation of thin films*", Marcel Dekker Inc.New york. (1992)
4. L.I.Maissel and R.Glang. (Eds) "*Handbook of thin film technology*", McGraw Hill Book Company, New York. (1970)
5. K.L.Chopra. "*Thin film Phenomena*", McGraw Hill Book Company, New york. (1969).
6. L.Holland. "*Vacuum deposition of thin film technology*", John Wieley and sons Inc., New York. (1961).
7. T.J.Coatts. (Ed) "*Active and Passive thin film devices*", Academic Press, London. (1978).
8. K.L.Chopra and L.K. Malhotra. (Eds) "*Thin Film technology and applications*", TMH publishing company, New Delhi. (1985).
9. K.Mitchell, A.L.Fahrenbruch and R.H.Bube *J. Vac. Sci. Technol.* **12** (1975) 909.
10. K.P. Mohanchandra, H.G.Shanbhauge and J.Uchil. *Phys. Stat. Sol. (a)* **130** (1992) K45.
11. J.Hamersky. *Thin Solid Films.* **44** (1977) 277.
12. N.G.Dhere, N.R.Parikh and A.Ferreira. *Thin Solid Films.* **44** (1977) 83.
13. G.K.M.Thutupalli and S.G.Tomlin. *J. Phys. D Appl. Phys.* **9** (1976) 128.
14. A.L.Fahrenbruch. *Proc. symposium on the Material Sci. Aspects of Thin Film systems for Solar Energy Conversion.* Tucson. (1974) p 384.
15. R.B.Shafizade, I.V.Ivanova, M.M.Kazinets. *Thin Solid Films.* **35** (1976) 169.
16. R.B.Shafizade, I.V.Ivanova and M.M.Kazinets. *Thin Solid*

Films. 55 (1978) 211.

17. B. Rezig, S. Duchemin and F. Guastavino. *Solar energy Mater.* 2 (1979) 53.
18. A. C. Rastogi and S. Salakalachen. *Thin Solid Films*. **97** (1982) 191.
19. L. L. Kazmerski, F. R. White, M. S. Ayyagiri, Y. J. Juang and R. P. Patterson. *J. Vac. Sci. Technol.* **14** (1977) 65.
20. W. Horig, H. Neumann, H. Sobotta, B. Schumann and F. Kuhn. *Thin Solid Films*. **48** (1978) 67.
21. D. Sridevi and K. V. Reddy. *Ind. J. Pure. Appl. Phys.* **24** (1986) 392.
22. K. W. Raine. *Thin Solid Films*. **38** (1976) 323.
23. H. M. Smith and A. F. Turner. *Appl. Optics*. **4** (1965) 147.
24. S. Mineta, N. Yasunga, N. Tarumi, E. Teshigawara, M. Okutomi and M. Ikeda. *Bull. Jpn. Soc. Process. Eng.* **18** (1984) 49.
25. M. Hanabusa, M. Suzuki and S. Nishigaki. *Appl. Phys. Lett.* **38** (1981) 385.
26. S. Maniv, W. D. Westwood, F. R. Shepherd, P. J. Scandon and H. Plattner. *J. Vac. Sci. Technol.* **20** (1982) 1.
27. F. Abou-Elfotouh, M. Soliman, A. E. Riad, A. Al-Jassim and T. Coutts. Proc. 22nd IEEE Photovoltaic Specialist Conf. IEEE, New York. (1991) p 1109.
28. R. B. Hall, R. W. Birkmire, J. E. Phillips and J. D. Meakin. *Appl. Phys. Lett.* **38** (1981) 925.
29. I. Martil, G. Gonzalez Diaz and F. Sanchez-Quesada. *Thin Solid Films*. **114** (1984) 327.
30. S. V. Krishnasamy, A. S. Manocha and J. R. Sxedon. *J. Vac. Sci. Technol. A* **1** (1983) 510.
31. J. Santamaria, F, Sanchez-Quesada, G. Gonzalez-Diaz, E. Iborra and R. Rodrguez-Vidal. *Thin Solid Films*. **125** (1985) 299.
32. A Krzesiuski. *Thin Solid Films*. **138** (1986) 111.
33. C. T. Lee, Y. K. Su and H. M. Wang. *Thin Solid Films*. **150** (1987) 283.
34. R. G. Goodchild, J. B. Webb and D. F. Williams. *J. Appl. Phys.*

57 (1985) 2308.

35. R.Banerjee and S.Ray. *J. Non. Cryst. Solids.* **89** (1987) 1.
36. S.Steven, R.E.Hegedus, W.Rocheleau, W.Buchman and B.N.Baron. *J. Appl. Phys.* **61** (1987) 381.
37. T.Saitoh, S.Matsubara and S.Minagawa. *Jpn. J. Appl. Phys.* **16** (1977) 807.
38. A.M.Mancini, P.Pierini , A.Quirini, A.Rizzo and L.Vasanelli. *J. Crystal Growth.* **62** (1983) 34.
39. A.M.Mancini, L.Vasanelli and C.DeBlasi. *J. Crystal Growth.* **79** (1986) 734.
40. M.Arienzo and J.J.Loferski. *Proc.* 2nd *EC Photovoltaic Solar Energy Conf.* (Eds. R.Van Overstraeten and W.Palz), Berlin. (1979) p 361.
41. R.Solanki and G.J.Collins. *Appl. Phys. Lett.* **42** (1983) 662.
42. P.K.Boyer, G.A.Roche, W.H.Ritchie and G.J.Collins. *Appl. Phys. Lett.* **49** (1982) 716.
43. R.R.Munz,.M.Rothschild and D.J.Ehrlich. *Appl. Phys. Lett.* **54** (1989) 1631.
44. F.A.Lowenheim *"Thin film Processes"* (Eds. J.L.Vossed and W.Kern). Academic Press, New York. (1978) p 209.
45. E.Fates, P.Herrasti, F.Arjona, E.G.Camerero and M.Leon. *J. Mater. Sci. Lett.* 5 (1986) 583.
46. K.S.Balakrishnan and A.C.Rastogi. *Thin Solid Films* **163** (1988) 279.
47. M.Fracastoro-Decker, J.L.S. Ferreira, N.V.Gomes and P.Decker. *Thin Solid Films.* **147** (1987) 291.
48. S.Chandra and R.K.Pandey. *Phys. Stat. Sol. (A)*.59 1980) 787.
49. Y.Ueono, H.Kawai, T.Sugiura and H.Minoura. *Thin Solid Films.* **157** (1988) 159
50. N.Khare, G.Razzina and L.P.Bicelli. *Thin Solid Films.* **186** (1990) 113.
51. M.Takahashi, K.Vosaki and H.Kite. *J. Appl. Phys.* **60** (1986)

2046.

52. P. Sircar. *Appl. Phys. Lett.* **53** (1988) 1184.

53. R. R. Chamberlin and J. S. Skarman. *J. Electrochem. Soc.* 113 (1966) 86.

54. A. G. Valyomana, Sunny Mathew, K. P. Vijayakumar and C. Purushothaman. *Bull. Mater. Sci.* **16** (1993) 55.

55. J. Nolly, K. K. Abdullah and K. P. Vijayakumar. *Phys. Stat. Sol. (A).* **101** (1987) K35.

56. O. P. Agnihotri, P. Rajaram , R. Thangaraj, A. K. Sharma and A. Raturi. *Thin Solid Films.* **102** (1983) 291.

57. C. R. Abernathy, C. W. Bates, Jr., A. A. Anani and B. Haba. *Thin Solid Films.* **115** (1984) L41.

58. A. K. Abass, Z. A. Ahmed and R. E. Tahir. *J. Appl. Phys.* **61** (1987) 2339.

59. G. Smestad and A. Da Silva. *Solar Energy Mater.* **18** (1989) 299.

60. F. J. Gracia, J. Muci and M. S. Tomar. *Thin Solid Films.* **97** (1982) 47.

61. J. Mimila-Arroya, J. A. Reynoso, E. Saucedo and J. C. Bourgoin. *J. Crystal Growth.* **68** (1984) 671.

62 K. Kulaszewicz, W. Jarmoc and K. Turowska. *Thin Solid Films.* **112** (1984) 313.

63. A. Ortiz, M. Garcia, S. Lopez and C. Falcony. *Thin Solid Films.* **165** (1988) 249.

64. C. Eberspacher, A. L. Fahrenbruch and R. H. Bube. *Thin Solid Films.* **136** (1986) 1.

65. P. K. Nair and M. T. S. Nair. *Solar Cells.* 22 (1987) 103.

66. I. Kaur, D. K. Pandya and K. L. Chopra. *J. Electrochem. Soc.* **127** (1980) 943.

67. S. G. Mokrushin and Yu. D. Tkachev. *Colloid. J. USSR.* **23** (1961) 366.

68. M. Ristov, G. J. Sinadinovski, I. Grozdanov and M. Miterski. *Thin Solid Films.* **149** (1987) 65.

69. J. C. Garg, R. P. Sharma and K. C. Sharma. *Thin Solid Films.* **164**

(1988) 269.

70. K.R.Murali. *Thin Solid Films.* **167** (1988) L19.
71. P.K.Vidhyadharan Pillai and K.P.Vijayakumar. *Proc. 36th DAE Solid State Symposium* 36C (1993) 230.
72. R.P.Goyal, P.Raviendra and B.R.K.Gupta. *Phys. Stat. Sol. (a)* 87 (1985) 79.
73. D.Raviendra and J.K.Sharma *J. Phys. Chem. Solids.* **46** (1985) 945.
74. N.Croitoru and S.Jakobson. *Thin Solid Films.* 56 (1979) L5.
75. N.Nakayama, H.Matsumoto, A.Nakano, S.Ikegami, H.Uda and T.Yamashita. *Jpn.J.Appl.Phys.* **19** (1980) 703.
76. S.Tolansky. "*Surface Microtopography*". John Wieley sons, New York.(1960).
77. R.M.A.Azzam and N.M.Bashara. "*Ellipsometry and polarised light*". North Holland, Amsterdam. (1977).
78. F.Braun. *Ann Phys.Chem.* **153** (1874) 556.
79. M.S.Tyagi. "*Introduction to semiconductor materials and devices*". John Wiely and Sons, New York. (1991).
80. G.Bush and H.Scanda "*Lectures in Solid state physics*" Pergamon Press, New York. (1973)
81. S.M.Sze. "*Introduction to Semiconductor Physics*". Wiely Eastern Ltd., New Delhi. (1981).
82. Stephen J.Fonash. "*Solar cells*". Academic Press, New York. (1985).
83. G.Milner and D.L.Feucht. "*Heterojunction and metal semiconductor junctions*". Academic Press, New York. (1972).
84. Robert K.Willardson and Alberst C.Beer (Eds.) "*Semiconductors and Semimetals*" Vol. **15** Academic press, New York (1981).
85. W.Schottky. *Naturwissenschaften.* **26** (1938) 843.
86. N.F.Mott. *Proc. Cambr. Philos. Soc.* **34** (1938) 568.
87. John Bardeen. *Phys. Rev.* **71** (1947) 717.
88. C.Y.Chang, Y.K.Fang, S.M.Sze. *Solid State Electron.* **14**

(1971) 541.

89. W.Shockley. *Bell Syst. Tech. J.* 28 (1949) 435.
90. C.T.Sah, R.N.Noyce and W.Shockly. *Proc. IRE.* 45 (1957) 1228.
91. J.L.Moll. *Proc. IRE.* 46 (1958) 1076.
92. R.L.Anderson. *Solid State Electron.* 5 (1962) 341.
93. Bulent M.Basol, Vijay K.Kapur, Aravind Halani and Craig Lerdholm. *Solar Energy Mater. Solar Cells.* 29 (1993) 163.
94. Lars Stolt, Jonas Hedstrom, John Kessler, Martin Ruckh, Karl-Otto Velthaus and Hans-Werner Schock. *Appl. Phys. Lett.* 62 (1993) 597.
95. Robert Hill and Hohn D. Mekin. in "*Current Topic in Photovoltaics*". (Eds. T.J.Coutts and J.D.Merkin). Academic Press, London. (1985) p 223.
96. M.S.Savelli and J.Bougnot. in "*Topics in Applied Physics (Solar Energy Conversion)*". Vol. 31, Springer-Verlag, Berlin Heidelberg. (1979) p 213.
97. J.M.Poate, K.N.Tu and J.W.Mayer (Eds.) "*Thin films-Interdiffusion and reactions*" John Wiely and sons, New York. (1978).
98. D.K.Pandya and K.L.Chopra. "*Vacuum-Science-Thin Film*" (Eds.K.L.Chopra and K.Goel) Vanity Books, New Delhi. (1981) p 246.
99. L.L.Kazmerski and Sigurd Wagner. in "*Current Topic in Photovoltaics*". (Eds. T.J.Coutts and J.D.Merkin). Academic Press, London. (1985) p 41.
100. Hobart H.Williard, Lynne.L Merritt, Johm A Dean and Frank A.Settle Jr. "*Instrumental methods of analysis*". CBS publishers and distributors, Delhi. (1986).
101. O.Hunderi. *Surf. Sci.* 96 (1980) 1.
102. O.Hunderi. *Thin Solid Films.* 57 (1979) 15.
103. B.J.Stagg and T.T.Charalampopoulos. *Appl. Optics.* 30 (1991) 4113.
104. D.E.Aspnes. *Thin Solid Films.* 89 (1982) 249.

105. Heavens O.S. "*Optical properties of thin solid films*". Butterworth, London (1955).

106. H.E.Bennett and Jean M.Bennett. "*Physics of thin films*" [Ed. Georg Hass and Rudolf E.Thun] . Vol.**4** Academic press, New York. (1964).

107. Zdenek Knittl."*Optics of thin films*". John Wiely and sons, London. (1976)

108. Xuantong Ying, Albert Feldman and E.N.Farabaugh. *J. Appl. Phys.* **67** (1990) 2056.

109. J.D.Klein, A.Yen and S.F.Cogan. *J. Appl. Phys.* 68 (1990) 1825.

110. Kent F.Palmer and Michael Z.Williams. *Appl. Optics.* **24** (1985) 1788.

111. J.C.Manifacier, J.Gasiot and J.P.Fillard. *J. Phys. E Sci. Instrum.* **9** (1976) 1002.

112. B.Sammanta, S.L.Sharma and A.K.Chaudhuri. *Ind. J. Pure Appl. Phys.* **32** (1994) 62.

113. C.L.Nagendra and G.K.M.Thutupalli. *Appl. Optics.* **20** (1981) 2747.

114. C.L.Nagendra and G.K.M.Thutupalli. *J. Phys. D. Appl. Phys.* **15** (1982) 1153.

115. S.G.Tomlin. *Thin Solid Films.* **13** (1972) 265.

116. S.G.Tomlin. *J. Phy. D Appl. Phys.* **1** (1968) 1667.

117. R.E.Denton, R.D.Campbell and S.G.Tomlin *J. Phy. D Appl. Phys.* **5** (1972) 852.

118. R.E.Denton and S.G.Tomlin. *Aust.J.Phys.* **25** (1972) 743.

Chapter 2

ELLIPSOMETRY: THEORY AND INSTRUMENTATION.

2.I Introduction.

Ellipsometry is a highly sensitive and non-destructive technique that deals with the measurement and interpretation of changes in the polarisation state of light upon reflection from a surface [1]. The theory that connects the changes in polarisation state and material properties, layer thickness etc., was first formulated by Drude in 1887 [2]. In 1933 Tronstad demonstrated the application of this technique as a serious diagnostic tool, which is non destructive and surface sensitive that could be used on samples in any transparent ambient [3]. Earlier instruments were null type which had serious technical limitations [4]. Based on the photometric ellipsometer demonstrated by Budde [5], Cahan and Spanier [6] developed Rotating Analyser Ellipsometer (RAE). The extensive development of instrumentation and method of data analysis in 1970's resulted in the application of ellipsometry to a wide variety of material and structural problem analysis. Earlier this technique was not widely used as a diagnostic tool due to the tedious computational work involved. Recently microcomputers could be used not only for the intensive computational task of analysing ellipsometric data, but also to collect, average and store these data in digital form for later analysis [7,8]. Very recently high speed ellipsometers are used for the insitu analysis of changes over sample surfaces and interfaces [9,10].

Ellipsometry can be defined as the optical characterization technique in which the changes in polarisation state of light that occurs upon non-normal-reflection from a specular surface of the sample is

measured and interpreted to determine the physical properties of the sample [1,11]. The changes in polarisation is described by two ellipsometric parameters ψ and Δ, (these are defined by Eqs. 1.59(a) and 1.59(b) in chapter 1) which correspond to relative amplitude attenuation and phase difference of the electric field vectors perpendicular and parallel to the plane of incidence. These ellipsometric parameters depend on surface and interface phenomena and other physical properties of the material under investigation. Using these parameters, angle of incidence ϕ and wavelength λ it is possible to calculate the various physical properties of the film like real refractive index (n), extinction coefficient (k), thickness (t), inter layer thickness (t_i), volume fraction (x) of added material in a layer, surface roughness, crystallinety etc. The advantage of ellipsometry over other optical techniques is that these two parameters (amplitude and phase) are available from a single measurement. More over ψ and Δ are independent of absolute intensity of light but depend only on the relative intensity.

Changes in surface layer thickness of the order of 0.01 nm can be measured using this technique. But accurate determination of (t) requires correspondingly accurate determination of (n) or vice versa [11]. A major advantage is that the spectral dependence allows microscopic surface roughness, surface contamination and crystalline damage to be distinguished from each other. Even though electron spectroscopy has better sensitivity, this can not be used for the analysis of surface in reactive ambient or buried interfaces. While Raman and IR spectroscopies have been applied to surface analysis, these techniques require layer thickness to be of the order of 5 nm thick to get adequate signals [11].

Another important application of ellipsometry is its capability to be used as a setup for *insitu* studies of

different reactions and thin film growth mechanism. It has application where other techniques fails, for eg., the study of reaction taking place in a solid-liquid interface, which can not be studied using an electron microscope, since the surface to be analysed should be kept in high vacuum. The area under investigation can be very small in the case of ellipsometry. More than that it is a non-destructive technique and requires no sample conditioning.

2.11 Brief report of works done using ellipsometry.

Film thickness measurement was the traditional application of ellipsometry. The fast development in the field of ellipsometry gave this technique wide application in the determination of composition, morphologies, grain sizes, surface roughness, interface thickness etc. If the film is sufficiently transparent to permit back reflection from the substrate (film/substrate interface), then the Spectroscopic Ellipsometry (SE) can be used to determine its thickness to an accuracy comparable to that achieved with cross-section transmission electron microscope (XTEM) and Rutherford Back Scattering (RBS) [12-14]. Ellipsometry is widely used for non-destructive characterization of the single and multilayer semiconducting material structure [14-20]. Vedam et al showed that under certain circumstances SE can provide more detailed microscopic information than that is provided by XTEM [12]. It is used for the accurate determination of dielectric function of intrinsic materials at room temperature [21-24], as a function of temperature [25-28] and doping concentration [29-31]. Composition of semiconductor alloys can be determined to an accuracy of 1 or 2 % [23,32], some what less than photoluminesence or modulation spectroscopy capabilities but acceptable for nearly all applications.

It is sensitive to the changes on surface atomic structure on a scale less than a monolayer. Thus it is

extremely surface sensitive and, this property is used for the study of the effect of atomic oxidation of materials [33,34]. Bertran et al performed real time ellipsometric analysis over the surface of Zn_3P_2 thin film in air at room temperature after etching to study the formation of oxide layer [35]. Ellipsometry is extensively used in plasma processing, since it is capable of reaching the reaction layer, analysing the microscopic surface roughness, subsurface damage etc. Various research groups have studied the effect of oxygen and hydrogen plasma on various semiconducting materials [11, 36-40]. Ellipsometry is highly useful for the determination of microscopic surface roughness of thin film and other samples using effective medium theory. Using this method the rms value of microscopic surface roughness is calculated. In this case roughness is taken as microscopic with an average size much smaller than the wavelength of light used and does not scatter light [41, 42]. Ellipsometry is also used for the determination of macroscopic surface roughness, where irregularities are large compared with wavelength and scatter light [43-48].

Interface thickness is the most important parameter which is analysed using SE in the case of semiconducting materials [49]. Erman and Frijlink investigated the AlGaAs/GaAs heterojunction [50]. Vijayakumar used ellipsometry to investigate Cu_2S/CdS heterojunction [18]. Ion implantation can affect the surface properties of thin films. Snyder et al have studied the smoothness of ion implanted copper [51] and molybdenum [52] laser mirrors. Optical coating are another ideal application of ellipsometry since these films are often deposited on flat smooth surfaces. Woollam et al have investigated different optical coatings, for example Diamond Like Carbon (DLC), ZnO/Ag/ZnO/glass, TiO_2/Ag/TiO_2/glass etc., [53-55]. Vijayakumar et al have studied the effect of temperature on the structural and surface properties of

metallic thin films [56-58]

Pioneering insitu ellipsometric studies were performed by Theeten, Hottier and co-workers on plasma deposition of Si and MOCVD of GaAs and related materials [59,60]. Application of SE for the study of crystal growth by MBE has also been reported [60]. Kawagoe et al has conducted insitu studies of the growth process of copper film at various condition using ellipsometry [62] and the oxidation on the surface of Zn_3P_2 film was monitored [35]. In compound semiconductors the optical penetration depth is limited to few tens of nm, meaning that only outer most layers and interface can be analysed. Such structures have yielded important information of surface and top layers. Under these condition the advantage of varying the angle of incidence and wavelength to enhance the sensitivity in the measurement of layer thickness, composition etc., have been recently stressed by Woollam and co-workers [14,15,63,64] and for the other types of ellipsometer [64,65]. Woollam et al have also introduced the 'sensitivity plots' to determine the experimental conditions in which the sensitivity is maximized [63].

2.2 Theory of Ellipsometry.

In this section we will consider the changes taking place in the state of polarisation of a beam of plane polarised light due to the interaction with optical components which constitute a polarising optical system. The following assumptions are made for this analysis [1]

1) Light beam is monochromatic and plane polarised.

2) The interaction between the light beam and optical system must be linear and frequency conserving.

3) The optical system must not be photo sensitive.

Here we will consider the theoretical aspects of the measurements of ellipsometric parameters ψ and Δ and hence the computation of the ρ. We will also consider the collection of

information regarding the properties of the surface under investigation, from these parameters. For this the most general ellipsometric setup consisting of polariser, compensator, optical system and analyser (PCSA) is taken into account and is shown in Fig.2.1. The monochromatic and well collimated light from the source is made plane polarised by a liner polariser (P), after which it passes through the compensator (C). The emergent beam from C is reflected by the optical system S, which is under investigation. This beam is analysed using a linear analyser (A) and is detected by Photomultiplier tube (PMT) (D).

The orientation of polariser, compensator and analyser around the beam axis are specified by azimuth angles P, C and A respectively in Fig.2.1. For the polariser and analyser the azimuth P and A define the orientation of their transmission axis (ie., the direction of transmitted linear eigen polarizations) while for the compensator the azimuth C defines orientation of its fast axis (ie., the direction of the fast linear eigen polarisation). All these azimuths P,C and A are measured from the plane of incidence which forms one of the two linear eigen polarisations of the optical system S. The angles are taken to be positive in anti clockwise direction when looking into the beam. In the description that follows the light beam is described by its Jones vector and the optical elements by the respective Jones matrices [1]. This is accepted because by this method one can easily follow the state of polarisation of light beam as it progresses through the components of the ellipsometer.

The notations used in the following treatment can be explained in a simple way as follows. The superscripts denote the coordinate system with respect to which the Jones vector or matrix is referenced. In the subscript the first letter denotes the components while the second shows whether the beam is its input or output. For example E_{co}^{fs} is the Jones vector

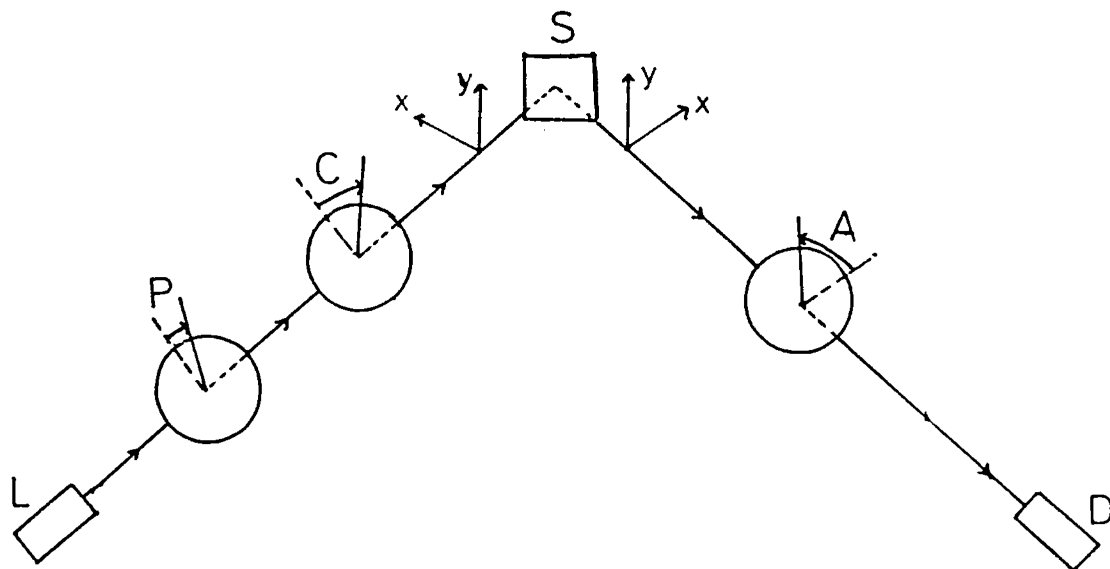

Fig.2.1 The PCSA ellipsometric arrangement that consists of a linear polariser P, compensator C, sample S, linear analyser A and the light detector D.

(electric field) of the light beam at the output of compensator, in its fast-slow principle frame of reference. (The frame of reference of an optical component is the coordinate system in which Jones matrix of the optical component is diagonal). Another important matter to be considered is the switching between two coordinate systems, which is necessary when light beam travels from one system to another. This can be implemented by using rotation matrix $R(\alpha)$ and counter rotation matrix $R(-\alpha)$ and is given as

$$R(\alpha) = \begin{bmatrix} \cos(\alpha) & \sin(\alpha) \\ -\sin(\alpha) & \cos(\alpha) \end{bmatrix} \tag{2.1}$$

A. Polariser.

Let us first consider the effect of polariser. The output of this system will be plane polarised light which can be represented as

$$E^{te}_{po} = A_c \begin{bmatrix} 1 \\ 0 \end{bmatrix} \tag{2.2}$$

Here A_c contains the information regarding the intensity and absolute phase of the wave emergent from the polariser. The superscript 'te' denotes the 'transmission-extinction' principal frame of reference.

B. Compensator.

Before examining the effect of the compensator one has to change the reference coordinate system, from transmission-extinction principal frame of polariser to the fast-slow principal frame of the compensator. This is achieved by the rotation matrix $R(P-C)$

$$E^{fs}_{ci} = R(P-C)\, E^{te}_{po} \tag{2.3}$$

$$= A_c \begin{bmatrix} \cos(P-C) & \sin(P-C) \\ -\sin(P-C) & \cos(P-C) \end{bmatrix} \begin{bmatrix} 1 \\ 0 \end{bmatrix}$$

$$E_{ci}^{fs} = A_c \begin{bmatrix} \cos(P-C) \\ \sin(P-C) \end{bmatrix} \quad (2.4)$$

The compensator is having a slow-to-fast complex amplitude transmittance given by

$$\rho_c = T_c\, e^{i\delta_c} \quad (2.5)$$

This shows that the component of the electric vector incident on the compensator parallel to its slow axis is retarded in phase by δ_c and is attenuated in amplitude by T_c relative to the orthogonal component parallel to its fast axis. The Jones matrix of the compensator is given by

$$T_c^{fs} = K_c \begin{bmatrix} 1 & 0 \\ 0 & \rho_c \end{bmatrix} \quad (2.6)$$

Where K_c accounts for the equal attenuation and phase shift along fast and slow axes. The Jones vector of the out put of the compensator is

$$E_{co}^{fs} = T_c^{fs}\, E_{ci}^{fs} \quad (2.7)$$

$$E_{co}^{fs} = K_c A_c \begin{bmatrix} \cos(P-C) \\ \rho_c \sin(P-C) \end{bmatrix} \quad (2.8)$$

C. Optical system.

Since the system under investigation is a reflecting surface its principal frame of reference is the X-Y coordinate system; but the X-axis coincides with the plane of incidence. In order to bring the Jones matrix to X-Y principal frame of the optical system S, one has to perform a coordinate counter

rotation by an angle C and the output is given as

$$E^{xy}_{co} = R(-C)E^{fs}_{co} \qquad (2.9)$$

$$R(-C) = \begin{bmatrix} \cos(-C) & \sin(-C) \\ -\sin(-C) & \cos(-C) \end{bmatrix}$$

$$= \begin{bmatrix} \cos(C) & -\sin(C) \\ \sin(C) & \cos(C) \end{bmatrix} \qquad (2.10)$$

$$E^{xy}_{co} = K_c A_c \begin{bmatrix} \cos(C)\cos(P-C) - \rho_c \sin(C)\sin(P-C) \\ \sin(C)\cos(P-C) + \rho_c \cos(C)\cos(P-C) \end{bmatrix} \qquad (2.11)$$

Now one can note the modification of the polarisation caused by the reflection at the optical system (S). The out put of the compensator is taken as the input of the system S.

$$E^{xy}_{so} = T^{xy}_{s}\ E^{xy}_{si} \qquad (2.12)$$

In the above equation the Jones matrix of the system T^{xy}_{s}, is diagonal since it is assumed to have orthogonal liner eigen polarisations, parallel to X-Y coordinate axes and the matrix can be written as

$$T^{xy}_{s} = \begin{bmatrix} V_{ex} & 0 \\ 0 & V_{ey} \end{bmatrix} \qquad (2.13)$$

where V_{ex} and V_{ey} represent the eigen values of X and Y liner eigen polarisations ie., these two parameters represent the changes taking place in the amplitude and phase of electric vector component. Substituting the values of E^{xy}_{si} and T^{xy}_{s} in Eq.2.12 we get,

$$E^{xy}_{so} = K_c A_c \begin{bmatrix} V_{ex}[\cos(C)\cos(P-C) - \rho_c \sin(C)\sin(P-C)] \\ V_{ey}[\sin(C)\cos(P-C) + \rho_c \cos(C)\sin(P-C)] \end{bmatrix} \qquad (2.14)$$

D. Analyser.

To study the effect of the analyser on the

polarisation of the beam, one has to make a coordinate rotation from the optical system's X-Y principal frame to the analyser's t-e principal frame as

$$E_{ai}^{te} = R(A)\ E_{so}^{xy} \tag{2.15}$$

Taking $E_{ai}^{xy} = E_{so}^{xy}$ and substituting for R(A) in the above equation, one can have,

$$\begin{bmatrix} E_{ai,t} \\ E_{ai,e} \end{bmatrix} = \begin{bmatrix} [\cos(A)E_{ai,x} + \sin(A)E_{ai,y}] \\ [-\sin(A)E_{ai,x} + \cos(A)E_{ai,y}] \end{bmatrix} \tag{2.16}$$

The third term in the subscript denotes the corresponding coordinate axis. The Jones matrix of the analyser is given by

$$T_a^{te} = K_a \begin{bmatrix} 1 & 0 \\ 0 & 0 \end{bmatrix} \tag{2.17}$$

where K_a represent the amplitude and phase changes experienced by the transmitted linear eigen polarisations.

Then the electric vector at the output of the analyser is obtained as

$$E_{ao}^{te} = T_a^{te} E_{ai}^{te} \tag{2.18}$$

ie.,

$$E_{ao}^{te} = K_a \begin{bmatrix} E_{ai,t} \\ 0 \end{bmatrix} \tag{2.19}$$

E. Detector.

Now the intensity of the detected light signal I_p is given by

$$\begin{aligned} I_p &= K_d\left(E_{ao}^{+}\ E_{ao}\right) \\ &= K_d\left(K_a K_a^{*}\right)\left(E_{ai,t} E_{ai,t}^{*}\right) = K_d |K_a|^2 |E_{ai,t}|^2 \end{aligned} \tag{2.20}$$

where K_d is the real factor which depends on the intensity profile of the light beam and nature of the photo

detector. From Eq. 2.16 it can be easily written as

$$E_{ai,t} = \cos(A)E_{ai,x} + \sin(A)E_{ai,y} \qquad (2.21)$$

substituting the value of $E_{ai,x}$ and $E_{ai,y}$

$$E_{ai,t} = K_c A_c \Big\{ V_{ex}\cos(A) \; [\cos(C)\cos(P-C) - \rho_c \sin(C)\sin(P-C)]$$

$$+ V_{ey}\sin(A) \; [\sin(C)\cos(P-C) + \rho_c \cos(C)\sin(P-C)] \Big\} \qquad (2.22)$$

$$I_d = GLL^* = G|L|^2 \qquad (2.23)$$

where $$G = |A_c|^2 \; |K_c|^2 \; |K_a|^2 \; K_d \qquad (2.24)$$

and $$L = \Big\{ V_{ex}\cos(A) \; [\cos(C)\cos(P-C) - \rho_c \sin(C)\sin(P-C)]$$

$$+ V_{ey}\sin(A) \; [\sin(C)\cos(P-C) + \rho_c \cos(C)\sin(P-C)] \Big\} \qquad (2.25)$$

The above results has been obtained by analysing the state of polarisation at different points along path of the beam.

The Eq. 2.22 shows that

$$I_d = f(P, C, A, \rho_c, V_{ex,} V_{ey}) \qquad (2.26)$$

which means that the detected light intensity is a function of

1. Azimuth angle of polariser, analyser and compensator.

2. Slow to fast relative complex amplitude transmittance of the compensator.

3. Complex eigen value V_{ex} and V_{ey} of the optical system to be analysed.

2.21 Different types of ellipsometer.

The principle of ellipsometer is based on the fact that the reflected light contain the information about the V_{ex} and V_{ey} and can be extracted by proper use of Eq. 2.22. The ellipsometer parameter ρ is defined as

$$\rho = \frac{V_{ex}}{V_{ey}} \qquad (2.27)$$

The information regarding V_{ex} and V_{ey} can be obtained from different type of experimental setup. Now we can classify ellipsometer into two main groups

1. Null Ellipsometer.
2. Photometric Ellipsometer.

2.211 Null Ellipsometer.

The principle of this setup is that by adjusting the azimuth angles of polariser, compensator and analyser (P,C,A) the light flux falling on the photodetector can be extinguished. This condition can be represented as

$$I_d = 0 \qquad (2.28)$$

for which the necessary condition is

$$L = o \qquad (2.29)$$

Using this condition in Eq.2.22 one gets

$$0 = \Big\{ V_{ex}\cos(A) \ \big[\cos(C)\cos(P-C) - \rho_c \sin(C)\sin(P-C)\ \big]$$

$$+ V_{ey}\sin(A) \ \big[\sin(C)\cos(P-C) + \rho_c \cos(C)\sin(P-C)\big]\Big\}$$

substituting Eq.2.27 in the above equation one can get,

$$\rho = \frac{-\tan(A)\ [\tan(C) + \rho_c \tan(P-C)\ ]}{1-\rho_c \tan(C)\ \tan(P-C)} \qquad (2.30)$$

using the ellipsometric relation given in Eq. 1.58 of section 1.52 we can write

$$\rho = \tan\psi e^{i\Delta}$$

From this equation one can calculate the ellipsometric parameters ψ and Δ of the optical system under investigation from the measured azimuth angles P, C and A and the slow to fast relative complex amplitude transmittance ρ_c of the compensator. Using this ψ and Δ one can calculate the

physical properties of the system and details of this calculation is discussed in chapter 3.

2.212 Photometric Ellipsometer.

In this type of ellipsometer the detected light intensity is never zero. Here the output light flux I_d is measured as a function of azimuth angles P, C, and A and phase retardation of compensator ρ_c and angle of incidence ϕ.

$$I_d = G|V_{ey}|^2 |\tan\psi e^{i\Delta}\cos(A) [\cos(C)\cos(P-C) - \rho_c\sin(C)\sin(P-C)]$$
$$+\sin(A)[\sin(C)\cos(P-C) + \rho_c\cos(C)\sin(P-C)]|^2 \quad (2.31)$$

Corresponding to different intensity or azimuth angles one can write different equation as above and three such equations can be solved to give the ellipsometric parameters ψ and Δ. Hence the physical properties of the system can be calculated.

There are two types of photometric ellipsometers,

1. Dynamic ellipsometer
2. Static Ellipsometer.

In dynamic ellipsometer some of the parameters (P, C, A and ρ_c) are periodically varied as a function of time and detected light intensity is analysed using fourier analysis. In static ellipsometer intensity is measured at different predetermined values of P, C, A, and ρ_c.

A. Static photometric ellipsometer.

In present study we have fabricated this type of ellipsometer. A static photometric ellipsometer does not require a compensator and this type is known as Polariser-System-Analyser (PSA) type ellipsometer. The detected light intensity is a function of P and A. The required relation can be obtained from the Eq.2.31 by setting C=0 and ρ_c=1.
ie.,

$$I_d = G|V_{ey}|^2 \; |\tan\psi \, e^{i\Delta} \cos(A)\cos(P) + \sin(A)\sin(P)|^2 \quad (2.32)$$

On further simplification the above equation simplifies to,

$$I_d = F^{\bullet} \Big[1-\cos(2\psi) \big(\cos(2A) + \cos(2P)\big) + \cos(2A)\cos(2P) + \sin(2\psi)\cos(\Delta)\sin(2A)\sin(2P)\Big] \quad (2.33)$$

where $F^{\bullet}$ is constant.

Let I_{d1}, I_{d2} and I_{d3} represent the detected light intensities at three different sets (P_1A_1), (P_2A_2) and (P_3A_3) of the polariser and analyser. These three intensities give three different equations of the type of (Eq.2.33) with three unknown quantities ($F^{\bullet}$, ψ and Δ). By solving these equations the required unknown quantities ψ and Δ can be obtained. Hence for determining the parameters ψ and Δ at least three sets of data are required. Even though additional measurements are redundant, for practical reasons a large number of measurements are required for the accurate determination of ψ and Δ.

The choice of setting azimuths P_1 and A_1 of the polariser and analyser is left arbitrary. Consider the following three sets of azimuths, to make the computations easier. One can select $\frac{\pi}{2}$ as the azimuth of polariser and $\frac{+\pi}{4}$, 0 and $\frac{-\pi}{4}$ to be the three setting of the analyser giving the three different intensities I_{d1}, I_{d2} and I_{d3}. From Eq.2.33 one gets

$$I_{d1} = I_{d(\pi/4,-\pi/4)} = F^{\bullet}(1-\sin2\psi \cos\Delta) \quad (2.34(a))$$

$$I_{d2} = I_{d(\pi/4,0)} = F^{\bullet}(1-\cos2\psi) \quad (2.34(b))$$

$$I_{d3} = I_{d(\pi/4,+\pi/4)} = F^{\bullet}(1+\sin2\psi \cos\Delta) \quad (2.34(c))$$

From the above equation ψ and Δ are obtained as

$$\psi = \frac{1}{2}\cos^{-1}\left[\frac{I_{d1} - 2I_{d2} + I_{d3}}{I_{d1} + I_{d3}}\right] \qquad (2.35)$$

$$\Delta = \cos^{-1}\left[\frac{\frac{1}{2}\sin(2\psi)(I_{d3} - I_{d1})}{I_{d1} + I_{d3}}\right] \qquad (2.36)$$

Knowing the value of ψ and Δ, the value of ρ and hence values of various physical properties of the optical system can be calculated.

B. Dynamic photometric ellipsometer.

Only a very brief report of this type of ellipsometer is included here. In this type one or more optical parameters are modulated and detected signal is fourier analysed. Depending upon the parameter or combination of parameters selected for modulation there are large number of possibilities and here the few important systems are considered.

The first one is Rotating Analyser Ellipsometer (RAE). This has either PCSA or PSA arrangement. Keeping the polariser and compensator at a fixed azimuth (P, C) the analyser alone is rotated at constant angular velocity ω and the intensity of detected signal is fourier analysed. The detailed description of the working, theory and computational techniques are given in several publications [1, 6, 67-70].

The next one is the Polarisation Modulated Ellipsometer (PME). In this the state of polarisation of light beam in its path is modulated at a suitable point in the prescribed fashion so that information of the optical system under investigation is retrievable from the harmonic analysis of the detected intensity. Here also several possibilities are available depending upon the position and method of modulation. A convenient arrangement is proposed by Jasperson

[71,72] in which the sequence of optical components are polariser (P), modulator (M), optical system under investigation (S) and analyser (A). The PMSA arrangement is considered to be the same as conventional PCSA arrangement, in which compensator's relative retardation (ρ_c) is periodically modulated as a function of time. The main advantage of PMSA is that all optical components remain stationary and it allows the measurements at vary high speed.

2.3 Experimental setup of the ellipsometer fabricated.

In this section we discuss the basic instrumentation and optical techniques of ellipsometer with due importance to the system fabricated for the present work. The basic theory of ellipsometry has already been covered in the previous section. In the present study we fabricated a static photometric type ellipsometer with facility to change both wavelength (λ) and angle of incidence (ϕ). This instrument is known as Variable Angle Spectroscopic Ellipsometer (VASE). The computation techniques using this technique is described in the next chapter. The ellipsometer is basically an optical instrument that consist of two arms, whose axes lie in one plane. One arm is usually stationary known as polarising arm and the other arm known as analyser arm which can rotate around a central axis that passes through the point of intersection of the two arms' axes. The angle between the two arms is measured on a graduated circular scale concentric with the central axis and having diametrically opposite verniers. The sample holder is mounted on a shaft that passes through the central axis of the instrument The sample holder is arranged over a sample table with leveling arrangements. Using these leveling screws the sample is arranged in such a way that the surface of the sample is perpendicular to the beam axis, so that the light reflected from the sample surface is in the same plane defined by the incident beam and arm axes.

The sample holder is attached to an electric heater capable of heating the thin film sample in a controlled manner up to 350°C. A chromel-alumel thermocouple is used for measuring the temperature of the sample. The Fig.2.2(a) shows the photograph of the experimental setup for ellipsometric measurement. Fig.2.2(b) shows the schematic diagram of the various elements arranged in the VASE fabricated. The various components in the setup are light source, lens system, optical beam chopper, monochromator, polariser, sample holder with heating and temperature measuring arrangement, analyser, light detector, tuned amplifier for signal processing and digital multimeter for read out. The following section contain the detailed description of important parts and alignment of ellipsometer.

A. Light source and monochromator.

The inset of Fig.2.2(b) shows the schematic diagram of the light source used in this setup. This contains a concave reflector at its back side and a plano concave condenser lens at the front side to increase the optical collection and for getting collimated beam output. In order to get continuous white spectrum, with more high frequency component a tungsten halogen source with 250 W power is used. Highly stabilized constant current source (15 A) is used as the power supply for the source. The collimated unpolarised light from the source S is used in ellipsometer. In earlier section it was described that for ellipsometric measurement the light should be monochromatic as far as possible. For this purpose a 0.20 Meter McPherson monochromator with a grating of 1200 g/mm is used. The entrance and exit slit widths are arranged to get narrow band light output. The dynamic range of this grating is 200-800 nm. In the present setup practical range of wavelength is limited by the spectrum of the light source and sensitivity of PMT used and it is ~400-750 nm.

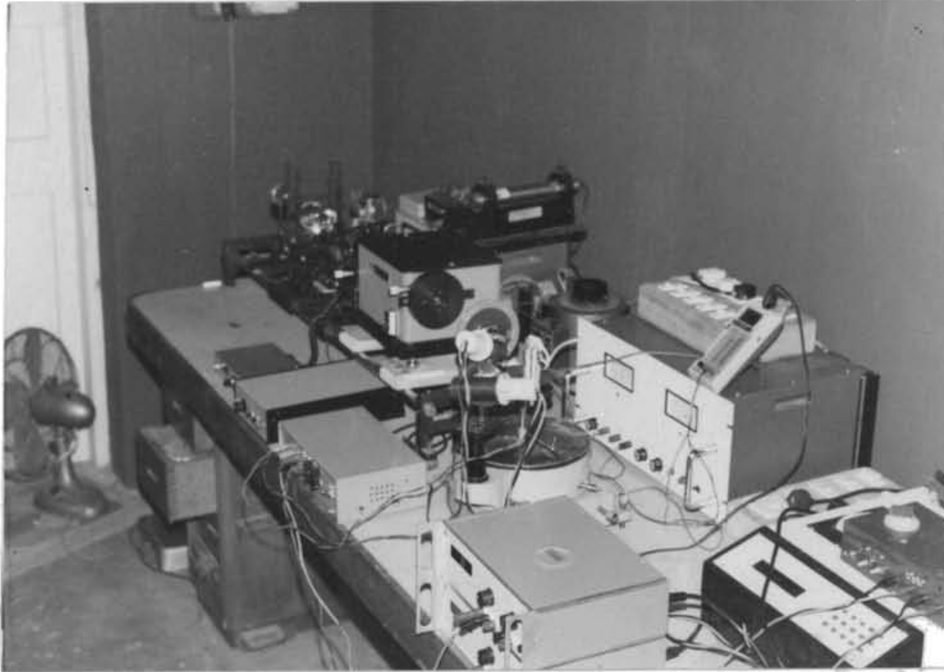

Fig.2.2. (a) Photograph of the VASE experimental setup fabricated.

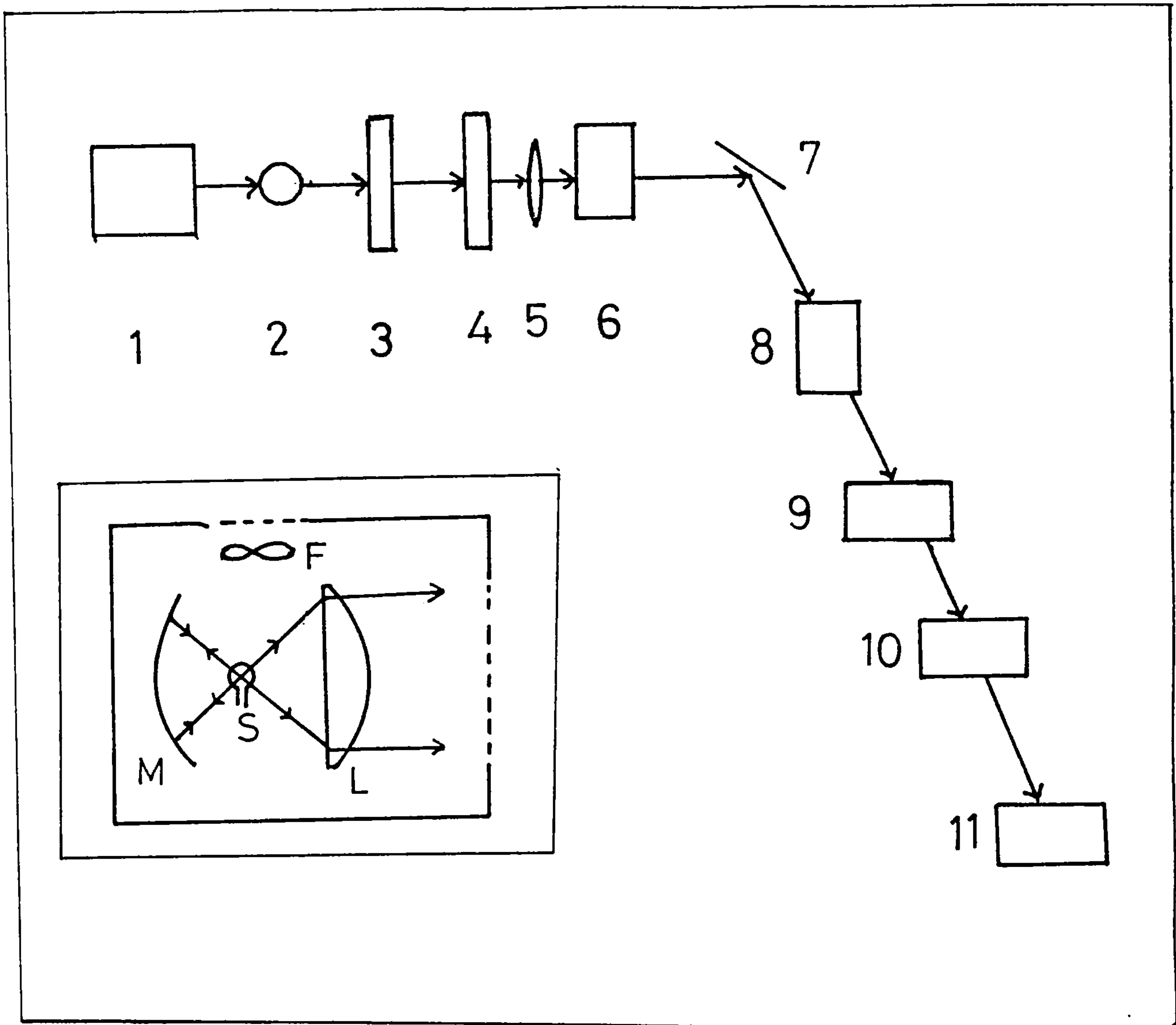

Fig.2.2. (b) Schematic diagram of VASE experimental setup fabricated. 1.light source, 2.lens system, 3.chopper, 4.monochromator, 5.long focal length lens, 6.liner polariser, 7.sample holder with heating and temperature measurement arrangement, 8.linear analyser, 9.light detector (PMT), 10.tuned amplifier and 11.digital multimeter. Inset of the figure shows the light source used in VASE. M.concave mirror, S.tungsten halogen lamp, L.condenser lens and F.cooling fan.

B. Polarising elements (Polariser and Analyser).

These are the most important optical elements in an ellipsometer. An ideal linear polariser is a device that transforms any state of polarisation of light at its input to a linear state of polarisation at its output. A real linear polariser has orthogonal linear eigen polarisations, say X and Y, with associated eigen values V_{ex} and V_{ey}, one of which is zero. If the Y eigen polarisation is almost extinguished ie., $|V_{ey}| << 1$. The extinction ratio of the polariser is defined as

$$\chi_r = \frac{|V_{ey}|^2}{|V_{ex}|^2} \qquad (2.37)$$

In the present setup a Glan-Thomson prism is used as linear polariser with extinction ratio $X_r \simeq 10^{-5}$. Two polarisers are coaxialy mounted on the two arms of the ellipsometer in such a way that the light beam passes through the centers of the polarising elements. The first one is known as polariser which converts the incident natural light into a linearly polarised one. The polarised light falls on the sample resulting in a change in polarisation state of the light due to reflection from the sample surface. The second element is known as analyser which is used to measure the change in polarisation of reflected light from the sample surface. These two optical elements are capable of rotation around an axis passing through their centers and the angle of rotation can be measured using a circular scale.

C. Light detector and signal processing.

In static photometric ellipsometer the ellipsometric parameters ψ and Δ are calculated from the intensity of light measured at different settings of the polariser and analyser. Photomultiplier tube (PMT) (R446, Hamamatsu, Japan) is used for the measurement of light intensity. PMT gives an output current which is independent of load. The output of the PMT is

fed into a current-to-voltage converter, that gives an output voltage which is proportional to the input current. This in turn is proportional to the intensity of light flux falling on the PMT. In order to avoid the ambient noise an electronic circuit consisting of tuned amplifier and an optical beam chopper (Stanford Instruments Ltd, USA) are used. The incident light beam is chopped at a frequency 169 Hz using an optical beam chopper and PMT detects this chopped light beam. To eliminate noise, only the AC component of the detected signal with frequency 169 Hz is amplified and all other components are filtered out using a band pass filter. The output of current-to-voltage converter is then amplified and fed into a band pass filter. The resonance frequency of the filter is arranged in such a way that it allows only the chopping frequency of light. [illegible] The AC output of the tuned amplifier is measured using a digital 4 1/2 (Aplab) multimeter.

2.30 **Alignment.**

The source is arranged to give collimated beam output. Using lenses it is further collimated to give parallel beam. All optical components and the light source are arranged along the axis that passes through the centre of the analyser and polariser arm. In order to have fine adjustments, all optical components are arranged on optical stands with two degrees (Z and Y axis) of movement. These optical stands are then fixed on an optical bench in such a way that the X-axis movement is also possible. Using fine pin holes, the diameter of the beam illuminating the sample surface is adjusted to be less than 2 mm in diameter.

The azimuth angles of the polariser and analyser are calibrated using the principle called 'polarisation of light by reflection' from a dielectric surface at a particular angle of incidence called Brewester angle (ϕ_b). At Brewester angle

the reflected light contains only s-component of polarisation ie., the component perpendicular to plane of incidence. If n_g is refractive index of glass, then the Brewster angle (ϕ_b) is defined as

$$\tan\phi_b = n_g \quad (2.38)$$

At first for the calibration of polariser, the analyzer is removed from the analyser arm. The angle of incidence of the beam on the glass plate mounted on the sample holder is arranged to ϕ_b (in the case of ordinary glass this angle is $56^\circ30'$) and the reflected intensity is noted using the PMT. Then the polariser is rotated in such a way that the reflected light intensity at ϕ_b is zero or minimum. At this point the azimuth angle of the polariser is taken as zero and in this position the polariser output contain only p component of light. Then using the known polarisation state of polariser the azimuth angle of the analyser is arranged to zero. In this setup the polariser is arranged to fixed azimuth $+45^\circ$. This is made possible by rotating the polariser through 45° in anticlockwise direction. The intensity of thin film sample is measured for different (at lest three) azimuth angle of the analyser. In the present case the intensity is measured for different azimuth angle of the analyser in the range $0-24^\circ$ with a step of 3°. This large number of measurements can avoid any possible error in the measurement of ellipsometric parameters ψ and Δ.

It is practically a tedious work to arrange a large number of elements without any deviation from optical axis unless the mechanical parts have very high precision. A small error in this can cause large deviation in optical path. In this setup it was observed that the rotation of polariser causes a small deviation in optical beam, which may affect the angle of incidence measurement. A long focal length lens was placed before the polariser in order to correct the path deviation due to the rotation of the polariser. Hence by the

slight adjustment of the lens the beam can be brought back to the original position and avoid the possible error in angle of incidence measurement as well as ellipsometric parameters ψ and Δ.

The dynamic range of angle of incidence of the ellipsometer fabricated is 20-85°. The angle can be measured with an accuracy of 30″. The azimuth angle of polariser and analyser can be measured with an accuracy of 1′. The accuracy of DMM is ±0.05% of full division. The monochromator gives a very narrow band optical output.

2.31 Standardization of the Ellipsometer- Measurements on glass slides.

As a standardisation process the surface of the ordinary type of glass slides were analysed using our ellipsometer. The Figs.2.3 to 2.6 shows the variation of ψ and Δ with angle of incidence in the case of the glass substrates (without any additional polishing). One side of the slide was grounded and blackned with carbon in order to avoid the back reflection from the glass/air interface. The glass slides were cleaned using soap solution and hot concentrated chromic acid. Then these slides were washed in double distilled water. Finally ultrasonic cleaning was given and the cleaned slides were dried inside a hot oven. The ellipsometric readings were taken at the wavelength 553 nm in this case. The glass slides were carefully mounted on the sample holder so that the surface was along the central axis of the ellipsometer and also perpendicular to the incident beam. The polariser azimuth was kept at constant value of 45°. The angle of incidence could be calculated from the readings on circular scale of ellipsometer. The intensities of reflected light corresponding to the different azimuth angles of the analyser were measured. The azimuth angle of the analyser was varied in the range 0-21° with a step of 3°. This gave eight measurements of light

intensity and using these eight values 56 ψ and Δ could be calculated by taking different possible combinations of (P,A). The average of these values were taken as the ψ and Δ corresponding to that particular angle of incidence and wavelength. The experiment was performed for angle of incidences in the range range 20-82.5° with a step value of 2.5° and with a still smaller step near the Brewester angle region 52.5-62.5°. Figs.2.3(a) and 2.4(a) show the experimental ψ and Δ of glass surface. The theoretically calculated ψ and Δ values of glass surface is shown in the same figure (Figs.2.3(b) and 2.4(b)). It is assumed that the deviation between the two graph may be due to the surface imperfections like surface roughness, or any contamination of these glass slides. The rough surface is considered as an imaginary surface layer having mixture of air and glass materials and this new layer is analysed (detailed analysis of these types of treatment is given in section 3 of chapter 3) using Bruggeman's effective medium approximation [73]. Very recently Jellison et al have reported such an analysis on different types of glass substrates [74]. In that analysis they have assumed that the surface layer contains 50% air and 50% material. But in the present study we have estimated the actual composition of the imaginary rough surface layer. Assuming that there is such an imaginary rough layer over the glass substrate, we calculated the ellipsometric parameters ψ and Δ for substrate at different angle of incidence. The calculated ψ and Δ of new optical model is shown in Figs.2.5(b) and 2.6(b) along with the experimental ψ and Δ plot. These figures shows that the new optical model agrees very well with experimental system except for a slight deviation at large angle of incidence region. This result suggest that the glass surface has a roughness (of average height ~35 nm) and the total volume fraction of air embedded in between these irregularities is about 0.30. (30%).

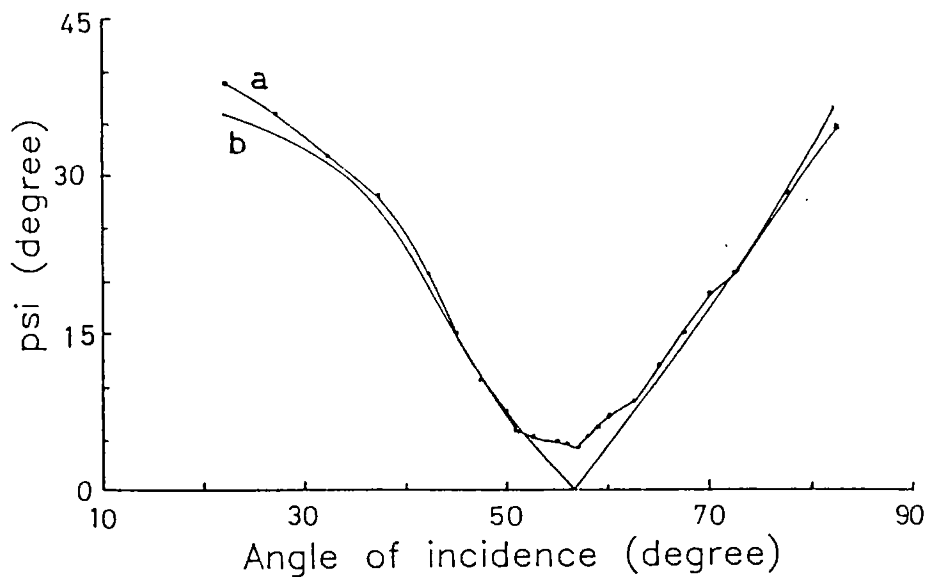

Fig.2.3 Ellipsometric parameter ψ as a function of the angle of incidence from a glass plate. (a) experimental ψ and (b) theoretical ψ from air/glass interface.

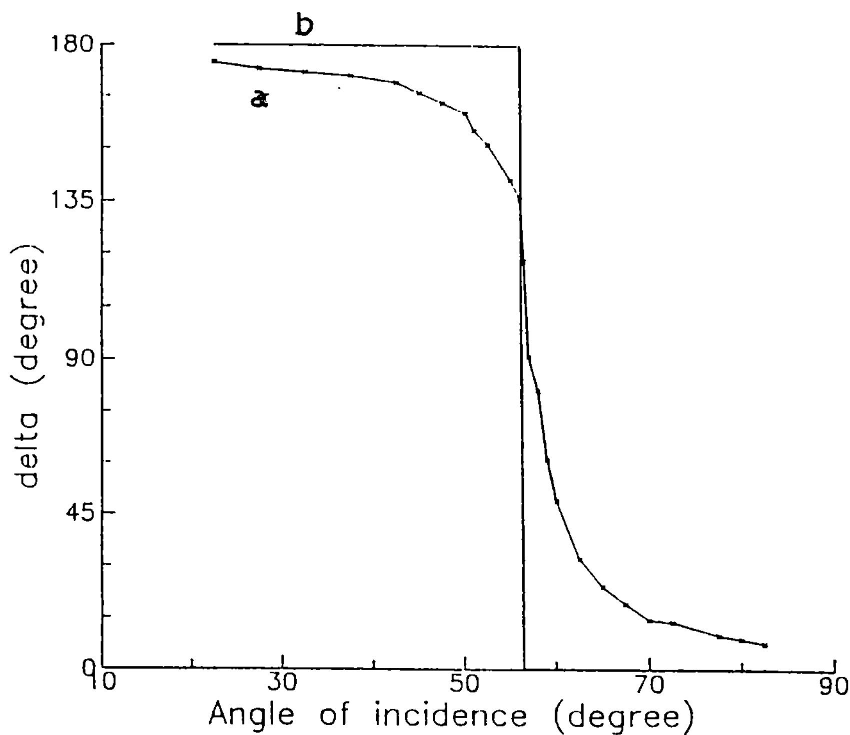

Fig.2.4 Ellipsometric parameter Δ as a function of the angle of incidence from a glass plate. (a) experimental Δ and (b) theoretical Δ from air/glass interface.

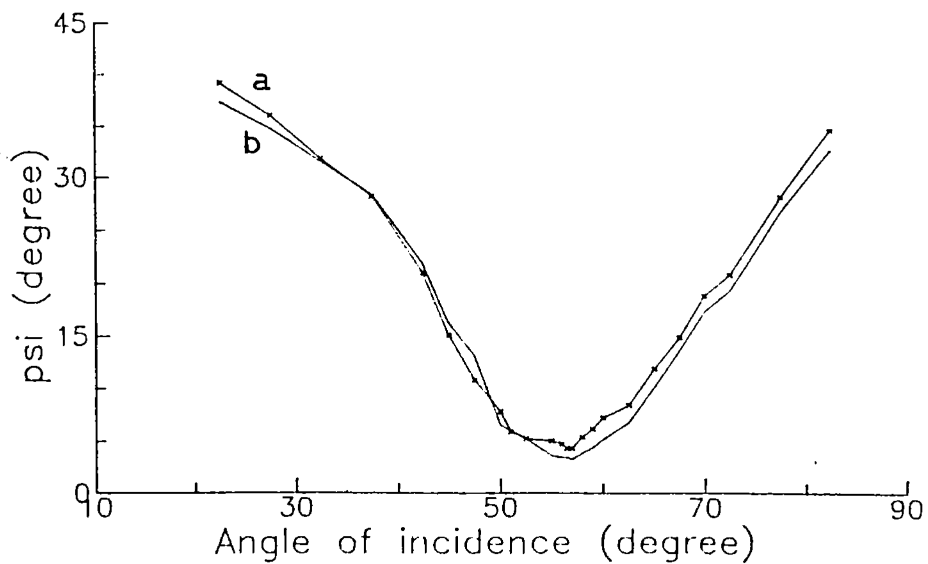

Fig.2.5 Ellipsometric parameter ψ as a function of the angle of incidence from a glass plate. (a) experimental ψ and (b) theoretical ψ for a model air/rough surface/glass interface.

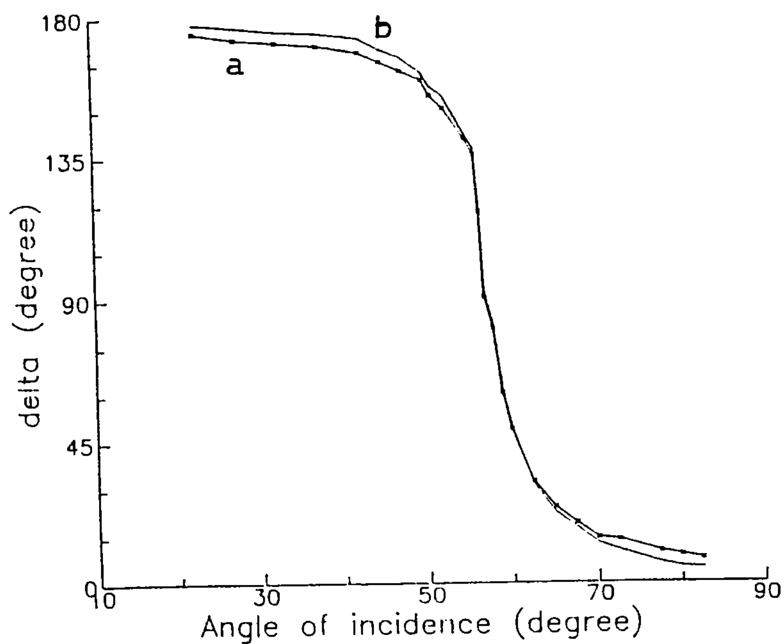

Fig.2.6 Ellipsometric parameter Δ as a function of the angle of incidence from a glass plate. (a) experimental Δ and (b) theoretical Δ for a model air/rough surface/glass interface.

2.4 Conclusion.

This chapter gave a detailed description of theory and the instrumentation of ellipsometer. An experimental setup for ellipsometric measurements (VASE) was fabricated with facility to vary the wavelength and angle of incidence. An ordinary spectrometer is used for this purpose. The collimator and telescope arms were converted into polariser and analyser arms respectively. The accuracy of the measurement of azimuth angles of the polariser and the analyser is 1' while that of angle of incidence is 30". The range of variation of angle of incidence is $20^{\circ} - 80^{\circ}$. 20 cm monochromator was used for wavelength selection and it can scan between 400nm and 750 nm. High power tungsten halogen lamp was used as the light source and this enabled measurement even on surfaces with very low reflectivity. A photomultiplier tube was used for the detection of the reflected light signals. Sine the signal was usually weak and it was further amplified. The chopper and tuned amplifier arrangement could eliminate noise from the system. The use of long focalength lens could avoid the path deviation due to the rotation of polariser.

A clean glass plate was used for the standardization of the system. The calculated ψ and Δ values were used for the determination of Brewster angle of glass plate and it was found to be in agreement with the standard values. This analysis also revealed that the glass surface had a roughness of the order of 40 nm.

References.

1. R.M.A.Azzam and N.M.Bashara. "*Ellipsometry and polarised light*", North Holland, New York. (1977).
2. P.Drude. *Ann. Phys.* (Leipzig) 32 (1887) 584.
3. L.Tronstad. *Trans. Faraday Soc.* 29 (1933) 502.
4. A.Rothen. *Rev. Sci. Instr.* **16** (1945) 26.
5. W.Budde. *Appl. Opt.* **1** (1962) 201.
6. B.D.Cahan and R.F.Spanier. *Surf. Sci.* **16** (1969) 166.
7. D.E.Aspnes. *Opt. Commun.* 8 (1973) 222.
8. P.S.Hauge and F.H.Dill. *I.B.M.J. Res. Develop.* **17** (1973) 472.
9. G.E.Jellison. *Optics Lett.* **12** (1987) 766.
10. R.M.A.Azzam, E.Masetti, I.M.Elminyawi and F.G.Grosz. *Rev. Sci. Instrum.* 59 (1988) 84.
11. D.E.Aspnes and R.P.H.Chang. "*Spectroscopic ellipsometry in plasma processing*" in "Plasma diagnostics", Eds. O.Auciello and D.L.Flamm. Academic press, New York. (1985).
12. K.Vedam, P.J.Mc Marr and J.Narayan. *Appl. Phys. Lett.* **47** (1985) 339.
13. J.Narayan, S.Y.Kim, K.Vedam and R.Manukonda. Appl. Phys. Lett. 51 (1987) 343.
14. J.A.Wollam, P.G.Snyder, A.W.Mc Cormick ,A.K.Rai, D.Ingram and P.P.Pronko. *J. Appl. Phys.* 62 (1987) 4867.
15. P.G.Snyder, M.C.Rost, G.H.Bu-Abbud, J.A.Woollam and S.A.Alterovitz. *J. Appl. Phys.* 60 (1986) 3293.
16. J.Nolly, K.K.Abdullah and K.P.Vijayakumar. *Phys. Stat. Sol.* (a) **101** (1987) K35.
17. J.Oikkonen. *J. Appl. Phys.* 62 (1987) 1385.
18. K.P.Vijayakumar. *J. Appl. Phys.* 69 (1991) 6771.
19. H.Haitjema and G.F.Woerlee. *Thin Solid Films.* **169** (1989) 1.
20. I.Ohlidal, E.Schmidt, M.Libezny, T.Varozek and I.Novotny.

Thin Solid Films. **169** (1989) 213.

21. D.E.Aspnes and A.A.Studna. *Phys. Rev. B* **27** (1983) 985.
22. D.E.Aspnes, S.M.Kelso, R.A.Logan and R.Bhat. *J. Appl. Phys.* **60** (1986) 754.
23. H.Arwin and D.E.Aspnes. *J. Vac. Sci. Technol. A* **2** (1984) 1316
24. H.Arwin and D.E.Aspnes. *Thin Solid Films.* **113** (1984) 101
25. G.E.Jellison Jr. and F.A.Modine. *J. Appl. Phys.* **53** (1982) 3754.
26. G.E.Jellison Jr. and F.A.Modine. *Phys. Rev. B* **27** (1983) 7466.
27. L.Vina, S.Logothetidis and M.Cardona. *Phys. Rev. B* **30** (1984) 1979.
28. G.E.Jellison Jr. and D.H.Lowndes. *Appl. Phys. Lett.* **51** (1987) 352.
29. L.Vina and M.Cardona. *Phys. Rev. B* **34** (1986) 2586.
30. L.Vina and M.Cardona. *Phys. Rev. B* **29** (1984) 6739.
31. P.Lautenschlager, M.Garriga and M.Cardona. *Phys. Rev. B* **35** (1987) 9174.
32. D.E.Aspnes, S.M.Kelso, A.A.Logan and R.Bhat. *J. Appl. Phys.* **60** (1986) 754.
33. J.Joseph and G.Gagnaire. *Thin Solid Films* **193** (1983) 257.
34. F.Lukes. *Surf. Sci.* **30** (1972) 91.
35 E.Pascual, A.Lousa and E.Bertran. *Thin Solid Films.* **214** (1992) 74.
36. R.W.Collins, C.J.Tuckerman, C.Y.Huang and H.Windischmann. *J. Vac. Sci. Technol. A* **3** (1985) 2077.
37. R.W.Collins and J.M.Cavese. *J. Vac. Sci Technol. A* **5** (1987) 2797.
38. R.P.H.Chang, S.Darack. *Appl. Phys. Lett.* **38** (1981) 898.
39. J.B.Theeten, R.P.H.Chang, D.E.Aspnes and T.E.Adams. *J. Electrochem. Soc.* **127** (1980) 980.
40. C.W.Tu, R.P.H.Chang and A.R.Schlier. *J. Vac. Sci. Technol.* **A1** (1983) 637.

41. Soe-Mie F Nee. *Appl. Optics*. **27** (1988) 2819.

42. D.E.Aspnes, J.B.Theeten and F.Hottier. *Phys. Rev. B* **20** (1979) 3292.

43. R.S.Sirohi. *J. Phys. D: Appl. Phys*. 3 (1970) 1407.

44. R.S.Sirohi. *Opt. Commun*. **1** (1970) 304.

45. T.Smith. *Surf. Sci*. **56** (1976) 252.

46. K.Vedam. *Surf. Sci*. **56** (1976) 221.

47. T.V.Vorburger and K.C.Ludema. *Appl. Optics*. **19** (1980) 561.

48. M.D.Williams and D.E.Aspnes. *Phys. Rev Lett*. **41** (1978) 1667.

49. G.Laurence, F.Hottier and J.Hallais. *Rev. Phys. Appl*. **16** (1981) 579.

50. M.Erman and P.M.Frijlink. *Appl. Phys. Lett*. **43** (1983) 285.

51. P.G.Snyder, A.Messengale, K.Memarzadeh, J.A.Woollam, D.C.Ingram and P.P.Pronko. *M R S Symp. Proc*. Vol. **74**, Mater. Res. Soc., Pittsburgh, PA. (1987) 535.

52. P.G.Snyder, M.C.Rost, G.H.Bu-Abbud, E.Oh, J.A.Woollam, D.Poker, D.E.Aspnes, D.C.Ingram and P.P.Pronko. *J. Appl Phys*. **60** (1986) 779.

53. S.Orzeszko, B.N.De, J.A.Woollam, J.J.Pouch and S.A. Alterovitz. *J. Appl. Phys*. **65** (1988) 4175.

54. K.Memarzadeh and J.A.Woollam. *Proc. Soc. Photo-Opt. Instrum. Eng*. 54 (1987) 823.

55. K.Memarzadeh, J.A.Woollam and A.Belkind. *J. Appl. Phys*. **64** (1988) 3407.

56. K.P.Vijayakumar and C.Purushothaman. *Thin Solid Films* 82 (1981) 225.

57. K.P.Vijayakumar K.P.and C.Purushothaman. *Thin Solid Films* **112** (1984) 71.

58. K.P.Vijayakumar and C.purushothaman. *J. Appl. Phys*. **59** (1986) 1787.

59. J.B.Theeten, F.Hottier and J.Hallais. *J. Crystal Growth*. **46** (1979) 245.

60. F.Hottier and R.Cadoret. *J. Crystal Growth*. **56** (1982) 304.

61. Y. Demay, D. Arnoult, J. P. Gailliard and P. Medina. *J. Vac. Sci. Technol.* **A5** (1978) 3139.

62. Takeshi Kawagoe and Talashi Mizoguchi. *Jpn. J. Appl. Phys.* 32 (1993) 2005.

63. Ping He and John A. Woollam. *Appl. Phys. Commun.* **10** (1990) 207.

64. G. H. Bu-Abbud, N. M. Bashara and John A. Woollam. *Thin Solid Films.* **138** (1986) 27.

65. J. Humlicek. *J. Opt. Soc. Am. A.* **2** (1985) 713.

66. Samuel A. Alterovitz, George H. Bu-Abbud, John A. Woollam and David C. Liu. *J. Appl. Phys.* **54** (1983) p 1559.

67. R. Greef. *Rev. Sci. Instr.* **41** (1970) 532.

68. J. C. Suits. *Rev. Sci. Instr.* **42** (1971) 19.

69. D. E. Aspnes. *Opt. Commun.* **8** (1973) 222.

70. D. E. Aspnes. *J. Opt. Soc. Am.* **64** (1974) 812.

71. S. N. Jasperson S. N. and Schnatterly. *Rev. Sci. Instr.* **40** (1969) 761.

72. S. N. Jasperson, D. K. Burge and R. C. O'Handley. *Surf. Sci.* **37** (1973) 548.

73. D. A. G. Bruggeman. *Ann. Phys. (Leipzig).* **24** (1935) 636.

74. G. E. Jellison Jr. and B. C. Sales. *Appl. Optics.* **30** (1991) 4310.

Chapter 3

ELLIPSOMETRIC CALCULATION TECHNIQUE AND APPLICATIONS

3.1 Introduction.

In general when a linearly polarised light is incident on a flat surface it becomes elliptically polarised upon reflection. Ellipsometry involves the measurement of the induced changes in polarisation [1]. The fundamental problem is then to understand those properties which characterize the material medium and are able to induce measurable changes in the polarisation. For this analysis, the system is considered as a non magnetic sample, exhibiting depth dependent optical properties, such as one with a layered structure over a substrate with uniform thickness and flat boundaries. The dielectric constant of each layer is considered as isotropic and homogeneous [2]. Each layer is characterized by at least two parameters ie., thickness and dielectric constant. If the medium is not homogeneous the dielectric constant of the mixed layer is expressed in terms of effective medium theory [3-8]. The effective medium theory helps us to analysis the nature of surfaces and interfaces of multilayer thin film systems. It can be used for the accurate determination of optical constants of thin film systems [9-11]. For the study of surface roughness usually, the rough layer is considered as a mixture of ambient and the medium and then analysed with the help of Bruggeman's Effective Medium Approximation (EMA) [9]. In the case of diffusion of one layer into another causing the formation of a mixed interface layer EMA can be used for the analysis of the inter layer [10,12]. In order to determine optical constants of thin film accuratly, the surface roughness of the film should also be taken into account; and which is possible with the help of EMA in ellipsometry [11]. But the correct estimate of the optical parameters and thickness of the structure depends on the number of the

independently obtained data from ellipsometer. The number of experimental data should be equal to or greater than the number of unknown parameters to be determined [13]. So the measurements should be made in such a way as to enhance the number of experimental data and hence the sensitivity of the measurement [14].

Ellipsometric measurement at one angle of incidence and wavelength yields two independent parameters, viz; the real and imaginary part of complex reflectance ratio (ψ and Δ). It has been observed that a reliable result can be obtained from the large number of data. There are different techniques for increasing the number of observations [15].

(i) by making measurements at multiple angle of incidence [16-18].

(ii) by making measurements at fixed angle of incidence and through a scan of wavelength (Spectroscopic Ellipsometry-SE-) [19].

(iii) by making measurements at multiple angle of incidence and multiple wavelengths (Variable Angle Spectroscopic Ellipsometry -VASE-) [20,21].

Among these techniques, the last one, VASE, is most important because it has all the advantages of the first two techniques like spectroscopic and variable angle ellipsometer. In the present work an ellipsometer with VASE facility is fabricated and used for the measurements.

In the ellipsometric technique the correlation between the calculated parameters is a major problem and may result in incorrect values. In the case of VASE this problem can be reduced by taking measurements at different angles of incidence and different wavelengths [15] and also by taking measurements at sensitive region of ϕ and λ. The sensitivity of ellipsometric parameters ψ and Δ of the thin film system varies with different regions of wavelength λ and angle of incidence ϕ region [14,22,23]. Using a VASE it is possible to take measurements at a particular λ and ϕ region, where the ψ

and Δ have more sensitivity to the thin film system under investigation and hence the accuracy of the calculated value will be better [23].

3.2 Ellipsometric data analysis.

3.21 Reverse and forward problems.

In the previous section we have seen the theory, instrumentation and data acquisition of ellipsometry. A FORTRAN programme is used for the analysis of the ellipsometric data and calculation of physical properties of the thin film. Section (2.2) contains the theory of ellipsometry and section 1.5 describes the theory of light reflected from the film atop a substrate. The Eq.2.33 gives the relation between the ellipsometric parameters (ψ and Δ) to the measured intensity of light reflected from the sample and Eq.1.60 relates the same parameters (ψ and Δ) to the optical properties of film system under (single layer) study using the Fresnel's coefficient of reflection. Using these two equations it is possible to calculate the physical parameters of the sample. In this case the calculation of a parameter like reflection coefficient for a given thin film structure of known optical properties is known as "forward problem" and is readily programmable [1]. But the ellipsometrically measured parameters (ψ and Δ) can also be used to determine the unknown physical properties (for example, refractive indices of the layer, thickness of the layer etc.) of the material, and this part of the calculation is known as "reverse problem" [1,2]. In order to characterize the layered structure of the sample it is necessary to invert the Eq.1.60. Because of the nonlinear nature of the Fresnel's equation that relates ψ and Δ to the physical properties of the system, usually it defies the analytical inversion except in few simple special cases. But with the help of a computer the numerical inversion of such nonlinear equations is possible. A numerical inversion computer programme inverts a set of equations that represent

an optical model of the system. Here one consider a sequence of forward problems, where each increment of the sequence involves different distinct steps. The steps include starting with a good estimate of values of the model parameters, determining the deviation (error factor Q defined in Eq.3.1) of experimental system from the optical model and updating the model parameters with the better values [2]. This is repeated until the magnitude of correction between the experimental and theoretical model becomes zero or very small.

For the ellipsometric analysis we have developed different FORTRAN programmes. Flow charts for different ellipsometric calculations are given in charts 3.1 to 3.3. The flow chart 3.1 is that of a general ellipsometric calculation for the determination of experimental values of ψ and Δ (ψ_e and Δ_e) using the measured values of intensity of light obtained from the ellipsometric measurements. These values of ψ_e and Δ_e are used in the reverse calculation for determining the unknown parameters of the thin film systems. The flow charts 3.2 and 3.3 show two types of calculations used in this work ie., multiple angle incidence (MAI) and variable angle spectroscopic ellipsometer (VASE). Flow chart 3.2 shows the calculation of refractive index spectrum (both real (n) and imaginary (k) parts of complex refractive index, N=n-ik) of a single layer thin film system. Using this programme the n and k calculation over the entire wavelength is possible. For each wavelength the measurement is performed at MAI. The n and k values are scanned over the given ranges and the error of the model is determined using least square error analysis. The best model is determined from the lowest value of unbiased estimator (δ) value (defined in Eq.3.2) obtained from the model fitting procedure. The flow chart 3.3 shows the calculation technique used in a VASE. It shows the calculation of thickness (t) and volume fraction (x) of additional material in a given layer. Bruggeman's effective medium approximation is used for this calculation. This technique is

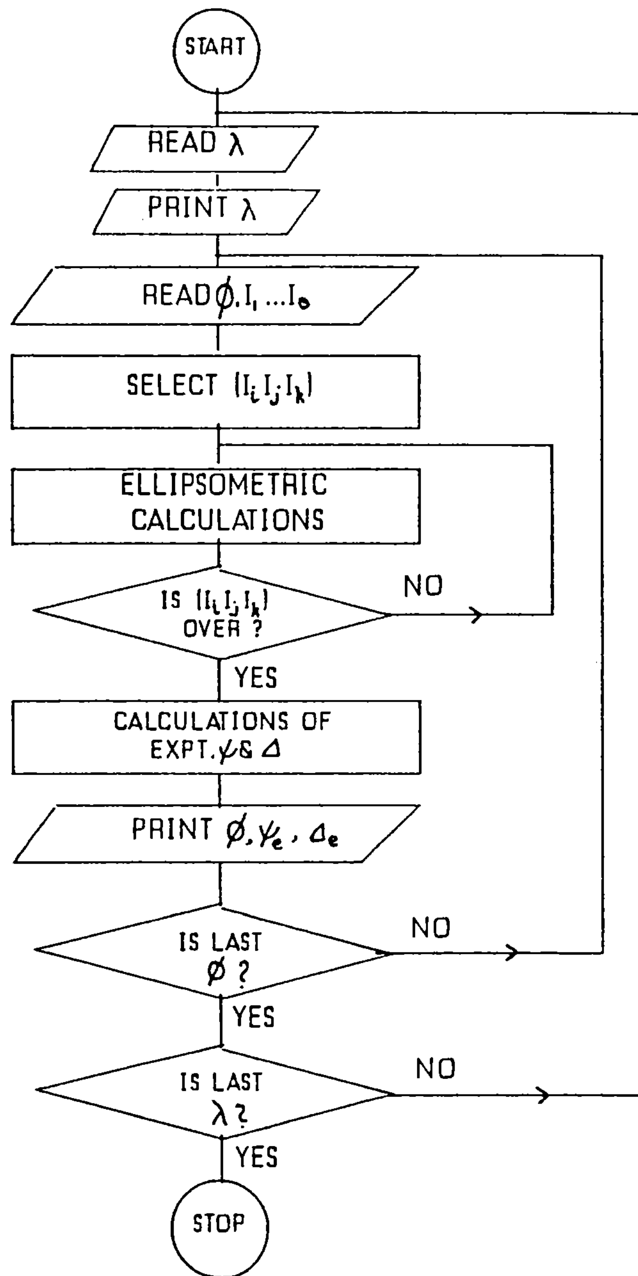

Flow chart 3.1 Flow chart of FORTRAN programme for the calculation of experimental ψ_e and Δ_e using the measured light intensity.

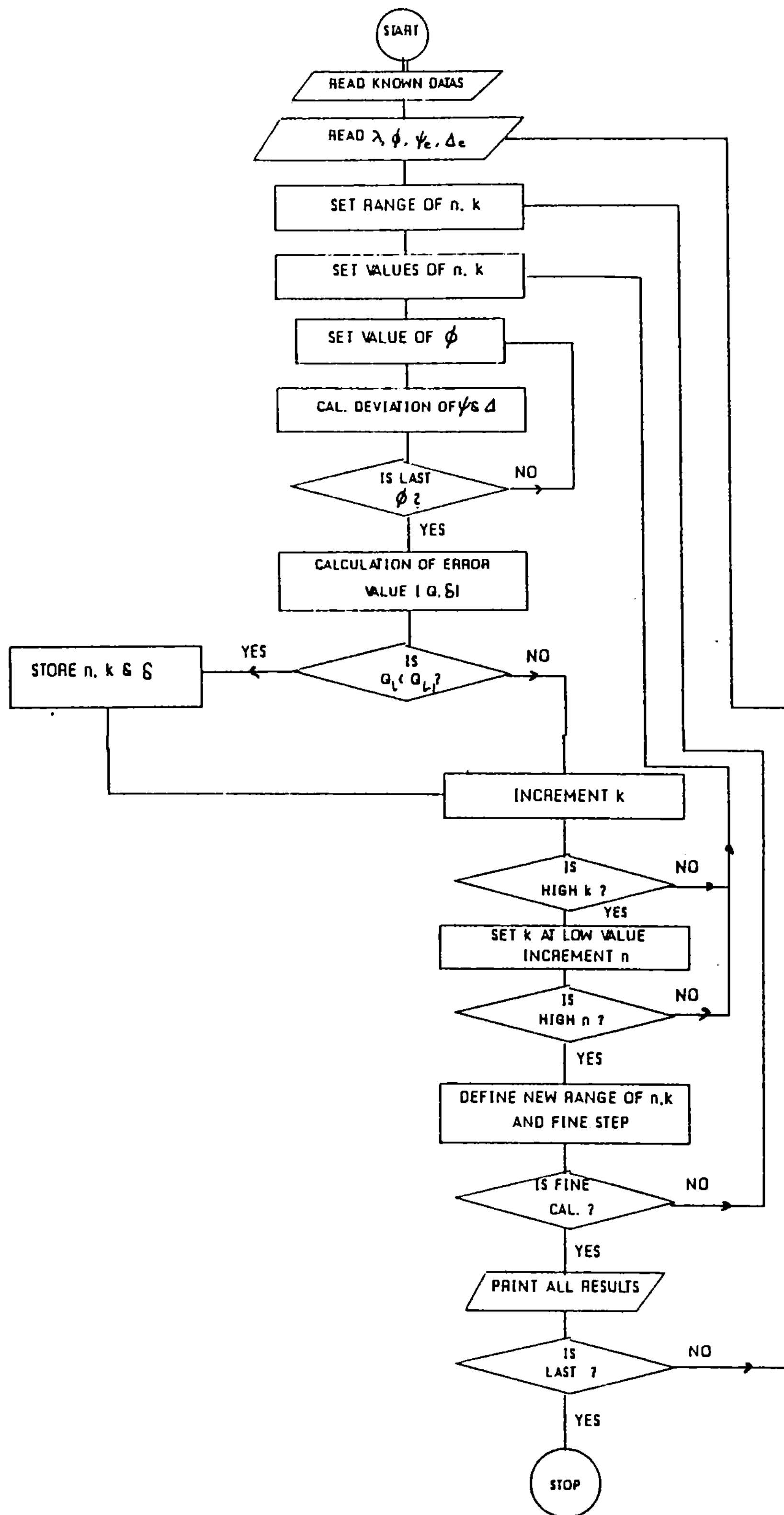

Flow chart 3.2 Flow chart of FORTRAN programme for the calculation of model parameters in MAI ellipsometer.

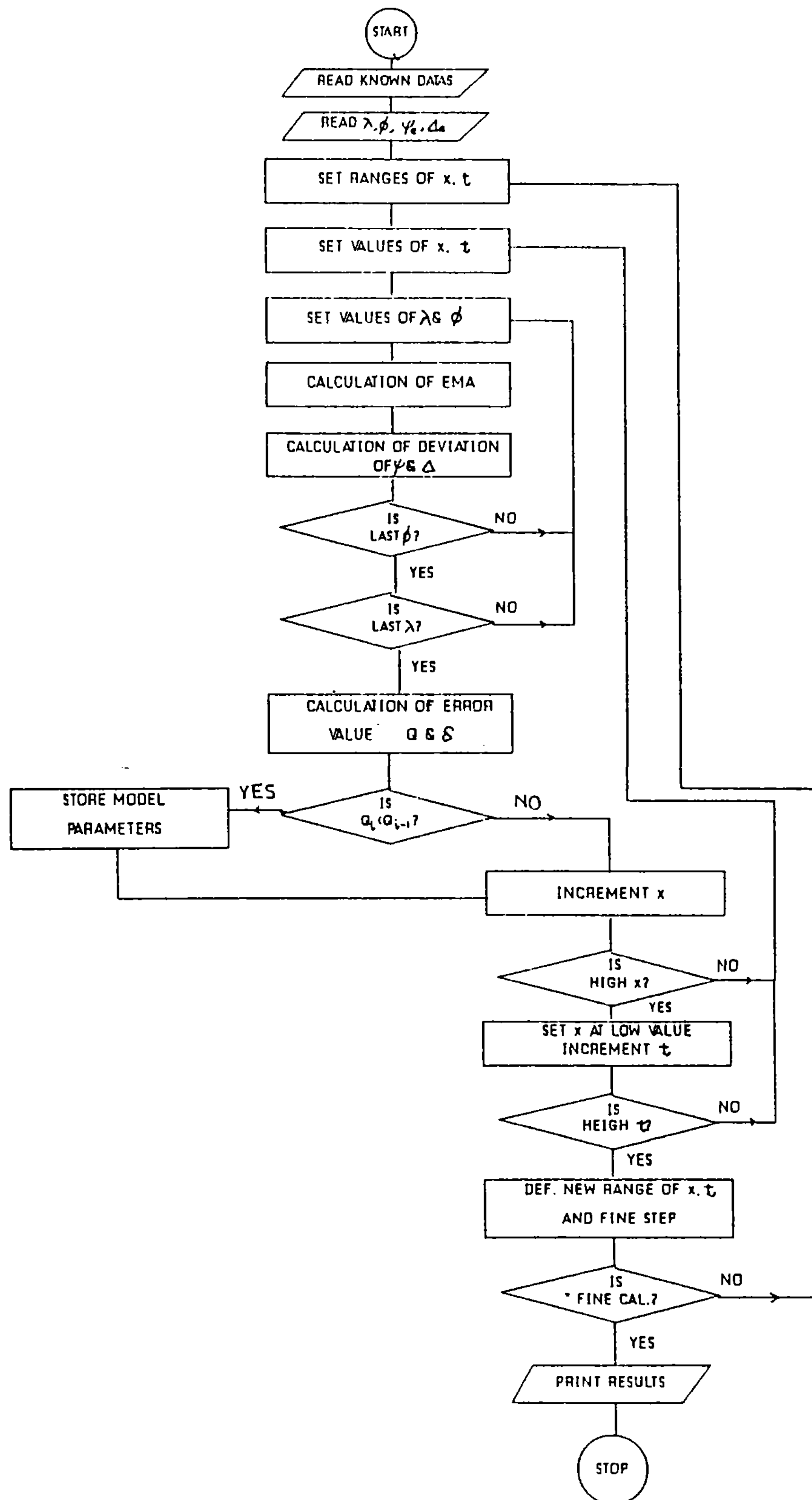

Flow chart 3.3 Flow chart of FORTRAN programme for the calculation of model parameters in VASE.

also used for the surface and interface analysis of a thin film system. The detailed description of various techniques involved in these calculations are given in the following sections. These are extended to multilayer thin films for the determination of physical properties of various layers together or independently and also for the analysis of interlayers between different layers.

3.22 Optical modelling.

A major drawback of optical analysis is that optical instruments measure only the variartion in the optical properties like reflectivity, transmission or polarisation; not the film thickness, relative volume fraction, grain size, or the dielectric function etc which the user really wants. These properties must be inferred from the optical data. A model is required for doing this. In other words a set of mathamatical equation based on a model is required to calculate theoretically the optically measured parameters. The values of unknown parameters (like dielectric constant, film thickness or grain size) will be just assumed for doing this theoretical calculation. When the computed value of the optically measured parameter exactly coinsides with its measured value, the model is correct and hence the value of the unknown parameter is just the assumed value itself. This is to be done in the case of ellipsometry also in which the measured parameter is ρ. This parameter has to be theoretically calculated using a optical model of the thin film system and this model is the computer simulation of the actual physical system using the known optical properties of the system [24]. A set of equations given in Eq.1.60 represent a simple system having structure (air-film-substrate system) and these equations can be used for calculating the measured ellipsometric parameters ρ theoretically. Fig.3.1 show how an optical model might be considered. In these Figs.3.1(a) and 3.1(b) show the actual structure of the system and the

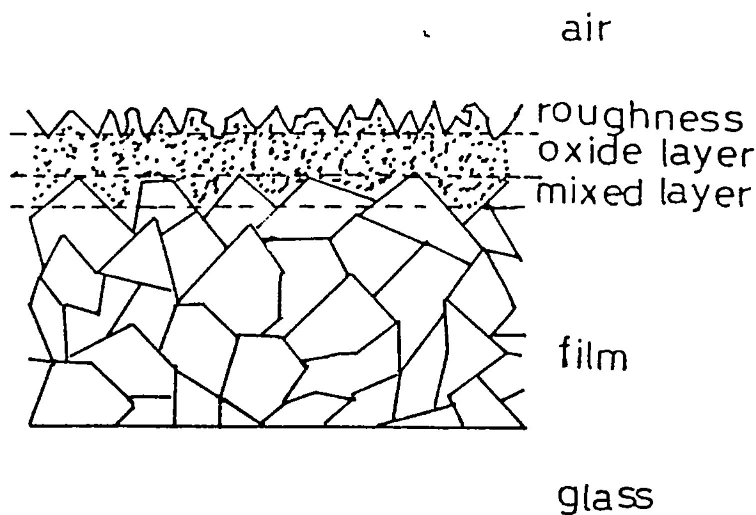

Fig. 3.1(a)

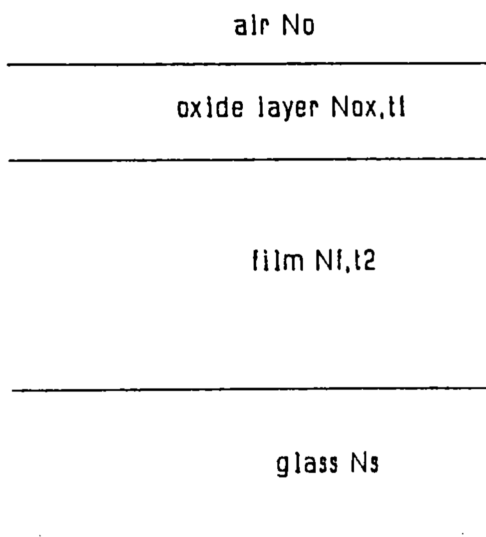

Fig. 3.1(b)

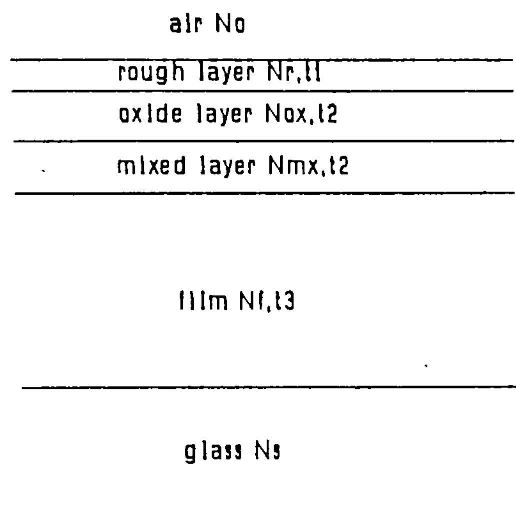

Fig. 3.1(c)

Fig. 3.1 (a) Schematic diagram of a thin film sample with top oxide layer with roughness deposited over the glass substrate.
3.1(b) One possible approximate optical model of the thin film system shown in (a).
3.1(c) Another optical model of the thin film system shown in (a) that contains the fine details like surface roughness and mixed layer.

approximate optical model of the physical system respectively. This system can be represented by a set of Fresnel's equations using complex refractive index of different layers N_s, N_f, N_{ox}, and N_o and thickness of the film t_1 and t_2. The objective is to determine t_1, t_2 and N_{ox}. Here N_s, N_f, N_{ox}, and N_o are the complex refractive indices of substrate, film, top oxide layer and ambient (air) while t_1 and t_2 are the thicknesses of the film and the oxide layer formed. Once an optical model has been selected the approximate material parameters are then determined by the numerical inversion of the Fresnel's equations. An assumed set of optical parameters is used to calculate the "calculated" results. This set is then changed by an iterative procedure until an optimum set of values is found by minimizing the least square difference between the experimental and calculated ellipsometric parameters, thus making the discrepancy between the calculated and measured spectra a minimum. The error function for calculating the discrepancy between the two ie, calculated value and experimental value is given by [11,25].

$$Q = \sum_{i,k} \left\{ \left[\tan\psi_e(\lambda_i \phi_k) - \tan\psi_c(\lambda_i \phi_k) \right]^2 + \left[\cos\Delta_e(\lambda_i \phi_k) - \cos\Delta_c(\lambda_i \phi_k) \right]^2 \right\} \qquad (3.1)$$

where the subscript c and e stand for the 'calculated' (using the Fresnel's equations) and 'experimental' (using ellipsometric technique) respectively. The subscript i and k stand for the different experimental condition that are varied during the measurements such as wavelength (λ) and angle of incidence (ϕ).

If finer details are required, (for example surface roughness, or interface formation) the model must be extended as shown in Fig.3.1(c) to include these phases also, provided there should be adequate data to deal with the more complicated models. If the data is independent to the added

parameters the uncertainty become very large. Experience and some basic knowledge of the structure of the sample are needed for choosing the correct models.

When comparing the suitability of the different optical models used in an experiment, the unbiased estimator (δ) value derived from the ellipsometric calculation is highly useful, and this is given by [11,25]

$$\delta = \frac{1}{s - p - 1} Q. \qquad (3.2)$$

where s is the number of independent readings corresponding to different experimental conditions ie., at different wavelengths and angle of incidence (in our experiment this (s) is in the range 40-50) at which the VASE measurements have been made and p is the number of unknown model parameters to be determined (for example if n, k and t are the parameters to be determined then p is 3, in the present experiments it varies from 1 to 4 depending on the system). The least value of δ corresponds to the best suitable model. The parameters corresponding to this model can be assumed to be the physical constants of the system under investigation. A more stringent test for the validity of an optical model is to use the optical data obtained from the model to determine any other parameters as a function of an experimental variable. For example in a three phase (eg., air/film/substrate) model the film thickness can be determined at different wavelengths. But if it turns out to be wavelength dependent, then it is clear that something is wrong with the data or the model used.

Another crucial problem coming up in the inversion procedure is that of correlation between the parameters of the system. The correlation between the parameters can be significantly reduced by taking reading in multiple angle and multiple wavelength mode [14].

3.3 Surface and Interface analysis.

3.31 Bruggeman's effective medium approximation.

All materials are inhomogeneous in the atomic scale. But macroscopically homogeneous materials can also consist of separate regions which possess their own dielectric identities but have dimensions that are small compared to the wavelength of light. The dielectric function of these materials can be described in terms of dielectric function of its constituents and its microstructure by effective medium theory. That is, if a medium is not perfectly filled with atoms of the same material, but has for example voids, or inclusion of some different materials, the optical properties of the medium can no longer be described by theories dealing with the ideal bulk materials [3-8]. Bruggeman's effective medium approximation theory (EMA) [8] and Maxwells-Garnett theory (MGT) [6] are the most widely used mean field theories for the calculation of dielectric constant of such composite media. Both these theories are derived on the assumption that the composite materials consist of grains which are much smaller than the wavelength of probing light. However they differ in the treatment of the two components in a composite system. In the EMA the two components are treated with equal importance. But in the MGT the grains of one component are taken to be embedded in the matrix of the other component [3,8] and this theory is valid only for small filling factors of inclusions. In the case of Bruggeman's EMA theory the two components with filling factors x and (1-x) are taken into account on an equal footing, and hence it is valid for all filling factors. Through out the present work for the analysis we have used Bruggeman's EMA.

In Bruggeman's EMA, the average dielectric function ε_c of a mixture $A_xB_{(1-x)}$ of two reference materials A and B with known dielectric function ε_a and ε_b and volume fraction x and 1-x can be calculated using the relation given below.

$$x \frac{\varepsilon_a - \varepsilon_c}{\varepsilon_a + 2\varepsilon_c} + (1-x) \frac{\varepsilon_b - \varepsilon_c}{\varepsilon_b + 2\varepsilon_c} = 0 \quad (3.3)$$

The dielectric constant (ε) of a material is related to complex refractive index (N) by the equation

$$\varepsilon = N^2 \quad (3.4)$$

3.32 Interface analysis.

Ellipsometry is commonly used for the interface analysis of semiconducting materials [10,28,27]. The characterization of the interdiffusion of different layers in the multilayer thin film system is done by measuring the volume fraction of one layer in the other and EMA is used for this this. In other words this is done by measuring the thickness and volume fraction (x) and (1-x) of the constituent materials in the hypothetical interlayer at the interface of two layers as shown in Fig.3.2. The figure shows the interface between the two layers A and B with dielectric constant ε_a and ε_b. If the interface is not perfect a small amount of material (A) diffuse into (B) and vice versa. This new layer which contain both material A and B is considered as the new interlayer. Thus for the ellipsometric analysis the bilayer system is now considered as a three-layer system with an interlayer in between the two having a volume fraction (x) for A and (1-x) for B. The thickness of the mixture layer gives a measure of the diffusion of material into each other. The dielectric constant of the mixed media is given by Eq.3.3. By incorporating EMA in the optical model of ellipsometric analysis it is possible to calculate the thickness, volume fraction of material A and B and the effective dielectric constant of the interlayer formed, if any between the layers A and B.

In the present work we have used the EMA in the ellipsometric analysis and applied the same iteration technique for minimising the error value between actual and

assumed models to get the actual model of the system and hence the physical parameters of the same.

3.33 Surface analysis.

It is observed that ellipsometry is highly sensitive to the variation on the surface, and this property is used to characterize the surface roughness of the film. This technique is used not only for measuring the thickness of surface roughness but also for the accurate determination of the refractive index of thin film samples. The surface roughness of the sample affects the measurement of the refractive index of the film [28,29]. Unlike the other technique ellipsometry can be used for the determination of accurate refractive index of thin films taking into account of surface roughness [30,31]. The surface is said to be macroscopically rough and scatter light if the average size of the irregularities is of the order of or exceeds the wavelength of light used. Ellipsometry is also used for the analysis of macroscopic surface roughness. The present study deals with microscopic surface roughness which has a dimension less than that of wavelength used and does not scatter light [9]. EMA is used for this microscopic surface roughness analysis of film [9]. In this technique surface roughness is treated as a combination of ambient (usually air) and thin film material. A simplified approach to study the surface roughness is to replace the top roughed layer by an equivalent film with plane parallel boundaries, whose effective thickness is equal to the rms value of roughness and optical constants are determined by EMA [1,11]. The Fig.3.3 shows the schematic representation of surface roughness and its optical model used in the ellipsometric calculations. Here the single layered rough film is considered as a smooth double layer film, where the imaginary top smooth layer contains the rough layer. The ellipsometer calculates the thickness of the top layer which is taken as the rms value of surface roughness of the film and

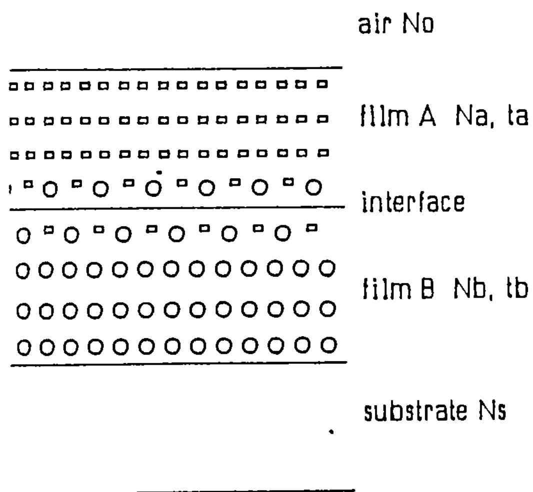

Fig. 3.2(a)

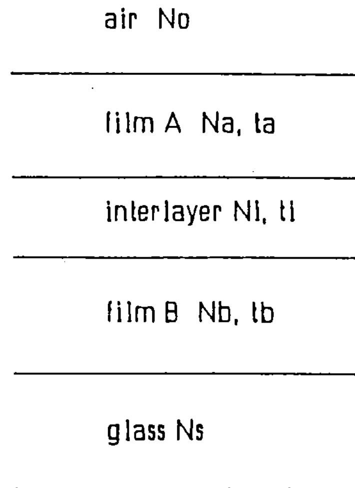

Fig. 3.2(b)

Fig.3.2 (a) Schematic representation of double layer thin film system with complex refractive index N_a and N_b and thickness t_a and t_b deposited over glass surface with refractive index N_s.

3.2 (b) Optical model of the bilayer thin film that shows the interlayer formed (thickness t_i and effective refractive index N_i) in between the layer A and B.

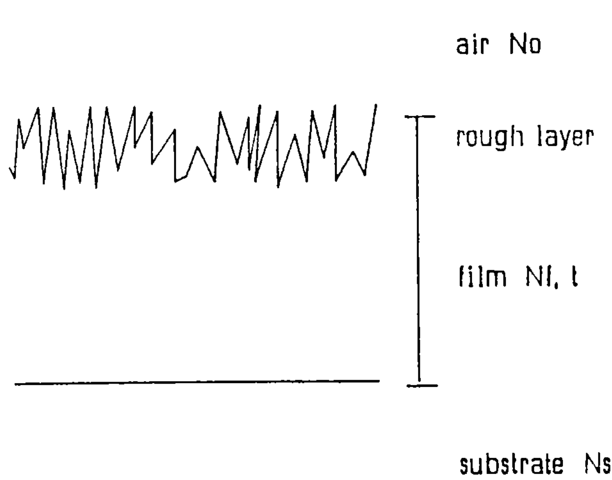

Fig. 3.3(a)

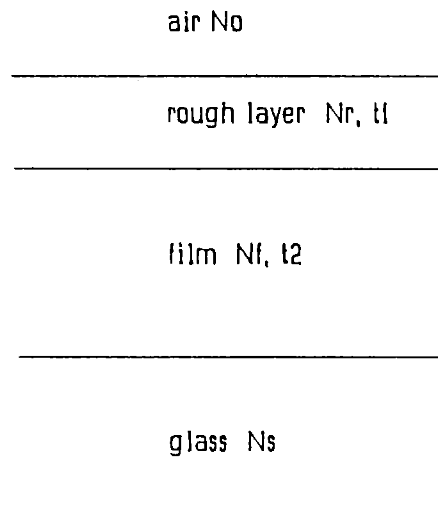

Fig. 3.3(b)

Fig.3.3 (a) Schematic diagram of thin film with surface roughness deposited on glass substrate.

3.3 (b) The optical model of the film; in this case the rough layer is replaced by a thin top layer with thickness (t_1) equal to the rms value of the roughness height and having an effective refractive index.

also determine the volume fraction of ambient (air) in this layer using EMA. The computer programming and optical modelling technique are same as that of interlayer analysis given in section 3.32.

3.4 sensitivity analysis.

Multilayer thin film structures are used in many different areas of science and technology. Thin film solar cell is an example. In the designing process, an accurate knowledge about the structure of different layers and interlayers are very important. Ellipsometry is widely used to obtain this type of information. But the major limitation of the accuracy of ellipsometric characterization of material is the decrease in sensitivity as one probes into greater depths below the surface. Another difficulty is caused by correlation between the model parameters in the data fitting procedure. In general, correlation tends to become more and more severe as the number of unknown parameters increases, number of experimental point decreases and as the parameter sensitivity decreases. Thus in studying a multilayer structure it is of crucial importance to maximize the sensitivity of ellipsometric measurements to the model parameters of interest. Several works were done to enhance the sensitivity of the ellipsometric measurements [22,23]. Alterovitz et al had studied the technique to increase the sensitivity of null ellipsometer and they reported that the suppression of either 'p' or 's' wave for a particular angle of incidence ϕ_i results in an increase in the sensitivity [32]. Snyder et al have plotted a 3 dimensional (3D) graph of ψ and Δ against wavelength λ and angle of incidence ϕ, by slightly changing the model parameters [14]. They have qualitatively estimated the error by mixing the simulated data with corresponding experimental errors and thus analyzed as if it were like the experimental data [14].

In the present study we have used the model

suggested by Woollam et al [23]. In this 3D or contour sensitivity plots are drawn and ellipsometric measurements of the multilayer thin film system are taken in the most sensitive region of wavelength λ and angle of incidence ϕ which are obtained from these plots. In the present work we have studied the following thin film systems using ellipsometry. It may be noted that these bilayer films are of practical importance in solar cell fabrication.

1. CdS/Glass.
2. CdS/SnO_2/Glass.
3. CdS/$CuInSe_2$/Glass.

For sensitivity analysis the 3D plots are to be drawn showing the variation of both $\delta\psi$ and $\delta\Delta$ with wavelength λ and angle of incidence ϕ based on the model of the system. The $\delta\psi$ and $\delta\Delta$ are calculated in the following way.

$$\delta\psi = \psi' - \psi'' \quad (3.5(a))$$

$$\delta\Delta = \Delta' - \Delta'' \quad (3.5(b))$$

First ψ' and Δ' for a structure given above, (eg. CdS/SnO_2/Glass, with CdS (thickness t_1-400 nm) and SnO_2 (thickness t_2- 450 nm)) are calculated in the wavelength range 400-740 nm and angle of incidence range 40-80° using a FORTRAN programme. Next a second set of ψ'' and Δ'' values of the same model is calculated after giving a small perturbation to one of the model parameters to be determined. For example in the above model a change equal to 10% is given to the value of t_1 (ie., t_1 changes from 400 to 440 nm) and ψ and Δ are again calculated as ψ'' and Δ''. The computer then subtract the new values (ψ'' and Δ'') from the corresponding values of earlier calculation (ψ' and Δ') and difference is denoted as $\delta\psi$ and $\delta\Delta$. The 3D graph is plotted with Z-axis representing the values of either $\delta\psi$ or $\delta\Delta$, ie., the changes in ψ and Δ due to applied perturbation of the model parameter. The sensitivity calculation can be repeated for any parameter and these help in choosing the ranges of λ and ϕ to be used in the experiment. Ellipsometric measurements at few wavelengths and

angles of incidence near the most sensitive region are sufficient to make reliable and accurate analysis [23].

3.41 CdS/Glass system.

CdS films have application in the field of thin film solar cells as a window material. It is prepared by different techniques. In chapter 4 a brief review of the properties of this film as well as preparation techniques are included. In the present studies we have used the film prepared over glass substrate by the spray pyrolysis technique. These films are treated as having a two layer structure, ie., on the top surface there is a microscopic rough surface layer and at the bottom a good quality film. In the sensitivity analysis we have used CdS film with thickness in the range 400-450 nm. The preliminary studies using VASE and SEM indicate the presence of surface rough layer and the thickness of this surface roughness is of the order of 25-60 nm. Therefore the simulated model of the film has a thickness t_2-400 nm, surface layer has a thickness t_1 - 30 nm and the volume fraction of air in the top rough layer is ~0.50. The different perturbation given are

1. Change in thickness of top layer by 10% ie., t_1 changes from 30 nm to 33 nm.

2. Change in thickness of bottom layer by 10% ie., t_2 changes from 400 nm to 440 nm.

3. Change in volume fraction (x) of air in top rough layer from 0.50 to 0.54.

The sensitivity plots corresponding to these perturbations are shown in Figs. 3.4 to 3.9. The Table 3.1 shows the sensitivity regions of λ and ϕ of these systems obtained from the sensitivity plots shown in Figs. 3.4 to 3.9. Table 3.1 shows the list of sensitive ϕ and λ region of ψ and Δ of CdS/glass system corresponding to different perturbations.

Fig. 3.4 Sensitivity ($\delta\psi$) of the ψ to the thickness of top rough CdS layer in air/rough CdS/CdS/glass system. The thickness t_1 is changed by 10%. (ie., $t_1 \rightarrow t_1 + 10\% t_1$).

G5645

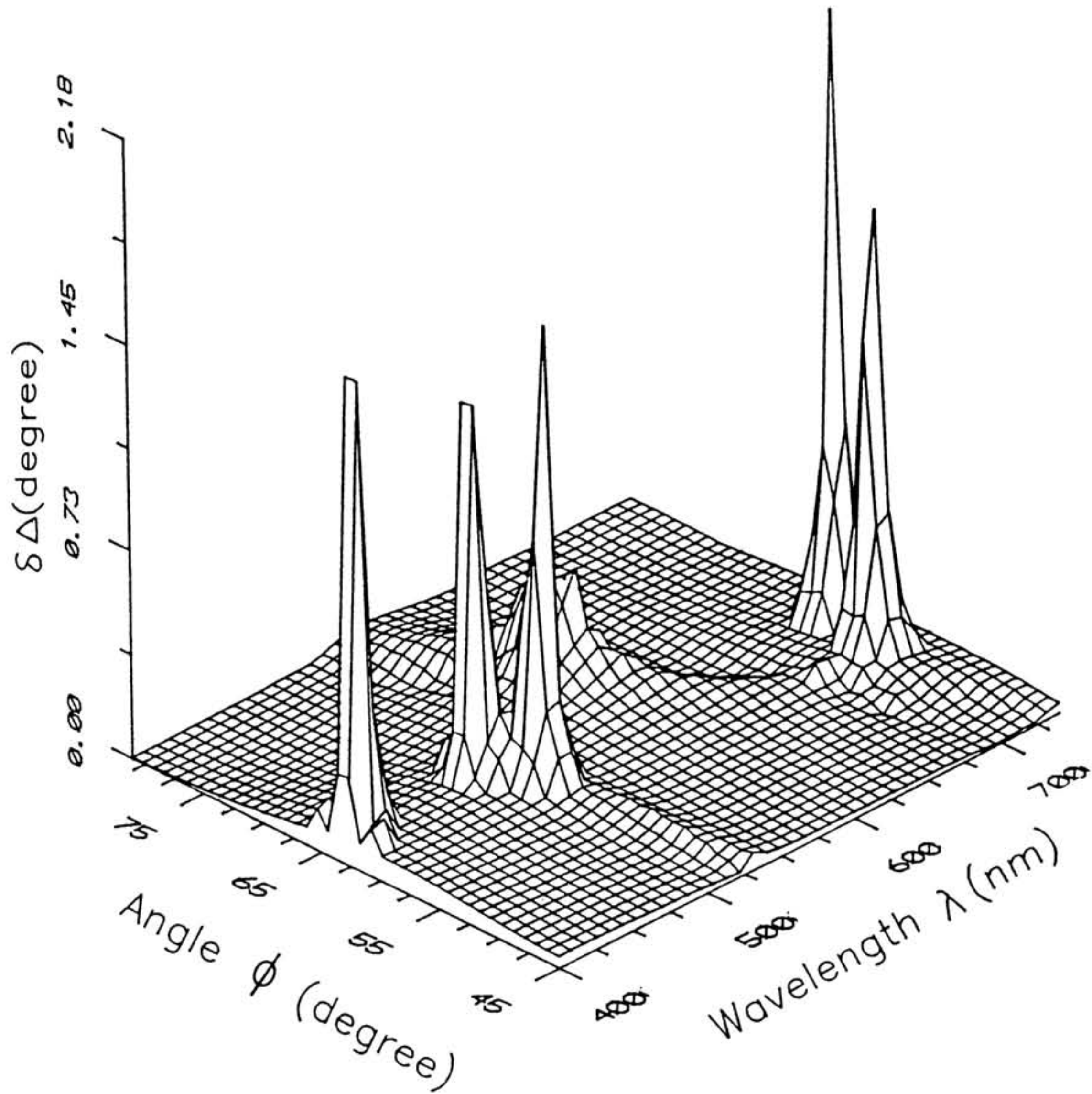

Fig. 3.5 Sensitivity ($\delta\Delta$) of the Δ to the thickness of top rough CdS layer in air/rough CdS/CdS/glass system. The thickness t_1 is changed by 10%. (ie., $t_1 \rightarrow t_1 + 10\% t_1$).

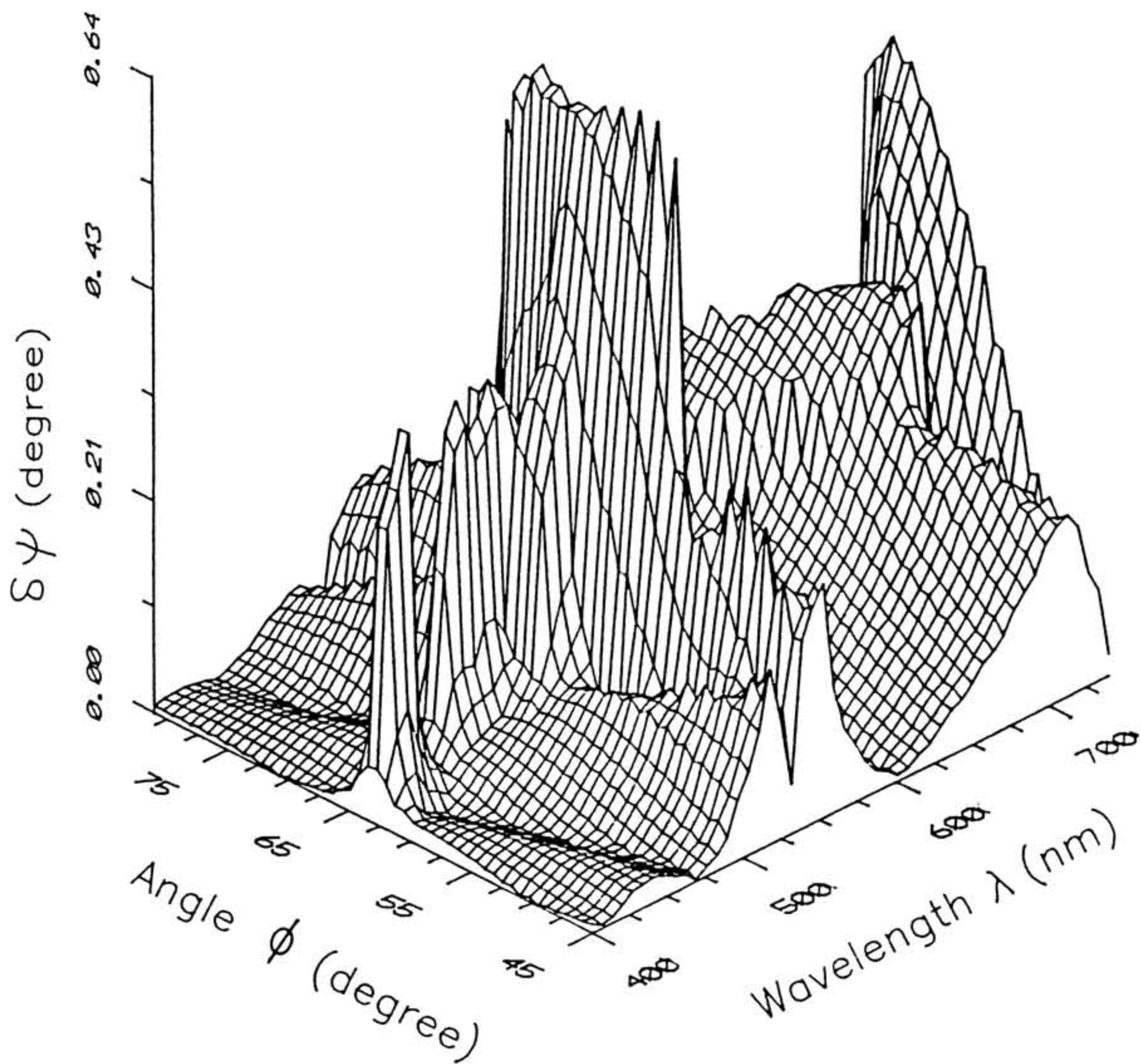

Fig. 3.6 Sensitivity ($\delta\psi$) of the ψ to the thickness of bottom CdS layer in air/rough CdS/CdS/glass system. The thickness t_2 is changed by 10%. (ie., $t_2 \rightarrow t_2 + 10\%t_2$).

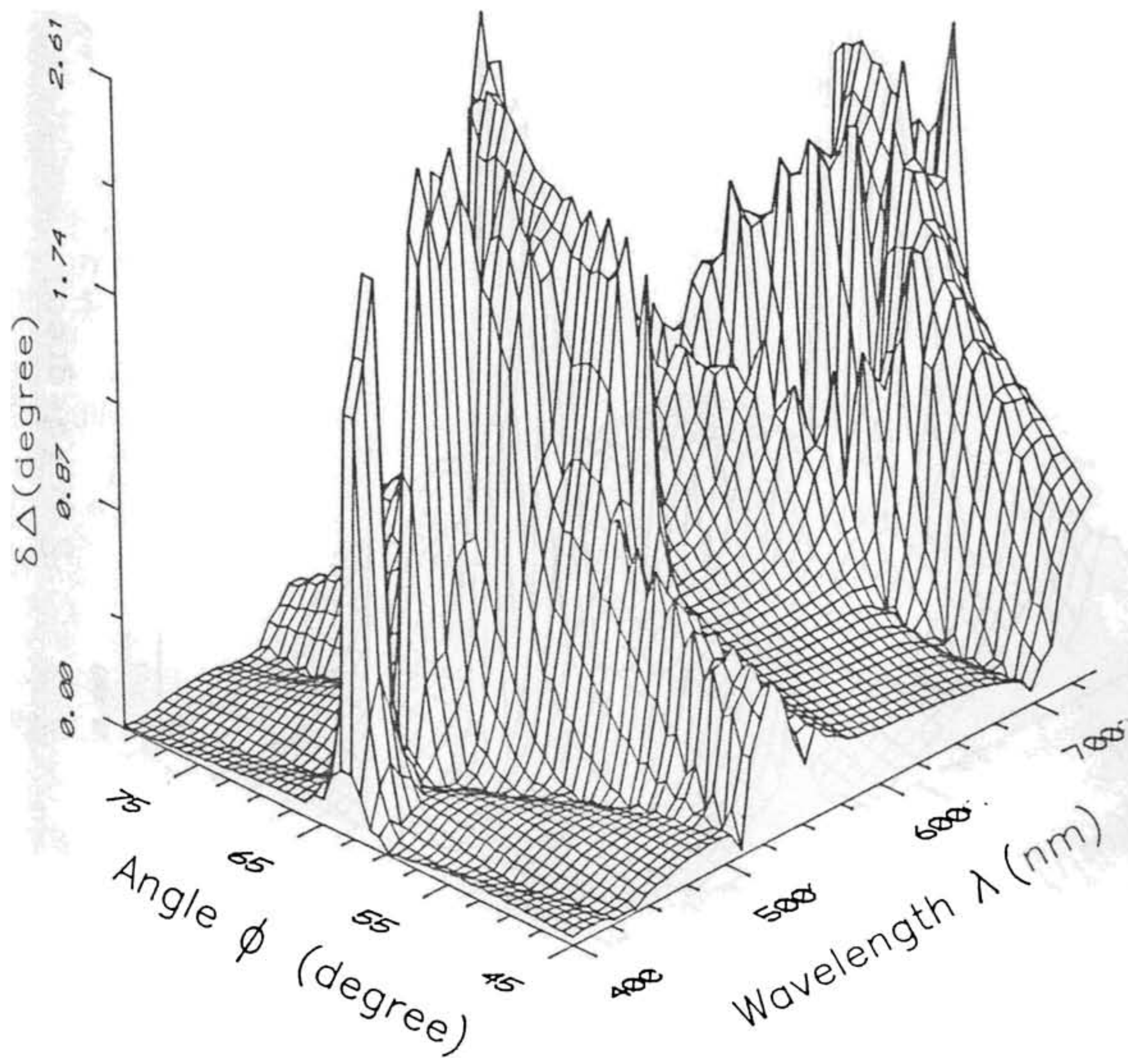

Fig. 3.7 Sensitivity (δΔ) of the Δ to the thickness of bottom CdS layer in air/rough CdS/CdS/glass system. The thickness t_2 is changed by 10%. (ie., $t_2 \rightarrow t_2 + 10\% t_2$).

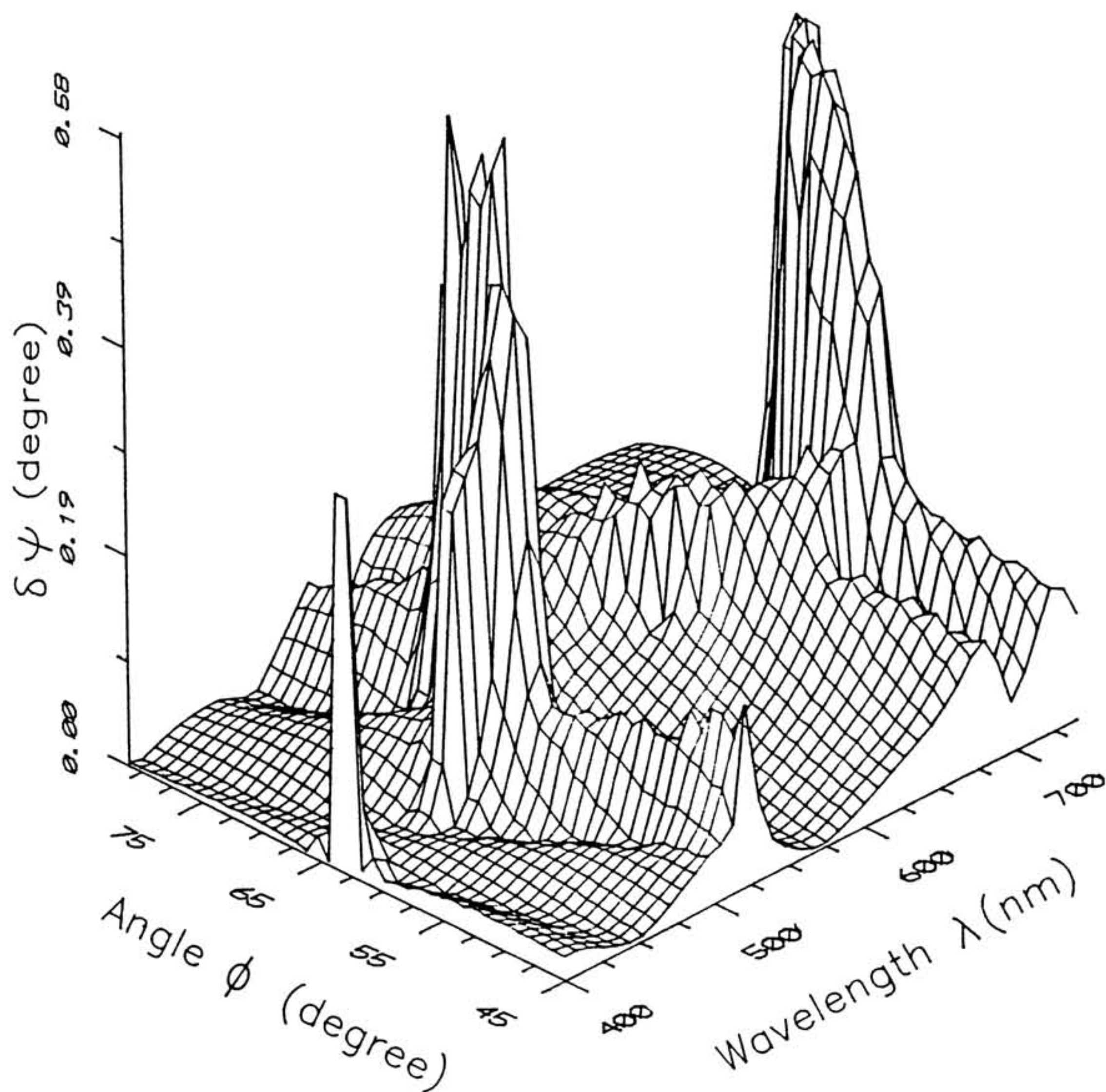

Fig. 3.8 Sensitivity ($\delta\psi$) of the ψ to the volume fraction of air in top rough CdS layer in air/rough CdS/CdS/glass system. The volume fraction x is changed by 0.04. (ie., $x \rightarrow x + 0.04$).

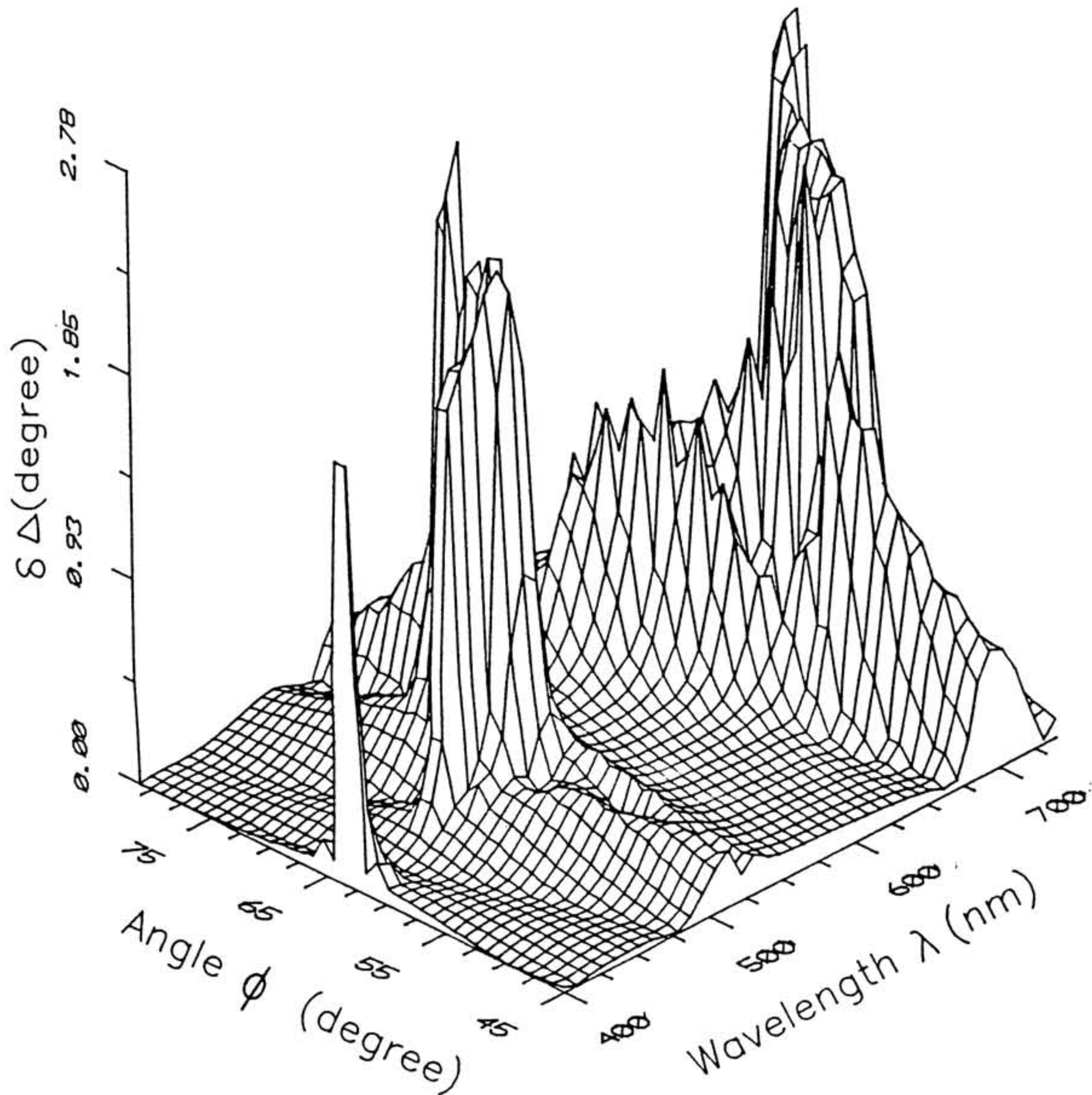

Fig.3.9 Sensitivity (δΔ) of the Δ to the volume fraction of air in top rough CdS layer in air/rough CdS/CdS/glass system. The volume fraction x is changed by 0.04. (ie., x → x + 0.04).

	Perturbations		
Sensitivity parameter	t_1+10%t_1	t_2+10%t_2	f+0.04
ϕ range for ψ	53-65°	56-72°	57-66°
ϕ range for Δ	54-65°	57-71°	55-68°
λ range for ψ	~ 400 nm, 480-540 nm & 680-720 nm.	500-600 nm & ~ 700 nm.	470-540 nm & ~ 700 nm.
λ range for Δ	~400 nm, 480-540 nm & 680-720 nm.	490-550 nm & 690-740 nm.	490-550 nm & ~700 nm.

Table 3.1 Summary of the most sensitive regions of ϕ and λ corresponding to various perturbations in air/rough CdS/CdS/glass thin film system.

3.42 CdS/SnO_2/Glass system.

This bilayer structure is also widely used in thin film solar cells. SnO_2 film is commonly used as transparent conducting electrodes in a large number of optoelectronic devices. A brief review of SnO_2 and its preparation techniques using spray pyrolysis are given in part I of chapter 6. The CdS/SnO_2/Glass structure is simulated with a CdS thickness t_1 - 400 nm and SnO_2 with a thickness t_2 - 450 nm. In this case also 10% perturbation has given to t_1 and t_2 and corresponding 3D plots are shown in Figs. 3.10 [illegible] to 3.13 [illegible]. Table 3.2 shows the list of sensitive region of ϕ and λ for the CdS/SnO_2/glass system corresponding to different perturbations.

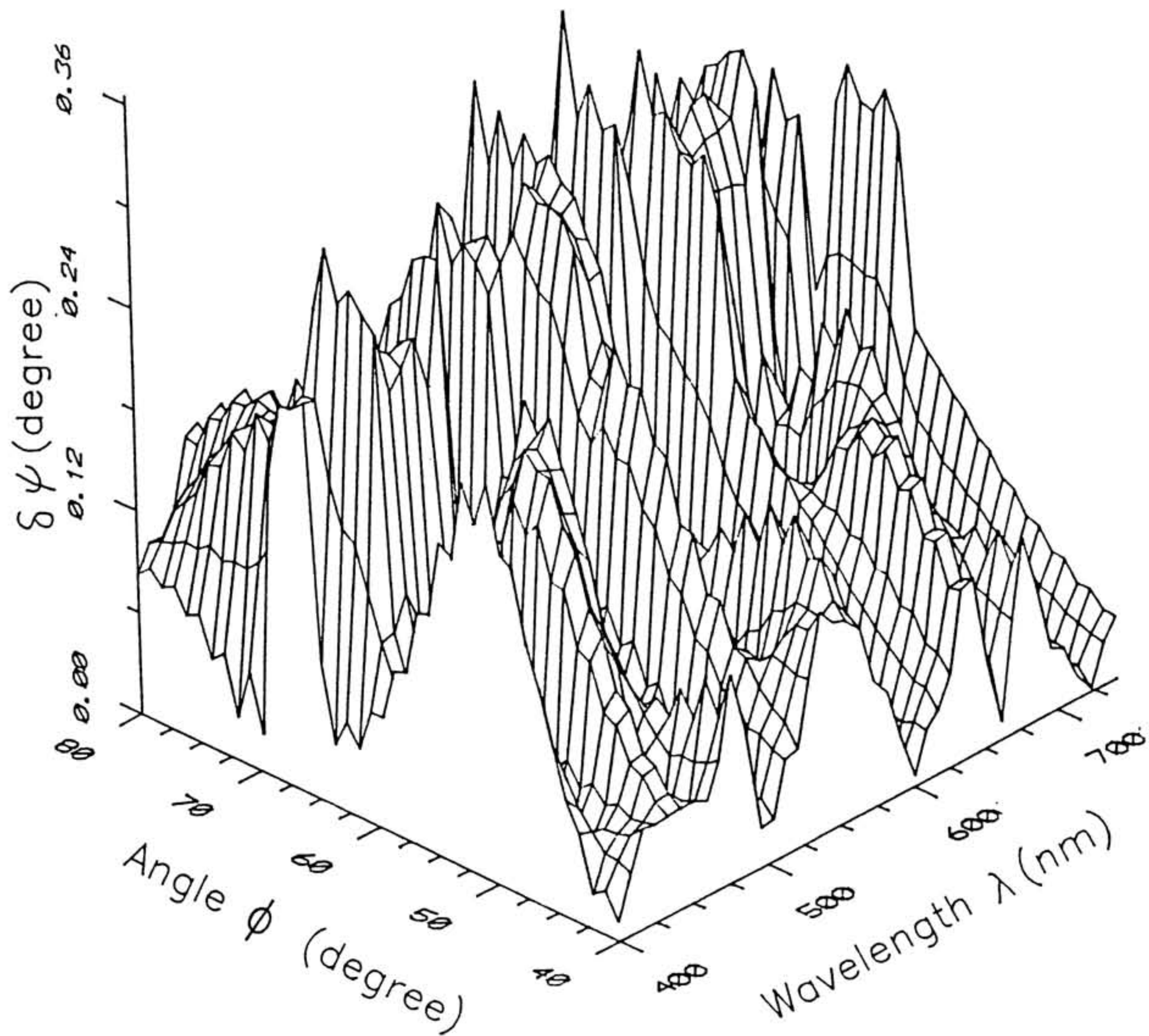

Fig. 3.10 Sensitivity (δψ) of the ψ to the thickness of top CdS layer in air/CdS/SnO_2/glass system. The thickness t_1 is changed by 10%. (ie., $t_1 \rightarrow t_1 + 10\% t_1$).

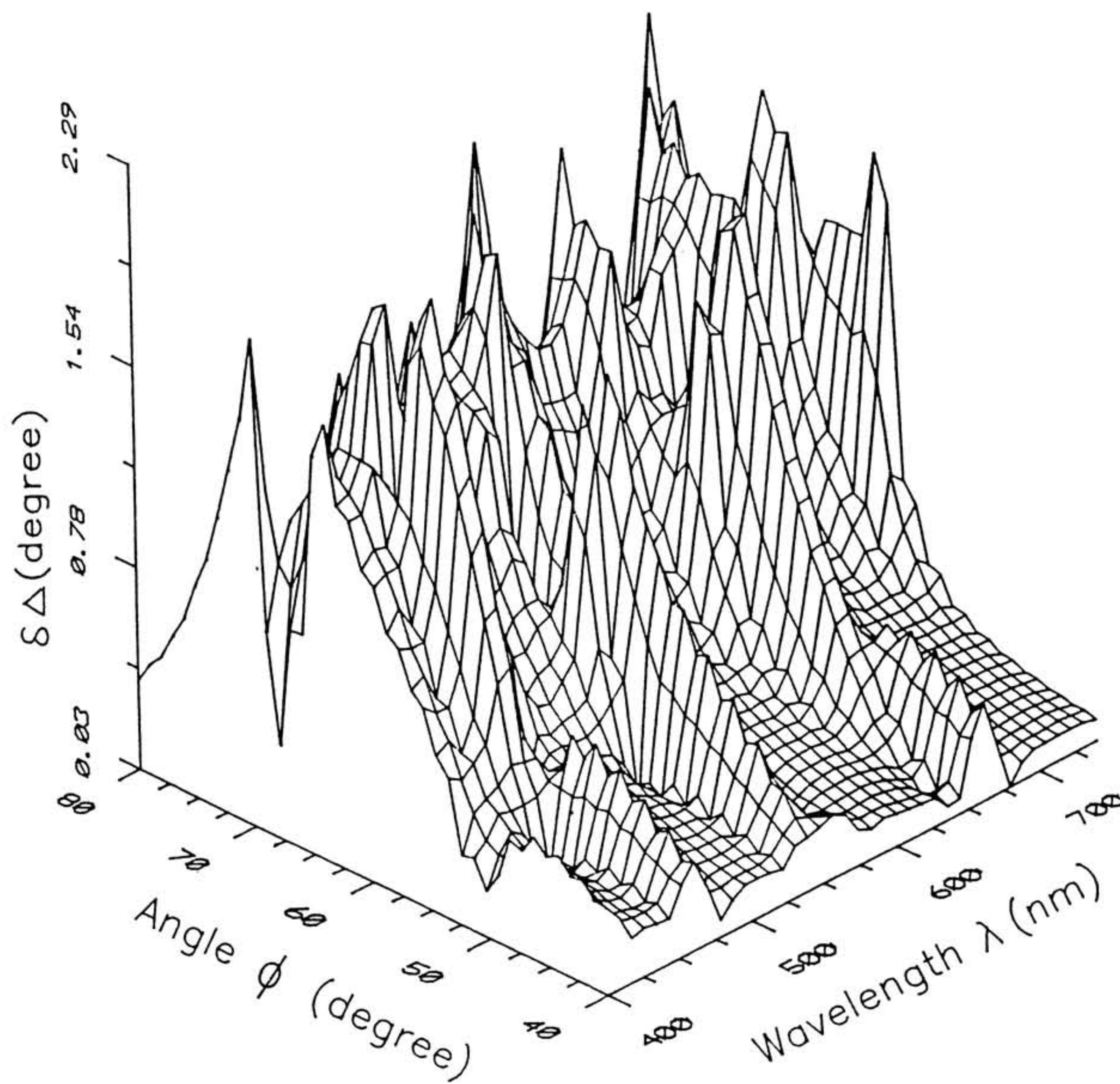

'ig. 3.11 Sensitivity ($\delta\Delta$) of the Δ to the thickness of top CdS ayer in air/CdS/SnO_2/glass system. The thickness t_1 is :hanged by 10%. (ie., $t_1 \rightarrow t_1 + 10\% t_1$).

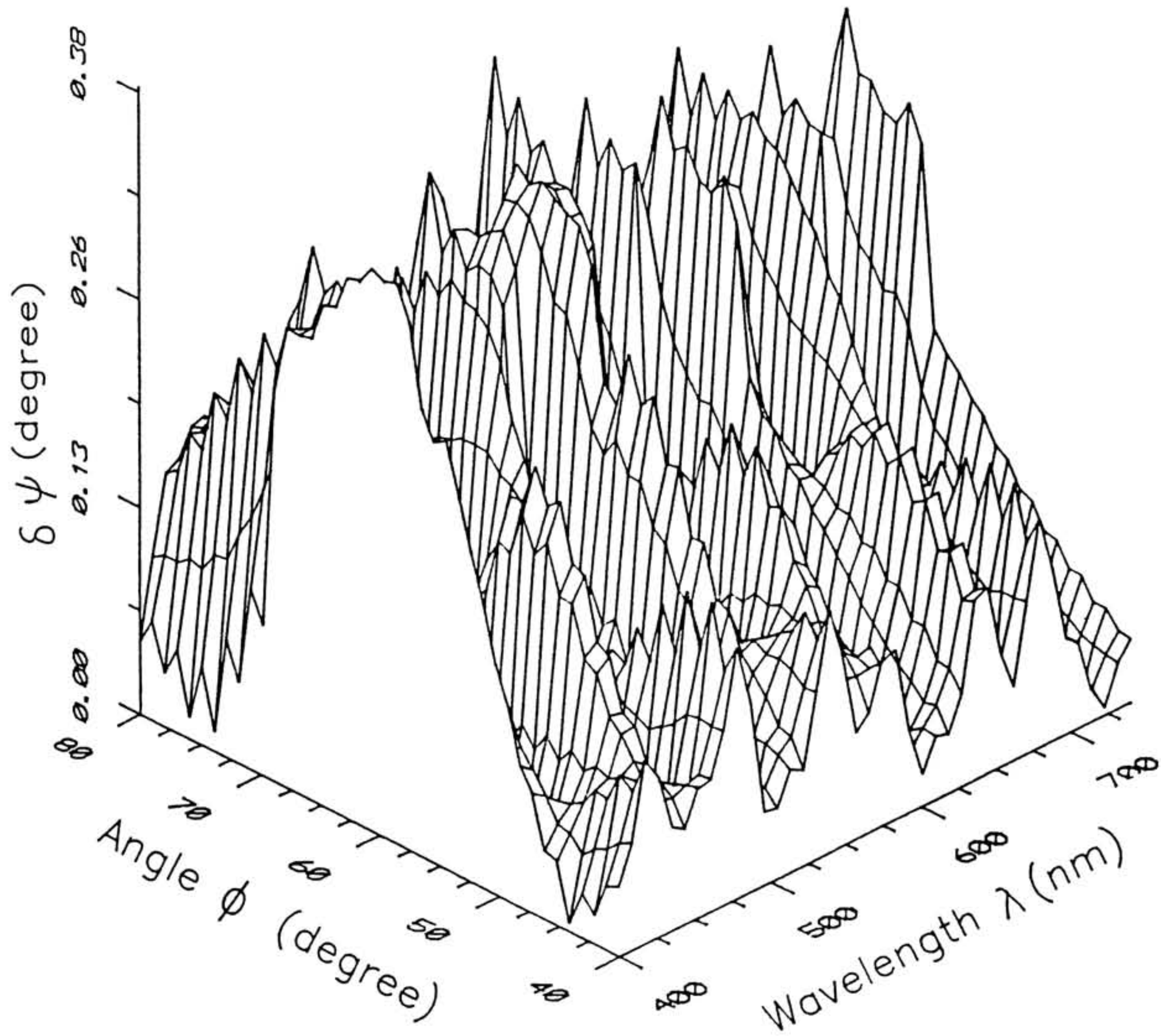

Fig. 3.12 Sensitivity ($\delta\psi$) of the ψ to the thickness of bottom SnO_2 layer in air/CdS/SnO_2/glass system. The thickness t_2 is changed by 10%. (ie., $t_2 \rightarrow t_2 + 10\% t_2$).

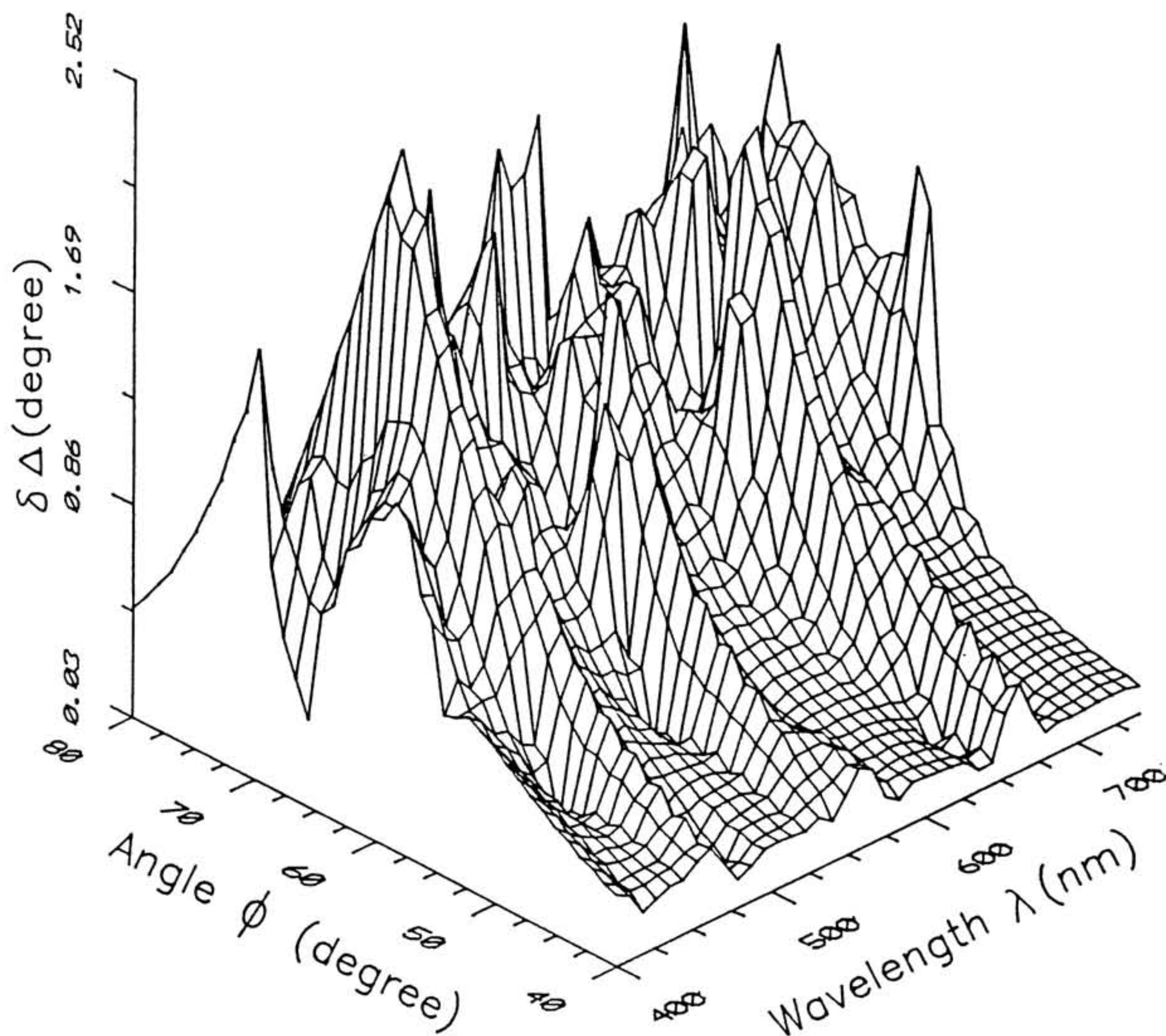

Fig. 3.13 Sensitivity (δΔ) of the Δ to the thickness of bottom SnO_2 layer in air/CdS/SnO_2/glass system. The thickness t_2 is changed by 10%. (ie., $t_2 \rightarrow t_2 + 10\%t_2$).

Sensitivity parameter	Perturbations	
	$t_1+10\%t_1$	$t_2+10\%t_2$
ϕ range for ψ	52-72°	52-74°
ϕ range for Δ	58-72°	59-70°
λ range for ψ	400-740 nm	470-740 nm
λ range for Δ	400-740 nm	470-740 nm

Table 3.2 Summary of the most sensitive regions of ϕ and λ corresponding to various perturbations in air/CdS/SnO_2/glass thin film system.

3.43 $CdS/CuInSe_2/Glass$ structure.

In a heterojunction solar cell pn junction is the most important and the studies of this junction is very much needed in the development of thin film solar cells (TFSC). $CdS/CuInSe_2$ is of current importance in TFSC. The p-type $CuInSe_2$ (CIS) acts as absorber layer and forms a junction with n-type CdS. This CdS/CIS bilayer was prepared on glass substrate by chemical bath deposition (CBD). The detailed preparation techniques of CBD for CdS and CIS are included in part II of chapter 6. The sensitivity analysis of CdS/CIS/Glass prepared by CBD technique is also conducted. Glass substrate was excluded from the optical model of the CdS/CIS/Glass system because CIS film has very high optical absorption and the light never reaches the glass substrate. The sensitivity analysis of CdS/CIS structure is performed by taking CdS thickness (t_1) equal to 50 nm. The 3D plots of this analysis are shown in Figs. 3.14 and 3.15. Table 3.3 gives the list of sensitive region of ϕ and λ of $CdS/CuInSe_2/Glass$ system corresponding to the change in top layer (CdS) thickness.

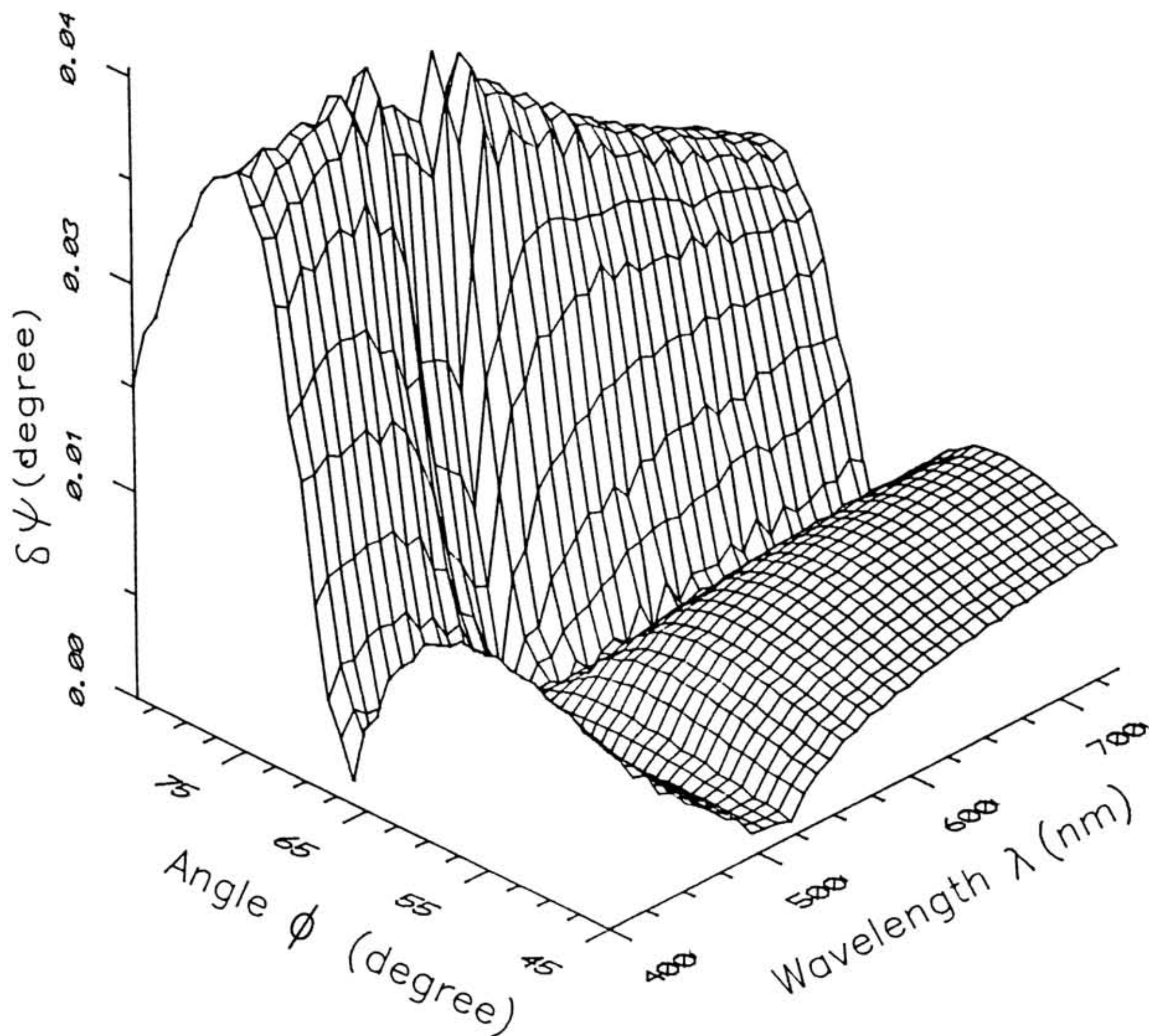

Fig. 3.14 Sensitivity ($\delta\psi$) of the ψ to the thickness of top CdS layer in air/CdS/$CuInSe_2$/glass system. The thickness t_1 is changed by 10%. (ie., $t_1 \rightarrow t_1 + 10\% t_1$).

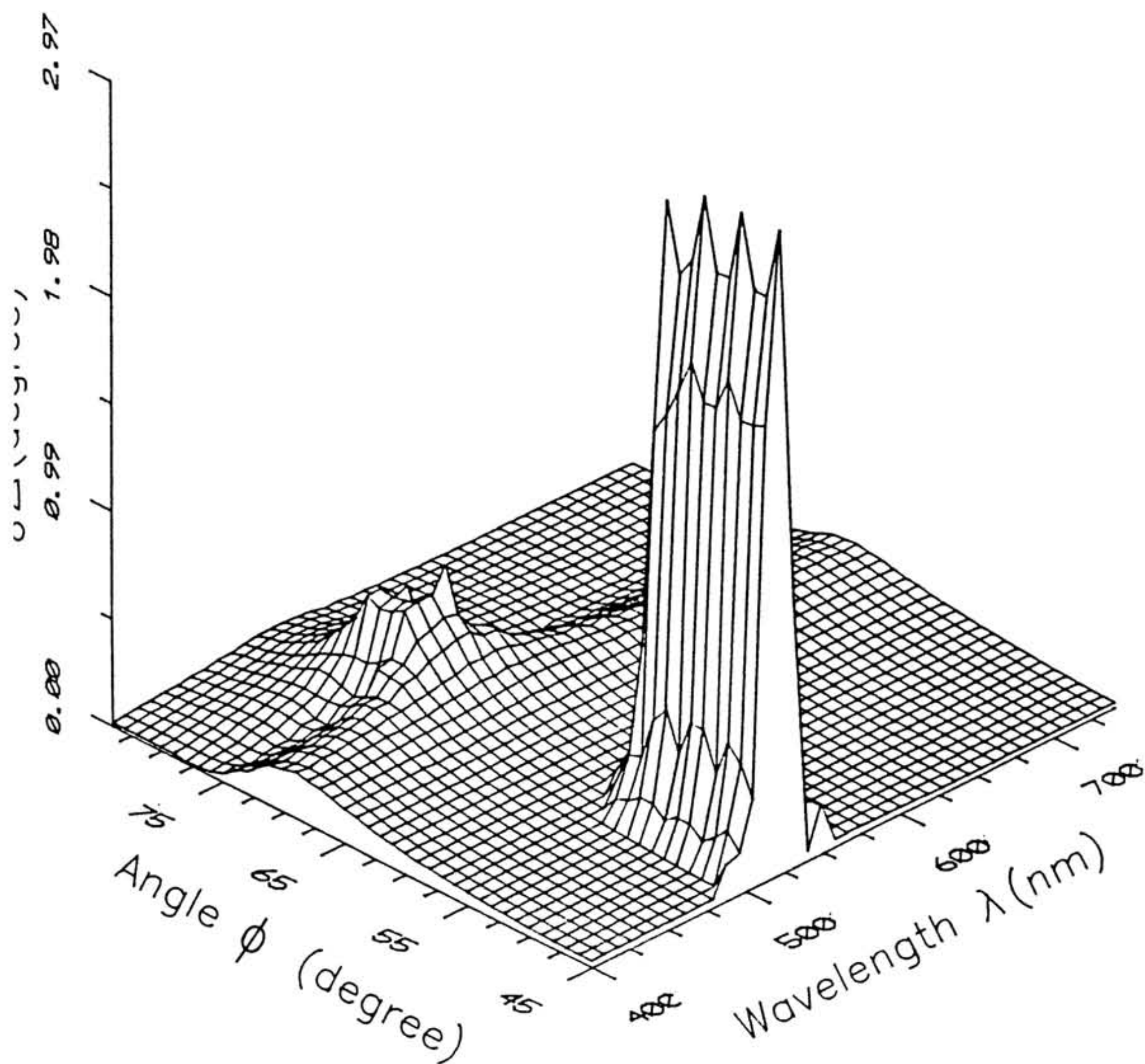

Fig.3.15 Sensitivity ($\delta\Delta$) of the Δ to the thickness of top CdS layer in air/CdS/$CuInSe_2$/glass system. The thickness t_1 is changed by 10%. (ie., $t_1 \rightarrow t_1 + 10\% t_1$).

	Perturbations
Sensitivity parameter	t_1+10%t_1
ϕ range for ψ	65-80°
ϕ range for Δ	45-55° &
	68-75°
λ range for ψ	400-740 nm
λ range for Δ	480-580 nm

Table 3.3 Summary of the most sensitive regions of ϕ and λ corresponding to various perturbations in air/CdS/$CuInSe_2$/glass thin film system.

3.5 Conclusion.

The ellipsometer is used in the two different modes,

1. Multiple Angle Incidence (MAI) ellipsometer.
2. Variable Angle Spectroscopic Ellipsometer (VASE).

The MAI mode was used for the calculation of refractive index of the film while in all other calculations VASE mode was used. In both the the techniques measurements were taken for different azimuth angles of the analyser. The minimum number of azimuth angles required for the determination of ψ and Δ was three. The details of computation technique (reverse and forward problems, optical modelling etc.) for ellipsometric calculation is included in this chapter. Different FORTRAN computer programmes were used for the MAI and VASE calculations. FORTRAN programmes were used for the optical modelling of thin film systems under investigation. The most suitable optical model was selected by minimizing the error function corresponding to the model and the parameters of the best fit optical model was taken as physical parameters of the thin film system. Along with refractive index and thickness calculations ellipsometry is used for the surface and interface analysis of single and multilayer thin film systems. The surface roughness and interface thickness are determined using present setup. Bruggeman's effective medium theory was used for the determination of volume fraction of inclusion in a mixed medium.

In the study of multilayer structures, sensitivity of the ellipsometric measurement is very important. In the present study the sensitivity of the multilayer system is enhanced by the technique suggested by Woollam. The sensitivity analysis of three thin film systems were done by this technique they are CdS/glass, CdS/SnO_2/glass and CdS/$CuInSe_2$/glass. The further ellipsometric measurements were taken at the sensitive regions of angle of incidence ϕ and wavelength λ.

References.

1. R.M.A.Azzam and N.M.Bashara. "*Ellipsometry and polarized light*", North Holland, New York. (1977).
2. J.F.Marchiando. "*A software programme for aiding the analysis of ellipsometric measurements, simple models*" *NIST Special publication* 400-83 (1989).
3. Ping Sheng. *Phys. Rev. B.* 22 (1980) 6364.
4. G.A.Niklasson, C.G.Granqvist and O.Hunderi. *Appl. Optics.* 22 (1981) 26.
5. G.W.Milton. *Appl. Phys. Lett.* **37** (1980) 300.
6. J.C.M.Garnett. *Philos. Trans. R. Soc. London.* **203** (1904) 385.
7. D.A.G.Bruggeman. *Ann. Phys. (Leipzig)* **24** (1935) 636.
8. A.Bittar, S.Berthier and J.Lafait. *J.Physique* **45** (1984) 623.
9. D.E.Aspnes, J.B.Theeten and F.Hottier. *Phys. Rev. B.* 20 (1979) 3292.
10. K.P.Vijayakumar. *J. Appl. Phys.* 69 (1991) 6771.
11. M.Oikkonen. *J. Appl. Phys.* 62 (1987) 1385.
12. D.E.Aspnes, S.M.KelsoM, R.A.Logan and R.Bhat. *J. Appl Phys.* **60** (1986) 754.
13. S.Y.Kim and K.Vedam. *Appl Optics.* 25 (1986) 2013.
14. Paul G Snyder, Martin C Rost, George H Bu-Abbud, John A Woollam, Samuel A Alterovitz. *J.Appl. Phys.* **60** (1986) 3293.
15. G.H.Bu-Abbud, N.M.Bashara and John A Woollam. *This Solid Films.* 138 (1986) 27.
16. J.E.Johnson and N.M.Bashara. *J. Opt. Soc. Am.* **61** (1971) 457.
17. M.M.Ibrahim and N.M.Bashara. *J. Opt. Soc. Am.* **61** (1971) 1622.
18. G.H.Bu-Abbud and N.M.Bashara. *Appl. Optics.* **20** (1981) 3020.

19. D. E. Aspnes, J. B. Theeten and R. P. H. Chang. *J. Vac. Sci. Technol.* **16** (1976) 1374.
20. G. H. Bu-Abbud, S. A. Alterovita, N. M. Bashara and J. A. Woollam. *J. Vac. Sci. Technol.* **1**(2) (1983) 619.
21. John A Woollam, Paul G Snyder, Martin C. Rost. *This Solid Films.* **166** (1988) 317.
22. John a Woollam, Paul G Snyder, Anthony W. McCromick, A. K. Rai David Ingram and Peter P Pronko. *J. Appl. Phys.* **62** (1987) 4867.
23. Ping He and John A Woollam. *Appl. Phys. Commun.* **10** (1990) 207.
24. D. E. Aspnes and R. P. H. Chang. "*Spectroscopic ellipsometry in plasma processing*", in "*Plasma Diagnostics*". Ed Auciello O and Flamm D L, Academic press, New York (1989).
25. K. Vedam, P. J. Mc Marr and J. Narayan. *Appl. Phys. Lett.* **47** (1985) 339.
26. G. Laurence, F. Hottier and J. Hallais. *Rev. Phys. Appl.* **16** (1981) 579.
27. M. Erman and P. M. Frijlink. *Appl. Phys. Lett.* **43** (1983) 285.
28. D. E. Aspnes. *Thin Solid Films.* **89** (1982) 249.
29. B. J. Stagg and T. T. Charalampopoulos. *Appl. Optics.* **30** (1991) 4113.
30. G. E. Jellison Jr and B. C. Sales. *Appl. Optics.* 30 (1991) 4310.
31. S. Y. Kim and K. Vedam. *Thin Solid Films.* **166** (1988) 325.
32. Samul A. Alterovitz, George H. Abbud, John A. Woollam and David C. Liu. *J. Appl. Phys.* **54** (1983) 1559.

Chapter 4

ANALYSIS OF SPRAY PYROLYSED CdS THIN FILMS

4.1 Introduction.

In the last three decades large amount of work has been devoted to the study of CdS thin films in view of its potential application in the field of optoelectronics devices. Wide band gap (Eg = 2.4 eV) CdS has been used as a window material in heterojunction solar cells with several narrow band gap semiconductors like Cu_xS (Eg = 1.2 eV) [1-4], InP (Eg = 1.35 eV) [5,6], $CuInSe_2$ (Eg = 1.01 eV) [7-10], CdTe (Eg = 1.45 eV) [11-14], Si (Eg = 1.1 eV) [15] etc. CdS material also forms homojunction with i-CdS [16] and p-CdS [17]. Other optoelectronic applications of CdS have been discussed in detail by Bube [18]. These include photocells, vidicons, phosphors and electroluminesent devices, electron beam pumped lasers etc. It is also used as an optoelectronic transducer [19]. Very recently high efficient ($\geq$ 14%) single junction solar cells fabricated using this material along with $CuInSe_2$ [9] and CdTe [12] were also reported. Again in another recent publication Basol et al have reported that the chemically prepared CdS films are more ideal window material in thin film solar cells [20]. They have used very thin (~ 50 nm) films of CdS as the window in CdS/$CuInSe_2$ solar cell and have reported that this structure of solar cell leads to high efficiency [20]. Niles et al have reported that junction can be formed on CdS/CdTe thin film system with a CdS film of thickness ~ 80 nm [11]. $CuInSe_2$ and CdTe are recently gaining importance in the fabrication of low cost and high efficient thin film solar cells with CdS film due to the high absorption coefficient and optimum band gap of these materials.

The main objective of the present study of CdS film is to identify the conditions for the preparation of

polycrystalline CdS film using chemical method -spray pyrolysis- with better electrical and optical properties in order to increase the efficiency of solar cells prepared using these films. The optical properties of CdS films are determined to a large extend by the microstructure of the films [21]. The evaporated and chemically grown CdS layers deposited on glass substrates are evaluated in terms of the optical properties of the film structure. These optical properties are the major factors which affect the efficiency of thin film solar cells. Therefore the information about the refractive index (n), extinction coefficient (k) and surface roughness are very useful for the analysis of the functioning of the cells as well as the characterization. This gains importance when we consider the fact that efficiency of the solar cells based on thin film is limited mainly by the surface roughness and grain boundaries [22].

Khawaja and Tomlin have determined the optical constants (n and k) of the evaporated CdS film [23]. But there are not much works reported in the case of the CdS film prepared using the spray technique even though these films find more use in solar cell fabrication. The major difficulty faced in the optical measurements of spray coated film is the surface roughness and this can affect the measured properties of the samples. In the present case the optical characterization of the CdS films are done using ellipsometry. This technique is used for the characterization of semiconducting materials [24-27] and detailed accounts are given in chapter 2 and 3. A good number of reports are available on the electrical and structural properties of the films prepared by spray pyrolysis [28-34].

CdS films were prepared by different techniques like vacuum evaporation [35-37], sputtering [38-41], MBE [42], CVD [43, 44], screen printing [45, 46], CBD [47-50] and spray pyrolysis [51-55]. In the present study, spray pyrolysis

technique is used for the preparation of these films. The main attraction of this technique is that, like any other chemical techniques, it is very simple and is a low coast technique. Again, this technique can be easily adopted by industries for the large scale production of films having large surface area mainly for the fabrication of thin film solar cells. Another feature of the films prepared using this technique is the strong adhesion to the substrate and coherence of the film at low thickness [21].

4.2 Experiment.

4.21 Sample preparation by spray pyrolysis.

The spray pyrolysis method was first described by Chemberlin and Sakarman in 1966 for the preparation of CdS and certain other sulfide and selinide films [51]. Spray pyrolysis has been extensively used for the preparation of thin films of several compound semiconductors and it is reviewed in detail by several authors [21,56].

Spray pyrolysis involves thermally stimulated chemical reaction between the constituent ions to form the required compounds. In this technique of film preparation, solution (usually aqueous) containing the soluble salts of the constituent atoms of the compound is sprayed onto a heated substrate, in the form of fine droplets by a sprayer with the help of compressed carrier gas. Upon reaching the hot surface, these droplets undergo pyrolytic decomposition to form the film over the substrate surface. The hot substrate provides heat energy for the decomposition and subsequent recombination. The other volatile by-products and excess solvent escape in the vapor phase and are removed from the site of chemical reaction usually by using an exhaust fan. The carrier gas may or may not play an active role in the pyrolytic reaction process. (eg., carrier gas may affect the preparation of SnO_2 film and not in the case of CdS). Doping

can be easily accomplished by simply dissolving the dopant in the required quantity in the spray solution. The different factors which affect the properties of the films prepared using this technique are the nature of the substrate and its temperature, the solution composition, the gas and solution spray rate, the size of droplets, the distance of spray head to substrate, the angle of incidence of solution droplets on substrate etc. A detailed description of the growth mechanism of this type of films is given by Chopra et al [57], along with the advantages of this technique.

Fig.4.1 shows the setup of spray pyrolysis technique fabricated in our laboratory. The spray head and substrate with heater are kept inside of a closed chamber provided with an exhaust for removing the gaseous by-products and other gases. The geometry of the carrier gas and liquid nozzle mainly determines the spray pattern, size and the distribution of droplets, spray rate etc., and hence the quality of the film prepared by this technique. For this, we have tried different spray heads. A very fine capillary tube is used for carrying the solution and another tube with comparatively larger diameter is used for carrying the carrier gas. Both the tubes were intercepted at an angle around 80° which gives better results. This avoids the formation of large size droplets in the spray. In the present case a number of trials were done to optimize the spray parameters. The glass plates (substrates) which have undergone thorough cleaning with detergent, chromic acid, distilled water and finally ultrasonic cleaning were placed on a hot plate made of thick iron block, which can be heated to the required temperature with the help of a controlled heater. The temperature over the glass substrate was measured using a digital thermometer (JUMO TDAt 70, W.Germany). During the spraying procedure the temperature of the hot substrate is kept constant with an accuracy of $\pm 2^{\circ}C$.

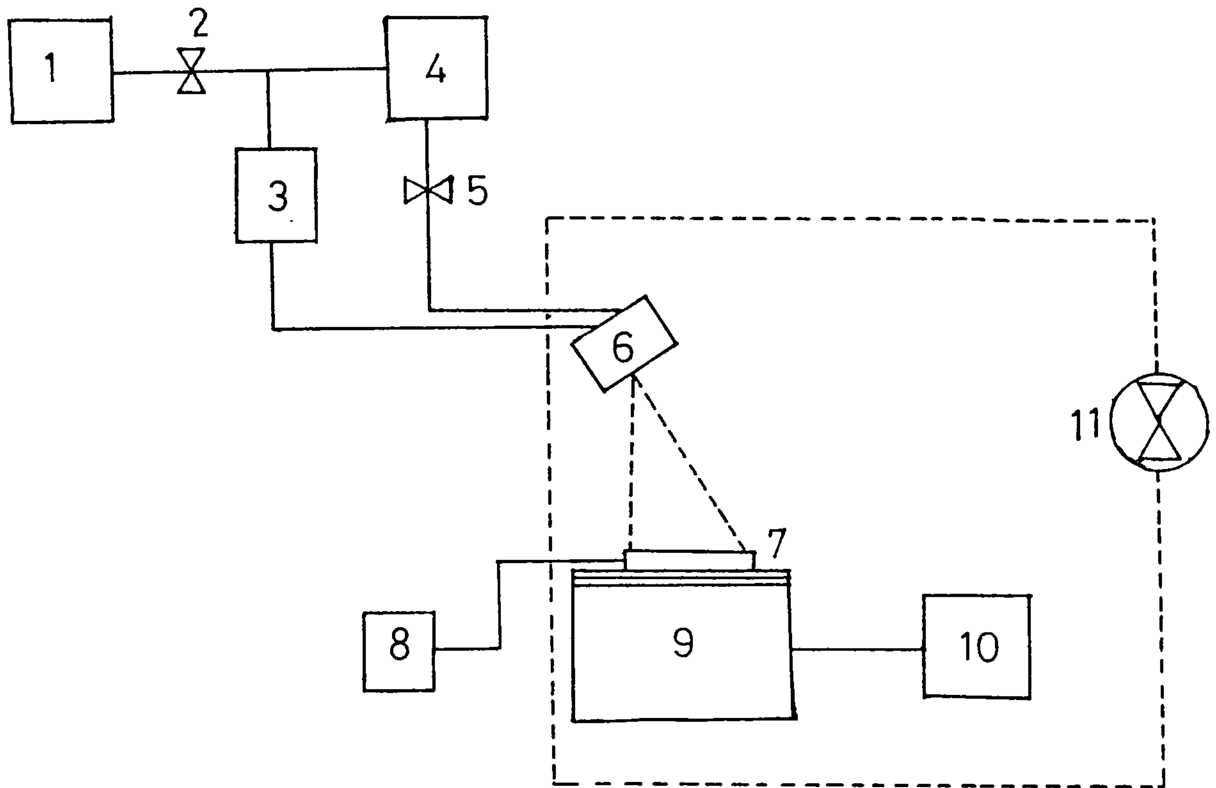

Fig. 4.1 Schematic diagram of experimental setup for spray pyrolysis coating. 1. air compressor, 2. gas flow control valve, 3. manometer, 4. solution reservoir, 5. solution flow control valve, 6. spray head, 7. substrate, 8. thermometer, 9. substrate heater, 10. heater controller and 11. exhaust fan.

The starting solution for CdS preparation was 0.01M thiourea (E. Merk, Darmstadt) and 0.01M $CdCl_2$ (Merk, Schuchardt) prepared using doubly distilled water. CdS is formed by the following chemical reaction

$$CdCl_2 + (NH_2)_2CS + 2H_2O \longrightarrow CdS + 2NH_4Cl + CO_2$$

The thickness of the prepared films were measured by gravimetric method using a microbalance and also by ellipsometry for thin CdS films. The film thickness can be controlled by the amount of solution sprayed. In the present case ~400 ml solution was used for getting ~600 nm thick film. The rate of flow of solution for the spray was ~12 ml/min and it was controlled with a valve. The size of the droplet was controlled by adjusting the pressure and gas flow rate. This was done with the help of a gas flow valve. The pressure of the air was kept around 130±1cm of Hg which was measured using a manometer connected to the gas line. The angle of incidence of the solution over the hot substrate was ~70° and the distance between the spray head and substrate was ~30 cm. The sprayed film had very good uniformity in thickness over the entire region of the sample (1X3 cm, 6 Nos. at a time). This thickness uniformity was obtained by the high scanning rate of spray head over the substrate during the deposition process. In the present case the scanning rate was ~100/min. The spray time for getting a film of thickness ~600 nm was ~35 min. CdS films were prepared at different substrate temperature in the range 200-360°C. The cooling of the samples was done in a very slow rate ie., 2°C/min.

4.22 Annealing.

Annealing of the samples was done in air, in the temperature range 100-300°C, keeping the samples at the annealing temperature for 45 min in all the cases. The

annealing chamber was made of glass which can be evacuated to rotary vacuum and the pressure was measured using a pirani gauge attached to the glass tube. The resistance wire was wound uniformly over the entire length of the chamber, inside which the thin film samples were kept for annealing. The temperature is controlled by controlling the current through the heater coil. A chromel-alumel thermocouple was used for measuring the temperature inside the glass chamber. The heating and cooling rate of all annealing were kept at the rate of 2°C/min.

4.23 Measurements.

VASE is used for the characterization of these CdS thin films prepared at different substrate temperatures and annealed at different temperatures. Detailed description of VASE as well as the experimental techniques are given in chapter 2 and the procedure for the calculation of the required film parameters using VASE is given in chapter 3. In order to avoid the back reflection from the glass/air interface during the ellipsometric measurements the samples were prepared on glass substrates with grounded back side, which is also blackened using carbon black. The ellipsometric readings of the films were taken in the angle of incidence range 60-75° with a step value 2.5° in the wavelength range 500-620 nm. These are the most sensitive regions of angle of incidence and wavelength for this thin film. The sensitivity analysis of these films are given in section 3.41 of chapter 3 and sensitivity plots are given in figures 3.4 to 3.9. In order to calculate the refractive index spectrum throughout the visible range, the ellipsometric measurements were taken in the wavelength range 400-750 nm.

Optical measurements like absorption as well as transmission were done using a double beam UV-Vis-NIR spectrophotometer (Hitachi U3410, Japan). The details of

measurements using a spectrophotometer is given in section ..521. Structural characterization of these films were done on a X-ray diffractometer as described in section 1.61. A Philips automated X-ray diffractometer (model PW 1710), using monochromated CuK$_\alpha$ (1.512 A^o) radiation was employed to obtain diffraction pattern from the films deposited on glass substrates. Composition analysis of these films was performed using X-Ray photoelectron spectroscopy (VG Scientific, England) which uses MgK$_\alpha$ (1235.4 eV X-ray source) as described in section 1.62. The preliminary surface testing of these films were done on a metallurgical optical microscope (Versamat-2, Union, Japan) and detailed morphological analysis of these films were carried out by using a scanning electron microscope (JSM JEOL, Japan) as described in section 1.63.

Sheet resistance of these films were measured using two probe technique. Aluminum electrodes were used for obtaining electrical contacts. Two thick aluminum electrodes were deposited on CdS film by vacuum evaporation as described in section 5.21. An electrometer (ECIL EA815, India) is used for the resistance measurement of the film. Using the measured sheet resistance value and known thickness of the film the resistivity of the CdS films was calculated.

4.3 Results and discussion.

4.31 Composition analysis.

The composition of the film is expected to depend on the kinetics of spray pyrolysis and the thermodynamics of the pyrolytic process. The stoichiometry of the sulfide films does not vary appreciably with metal-to-sulfur ion ratio in the spray solution [57]. At low temperature, if the pyrolytic reaction is not completed, some by-product or intermediate compound will be traped as impurities in the film. At high temperature, due to the cooling effect at the growing surface, a higher concentration of impurities are observed at the

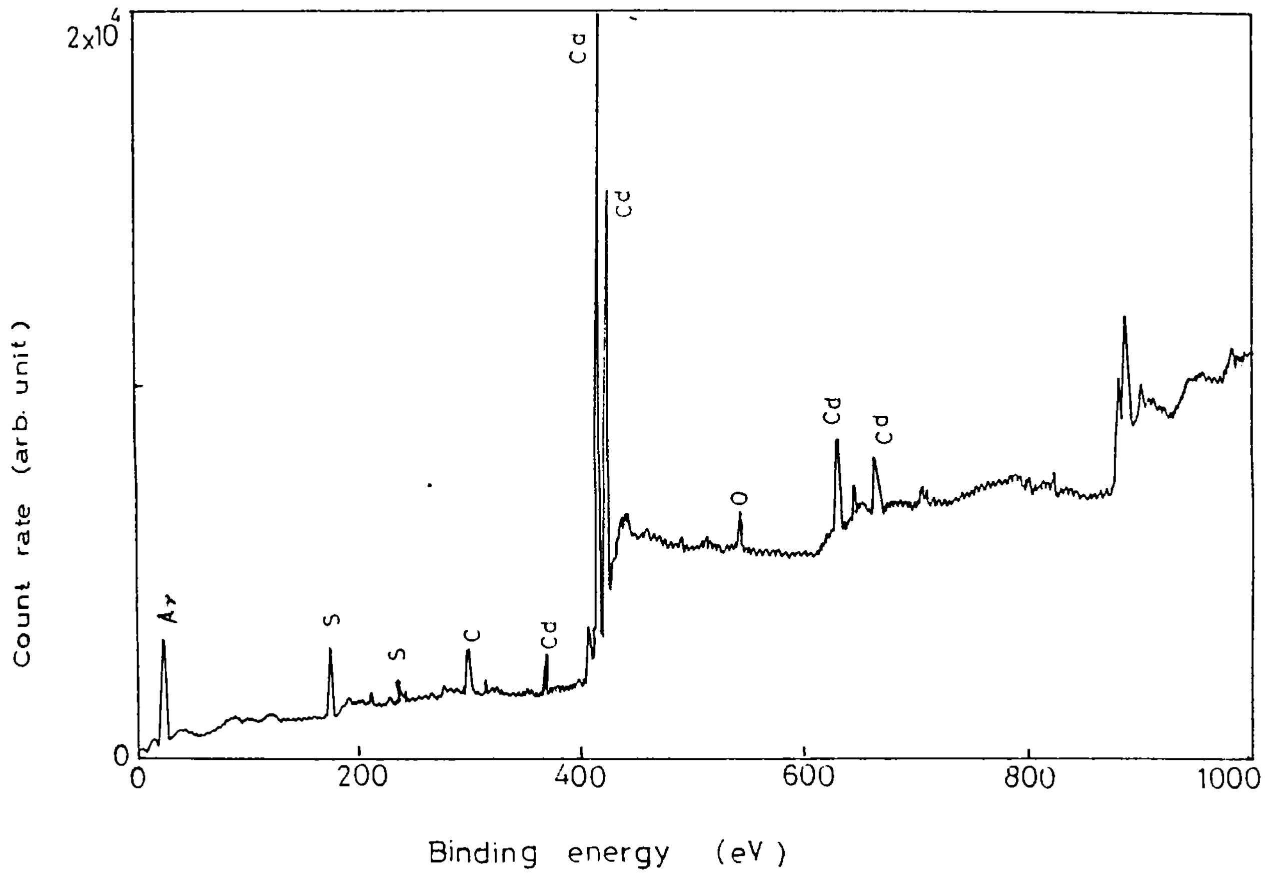

Fig. 4.2 XPS spectrum of CdS film prepared at 300°C by spray pyrolysis technique. This indicates the presence of impurities like Cl, O and C.

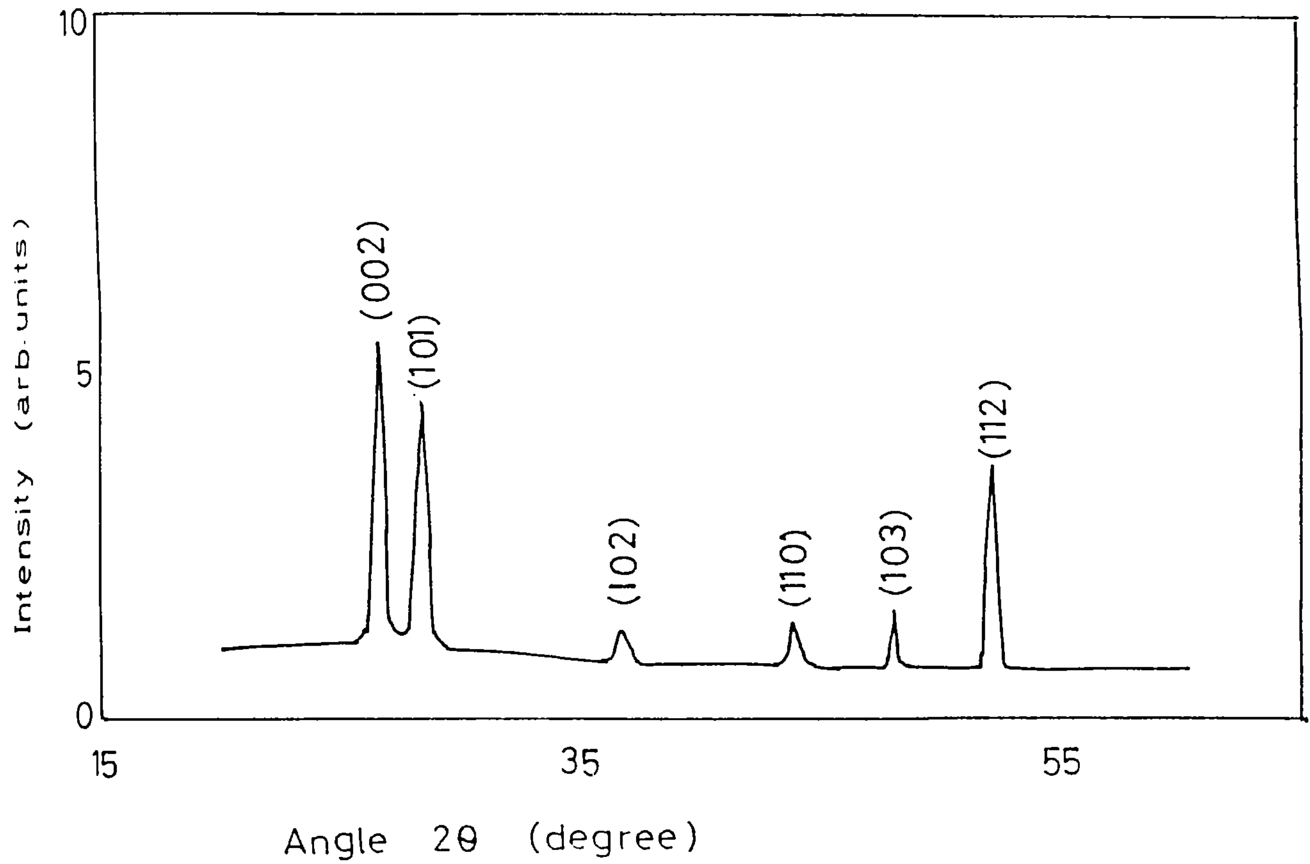

Fig.4.3 XRD spectrum of CdS film prepared at 280°C by spray pyrolysis technique.

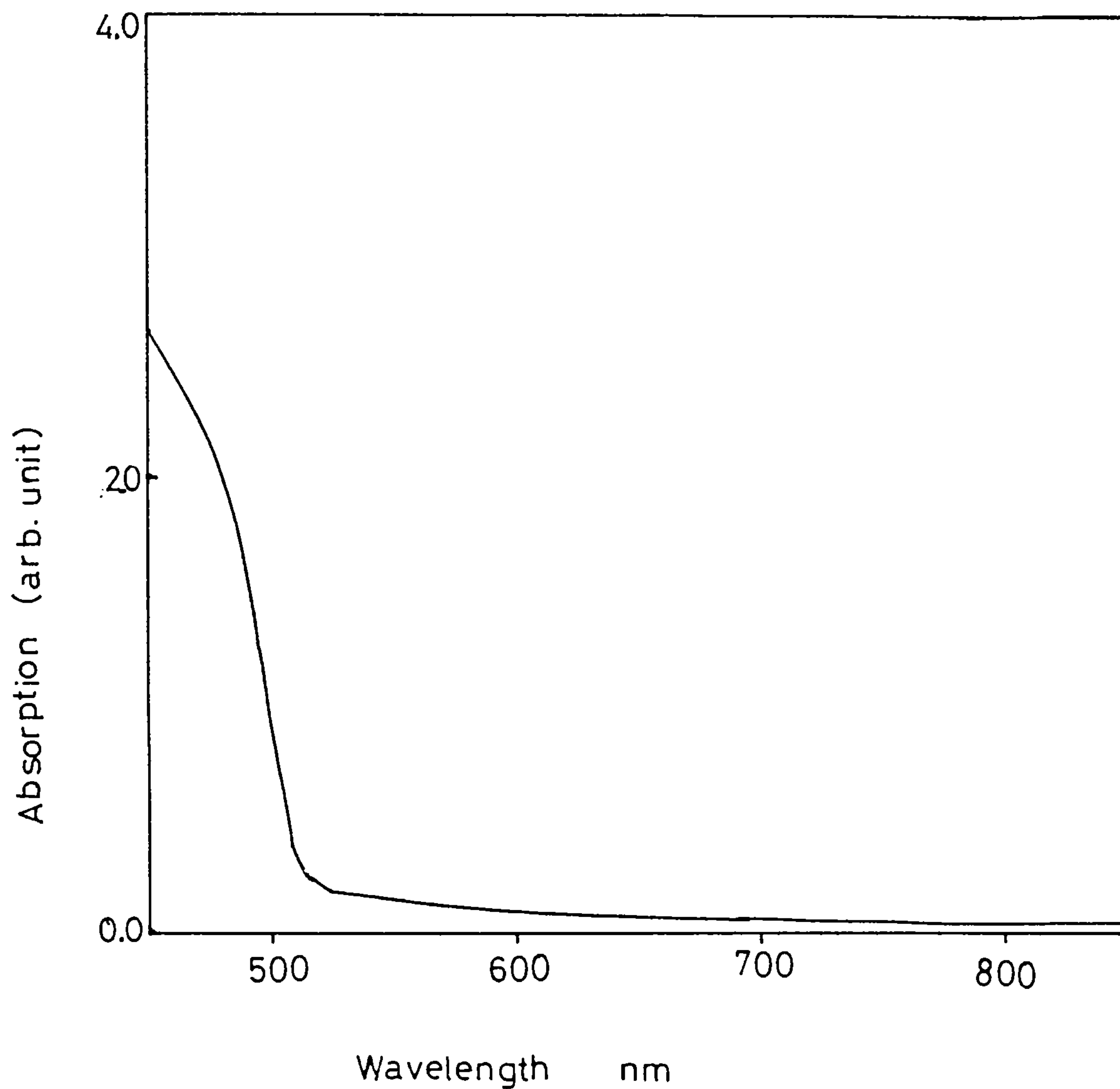

Fig. 4.4 Absorption spectrum of CdS film prepared at 280°C by spray pyrolysis technique. The figure shows that the absorption starts at 515 nm.

surface [57]. The XPS spectrum of CdS film prepared at 300°C is shown in Fig. 4.2, indicating the presence of impurities like Cl, O and C, over the surface of CdS thin film. These impurities are present in the starting solution ie., from $CdCl_2$ and thiourea. The structural and compound identification of the sprayed CdS is done by XRD. The XRD pattern shows that the films have hexagonal crystalline structure with highest peak for [002] reflection. The XRD pattern is shown in Fig. 4.3. The calculated d values of the spectrum is compared with JCPDS data cards for the structural and compound identification and is found to be in good agreement with the reported values. The band gap of the CdS film is calculated from the absorption spectrum (shown in Fig. 4.4.) and it is equal to 2.4 eV.

4.32 Surface roughness of sprayed thin film.

Different optical models were used in ellipsometric calculation of CdS thin film. The Table 4.1 gives the unbiased estimator (δ) values obtained from ellipsometric model analysis of the films with thickness >600 nm and prepared at 300°C. The preliminary optical microscopic analysis shows that this is the optimum substrate temperature for good surface CdS films. Figs. 4.5(a) to 4.5(c) show the optical micrograph of these CdS films prepared at different substrate temperatures. The different optical models selected for the ellipsometric analysis of thin film is listed below.

Model a. air/CdS/glass.

Model b. air/rough layer of CdS/CdS/glass - (air/rough CdS/CdS/glass).

Model c. air/rough layer of CdS/CdS (air/rough CdS/CdS).

The δ values tabulated in Table 4.1 shows that the model (a) has the least fitting, ie., it has the maximum deviation from the physical system. This indicates that the

optical models	estimator value δ
model a	1.970
model b	0.195
model c	0.026

Table 4.1 Unbiased estimator value (δ) of as-prepared CdS thin film for different optical models. The table shows that the model (c) air/rough CdS/CdS/[illegible] has lowest δ value.

Correlation of ψ for model (c) is 0.990

Correlation of Δ for model (c) is 0.995

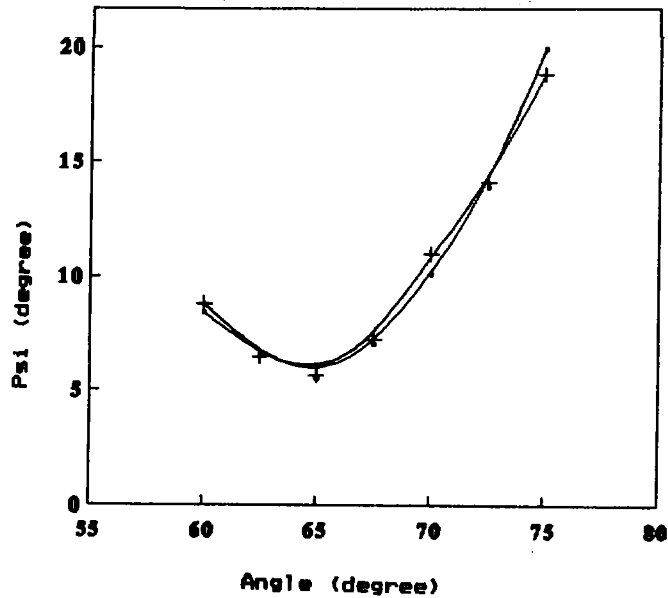

Fig.4.4a Shows the graphical fitting of ψ of air/rough CdS/CdS model (c) for the best fit value. + shows the experimental curve of ψ and • shows the theoretical curve of ψ. This graph is plotted using the ψ value corresponding to wavelength 650 nm.

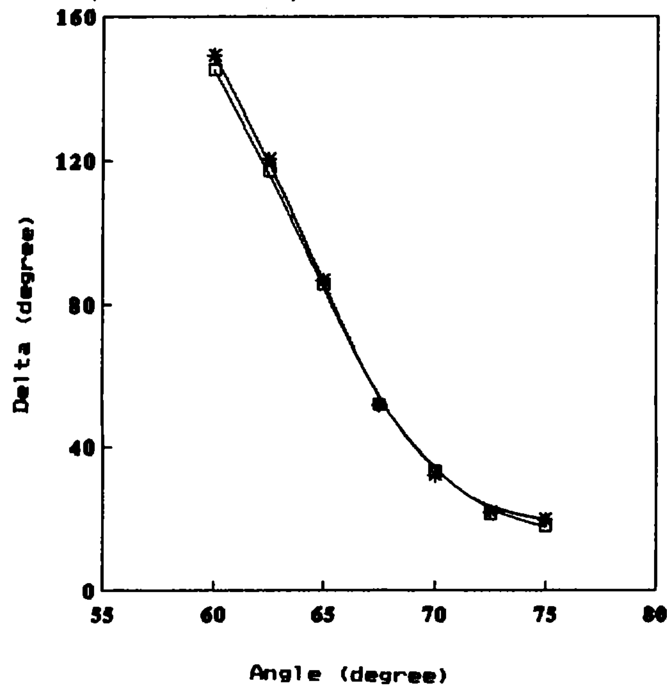

Fig.4.4b Shows the graphical fitting of Δ of air/rough CdS/CdS model (c) for the best fit value. □ shows the experimental curve of Δ and * shows the theoretical curve of Δ. This graph is plotted using the Δ value corresponding to wavelength 650 nm.

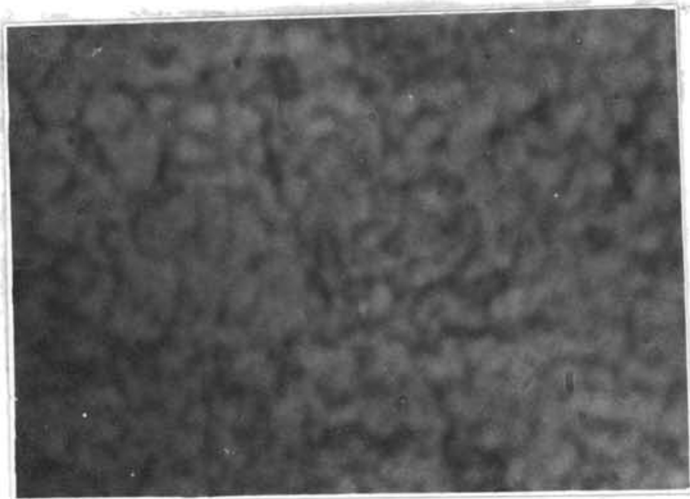
(a)

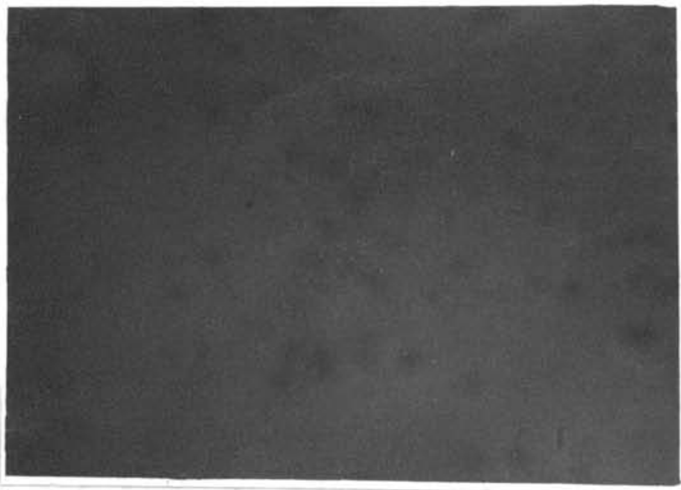
(b)

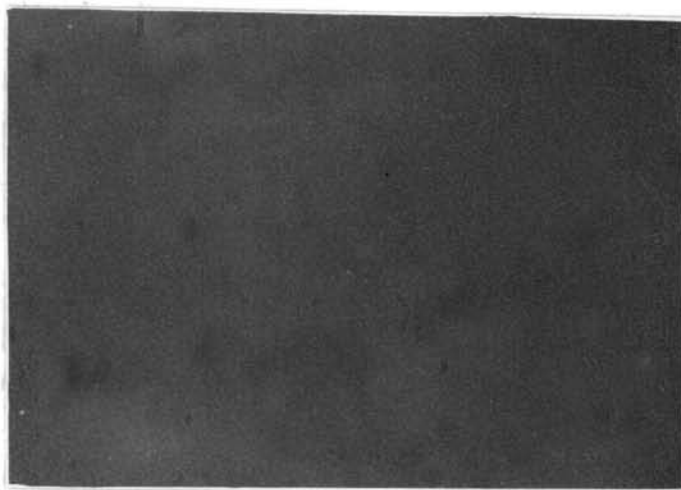
(c)

Fig. 4.5 Optical micrograph (2000X) of spray pyrolysed CdS thin film surface prepared at different temperature. (a) 200°C, (b) 300°C and (c) 360°C.

CdS film is not homogeneous with plane parallel boundaries and this may be due to the surface roughness of the film. Hence a different optical model is tried. Here one can consider the surface roughness as a hypothetical layer over the CdS surface. This layer can be considered as a mixture of air and CdS material as shown in Fig.3.3 of chapter 3. Bruggeman's EMA is used for the analysis of this layer [58,59]. In EMA the surface roughness is considered as an ambient-film mixture and the rough layer is treated as an equivalent top layer with thickness equal to the rms value of roughness and the optical constants of this layer is determined by EMA [60]. The roughness over CdS is considered as microscopic and does not scatter light. Details of this analysis is included in section 3 of chapter 3.

As the model (a) is not fitting, another model is selected. In the second model (model b) the film is considered to be having two layers. Taking into account of the surface roughness on the top of CdS layer, it is now necessary to calculate the optical constants of this layer (as shown in Fig.3.3) and this is determined by EMA using the refractive index of air and CdS material which are the constituents of this imaginary layer. The ellipsometric analysis shows that the model (b) has comparatively good accuracy than model (a). This confirms the presence of surface roughness over spray pyrolysed CdS film. After this another optical model is selected, (model c) Table 4.1 shows that this model is better compared to other two models. In this analysis, the wavelength used is in the range 500-600 nm which is found the sensitive wavelength region of CdS film structure. Relatively high optical absorption of CdS in this wavelength range may be the reason for the good accuracy of the model without glass. Due to the absorption of the light by CdS layer the reflected light from the CdS/glass interface may not be coming out and hence glass is not taken into account. The surface roughness

calculated from this analysis over different samples are in the range 25-30 (27.5±2.5) nm and the volume fraction of air in this rough layer is 0.30-0.40 (0.35±.05). All these experiments confirm the presence of rough CdS layer over the sprayed CdS film and surface roughness is taken into account of refractive index calculation.

4.321 Effect of annealing.

The Fig.4.6 shows the variation of thickness of the rough surface layer with annealing in air in the range 100-300°C. The inset of the figure shows the volume fraction of air in the top rough layer. Here also the calculations were done in the most sensitive regions of wavelength and angle of incidence. It is observed that the film annealed at 300°C has very thin surface layer while annealed at 200°C has the largest thickness. We have done annealing to increase the surface quality of the film, but it is observed that the initially it is disturbed and getting corrected only at around its preparation temperature. In this analysis also all the three optical models used for the surface analysis were employed. viz.,

model a (air/CdS/glass),

model b (air/rough CdS/CdS/glass).

model c. (air/rough CdS/CdS).

In all these calculations the refractive index of unannealed CdS film is used. The Table 4.2 shows the unbiased estimator (δ) value for different optical models for different annealing temperatures. It is very clear from the table that in the case of annealed film also this model (a) is not suitable while model (c) is found to be most suitable. This hints that the roughness continue to exit over annealed films.

4.33 Refractive index spectrum of CdS.

It is known that the optical properties of thin film

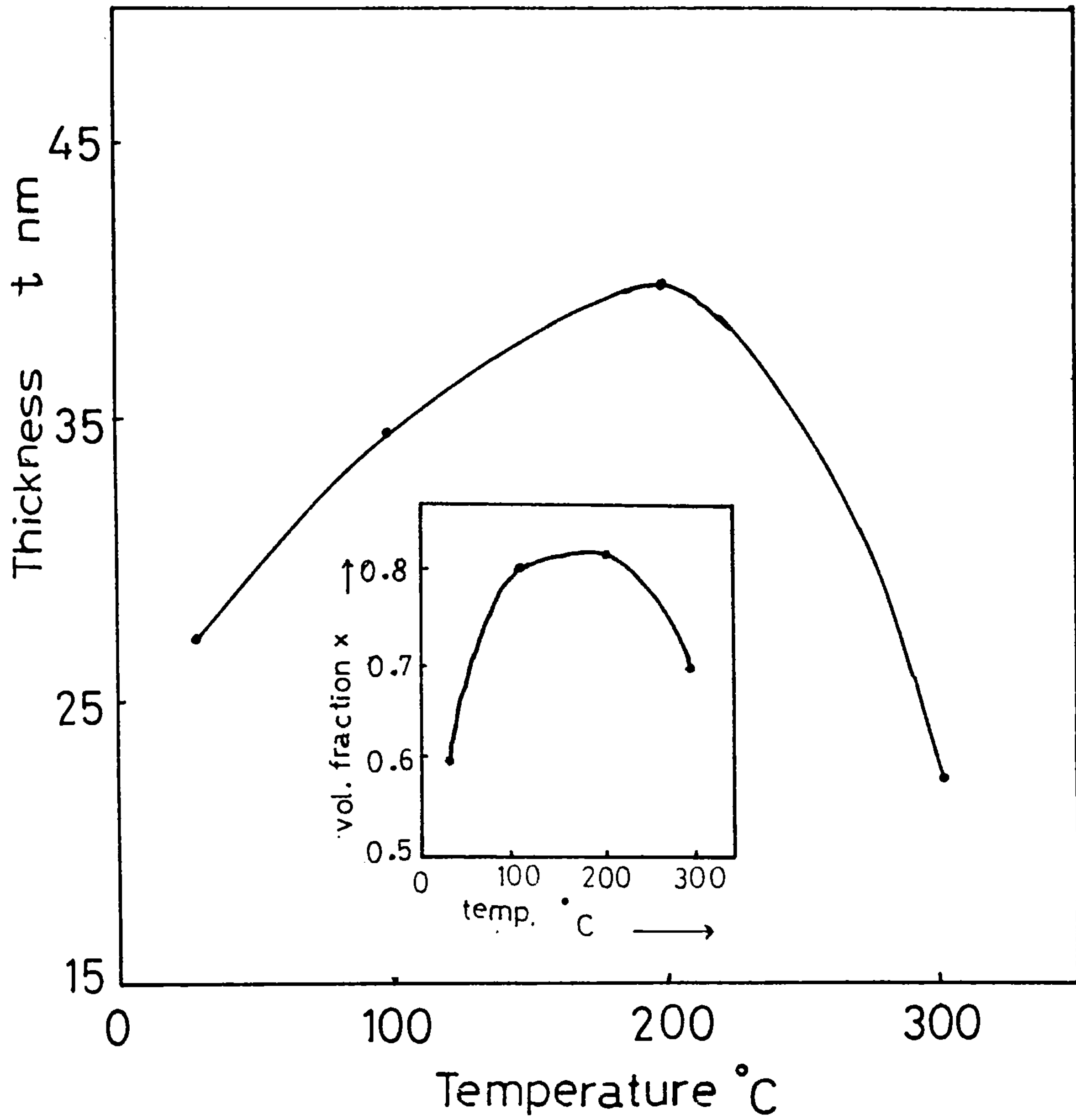

Fig. 4.6 Variation of thickness of top rough surface layer of CdS film with annealing temperature. Inset of the figure shows the volume fraction of air in rough CdS layer.

Temperature °C	estimator value δ		
	air/CdS/glass model (a)	air/rough CdS/CdS/glass model (b)	air/rough CdS/CdS model (c)
as-prepared	1.97	.195	.026
100	1.08	.197	.018
200	1.13	.172	.021
300	1.11	.206	.024

Table 4.2 Unbiased estimator value (δ) of different optical models of CdS thin film annealed at different temperatures The table shows that the model (c) air/rough CdS/CdS/... has the lowest δ value.

usually differs from those of bulk material [26]. The grain boundaries, voids, disordered regions, surface roughness and other inhomogeneities on the microstructural length scale 1-1000 nm significantly affect the UV-visible optical properties of thin films even if the films are macroscopically uniform. The role of surface roughness is also very important while doing the optical analysis of thin films [60]. The refractive index of CdS obtained in the wavelength range 400-740 nm using ellipsometer is given in Fig.4.7 and Fig.4.8. Ellipsometry is widely used for the accurate determination of refractive index of thin films because in this technique it is possible to avoid the effect of surface roughness by selecting suitable optical models. For the refractive index calculation, CdS film is considered as a double layer structure ie., the top layer as a mixture of air and bulk material (as shown in Fig.3.3). The 'effective' value of n for this layer is smaller than the bulk material due to the factors cited above. Now the refractive index spectrum of bottom CdS layer is determined, which is considered as more or less perfect. EMA is used for this analysis. Details of the EMA and refractive index calculation is given in section 3.3 The variation of n with wavelength for the sprayed CdS is shown in Fig.4.7 and this indicates that the value of n is slightly less than that of CdS film prepared by vacuum evaporation as reported by Khawaja and Tomlin [23]. This may be due to the comparatively smaller grain size of the film prepared by this technique. Basol et al have reported that chemically prepared (-CBD-) CdS thin film has low n-value in the range 1.8-2.0 [20], which is much smaller than the present values of spray coated thin films. It is also reported that the n-value of spray coated CdS film vary from one sample to another in the range 2.4-2.7 at 500 nm [61]. But in the present case we are getting repeatable n-value for a particular preparation condition. The real part of the refractive index changes considerably when the

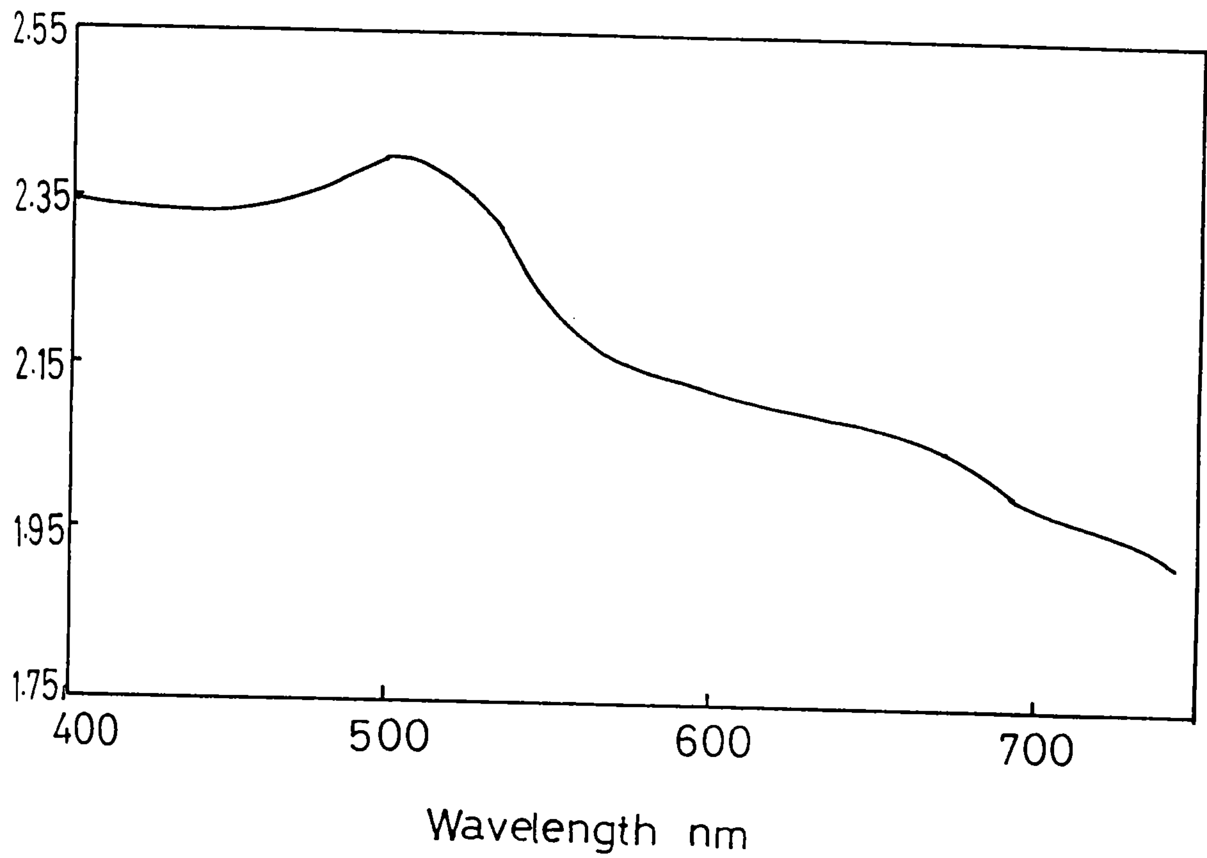

Fig. 4.7 Real part of complex refractive index (n) spectrum of CdS film prepared by spray pyrolysis technique at 300°C.

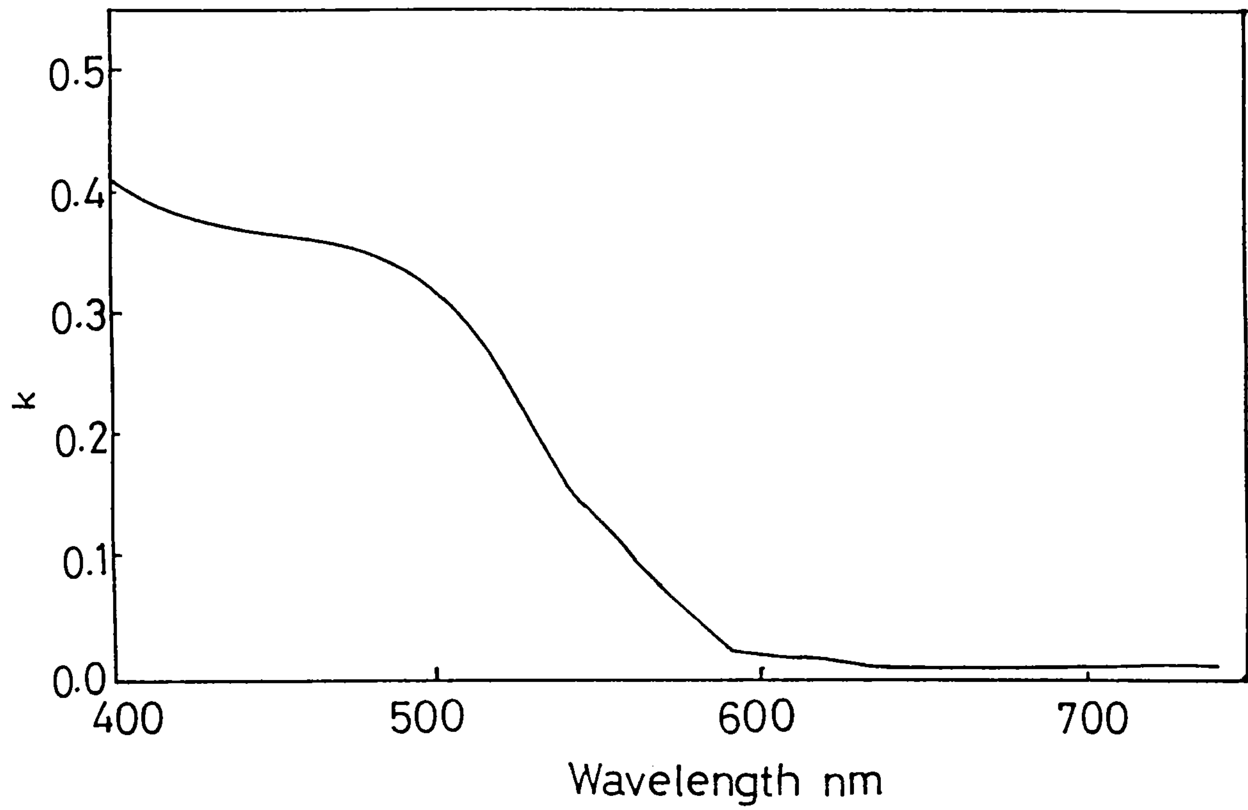

Fig. 4.8 Imaginary part of complex refractive index (k) spectrum of CdS film prepared by spray pyrolysis technique at 300°C.

preparation condition changes. For example n-value changes with substrate temperature as described in section 4.34. The optical properties of CdS films are determined to a large extent by the microstructural aspects of the film and hence by the deposition conditions. The k-value of sprayed CdS is depicted in Fig.4.8 and this observed to be slightly higher than that of the vacuum coated CdS film reported earlier [23]. In bulk material, the extinction coefficient (k) of light can be considered as the result of the absorption of light by atoms alone. In the case of thin films it is modified by other factors such as surface roughness, boundaries between grains etc. Near the absorption edge k value increases rapidly due to the high optical absorption as shown in Fig.4.4.

4.34 Optical, structural and electrical studies.

In Fig.4.9 the variation of real part (n) of complex refractive index with substrate temperature is shown for different wave lengths in the range 530-620 nm. In Fig.4.10 the variation of imaginary part (k) of complex refractive index of the same film in the same wavelength range and substrate temperature is depicted. In this case also the same technique mentioned earlier is used for the refractive index calculation. From the Fig.4.9 it is clear that the real part of refractive index of polycrystalline is lower than the bulk material. As suggested earlier this may be due to the non-perfect (grain boundaries) structure of thin films prepared by this technique. The ratio of solid volume to the total volume of the film has been termed as the packing density (p). Refractive index data is used to determine the packing density of the film using the relation [62]

$$n_f = n_b p + (1-p) n_v \quad (4.1)$$

where n_f is the refractive index of the film, n_b is the refractive index of the bulk material and n_v is that of ambient material present in surface roughness and between the

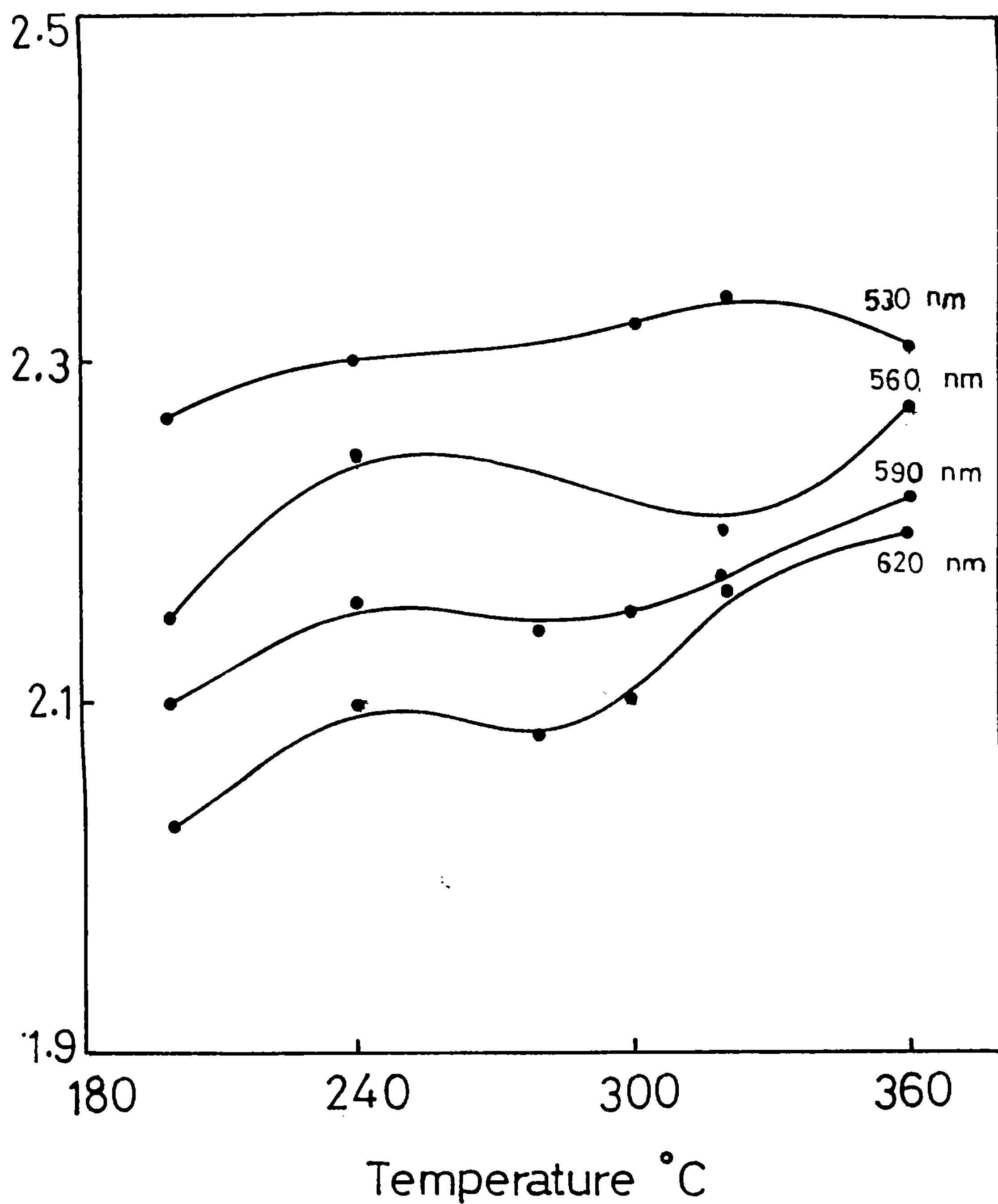

Fig. 4.9 Variation of real part of refractive index (n) with preparation temperature. 'n' increases along with the substrate temperature.

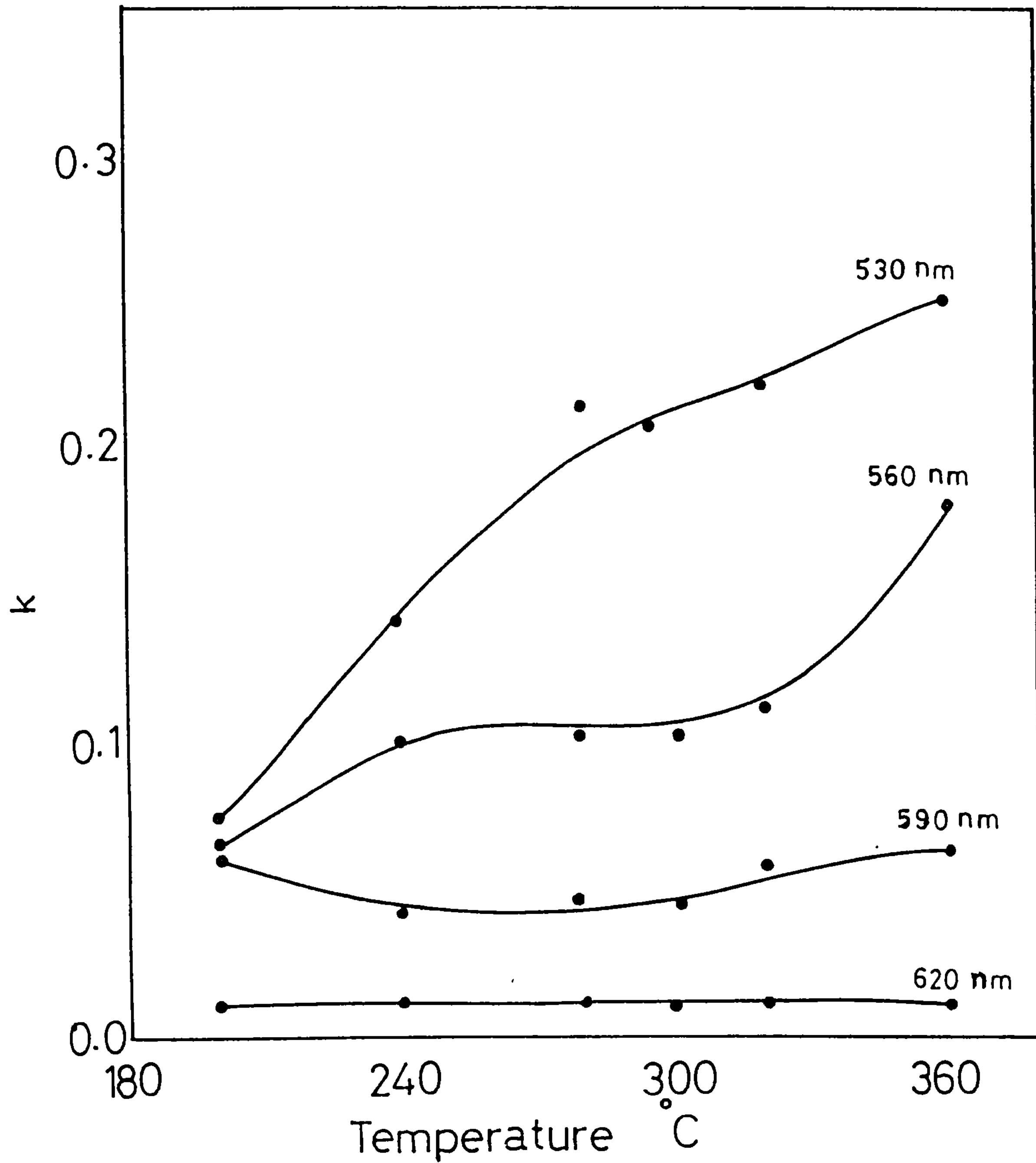

Fig. 4.10 Variation of imaginary part of refractive index (k) with preparation temperature. Near the absorption region, k shows an increase with the in substrate temperature.

grains in the boundaries, which is generally air. The packing densities of these films prepared at different substrate temperatures are given in Table 4.3. In the present studies, the calculated packing density has a higher value for the film prepared at high temperature (360°C) than that of the film prepared at low temperature (200°C) by an amount 12%. It is clear that the polycrystalline growth of the film reduces the packing density due the presence of grain boundaries. From the Fig.4.9 it can be seen that the preparation of film at comparatively lower substrate temperature leads to lower value of n and the value of n readily increases with the substrate temperature. This is due to the better crystalline quality of the film prepared at high temperature as already indicated by the packing density variation.

The Fig.4.10 depicts the variation of the imaginary part (k) of complex refractive index of these films with substrate temperature and wavelength. This shows that the k value of the film increases with substrate temperature for wavelengths near the absorption edge.

XRD spectra of these films are shown in Figs.11(a)-(e) corresponding to different substrate temperature 200, 240, 300, 320 and 360°C respectively. The XRD pattern makes it clear that the peak height corresponding to the reflection from [002] plane alone increases with substrate temperature while the height of all other peaks decreases with increase in temperature. It is to be specifically noted here that almost all other peaks other than [002] plane become very small at the preparation temperature 360°C. From the XRD spectra it can be seen that the film prepared at low temperatures have hexagonal phases and there is no preferential orientation for crystalline growth of film. Gupta et al, [63] have reported that the peak height of [002] reflection increases as the substrate temperature is increased from 300 to 500 °C. At high temperature also (360°C) the film

Temperature °C	Packing density
200	0.7207
240	0.7635
280	0.7229
300	0.7432
320	0.8108
360	0.8108

Table 4.3 Packing density of CdS film prepared at different substrate temperatures. This parameter has high value for films prepared at high substrate temperature.

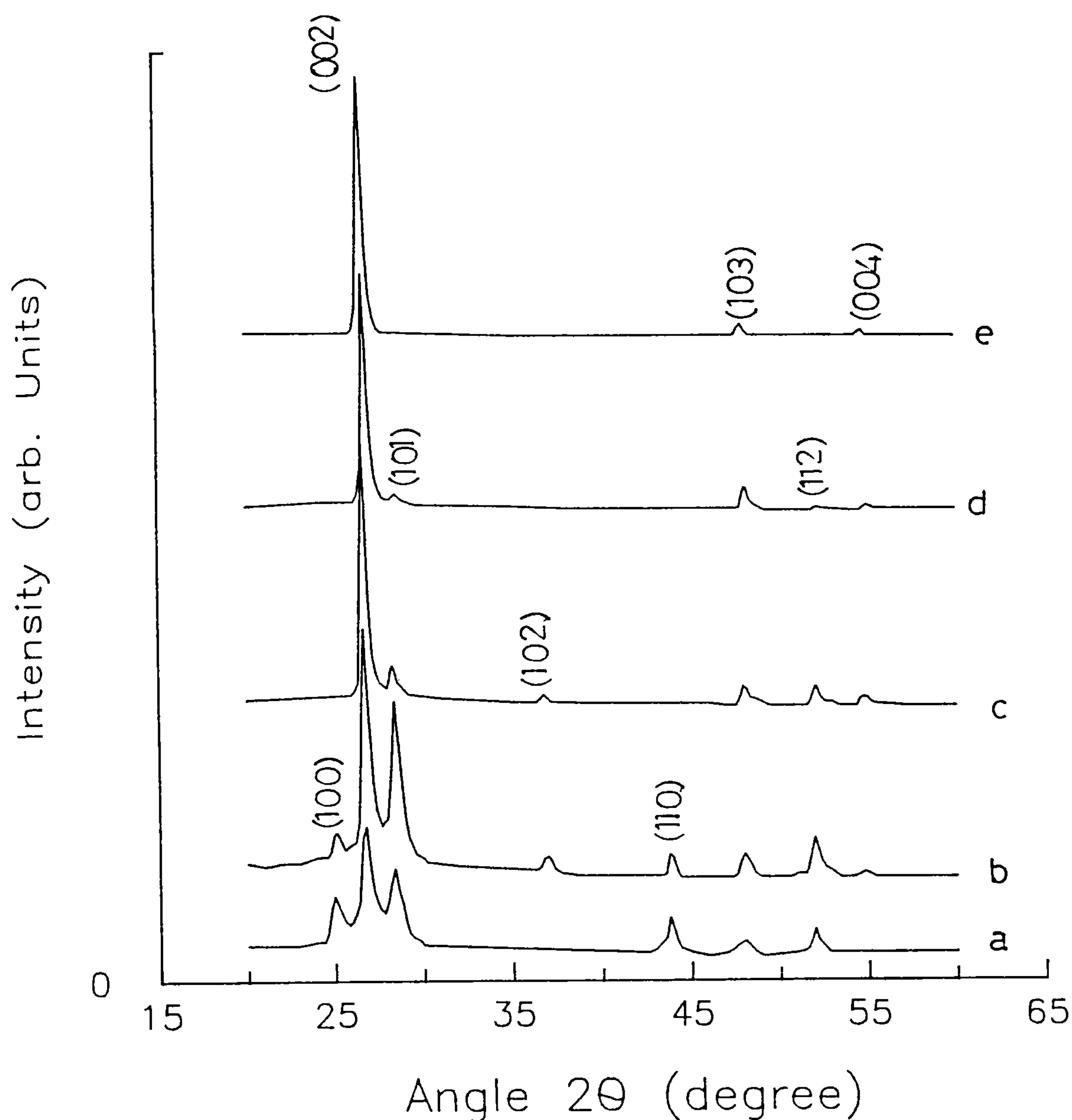

Fig. 4.11 XRD spectra of CdS film prepared by spray pyrolysis technique at different substrate temperature. (a) 200°C, (b) 240°C, (c) 300°C, (d) 320°C and (e) 360°C. The spectra show that the crystalline quality of the film becomes better with increase in preparation temperature.

Preparation temperature °C	Grain size of CdS in (micron)
200	1.24
240	2.02
300	2.95
320	3.10
360	3.10

Table 4.3(a). Variation of grain size of CdS film with preparation temperature.

Scherrer's formula [66] was used for the calculation of grain size from the XRD pattern given in Fig.4.11.

$$L = k\lambda/\beta\cos\theta$$

where k is constant approximately equal to unity, λ is the avelength of X-ray used, θ is the angle and β is the width easured in radians at an intensity equal to half maximum ntensity of the peak.

has mainly hexagonal structure and it has [002] preferential growth. CdS can exist in a hexagonal (wurtzite) structure or in zinc blend or rocksalt cubic structure. Ma and Bube recorded the XRD pattern of CdS film prepared in the temperature range 322-500°C [64]. They have reported that below 400°C the cubic structure is stable. However Banerjee et al [52] have reported that crystallographic structure of spray pyrolysed film does not depend upon deposition temperature in contrast to evaporated films where it is sensitive to the deposition temperature. In our studies also it is observed that films prepared in the temperature range 200-360°C have hexagonal structure and there is no indication of the presence of cubic structure.

The XRD pattern also shows that the grain size of the polycrystalline film increases with substrate temperature and above 300°C the film has comparatively large grain size. These results are supporting the VASE analysis on packing density, which is also indicating that the grain size is increasing with substrate temperature.

The Fig.4.12 shows the variation of resistivity of the CdS film prepared at different temperatures. The electrical resistivity of the film is calculated (using Eq. 5.1) as described in section 5.35.This study indicates that the resistivity reduces considerably for the films prepared above 300°C. (The variation of resistivity is from 10^4 Ω cm to 10^2 Ω cm). It has been observed that above 300°C the crystalline quality of the film increases. The better crystalline quality may be the reason for the high conductivity of the film measured at low ambient light. The fundamental advantage of polycrystalline thin films over others is its high mobility-life time product [47]. The better crystalline quality of CdS film prepared at high temperature may cause an increase in the mobility of charge carriers and this in turns may result in the low resistivity of the film

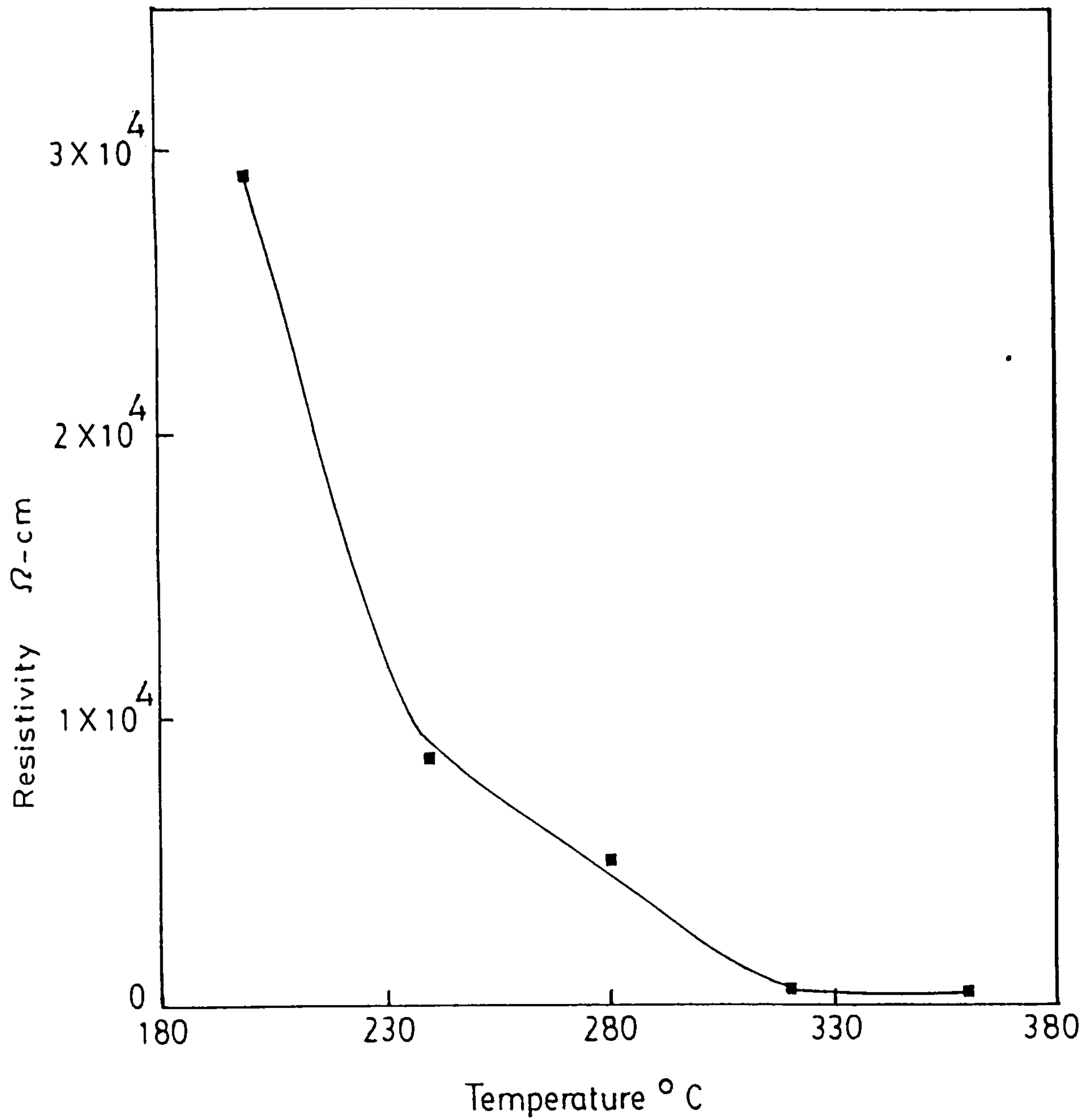

Fig. 4.12 Variation of resistivity of spray pyrolysed CdS film at different substrate temperature. The film has very low resistivity at high temperature.

prepared at high temperature.

4.35 Deposition rate and surface topography.

The Fig.4.13 gives the variation of thickness of the rough surface layer over the CdS film prepared at different temperatures. Figs.4.14(a)-(f) show the SEM photographs of the surface of CdS film prepared at different temperature in the range 200-360°C. VASE is used for the surface roughness calculation of these CdS films. The details of the analysis is given in sections 3.3 and 4.32. From the Fig.4.13 it is observed that the film prepared at low temperature has high surface roughness and this roughness decreases with the increase in substrate temperature. The surface roughness reaches a minimum for films prepared at 280-300°C and thereafter it increases slowly with temperature. The SEM photographs are also supporting the VASE measurements. The variation of surface roughness can be explained from the deposition mechanism of the spray coated CdS thin films.

In spray pyrolysis, the liquid droplets tend to flatten out into a disk on impact with substrate surface. The disk geometry depends on the momentum and volume of this droplets, substrate temperature and the balance of the dynamical surface energy and thermal process. The deposition process is the result of pyrolytic reaction between the decomposed reactants and evaporation of solvents. The random disk-by-disk growth, exposed to a continuous flow of pressurized liquid droplets eliminates microscopic and macroscopic voids as well as pin holes in the growing film, provided the substrate temperature is high enough to cause the complete pyrolytic reaction [54]. Fig.4.15 shows the deposition rate of CdS film at different substrate temperatures in the range 200-360°C. This figure makes it clear that the deposition rate decreases with increase in substrate temperature. At first, this occurs in a very slow

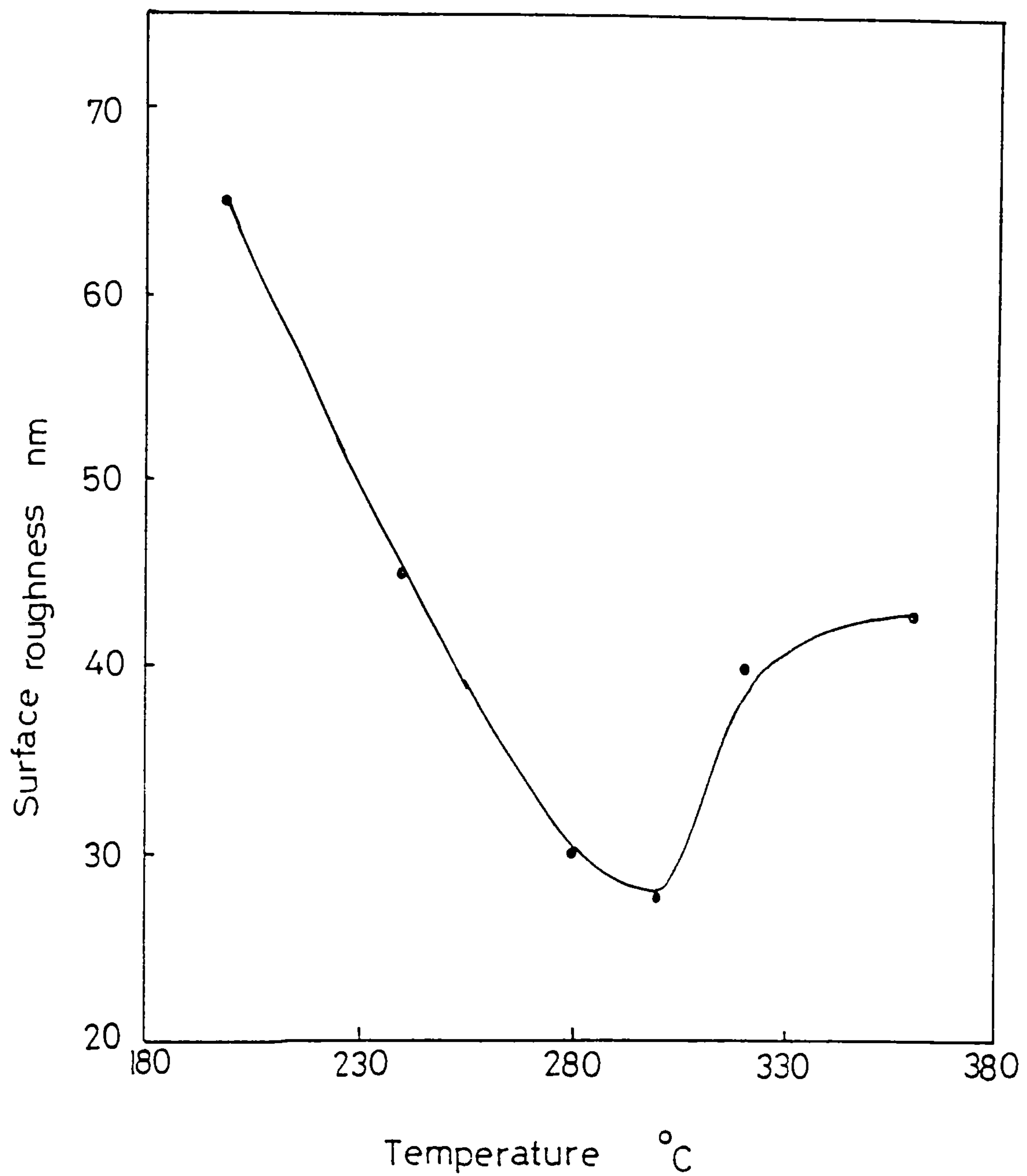

Fig.4.13 Variation of thickness of rough surface of the CdS layer with different preparation temperature. The figure shows that at medium temperature (280-300°C) the film has smooth surface.

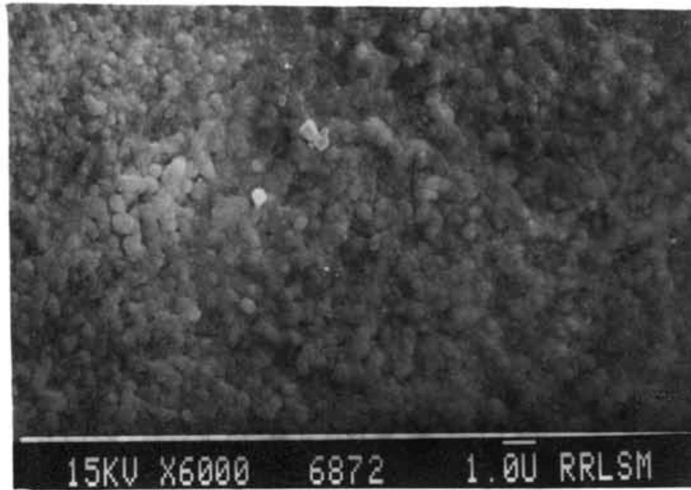

(a)

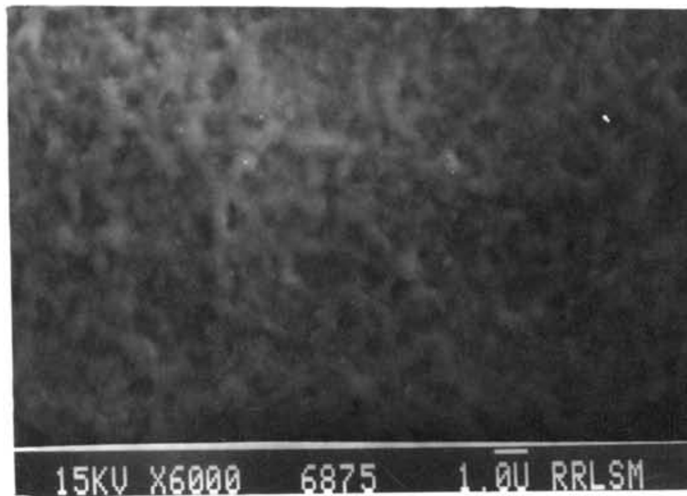

(b)

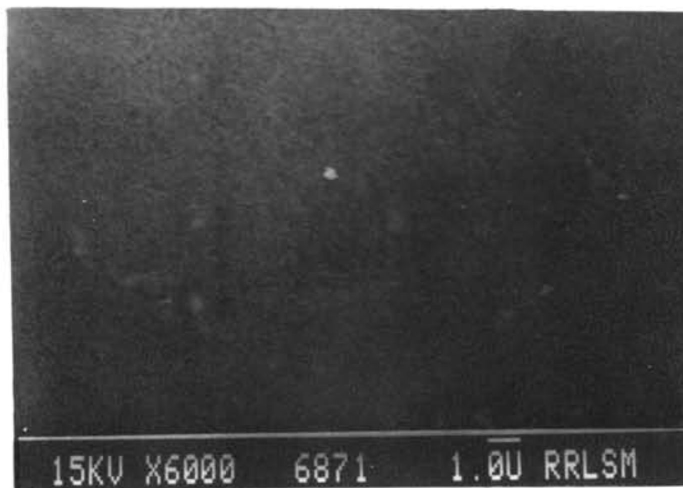

(c)

Fig. 4.14 (a-f)

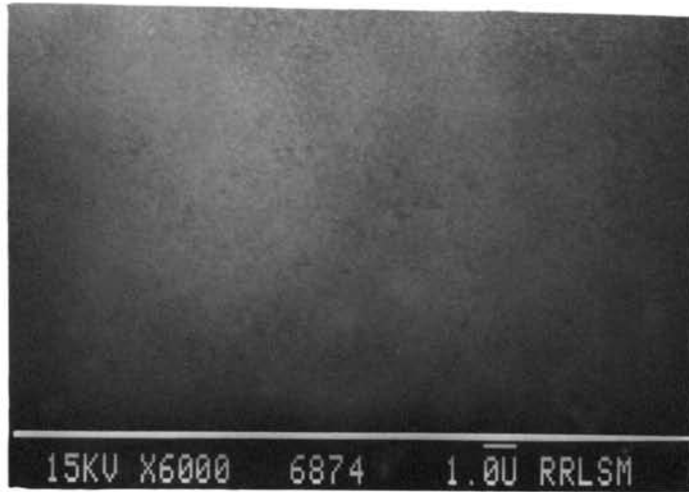

(d)

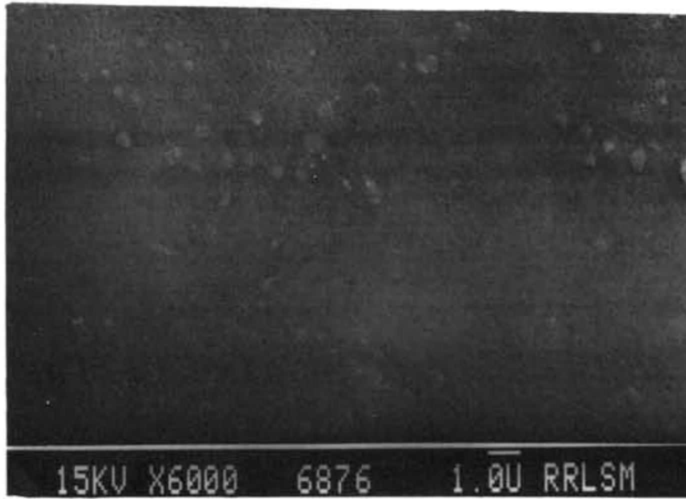

(e)

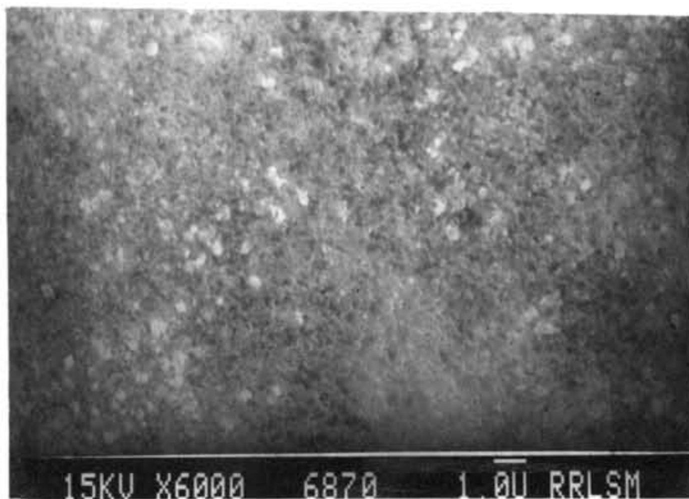

(f)

Fig. 4.14 SEM photograph of CdS film prepared at different substrate temperature. (a) film prepared at 200°C, (b) 240°C, (c) 280°C, (d) 300°C, (e) 320°C and (f) 360°C.

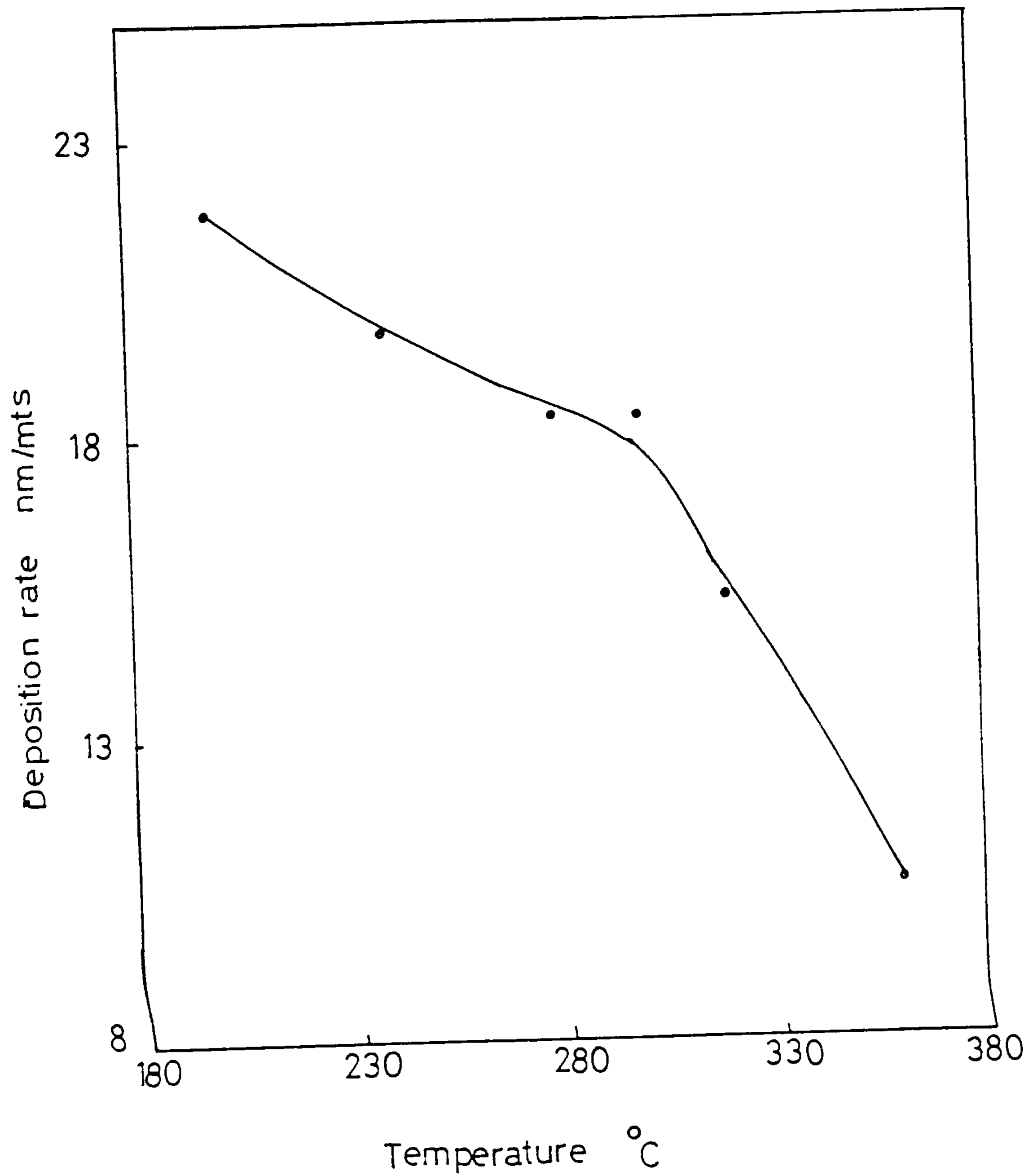

Fig.4.15 Variation of deposition rate of CdS film with different preparation temperature. It shows that above 300°C the deposition rate decreases rapidly

manner and as the substrate temperature goes above 300°C the rate of deposition decreases rapidly. In spray process, usually the generation of droplets of uniform size cannot be attained and in fact the thermal behaviour of droplets (ie., variation of size, evaporation of solvent after reaction etc.) depends on their mass and the temperature of the substrate. So one can see that the substrate temperature will readily affect the film formation process depending on the droplet size [65].

At low temperature the growth rate is very high because the size of the droplet reaching the substrate surface may be quite large. This is because of the fact that the temperature may not be sufficient to vaporize the droplets before reaching the substrate surface. Because of the vaporization of the large size of droplets over the substrate there can be considerable decrease in temperature on the substrate surface. This affects adversely the kinetics of the reaction, leading to the formation of a rough film. This is verified by VASE analysis, which shows that the surface roughness is very high at low temperature (Fig.4.13). These results are confirmed by the SEM photograph shown in Figs.4.14(a) and (b) corresponding to low temperatures 200 and 240°C respectively. As the substrate temperature is low the reaction leading to the formation of CdS may not be perfect and this may affect the grain size also. It is also inferred from the refractive index calculation as well as XRD spectrum that the grain size of these films are very small. Probably this may be the reason for the low transmission exhibited by these films (Figs.4.16(a) and (b)). This is again supported by the electrical resistivity measurements (Fig.4.12). The samples prepared at low temperature have very high resistivity ($\sim 10^4$ Ω cm) while those prepared at high temperature above 280°C shows low resistivity ($\sim 10^2$ Ω cm).

At moderately high temperature the size of the

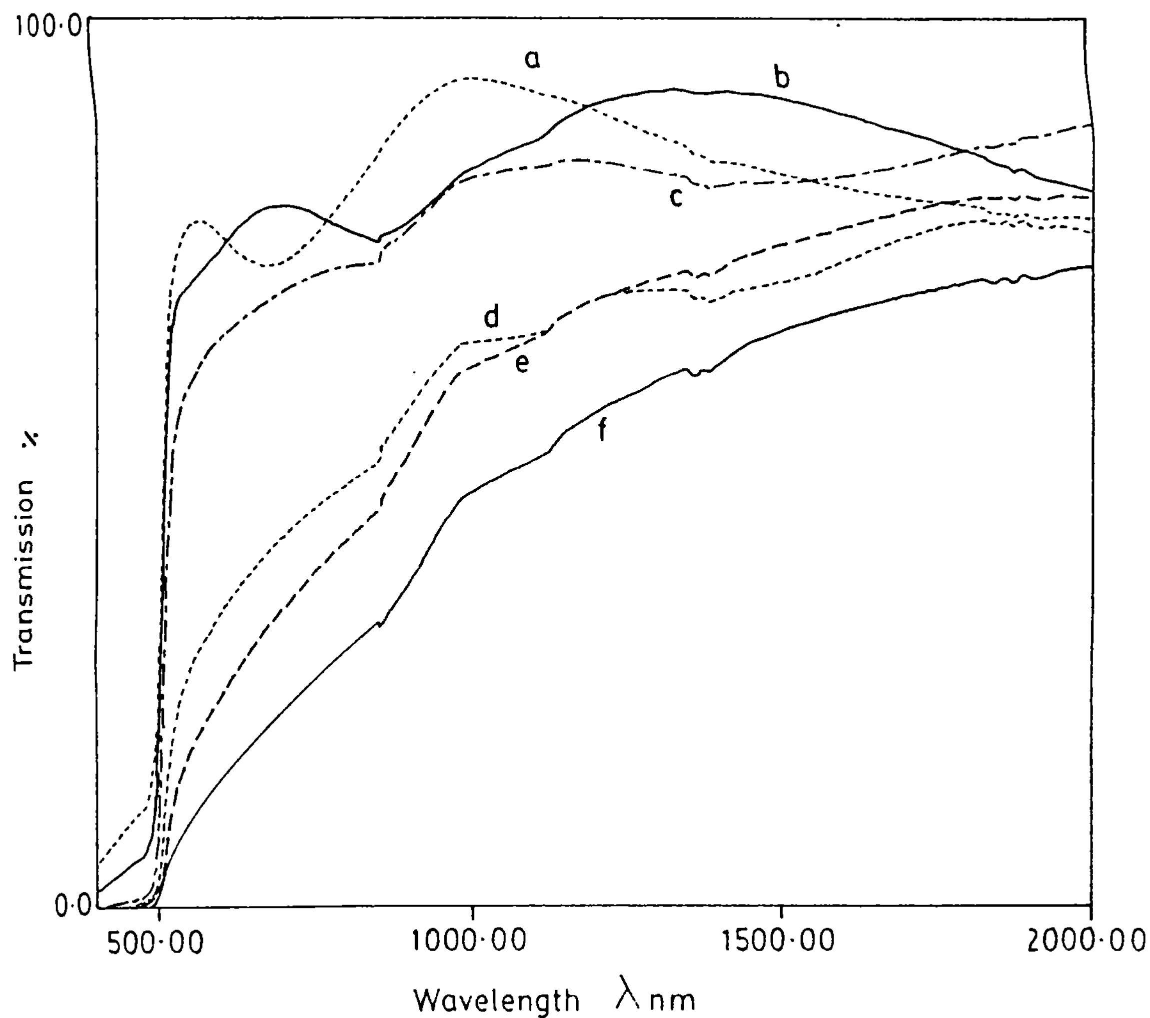

Fig. 4.16 Transmission spectrum of CdS prepared at different substrate temperatures. (a) 360°C, thickness 300 nm, (b) 320°C, thickness 230 nm, (c) 300°C, thickness 400 nm, (d) 240°C, thickness 420 nm, (e) 200°C, thickness 500 nm, (f) 170°C, thickness 500 nm.

droplets reaching the substrate may be getting further reduced due to the vaporization of solvent resulting from the higher temperature of the substrate. In this temperature range smaller droplets vaporize just over the substrate leading to the chemical reaction taking place over the substrate in a well ordered manner. Probably this is the reason for the smoothness of the film prepared at this temperature range 280-300°C as shown by SEM photographs Figs.4.14(c) and (d) and VASE analysis (Fig.4.13). These films also have good optical transmission as shown in Fig.4.16 and are possessing larger grain size as indicated by XRD spectrum and VASE analysis. As the droplet size is smaller in this case the growth rate is found to be lower and this is indicated in Fig.4.15.

At very high temperature (ie., above 300°C) smaller droplets may be vaporized to a very large extend away from substrate itself chemical reaction may occur before reaching the substrate surface resulting the formation of the compound in powder form and this does not contribute much to the growth of film. Thus the growth rate of film at very high temperature is very small as shown in Fig.4.15. More over the CdS formed above the substrate surface in powder form may just adhere to the film surface causing an increase in surface irregularities. This is indicated in SEM photograph Fig.4.14(e) and (f). The VASE also shows an increase in surface roughness of film deposited above 300°C. The XRD and VASE show that these films have large grain size. The optical spectrum shows good transmission while these exhibit very low resistivity. Hence from these studies, it is clear that critical temperature required for the film formation in spray pyrolysis is not merely linked with the chemical reaction and has connection with growth rate as well as surface nature of the film.

4.4 Conclusion.

In this chapter we have reported single layer CdS thin film preparation by spray pyrolysis technique. Spray pyrolysed CdS films were prepared from aqueous solution of 0.01M $CdCl_2$ and 0.01M thiourea. The geometry of gas and liquid nozzle largely determined the quality of the film prepared by this technique. A fine capillary tube was used for carrying the solution and another tube with comparatively large diameter was used for carrying the carrier gas and both tubes were intercepted at an angle of 80° which gave better results. The other conditions for the film preparation were (1) the substrate to spray head distance was ~30 cm, (2) angle of incidence of solution on glass substrate is ~75°, (3) spray rate of solution was ~12ml/min, (4) pressure of carrier gas was ~130 Cm of Hg and (5) the best substrate temperature for the film preparation was 280 -300°C.

Composition analysis of the CdS samples prepared by spray pyrolysis at temperature 300°C, was performed using XPS. It showed that the film contained impurities like Cl, C, and O_2. The calculated band gap of CdS is 2.4 eV. The preparation temperature had influence on the film structure. Ellipsometry was used for optimising the preparation temperature of the CdS film and it was verified using other techniques like XRD and SEM. The ellipsometric studies indicated that the film prepared by this techniques had rough surface. The roughness had very high value (65nm) for films prepared at low temperature and was having a minimum value (27nm) for films prepared at 280-300°C. Above this temperature surface roughness is also high. This VASE results were verified using SEM. The annealing of these films (prepared at 300°C) at first casuse an increase of the surface roughness with annealing temperatures and then decrease with temperature. Annealing at the preparation temperature lead to a very low surface roughness. The XRD and VASE analysis showed that the crystalline quality of the film increased with the substrate

temperature. It is observed that at low substrate temperature, the deposition rate of the CdS film is very high and this slowly decreased with increase in substrate temperature. When substrate temperature is above 300°C the growth rate again decreased drastically. Electrical and optical transmission studies showed that film prepared above 280-300°C had comparatively low resistivity and good optical transmission. All these studies indicated that the film prepared at 300°C had good quality and can be used for the fabrication of thin film solar cells. Using ellipsometer the real (n) and imaginary (k) part of complex refractive index of CdS film in the visible region (400-740nm) was also calculated by eliminating the effect of surface roughness of these film by appropriate optical modelling.

References.

1. A. Vervaet, M. Burgelman and D. Van Wassenhove. *Thin Solid Films* 151 (1987) 133.
2. A. C. Rastogi and S. Salkalchen. *J. Appl. Phys.* 58 (1985) 4442.
3. A. M. Al Dhafiri, P. C. Pande, G. J. Russel and J. Woods. *J. Cryst. Growth.* 86 (1988) 900.
4. Jacques Vedel. *Thin Solid Films.* **111** (1984) 121.
5. J. A. Bragaganolo. *IEEE. Trans. Electron. Devices.* **ED27** (1980) 645.
6. L. M. Fraas and Y. Ma. *J. Cryst. Growth* 39 (1977) 92.
7. R. R. Arya, T. Lommasson, Fieselmann, L. Russell, L. Carr and A. Catalno. *Proc. 22nd IEEE Photovoltaic Specialist Conf.* (IEEE, New York, 1991) p 903.
8. John T Tuttle, Miguel Contreras, David S Albin and Rommel Noufi. *Proc. 22nd IEEE Photovoltaic Specialist Conf.* (IEEE, New York, 1991) p 1062.
9. Lars Stolt and Jonas Hedstrom, John Kessler, Martin Ruckh, Karl-otto Velthaus and Hans-Werner Schock. *Appl. Phys. Lett.* 62 (1993) 597.
10. R. A. Sasala and J. R. Sites. *Solar cells.* 30 (1991) 101.
11. David W Niles, Dennies Rioux and Hartmut Hochst. *J. Appl. Phys.* 79 (1993) 4586.
12. D. A. Fardig and J. E. Phillips *Proc. 22nd IEEE Photovoltaic Specialist Conf.* (IEEE, New York, 1991) p 1146.
13. B. E. Mc Candless and S. S Hegedus. *Proc. 22nd IEEE Photovoltaic Specialist Conf.* (IEEE, New York, 1991) p 967.
14. S. K. Das and G. C. Morris. *Sol. Energy Mater. Sol. Cells.* 28 (1993) 305.
15. F. M. Livigstone, W. M. Tsang, A. J. Barlow, R. De La Rue and W. Duncan. *J. Phys. D. Appl. Phys.* **10** (1977) 1959.
16. Yasube Kashiwaba, Hitoshi Kirita, Hideshi Abi and Toshio Ikeda. *Jpn. J. Appl. Phys.* 29 (1990) 1733.

17. Yasube Kashiwaba, Itaru Kanno and Toshio Ikeda. *Jpn. J. Appl. Phys.* 31 (1992) 1170.

18. R.H.Bube. "*Photoconductivity of solids*". Wiely, New York, (1960).

19. S.S.Elliot, V.Domarkas and G.Wade. *IEEE Trans. Sonics Ultrasonis.* 25 (1978) 346.

20. Bluent M Basol, Vijay K Kapur and Aravind Halani. *Proc. 22nd IEEE Photovoltaic Specialist Conf.* (IEEE, New York, 1991) p 893.

21. K.L.Chopra and S.R.Das. "*Thin Film Solar Cells*". Plenum press, New York (1983) Ch. 6.

22. P.KPandya and K.L.Ckopra. "*Vacuum-Science-Thin Films*". Ed. K.L.Chopra and K.Goel. Vanity Book, Delhi (1982) p 246.

23. E.Khawaja and S.G.Tomlin. *J Phys. D Appl. Phys.* 8 (1975) 581.

24. J.Nolly, K.K.Abdullah and K.P.Vijayakumar. *Phys. Stat. Sol. (A).* 101 (1987) K35.

25. K.Vedam, P.J.Mc Marr, J.Narayan. *Appl. Phys. Lett.* **47** (1985) 339.

26. M.Oikkonen. *J. Appl. Phys.* 62 (1987) 1385.

27. Paul G Snyder, Martic C Rost, George H Bu Abbud, John A Woollam and Samuel A Alterovitz. *J. Appl. Phys.* 60 (1986) 3293.

28. Yale Y Ma and Richard H Bube. *J. ElectroChemical Soc.* **124** (1977) 1430.

29. A.G.Valyommana, K.P.Vijayakumar and C.Purushothaman. *J. Mater. Sci. Lett.* 9 (1990) 1025.

30. A.G.Valyommana. *Ph.D Thesis.* Cochin University of Science and Technology. (1992).

31. C.H.Wu and R.H.Bube. *J. Appl. Phys.* **45** (1974) 648.

32. V.P.Panov, I.I.Polezhaev and G.D.Sizova. *Soviet Phys.-Semiconductor.* 10 (1976) 1202.

33. H.L.Kwok, W.C.Siu. *Thin Solid Films.* 61 (1979) 249.

34. J.W.Orton, B.J.Goldsmith, J.A.Chapman and M.J.Powell *J. Appl. Phys.* 53 (1982) 1602.
35. A.Ashour, R.D.Gould and A.R.Ramandan. *Phys. Stat. Sol. (A)*. 125 (1991(541.
36. N.Romeo, G.Sherveglieri and L.Terrcone. *Thin Solid Films*. 55 (1978) 413.
37. F.J.Bryant, A.K. Hariri, S.Salkalachen and C.G.Scott. *J. Phys. D Appl. Phys.* 16 (1983) 1755.
38. I.Martil, G.Gonzalez-Diaz and F.Sanchez-Quesada. *Thin Solid Films*. **114** (1984) 327.
39. S.Durand. *Thin Solid Films*. **44** (1977) 43.
40. A.Piel and Murray. *Thin Solid Films*. **44** (1977) 65.
41. R.Hill. *Solid State Electron Div.* 2 (1978) s49.
42. D.C.Cameron, W.Duncan and W.M.Tsang. *Thin Solid Films*. 58 (1979) 61.
43. M.Arienzo and J.J.Loferski. *Proc. 2nd IEEE Photovoltaic Specialist Conf.* (IEEE, New York 1979) p 361.
44. A.M.Mancini, L.Vasanelli and C.De Blasi. *J. Cryst. Growth*. 79 (1986) 734.
45. A.Yoshikawa and Y.Sakai. *J. Appl. Phys.* **45** (1974) 3521.
46. N.Croitoru and S.Jakobson. *Thin Solid Films*. 56 (1979) L5.
47. P.K.Nair, M.T.S.Nair, J.Campos and L.E.Sansores. *Solar Cells*. 22 (1987) 211.
48. I.Kaur, D.K.Pandya and K.L.Chopra. *J. Electrochem. soc.* 127 (1980) 943.
49. P.K.Nair, M.T.S.Nair, and J.Campos. *Solar Energy Mater.* 15 (1987) 441.
50. Hiroshi Uda, Seiji Ikegami and Hajimu Sonomura. *Jpn. J. Appl. Phys.* 29 (1990) 30.
51. R.R.Chemberlin and J.R.Sakarman. *J. Electrochem. soc.* **113** (1966) 86.
52. A.Baneerjee, P.Nath, V.D.Vankar and K.L.Chopra. *Phys. Stat. Sol. (A)* **46** (1978) 723.

53. D.S.Albin and S.H.Risbud. *Thin Solid Films. Thin Solid Films* **147** (1987) 203.

54. K.P.Vijayakumar. Bull. Mater. Sci.**14** (1991) 57

55. A.G.Valyommana, Sunny Mathew and K.P.Vijayakumar. Bull. Mater. Sci.**16** (1993) 55.

56. Joy George. "*Preparetion of thin films*" Marcel Dekker Inc., New York (1992) Ch. 8.

57. K.L.Chopra and S.R.Das. "*Thin Film Solar Cells*".Plenum press, New York (1983) Ch. 5.

58. D.A.G.Bruggeman. Ann. Phys. Leipzig. **24** (1935) 636.

59. G.A.Niklasson, C.G.Granqvist and O.Hunderi. Appl. Optics. **20** (1981) 26.

60. D.E.Aspnes and J.B.Theeten, F.Hottier. Phys. Rev. B.**20** (1979) 3292.

61. L.Escosura, E.Grarcia-Camarero, F.Arjona and F.Rueda. Solar Cells.**11** (1984) 211.

62. K.P.Mohanachandra, H.G.Shcnbhouge and J.Uchil. Phys. Stat. Sol. (A).**130** (1992) K45.

63. B.K.Gupta and O.P.Agnihotri. *Phil. Mag. B* **37** (1978) 631.

64. Yale Y Ma abd Richard H Bube. *J. Electrochem. Soc.***124** (1977) 1430.

65. W.Siefert. Thin Solid Films. **121** (1984) 275.

66. B.D.Cullity. "*Elements of X-ray diffraction*", Addison Wesley pub. comp., Reading (1967).

Chapter 5

ANALYSIS OF Cu/CdS BILAYER THIN FILMS AND PREPARATION OF p-TYPE CdS FILMS

5.1 Introduction.

Thin film photovoltaic solar cells based on CdS have received considerable attention for the economical reasons, as well as due to the feasibility of fabricating large area devices. CdS thin film is widely used as a window material in several thin film solar cells [1]. It forms heterojunction with several p-type materials such as Cu_2S [2], InP [3] CdTe [4,5], $CuInSe_2$ [6,7], Si [8] etc. It can also form homojunctions with intrinsic CdS [9] and p-type CdS [10]. Reynolds et al first observed the photovoltaic effect in CdS with several metal electrodes [11] while Hussain could observe the rectifying effect of Cu/CdS [12]. Reynolds et al [13] considered the device to be a metal-semiconductor junction whose response was that of CdS, modified by impurities. Woods and Champion [14] suspected an unspecified p-layer that gave rise to the pn junction. Williames et al compared the electroplated junctions of several metals on n-type CdS crystals and found that copper gave the highest response and suggested that a metal semiconductor junction was formed [15]. They assumed a model of photoemission from the copper metal into the CdS for the photovoltaic effect. Grimmeiss et al [16] showed that, for copper diffused CdS crystal, the photovoltaic phenomena can be interpreted by pn photovoltaic effect in CdS crystal. They also assumed that a p-type CdS was formed by high copper concentration and argued that a pn homojunction was formed [16]. Cusano suggested the formation of Cu_2S and the possibility of a heterojunction [17]. They produced Cu_2S/CdS heterojunction by the chemical reaction of CdS with copper ion solution ($CuCl_2$). This reaction is known as

chemiplating. Spakowski et al considered the copper sulfide over CdS to be entirely degenerate, giving the equivalent of a metal-semiconductor junction [18].

It has been generally concluded that the formation of p-type CdS is very difficult because of the self compensation effect due to the sulfur vacancies [19]. But few authors has reported the formation of p-type CdS crystals by compensation of donors with copper accepters [12,16,20] and the ion implantation of various accepters [21-23]. These authors prepared pn junction and observed rectifying characteristics and photovoltaic effects. Again Hall and Seebeek coefficients measurements gave a direct evidence for p-type conduction [20,14]. Preparation of p-type CdS thin films was reported by few authors by vapor deposition of copper over pre deposited CdS film followed by heat treatment [24]. p-CdS crystalline films were prepared by rf sputtering in argon atmosphere containing small amount of phosphine [25] and very recently by deposition of CdS film over predeposited copper film at high temperature followed by high temperature annealing [10]. Kashiwaba et al demonstrated thin film photovoltaic cell using copper diffused CdS layers [9,10]. The measurements of conductivity, the Hall and Seebeek coefficients confirm the possibility of p-type CdS due to the copper doping [10]. However so far nobody has reported p-type conduction in spray pyrolysed CdS film. This chapter gives a detailed description of the conversion of spray pyrolysed CdS films into p-type and the experiments performed for the analysis of the p-type film.

5.2 Experiment.

5.21 Cu film preparation.

Vacuum evaporation is a widely used technique for the preparation of thin films [26-29]. The home made vacuum evaporation unit consist of a bell jar (diameter 12")

evacuated using a four inch oil diffusion pump via, a baffle and diaphragm valve. The diffusion pump is backed by a rotary vacuum pump of capacity 200 Liters/minute. The diffusion pump is connected to the chamber through a liquid nitrogen trap. For the copper evaporation molybdenum boat is used as the source. The evaporation rate is controlled by adjusting the high current through the source and it is monitored using a quartz digital thickness monitor (QTC 101, Vacuum Techniques, India). High pure copper (99.999%, Koch-Light Laboratories Ltd, England) is used for the sample preparation of Cu film, which is deposited on a clean glass substrates and the thickness of the film was ~30nm.

5.22 Cu/CdS bilayer sample preparation.

CdS thin films were prepared by spray pyrolysis technique by spraying an aqueous solution of $CdCl_2$ (0.01M) and thiourea (0.01M) on a clean glass substrate kept at a high temperature of 300°C. The glass substrates were given usual cleaning procedure as described earlier using strong detergent solution, hot concentrated chromic acid and washing in doubly distilled water and finally ultrasonic cleaning. Air is used as the carrier gas and the thickness of the film is controlled by the amount of solution used. Detailed description of spray pyrolysis is given in chapter 4.

The Cu/CdS thin film systems were prepared by vacuum deposition of copper film over the spray pyrolysed CdS film at room temperature in a high vacuum coating unit at a pressure less than $1X10^{-5}$ Torr. The source to substrate distance was kept at 23 cm. The thickness of copper films was controlled using a quartz thickness monitor kept along the side of glass substrate. The rate of deposition was about 7 A°/sec, and this was achieved by keeping the current through the molybdenum source at ~120 A. The copper films were coated on unannealed (as-prepared) CdS samples and these bilayer films were later

annealed at different temperatures in the range 100-300°C. In all these experiments the thickness of CdS film was in the range 525±25 nm. The thickness of Cu film deposited over CdS samples was in the range 5 to 50 nm. These samples were labeled according to the thickness of Cu over CdS as CS005, CS010, CS011, CS015, CS020, CS027, CS030 and CS050. These represent the Cu/CdS system with as-prepared CdS of thickness ~550 nm and Cu with thickness 5, 10, 11, 15, 20, 27, 30 and 50 nm respectively.

Another set of Cu/CdS bilayer films were also prepared in which the CdS films were annealed prior to the deposition of Cu film (pre-annealing). The pre-annealing were done at different temperature in the range 100, 200 and 300°C and was done in air for 45 min. These Cu/CdS samples were labeled according to the pre-annealing temperature of CdS film. CS111, CS211 and CS311 represent Cu/CdS system fabricated on CdS film pre-annealed at 100, 200 and 300°C.

In the case of electrical measurements Al electrodes were used [30] for making electrical contacts. It is also prepared by vacuum evaporation and usually the thickness of these electrodes was kept above 300 nm. The Cu/CdS samples were also prepared by all evaporation technique. For this, at first CdS films of thickness ~500 nm were prepared on a clean glass substrate by vacuum evaporation of high pure CdS powder (Koch-Light Ltd, England). Later copper films were deposited at room temperature over this film by the same technique at room temperature as described earlier.

5.23 Annealing

Annealing of the samples were done both in air and vacuum. The details of the annealing chamber and method is described in chapter 4. Annealing in air was done at different temperatures in the range 100-300°C. Vacuum annealing of the samples was done at a pressure of $\sim 10^{-4}$ Torr inside a high

vacuum chamber at the temperature 350°C. In all the cases the annealing time was 45min while heating and cooling rates were ~2°C/min.

5.24 Ellipsometric measurements.

VASE measurements were done at room temperature as described in early chapters. Angle of incidence was in the range 57.5–75.0° with an interval of 2.5° while the wavelength was in the range 500-620 nm. These ranges were selected from the sensitivity analysis of CdS film system and its details are included in section 4 of chapter 3. For each angle of incidence full wavelength range was scanned and the total number of experimental points (s) was greater than 42. A FORTRAN programme was used for the optical modelling of the thin film system and the ellipsometric data analysis. Detailed description of ellipsometric technique and calculations are given in chapters 2 and 3.

5.25 Other techniques used for the characterization of the film.

The structural, electrical and optical behaviour of a film is very sensitive to the film composition. In the present investigation, for the characterization of the copper diffused CdS films we have used different techniques like X-ray diffractometer (Philips automated PW 1710), X-ray photoelectron spectrometer (VG Scientific England) and UV-VIS-NIR double beam spectrophotometer (Hitachi U3410) along with VASE which is used for the determination the nature and profile of copper diffusion in CdS. Hot probe and Hall effect measurements were performed for determining the type of conductivity of the doped films and the carrier concentration of heavily doped films. Electrical resistivity measurements of the samples were also conducted at room temperature in air at low ambient light. Detailed description of XRD, XPS and

spectrophotometer analysis is given in chapter 1.

5.3 Results

The Fig.5.1 gives the results of ellipsometric studies and it depicts the penetration of copper into CdS film due to annealing of Cu/CdS system in air at different annealing temperature. The ellipsometric analysis was done mainly to study about the nature of diffusion of copper into CdS. This is also used to measure the thickness of copper diffused CdS and the results are given in the Tables 5.1 to 5.4. It can be seen that the depth of penetration increases with increase in annealing temperature. In this case the thickness of copper film is 11 nm and that of CdS is 500 nm. The results of the other studies like XRD, XPS, absorption spectra and electrical studies are shown in Figs.5.2 to 5.10 and these readily support the results from VASE studies.

5.31 Ellipsometric analysis.

5.311 Diffusion of Cu into unannealed CdS.

Different optical models of the Cu/CdS system were used for the study of the nature of copper diffusion into CdS due to annealing at different temperature. Sample CS011 is used for this analysis. The different optical models selected for this analysis are given below. (In all the cases glass substrate is not taken into account due to the high absorption of Cu/CdS bilayer thin film system in the wavelength range used for the VASE study).

a. Cu/CdS

b. Cu/(CdS+Cu)/CdS

c. (CdS+Cu)/CdS

d. $(CdS+Cu)_1/(CdS+Cu)_2$

e. $(CdS+Cu)_1/(CdS+Cu)_2/CdS$

The Table 5.1 & 5.2 show the variation of the

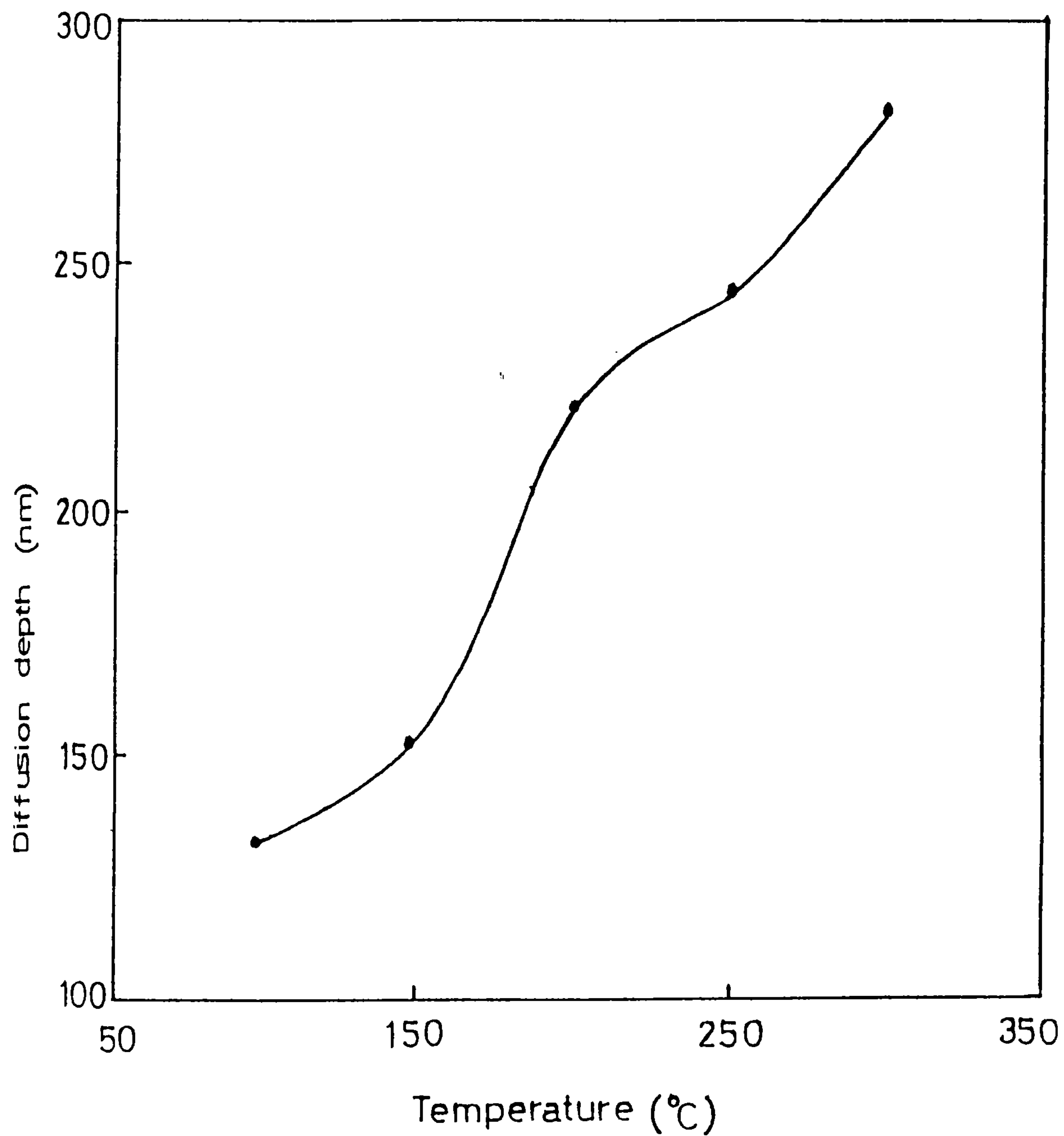

Fig.5.1 Diffusion of Cu in to CdS film due to annealing at different temperature.

Annealing Temperature °C	δ values of different Optical models				
	(a)	(b)	(c)	(d)	(e)
Un annealed	0.0944	——	——	——	——
100	0.1064	0.046	0.0160	0.0680	0.0580
150	0.3720	0.099	0.0530	0.0405	0.0183
200	0.2390	0.100	0.0620	0.0259	0.0166
250	0.4500	0.200	0.0660	0.0227	0.0080
300	0.7598	0.380	0.0107	0.0199	0.0046

Table.5.1 The variation of unbiased estimator value δ with annealing temperature for different optical models.
(a) Cu/CdS (b) Cu/(CdS+Cu)/CdS (c) (CdS+Cu)/CdS
(d). $(CdS+Cu)_1/(CdS+CdS)_2$ and (e). $(CdS+Cu)_1/(CdS+Cu)_2/CdS$.
Model (e) is the most suitable.

unbiased estimator (δ) value of different optical models of the Cu/CdS system with annealing in air at different temperatures in the range 100-300°C. At first a simple optical model is selected having Cu/CdS structure over the glass substrate. In order to select the best fit model the unbiased estimator δ derived from the ellipsometric analysis [31] is used. The low value of the unbiased estimator δ is an indication of best fit model. This model (a) is tried on as-prepared and annealed bilayer film systems so as to know the suitability of the model and to have an idea about the variation of Cu/CdS bilayer thin film systems due to the penetration of copper into CdS. From the unbiased estimator value, it is clear that this model is valid only for the as-prepared (unannealed) samples, which probably have a sharp Cu/CdS interface. As annealing temperature increases this model becomes unsuitable, which indicates that Cu/CdS interface is no longer well defined ie., copper diffuses into CdS. The next model selected for this analysis is (b) Cu/(CdS+Cu)/CdS. It is selected on the assumption that copper film is not fully diffused into CdS. Hence under this model the Cu/CdS system forms a three layer structure like Cu/(CdS+Cu)/CdS. The value of the estimator δ shows that this model is also not suitable for films annealed at high temperature and is comparatively suitable for films annealed at temperature upto 150°C. This result rules out the presence of copper layer over Cu/CdS bilayer system annealed at temperature above 200°C.

The next model applied is (c) (CdS+Cu)/CdS. The variations in the value of the estimator δ shows that this model gives good results especially for films annealed at temperature in the range 100-200°C, indicating that in this temperature range a thin mixed layer is formed over CdS film due to copper diffusion. Comparing the δ value of model b and c at 100°C shows that even at 100°C itself Cu diffuses into

CdS and a very thin diffused layer (Cu+CdS) is formed on the top of CdS film. Due to annealing, copper diffuses more and more into CdS with varying percentage of copper at different levels. Hence after high temperature annealing the diffused layer cannot be treated as single homogeneous layer. This is the reason of the high δ value for model (c) at high temperature. On this experience we have selected a new optical model (d) $(CdS+Cu)_1/(CdS+Cu)_2$ such that the diffused layer is treated as two layers with different amount of copper in each layer. The δ values of ellipsometric calculation shows that comparatively better accuracy and the suitability of the model becomes better as the annealing temperature increases. The high value of δ for this model at low temperature may be due to the very thin copper layer at the top or may be due to the homogeneous distribution of copper in the mixed layer. The last model selected for this analysis (model e) is $(CdS+Cu)_1/(CdS+Cu)_2/CdS$. This is on the assumption that copper does not penetrate completely into CdS film and so, there will be a thin CdS layer without any copper, at the bottom of the film near to the glass surface. The unbiased estimator value of this model shows that this model has very good accuracy especially for the film annealed at high temperature and this makes it clear that the copper has completely diffused into CdS leaving no copper layer on the top.

The volume fraction of copper in each layer is calculated using the Bruggeman's effective medium theory [32]. The section 3.3 contains the detailed aspects of the calculation of interlayer diffusion of two layers using Bruggeman's EMA. Table 5.3 gives the depth of copper diffusion into CdS and the volume fraction of copper present in the top layer of CdS. In this analysis the volume fraction of only the top layer ie., $(CdS+Cu)_1$ is calculated. This has been done in in order to reduce the number of unknown parameters in the ellipsometric analysis. Now the volume fraction of bottom

layer ie., $(CdS+Cu)_2$ is calculated and for computing this the values of thickness of the Cu layer, thickness of top layer $(CdS+Cu)_1$, its volume fraction and thickness of the second layer $(CdS+Cu)_2$ are taken to be known parameters. From the Table 5.3 it can be understood that the volume fraction of copper in the top diffused layer decreases with increase in annealing temperature. The thickness of the top layer also decreases with increase in annealing temperature. These results give an indication that more and more copper diffuse into CdS and the mixing is becoming more and more uniform at high temperature.

5.312 Effect of pre-annealing of CdS on copper diffusion.

The diffusion of Cu deposited on preannealed CdS samples was also analysed using ellipsometry. The different samples CS111, CS211 and CS311 were annealed at different temperatures in the range 100-300°C. The same analysis described in 5.311 was done in this case also. The Table 5.4 gives the results of the best optical model (e) $(CdS+Cu)_1/(CdS+Cu)_2/CdS$ of the present study and it is found that here copper diffuses to a smaller depth compared to that of unannealed CdS. Again diffusion decreases with increase in pre-annealing temperature of CdS film. This may be due to the better crystalline quality of the film annealed at high temperature. Lepley et al has reported that Cu diffusion into crystalline CdS is very slow while faster for polycrystalline and thin films [33]. In thin films grain boundaries and intergranular cracks enhance diffusion.

5.313 Effect of annealing in vacuum.

For this analysis Cu/CdS systems were prepared, as mentioned earlier, on unannealed CdS films. The Cu/CdS system with different copper thicknesses (in the range 5-50 nm) were prepared at room temperature in a high vacuum coating unit

Annealing temperature °C	Cu Diffusion (total) T nm	Cu diffusion (top layer) t nm	Volume fraction of Cu in top layer
100	130	20	0.40
150	150	25	0.10
200	220	20	0.10
250	240	17	0.05
300	280	15	0.04

Table.5.3 Variation in the thickness (T) of Cu diffused layer of [$(CdS+Cu)_1$/$(CdS+Cu)_2$] of CdS due to annealing calculated using the model (e) $(CdS+Cu)_1$/$(CdS+Cu)_2$/CdS. It also shows the thickness (t) of the top layer $(CdS+Cu)_1$ and volume fraction of Cu in this layer.

Annealing Temperature ^{o}C	δ value of optical model $(CdS+Cu)_1/(CdS+Cu)_2/CdS$	Cu diffusion (total) T nm
Unannealed	0.0046	280
100	0.0160	250
200	0.0060	200
300	0.0230	200

Table.5.4 The unbiased estimator value δ calculated using model (e) for Cu/CdS system prepared on preannealed (at different temperature) CdS film. This bilayer films are annealed at 300°C. T is the copper diffusion depth of into these samples.

over the spray coated CdS film (thickness ~ 500 nm). All these bilayer thin film systems were annealed at 350°C for 45 minutes in a vacuum of 10^{-4} Torr. In this case also different optical models were applied as described in earlier sections. From this analysis it is observed that Cu diffuses completely into CdS and uniform mixing occurs at 350°C. By doping different amount of Cu, (this was achieved by depositing Cu films of different thickness in the range 5-50 nm) it is possible to control the properties of Cu/CdS film system. The electrical and optical studies of these samples were done to study the variation of properties of CdS.

5.32 XRD analysis.

XRD is widely used as characterization technique for materials. Analysis of diffraction patterns obtained and comparison with standard JCPDS powder diffraction data can reveal the existence of different crystallographic phases in the film, their relative abundance etc. The details of XRD analysis are given in section 1.61. The Fig. 5.2 give the XRD pattern of copper film (thickness 30 nm) and CdS film (thickness 600 nm) deposited on a glass substrate respectively. In the case of CdS the main peak corresponds to that of the [002] reflection of hexagonal structure and the other peaks also correspond to the hexagonal structure of CdS. The XRD pattern of the sample CS027 annealed at 300°C is given in Fig.5.3. The Cu/CdS film having a larger thickness for copper layer is specifically selected for XRD analysis because the chance for any compound formation is very high in this case. Again it is easy to notice the formation of any compound when the layer over which the compound is formed is quite thick. The XRD pattern of annealed film shows that [002] peak is quite high in the case of annealed Cu/CdS bilayer film also. All the peaks correspond to the CdS film only (as shown in Fig.5.2(b)). The main observation in this case is that

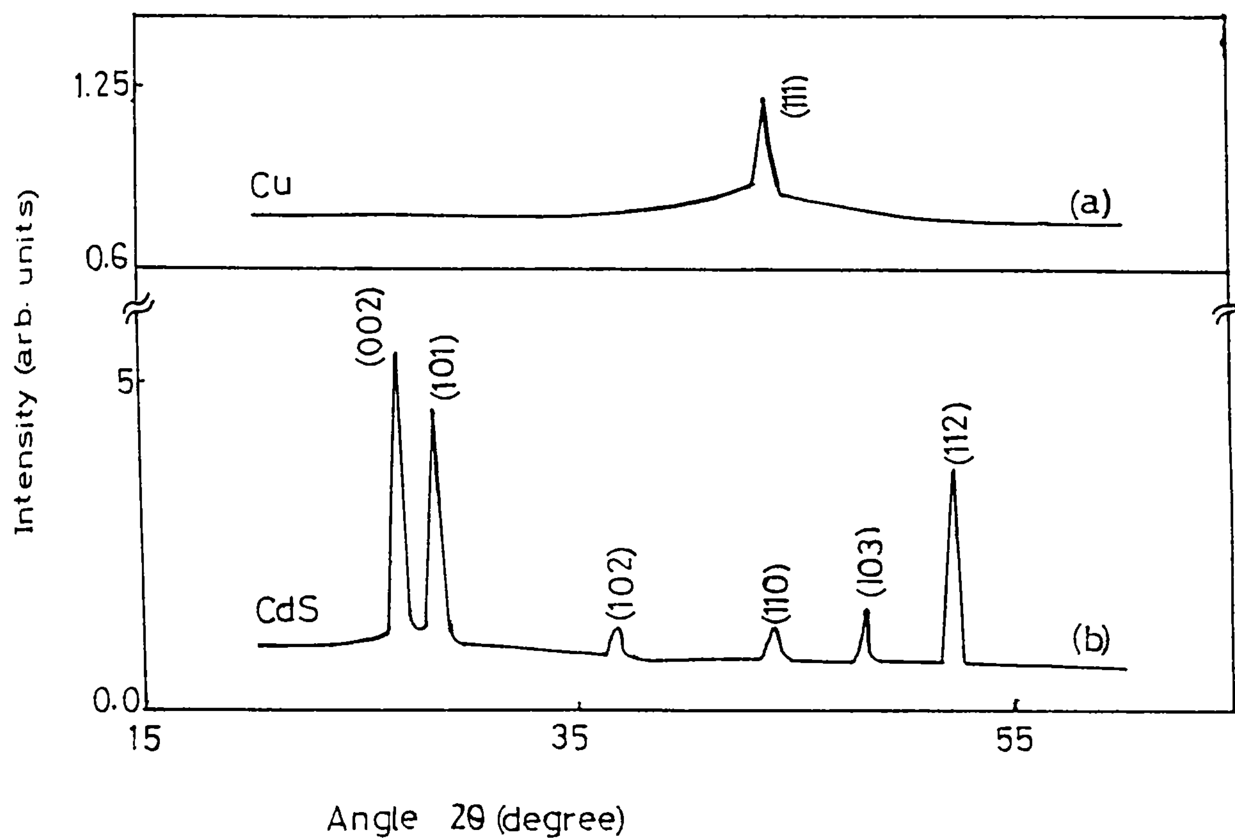

Fig.5.2 XRD spectra of Cu and CdS film. (a) Cu film (thickness 30 nm) prepared by vacuum evaporation. (b) CdS film (thickness 600 nm) prepared by spray py ysis.

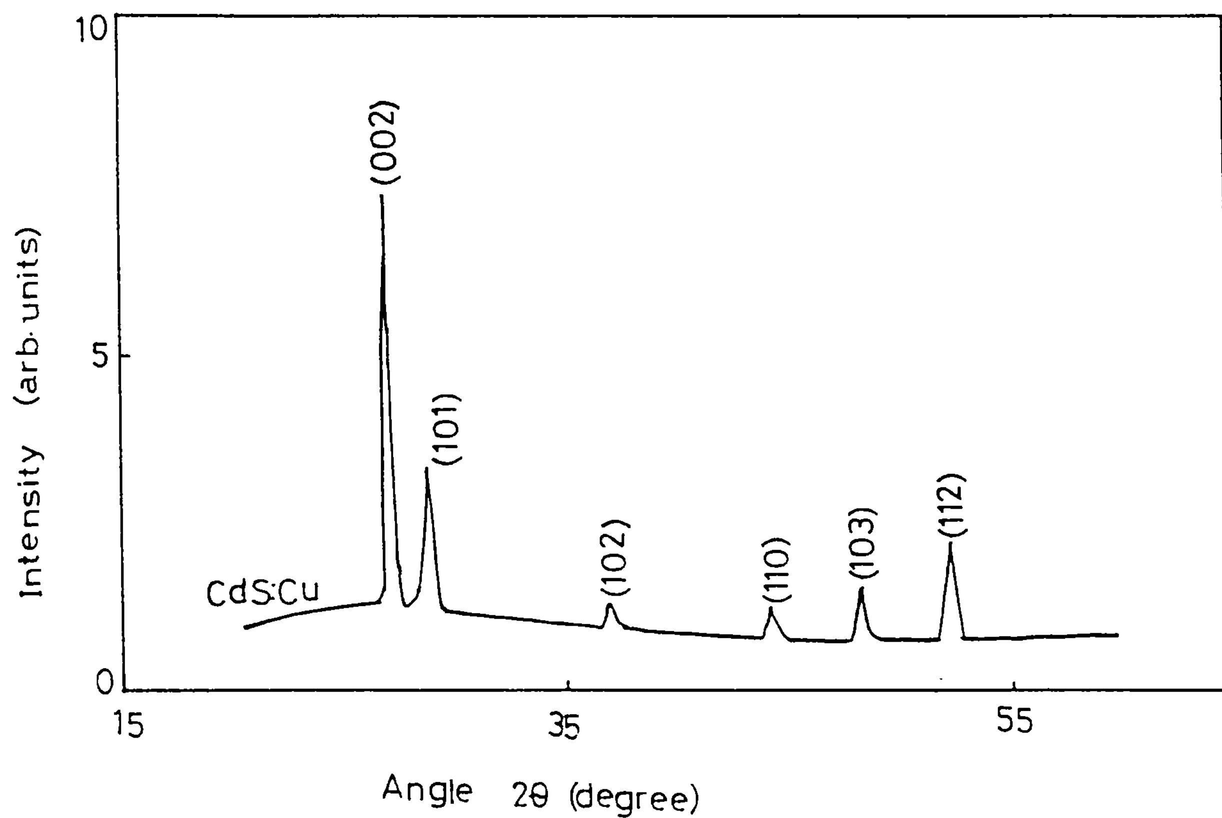

Fig.5.3 XRD spectrum of Cu doped CdS film (Cu/CdS system annealed at 300°C). All peaks correspond to CdS only.

there are no peaks corresponding to either copper or new compounds like Cu_2S formed by the chemical reaction between copper and sulfur.

The same XRD analysis was repeated on annealed bilayer thin film samples prepared on pre-annealed CdS samples (mentioned in section 5.312) (spectrum is not shown) and we could get the same results as in the case of copper film deposited over unannealed CdS films described just above. We have repeated the same experiments on all-evaporated Cu/CdS bilayer thin film system, annealed at 300°C. In this case also annealed bilayer thin film systems show the same XRD pattern of undoped CdS film (spectrum is not shown in the text). All these studies indicate that copper completely diffuses into CdS and also no chemical bonding is formed.

5.33 Optical Analysis.

Optical measurement is the most important method for determining the band structure of semiconductors. Photon-induced electronic transitions can occur between different bands, which leads to the determination of band gap energy, or electron (or hole) transitions within a band from one single-particle state to another such as free carrier absorption. Fig.5.4 shows the absorption spectra of copper film (of thickness 30 nm, vacuum evaporation) and that of CdS film (of thickness 500 nm prepared by spray pyrolysis at the temperature 300°C) respectively. Fig.5.5 shows the absorption spectra of Cu/CdS samples CS005, CS010, CS015, CS020, CS030 and CS050 without any heat treatment. The Fig.5.6 shows the absorption spectra of Cu/CdS system shown in Fig.5.5 after annealing at 350°C at a pressure 10^{-4} Torr. The Fig.5.7 shows the absorption spectra of the sample CS050 before and after annealing at 350°C in a vacuum 10^{-4} Torr. The absorption of as-prepared Cu/CdS film (Fig.5.5) is very high and has the characteristics of copper film (Fig.5.4(a)). Due to annealing

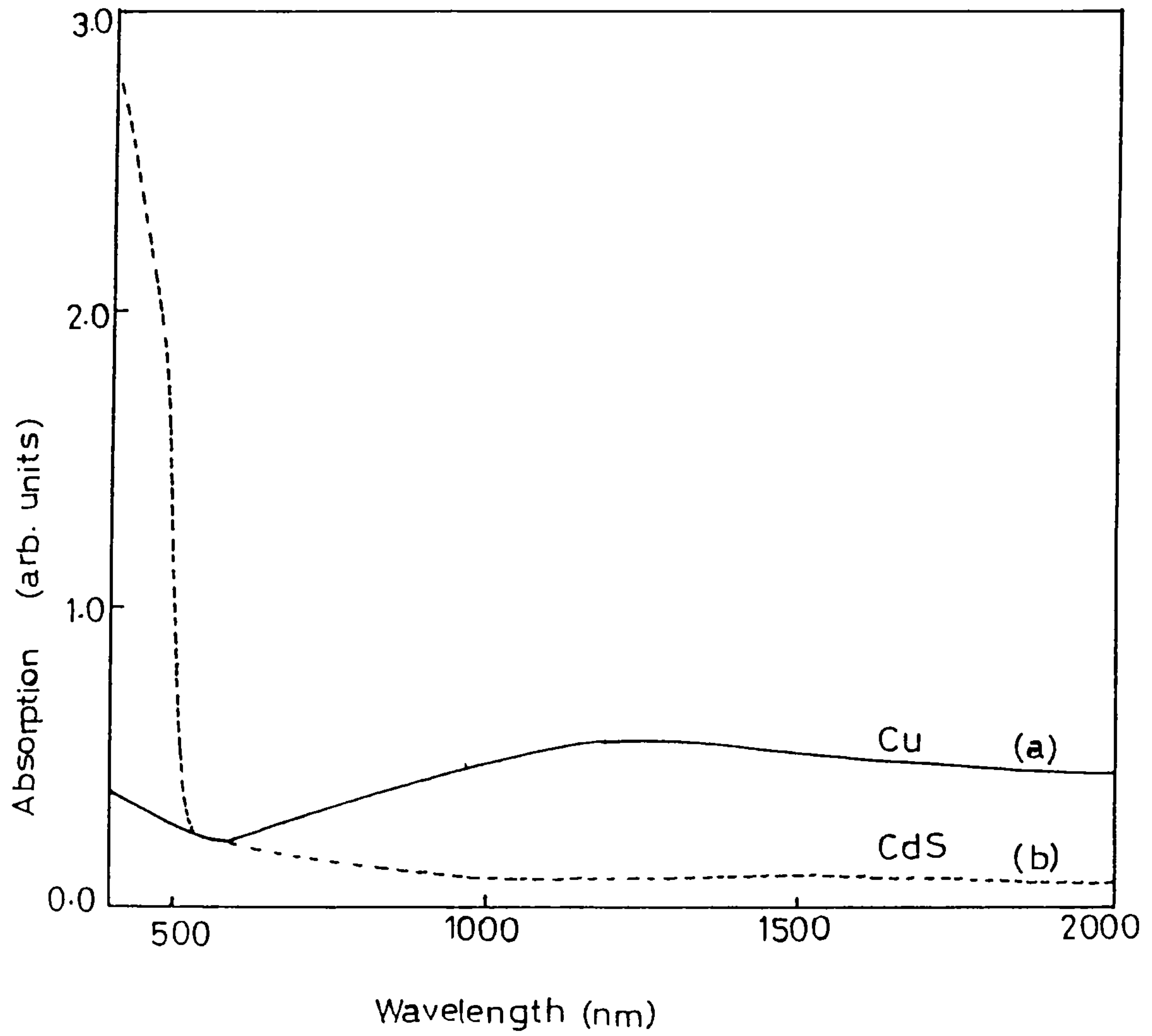

Fig.5.4 Absorption spectra of Cu and CdS film. (a) Cu film (thickness 30 nm) prepared by vacuum evaporation. (b) CdS film (thickness 600 nm) prepared by spray pyrolysis.

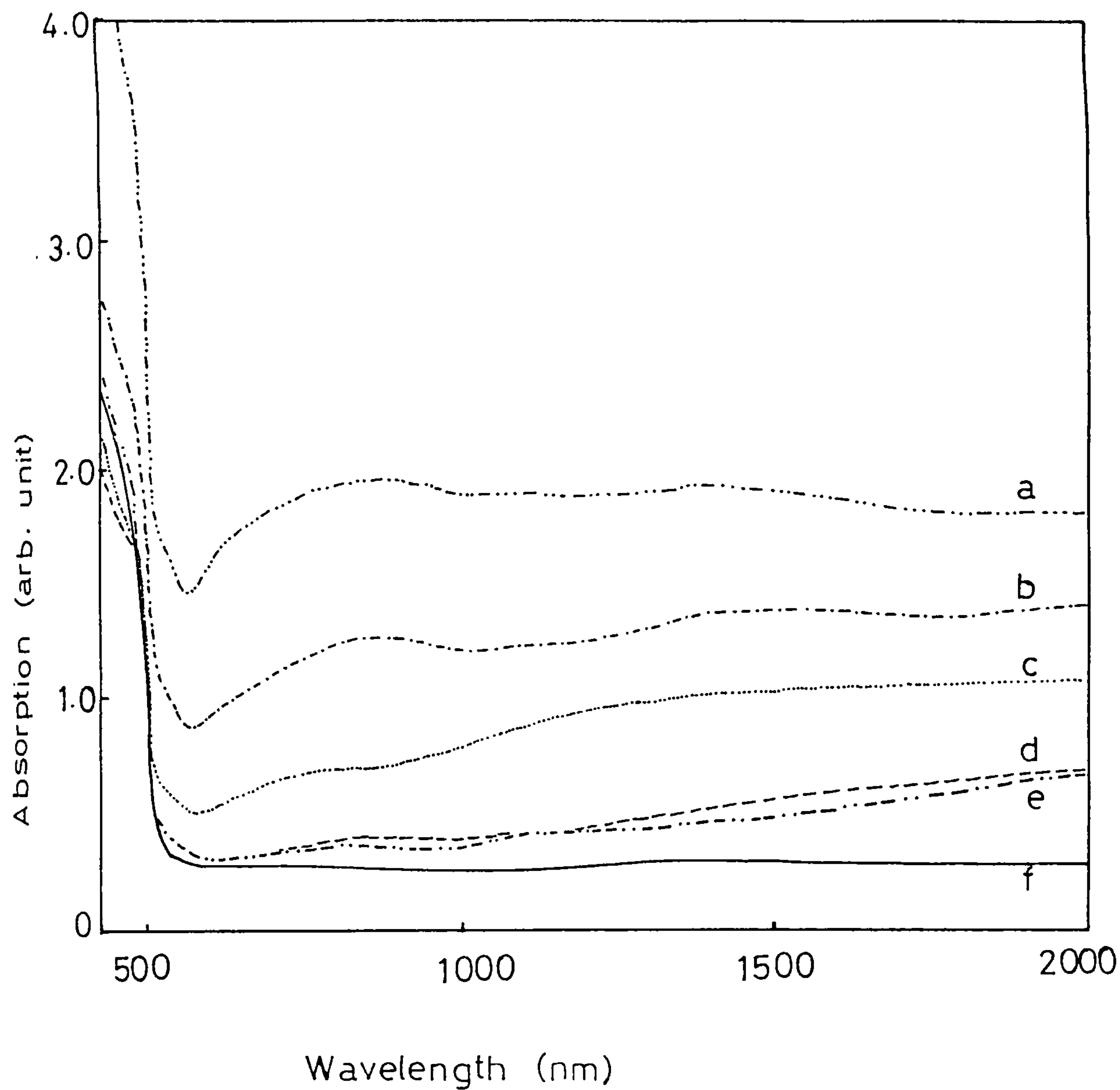

Fig.5.5 Absorption spectra of as-prepared Cu/CdS bilayer thin film with CdS thickness 500 nm and different Cu thicknesses. (f) 5 nm, (e) 10 nm, (d) 15 nm, (c) 20 nm, (b) 30 nm and (a) 50 nm.

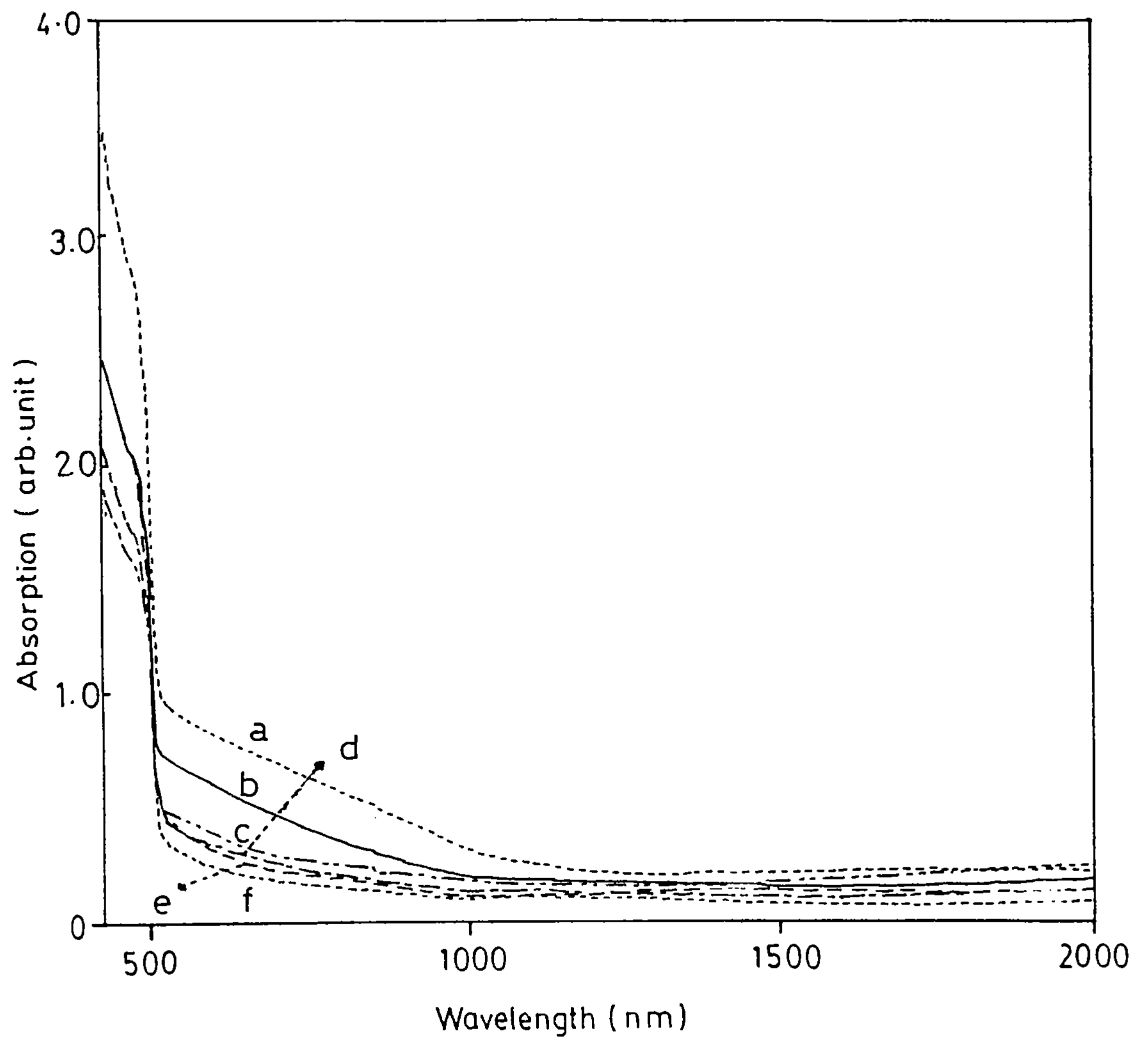

Fig.5.6 Absorption spectra of annealed (at 350°C) Cu/CdS bilayer thin film with CdS thickness 500 nm and different Cu thicknesses.
(f) 5 nm, (e) 10 nm, .(d) 15 nm, (c) 20 nm, (b) 30 nm and (a) 50 nm.

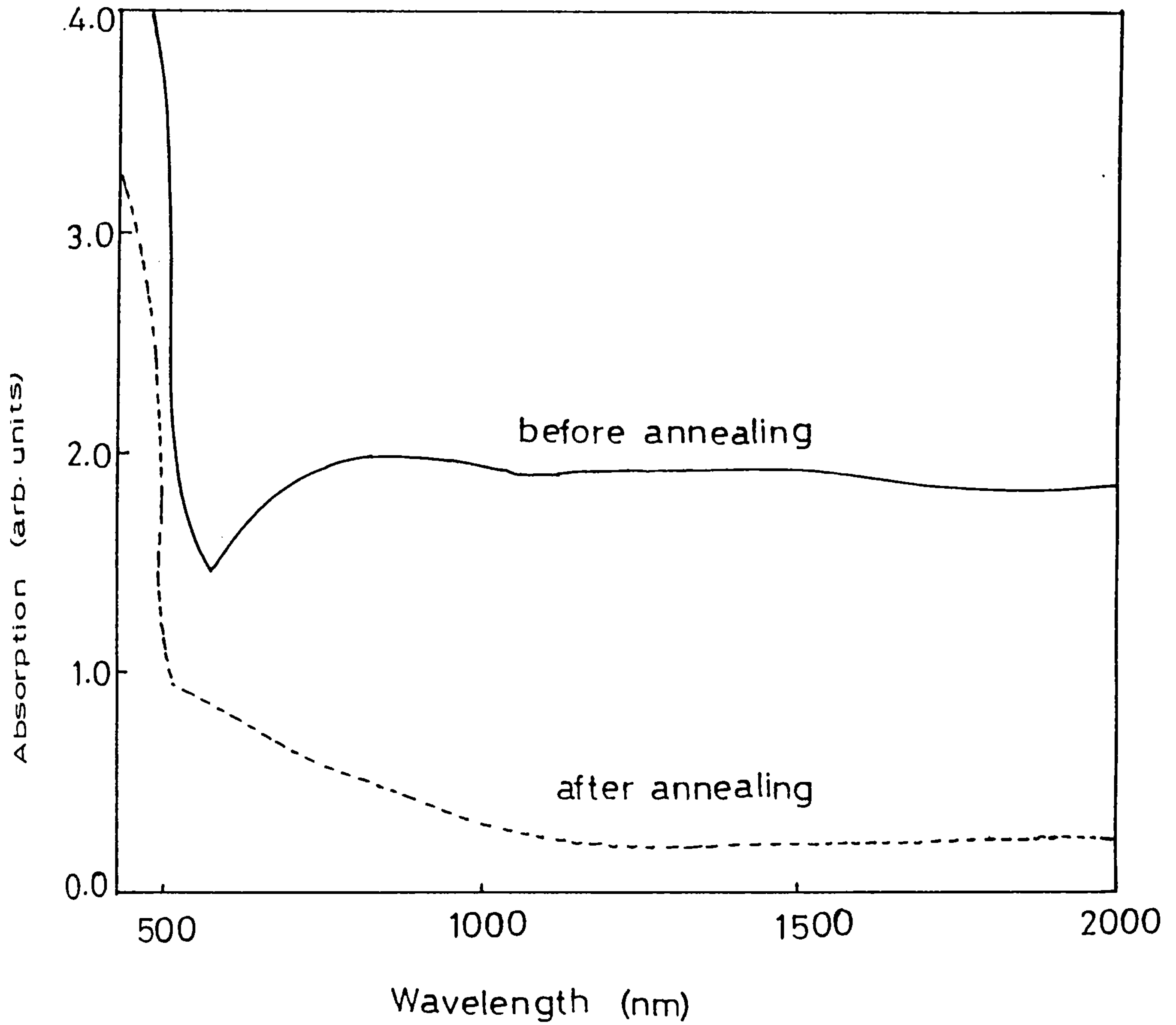

Fig. 5.7 Absorption spectra of Cu (50 nm)/CdS (500 nm) bilayer thin film before and after annealing (at 350°C). After annealing it has the characteristics of CdS film shown in Fig. 5.4(b).

the absorption of Cu/CdS film system decreases and all characteristic features of copper film disappears. This suggests that copper atoms diffuse into CdS film during the post-deposition annealing at 350°C. The absorption spectrum has the same characteristics as that of CdS film except for film which has very high copper thickness. In this case (with very thick copper film) an enhanced absorption starting at about 1eV possibly due to some mid-band gap defects created by heavy doping of Cu is observed. Again it has to be specifically noted that no traces of Cu_2S (which has a band gap ~1.2eV [34]) is revealed from optical absorption studies.

5.34 XPS Analysis.

The VASE, XRD and the absorption studies show that copper completely diffuses into CdS film due to annealing and those studies could not detect any trace of new compound formed between CdS and Cu. The utility of XPS for the chemical analysis results from the chemical shift that is observed in electron binding energies after the formation of compounds. The binding energy of the core electrons are affected by the valence electrons and therefore by the chemical environment of the atom. Or in a simple sense, the shift of the photoelectron lines in a XPS spectrum reflect the change in binding energy as the oxidation state of the atom changes.

The XPS spectrum of annealed (at a temperature 300°C) sample CS011 (shown in Fig.5.8) taken in the binding energy range 0-1000 eV shows the peaks of Cd and S along with copper and this also confirms the results of VASE analysis (given in section 5.311) ie., the formation of a diffused layer (CdS+Cu) due to the diffusion of copper into CdS layer. This also confirms the assumption that the copper fully diffused into CdS and in fact one reaches at this conclusion from the presence of Cd and S on the surface of Cu/CdS sample along with copper. The Fig.5.9 shows the XPS spectrum of

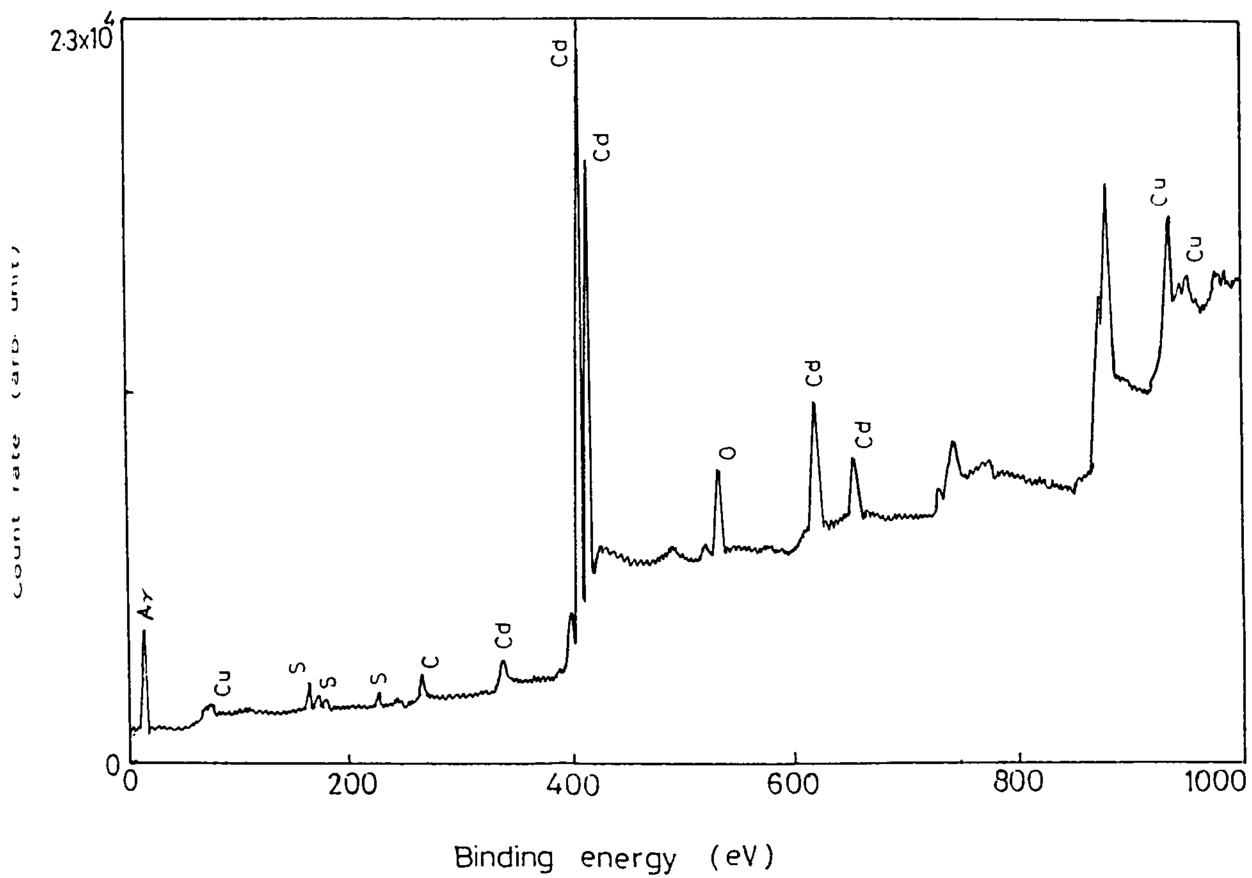

Fig.5.8 XPS spectrum of Cu/CdS system annealed at 300°C. The spectrum shows the peaks of Cu along with Cd and S.

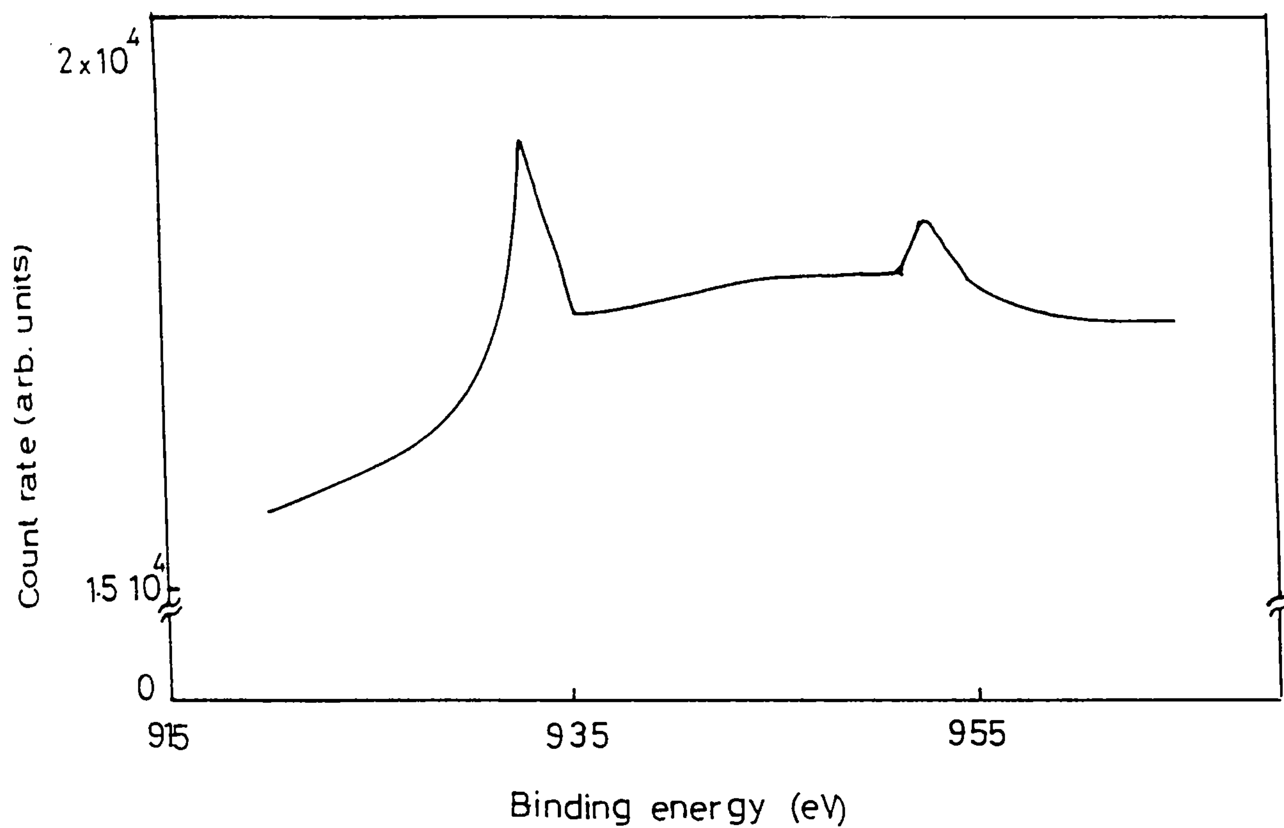

Fig.5.9 XPS spectrum of annealed Cu/CdS system in the region of copper. These peaks correspond to pure copper.

copper in Cu/CdS thin film system . It can be easily seen from the Fig.5.9 that the two peaks (932.8 eV and 953.5 eV) are corresponding to the binding energy of pure copper alone. The XPS spectrum does no hints at any shift in binding energy peaks, which indicates that no changes in oxidation state of copper. This also confirms that no additional compounds like Cu_xS were formed due to the annealing of Cu/CdS thin film system.

5.35 Electrical measurements.

Sheet resistance (R_s) of the films were calculated by two probe method using an electrometer (ECIL EA815) for the highly resistive samples and a 4½ Digital Multimeter (DMM) for other samples. Aluminum electrodes were used for giving electrical contacts. The electrical resistivity (ρ) of the films was calculated using the relation

$$\rho = R_s \, t \; (\Omega - cm) \qquad 4.1$$

where t is the thickness of the film. Carrier concentration of the heavily doped CdS:Cu system was calculated by the Hall effect technique for which a magnetic field of 0.6 Tesla, was applied and corresponding voltage was measured [35]. The type of conductivity of the films was determined using hot probe technique [36]. For this one probe of a DMM is kept at room temperature and the other is heated to high temperature ~90° which was kept in touch with the film surface. All these electrical measurements were done in air at room temperature.

The Fig.5.10 shows the variation of resistivity of CdS film with the amount of copper diffused in it.(ie., the resistivity of the Cu/CdS system annealed at 350°C in a vacuum 10^{-4} Torr). The quantity of copper diffused into CdS was varied by depositing Cu films of different thicknesses (in the range 5 - 50 nm) over CdS and annealing it. From the graph it can be seen that the diffusion of small quantity of copper

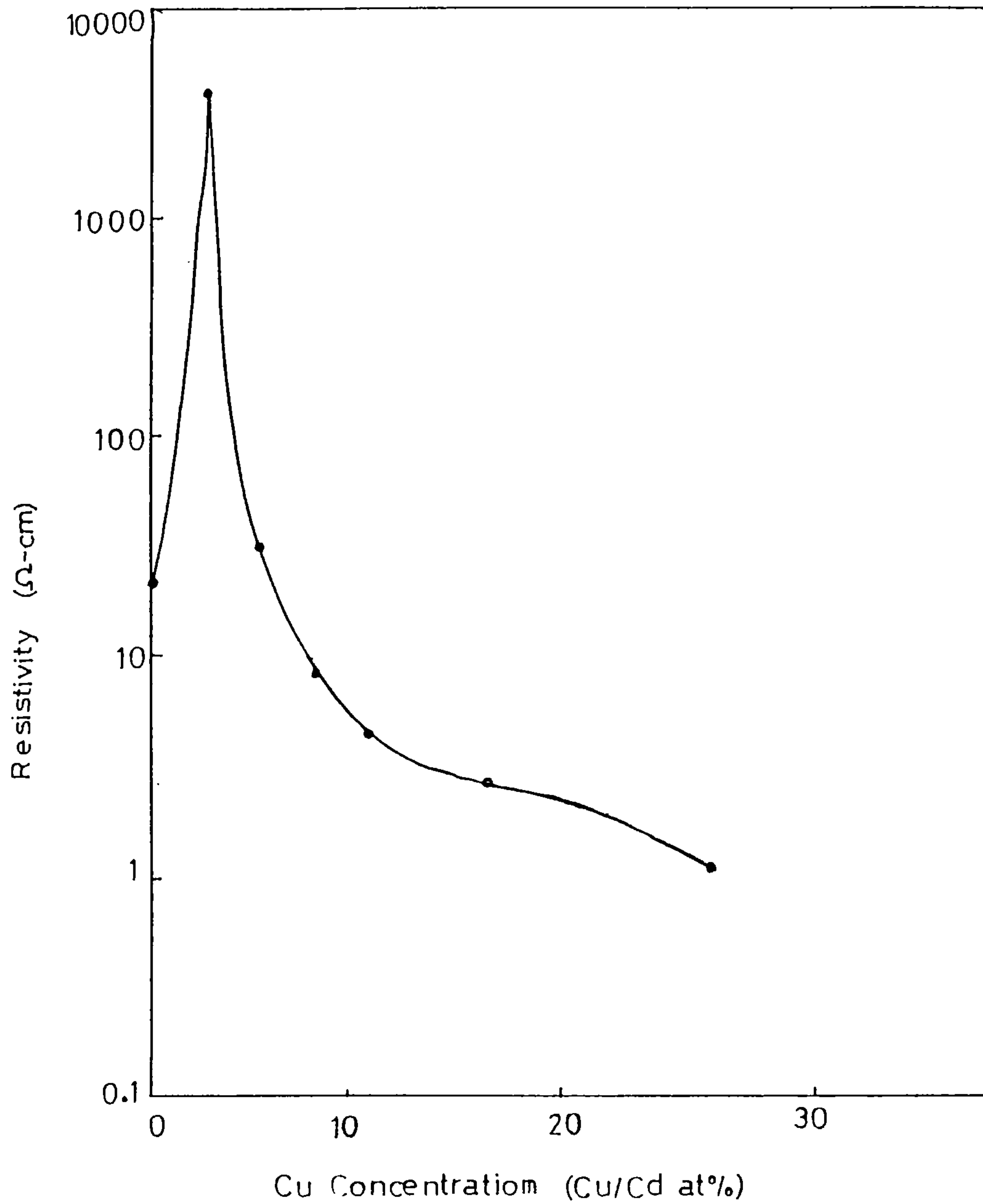

Fig.5.10 Variation of resistivity of CdS film with copper concentration. The resistivity of CdS decreases with copper percentage due to the p-type conductivity of CdS.

results in a drastic increase of the resistivity of the film. This may be due to the intrinsic nature of the CdS film caused by the compensation of donors with Cu accepters. The hot probe technique indicates that the CdS film doped with Cu has p-type conductivity when the thickness of Cu film is >10 nm. The CdS film having the over layer of thickness 5 nm shows intrinsic character. The Hall effect measurements on Cu (50 nm)/CdS (600 nm) thin film system shows a carrier density of $2X10^{18}$ $/cm^{3}$ and also positive Hall coefficient, as obtained from hot probe technique.

5.4 Discussion.

In the introduction part of this chapter it was mentioned that a small number of groups reported the p-type conductivity for CdS films prepared by various methods [9,10,24,25]. Very recently Kashiwaba et al [9,10] have reported the conversion of vacuum evaporated CdS into p-type for the first time. In this work we have converted the spray pyrolysed CdS into p-type. In this study the samples were prepared with different atomic percentage of copper in the range 3.5 to 31%. From the results of VASE analysis it is clear that copper completely diffused into CdS due to annealing and there is no copper layer existing over the CdS film. If copper atoms combine with sulfur atoms, a new p-type compound such as Cu_xS may be formed. Some workers have reported that the Cu/CdS (in the case of crystal) interface cause the formation of Cu_xS layer on CdS crystal. [37,38]. Lepley et al [33] have reported the possibility of Cu_2S formation at Cu-CdS interface. They have also reported the possibility of deep level trap acting as acceptor in the CdS due to the Cu diffusion [33]. In an earlier paper Brillson reported the possibility of Cu_xS formation at the interface of Cu/CdS (crystal) [39,40]. Later they have reported that the Cu impurity level cannot be ruled out in explaining the features

produced by copper deposition and annealing on CdS crystal. [41]. The results of our studies rules out the formation of any new compound due to copper diffusion into CdS layer. The VASE analysis confirms that there is no copper diffusion into CdS at room temperature (Table 5.1). Zurawasky et al [42] have reported almost a similar observation on CdS crystal in which it is stated that copper diffuses into CdS at very small rate for unheated system. Their ESCA analysis rules out the chance for the formation of any new compound. Kashiwaba et al also do not find any trace of a new p-type compound [9,10] and they have also reported the conversion of vacuum deposited CdS film into p-type. Our studies on spray coated CdS confirms their results. We have observed that at first n-type spray coated CdS is converted into intrinsic by the addition of [illegible] of copper (~2.3 Cu/Cd atomic%) as observed by the resistivity measurements. This is due to compensation of donors by the copper accepter. Further addition of copper (>4.5 Cu/Cd atomic %) results in the conversion of this intrinsic CdS film into p-type CdS. Kashiwaba et al have reported the same type changes in vacuum coated CdS film deposited over pre-deposited copper film at elevated temperature (200°C) [10]. Szeto et al have merely reported an increase in resistivity of n-type CdS crystal due to copper diffusion [43].

The absorption spectra of Cu/CdS system also confirm the absence of any new compounds like Cu_xS and an enhanced absorption is observed at the mid band gap region. Copper is known to form deep levels in CdS. The main role of copper levels is to cause a longer wavelength response (red shift) due to the photo excitation of electrons from these levels lying in the forbidden gap of the host CdS to the conduction band [44].

The XRD and XPS studies also confirm the absence of any new chemical compounds. The resistivity studies as well as hot probe method show that the addition of copper changes the

type of conductivity of CdS ie., from n-type to p-type.

5.5 Conclusion.

Cu/CdS bilayer thin films were prepared by vacuum evaporation of copper films on spray pyrolysed CdS thin films. The copper deposition was done on CdS samples kept at room temperature. n-type CdS films which were prepared by spray pyrolysis were converted into p-type for the first time by doping with copper. Ellipsometer is used for the study of Cu/CdS bilayer thin films and this study shows that the copper easily diffuses into as-prepared CdS films and the diffusion depth increases with annealing temperatures. Copper diffusion into pre-annealed CdS film is less than that into as-prepared CdS and it decreases with increase in pre-annealing temperature.The VASE analysis also indicates that the copper diffuses into CdS layer fully due to the annealing of Cu/CdS bilayer films at 350°C in vacuum.

It is observed that the CdS films have very high resistivity at low copper concentration and resistivity decreases with increase in copper concentration. The hot probe and other electrical measurements give the hints that the addition of low amount of copper causes the formation of intrinsic CdS and further addition results in the formation of p-type CdS. The XRD, XPS and absorption studies confirm the absence of any p-type compounds formed due to the chemical reaction between copper and sulfur. The Hall effect measurements on CdS film containing maximum amount of copper in the present work, has shown that the hole concentration in that film is $2X10^{18}/cm^3$. The XRD, XPS and absorption studies confirm that the p type conductivity is due to the presence of copper acceptor in CdS film. All these studies rule out the chance for the formation of p-type Cu_xS film.

References.

1. Bulent M Basol, Vijay K Kapur and Aravind Halani. Proc. 22nd IEEE Photovoltaic Specialist Conf. (IEEE, New York 1991) p 893.
2. K.H.Norian and J.W.Edigton. *Thin solid Films*, 75 (1991) 53.
3. I.M.Fraas and Y.Ma. J. Cryst. Growth. 39 (1977) 92.
4. T.Arita, H.Hanausa, S.Kitamura and H.Takakura. Proc. 22nd IEEE Photovoltaic Specialist Conf. (IEEE, New York 1991) p 946.
5. S.K.Das and G.C.Morrie. Solar Energy Mater. Solar Cells. 28 (1993) 305.
6. R.J.Schwartz, J.L.Gray and Y.J.Lee. Proc. 22nd IEEE Photovoltaic Specialist Conf. (IEEE, New York 1991) p 920.
7. Lars Stolt, Jonas Hedstrom, John Kessler, Martin Ruckh, Karl Otto Velthaus and Hans-Werner Schock. Appl. Phys. Lett. 62 (1993) 597.
8. F.M.Livigstone, W.M.Tsang, A.J.Barlow, R.M.De La Rue and W.Duncan. *J. Phys. D.* 10 (1977) 1959.
9. Y.Kashiwaba, H.Kirita, H.Abe and T.Ikeda. *Jpn. J. Appl. Phys.* 29 (1990) 1733.
10. Yasube Kashiwaba, Haru Kanno and Toshio Ikeda. *Jpn. J. Appl. Phys.* 31 (1992) 1170.
11. D.C.Reynold, G.Leiss, L.L.Antes and R.E. Marburger. *Phys. Rev.* 96 (1954) 533.
12. S.B.Hussain. *Thin Solid Films.* 23 (1974) 513.
13. D.C.Reynolds, S.J.Czyzak. *Phys. Rev.* 96 (1954) 1705.
15. R.W.Williams and R.H.Bube. *J. Appl. Phys.* 31 (1960) 960.
14. J.Woods and J.A.Chapion. *J Electron. Control.* 7 (1959) 243.
16. H.G.Grimmeiss and R.Memming. *J. Appl. Phys.* 33 (1962) 2217.
17. D.A.Cusno. *Solid State Electron.* 6 (1963) 217.

18. A.E.Spakowski, A.E.Potter and R.L.Schalla. Proc. 2th IEEE Photovoltaic Specialist Conf. (IEEE, New York 1967). p 217.
19. A.L.Fahrenbruch and R.H.Bube. "*Fundamentals of solar cells*", Academic press, New York (1983) p 425.
20. D.C.Reynolds, L.C.Greene, R.G.Wheeler and R.S.Hogan. *Bull. Am. Phys. Soc.* **1** (1956) 111.
21. W.W.Anderson and J.T.Mitchel. *Appl. Phys. Lett.* **12** (1968) 334.
22. Chernow F, Eldridge, G.Ruse and L.Washlin. *Appl. Phys. Lett.* **12** (1968) 339.
23. Y.Shirakai, T.Shimada and K.F.Komatsubara. *J Appl. Phys.* **43** (1972) 710.
24. H.G.Grimmeiss and R.Mamming. *J. Appl. Phys.* **33** (1962) 3596.
25. M.Lichtensteiger, I.Lagndo and H.C.Gatos. *Appl. Phys. Lett.* **15** (1969) 418.
26. Joy George "*Preparation of Thin Films*". Marcel Dekker, (1993) Chpter 1.
27. L.I.Maissel and R.Glang. " *Hand book of thin film technology*". Mc Graw Hill book company, New York. (1970) 1-7, 1-81, 1-85, 1-92.
28. L.Holland. " *Vacuum deposition of thin films*" John Wiley and sons Inc. New York. (1961) p 108.
29. K.I.Behrndt. " *Techniques of metal research*" Vol. 1, pt. 3. Interscience publishers Inc. New York. (1968) p 1225.
30. P.K.Weimer, F.V.Shallcross and H.Borkan. *RCA Rep.* **24** (1963) 661.
31. K.Vedam, P.J.Mc Marr and J.Narayn. *Appl Phys. Lett.* **47** (1985) 339.
32. D.A.G.Bruggeman. *Ann. Der Phy.* (Leipzig) **24** (1935) 636.
33. B.Lepley, P.H.Nguyen, C.Boutrit and S.J.Ravelet. Phys. D. Appl. Phys.12 (1979) 1917.
34. K.L.Chopra and S.R.Das. "*Thin Film Solar Cells*". Plenum

Press, New York (1983). Chapter 6.

35. K. Jacob John, B. Pradeep and Elizabeth Mathai. Solid Stat. Commun. 85 (1993) 879.
36. M. S. Tyagi. "*Introduction to semiconductor material and devices*" John Wiley and sons, New York, (1991) p 613.
37. N. G. Stoffel, R. R. Daniels and M. Magartonda, C. F. Brucker and L. J. Brillson. *Vac. Sci. Technol.* 20 (1982) 701.
38. C. F. Brucker and L. J. Brillson. *J. Vac. Sci Technol. (A).* 3 (1985) 1011.
39. L. J. Brillson. *Phys. Rev. B.* **18** (1978) 2431.
40. L. J. Brillson. *Phys. Rev. lett* **40** (1978) 2460.
41. L. J. Brillson, H. W. Richter, M. L. Slada, Weinstein and Y. Shapira. *J. Vac. Sci. Technol. (A).* **3** (1985) 1011.
42. W. P. Zurawshky, Kaj Stolt and H. G. Drickamer. *J Appl. Phys.* **57** (1985) 2817.
43. Whalun Szeto and G. A. Somarajai. *J. Chem. Phys.* **44** (1965) 3490.
44. Hideki Minoura, Takashi Sugiura, Ellchi Suzuki, Yoshinon Mizuno and Yasusada Ueno. " *J. Electron. Scc.* **136** (1970) 1346.

Chapter 6

STUDIES ON BILAYER FILMS IMPORTANT IN SOLAR CELL APPLICATION

Part I.

CdS/SnO_2 bilayer thin films

6.1 Introduction.

Transparent conducting film of metallic oxides such as SnO_2 or In_2O_3 etc have been studied for many years because of their practical applications [1-3]. An intrinsic and stoichiometric material does not show simultaneous high optical transparency and high electrical conductivity. Partial transparency and fairly good conductivity may be obtained in thin films of a variety of materials. But non-stoichiometric and doped films of oxides of Sn, In, Cd, Zn etc deposited by various techniques exhibit high optical transparency in the visible region, high optical reflectivity in the IR region and nearly metallic conductivity. The most prominent oxide materials are those mentioned at the beginig. The oxide films, which exhibit high conductivity along with high transparency in the visible region are widely used in making optoelectronic devices such as displays and solar cells [2,4,5] because of their high stability, hardness and adherence to many type of substrates. More than that, film of SnO_2 and other oxides find a number of applications such as transparent heating elements for air crafts and automobile windows, anti-static coating for instruments windows, heat mirrors for glass windows, anti-reflection coatings, gas sensors etc [2].

SnO_2 film can be produced by various deposition methods [6-10] including spray pyrolysis technique [11-14]. Spray pyrolysis involves spraying of a solution, (usually alcoholic/aqueous) containing soluble salt of the constituent

atoms of the desired compound onto a heated substrate. This is a very simple technique and more details are included in section 4.2. SnO_2 films prepared at low temperature are amorphous and while film prepared at high temperature are ploycrystalline in nature [15,2]. It has also been noted that the grain size increases with substrate temperature. In order to increase the conductivity of the film various dopents are added like Sb [16,17] F [12,18] and In [11,19].

As satated in earlier chapters CdS thin film is widely used as a window material in several thin film heterojunction solar cells using the p-type materials like Cu_2S, $CuInSe_2$, CdTe etc. The most common problems in these cells are those occuring at interface in the pn junction and in the semiconductor-metal electrode contact region. The interface probleums occuring in the pn junctions and semicondutor-metal electrode contact region are reviewed by many others [20-23]. But there are not much studies aimed at the analysis of probleums occuring at the interface between SnO_2 and other semiconducting materials eg., (SnO_2/CdS interface). There are only few reports about this interface [24].

The drive for solar cells of high efficiency and long life has necessitated a more detailed understanding of CdS/SnO_2 interface. Very recently Niles et al reported the results of CdS/SnO_2 interface [24]. For high efficiency the CdS window layer must be very thin to allow maximum transmission into the absorber layer [25,26]. In these present work we have studied the interlayer diffusion of CdS and SnO_2 due to high temperature treatment.

6.2 Experiment.

6.21 Sample preparation.

The spraying technique is used for the preparation of CdS/SnO_2 samples. In the case of SnO_2 this technique

involves decomposition of alcoholic solution of stannic chloride at high temperature ($450^{\circ}C$) in the presence of an oxidizing agent [27]. This endothermic reaction is given below

$$SnCl_2 + 2H_2O \longrightarrow SnO_2\ 4HCl$$

Detailed description of experimental setup and theory of spray pyrolysis is given in section 4.2. The solution used for this contains $SnCl_2.5H_2O$ at a molarity of 0.9M. The distance from the spray head to substrate is kept at ~30 cm and the angle of incidence of solution droplets on the substrate is ~75°. The flow rate of the liquid is controlled to ~10 ml/mts. 20 ml of. the solution is sprayed for getting 450 nm thick SnO_2 film. Air is used as carrier gas. High scanning rate of spray head (100/mts) ensure a uniform film thickness. For optimizing the condition for good quality SnO_2 films, the films were prepared over glass substrates at different substarte temperature in the range 350-500°C.

Optical transmission and electrical resistivity show that the film prepared at 450°C has optimum results and this film is used for the bilayer (CdS/SnO_2) preparation. For this purpose SnO_2 (thickness ~450 nm) film was prepared at 450°C on glass substrate and above this CdS film (thickness ~400 nm) was deposited at 300°C. The CdS films were also prepared by spray pyrolysis technique using a solution of thiourea (0.01M) and $CdCl_2$ (0.01M). The details of CdS film preparation by spray pyrolysis is given in section 4.2. and also given elsewhere [28].

The CdS/SnO_2 film system was annealed at different temperatures in the range 100-300°C in air. The heating and cooling rates were 2°C/mts for all cases. The details of annealing is described in section 4.2.

6.22 Measurements.

Spectrophotometer is used for transmission studies

of the films prepared at different substrate temperature. VASE is also used for the optical studies of the films. Electrical resistivity of the film is determined as described in section 5.35. VASE is used for the analysis of inter-diffusion taking place in the CdS/SnO_2 bilayer structure due to annealing. All VASE measurements were done at room temperature and in air. The sensitivity analysis of CdS/SnO_2 bilayer structure is given in section 3.4 and plots are given in Fig.3.10 to 3.13. These studies show that this system has high sensitivity over a wide range of wavelength and wide range of angle of incidence. The VASE measurements were done in the angle of incidence range 60-75° and the wavelength range 500-620 nm as suggested by sensitivity analysis.

6.3 Results and discussion.

The CdS/SnO_2 bilayer thin film system were prepared over glass substrate by spray pyrolysis technique. The summarised results of optical and electrical measurements of these films are given in Table 6.11. From this table, it is clear that the film prepared at 450°C has better properties. At low temperature the thickness of SnO_2 film is very low (In all cases same quantity of solution is used). Thickness of the film increases rapidly at 400°C and remain more or less constant. The electrical resistivity of the film at first decreases with increase in substrate temperature and reaches a minimum at 450°C and thereafter it increases slowly. Refractive index of the film measured using ellipsometer shows that the real part of refractive index has high value for the films prepared at 450°C. This may be due to the better structure of the film. The Fig.6.11 depicts the variation of optical transmission with wavelength for films prepared at different temperatures. The Fig.6.12 shows the refractive index spectrum of SnO_2 film prepared at 450°C determined using ellipsometer. In this calculation imaginary part k of complex

Preparation temperature (°C)	Thickness (nm)	Resistivity (Ω cm)	Index of refraction 590 nm	620 nm	Transmission (680 nm) %
350	195	12×10^{-4}	1.88	1.85	52
400	290	7.5×10^{-4}	1.87	1.86	68
450	300	7.0×10^{-4}	2.09	2.05	78
500	315	9.0×10^{-4}	1.89	1.90	57

Table 6.11 Properties of SnO_2 film at different substrate temperatures. Table shows that the film prepared at 450°C has good optical and electrical properties.

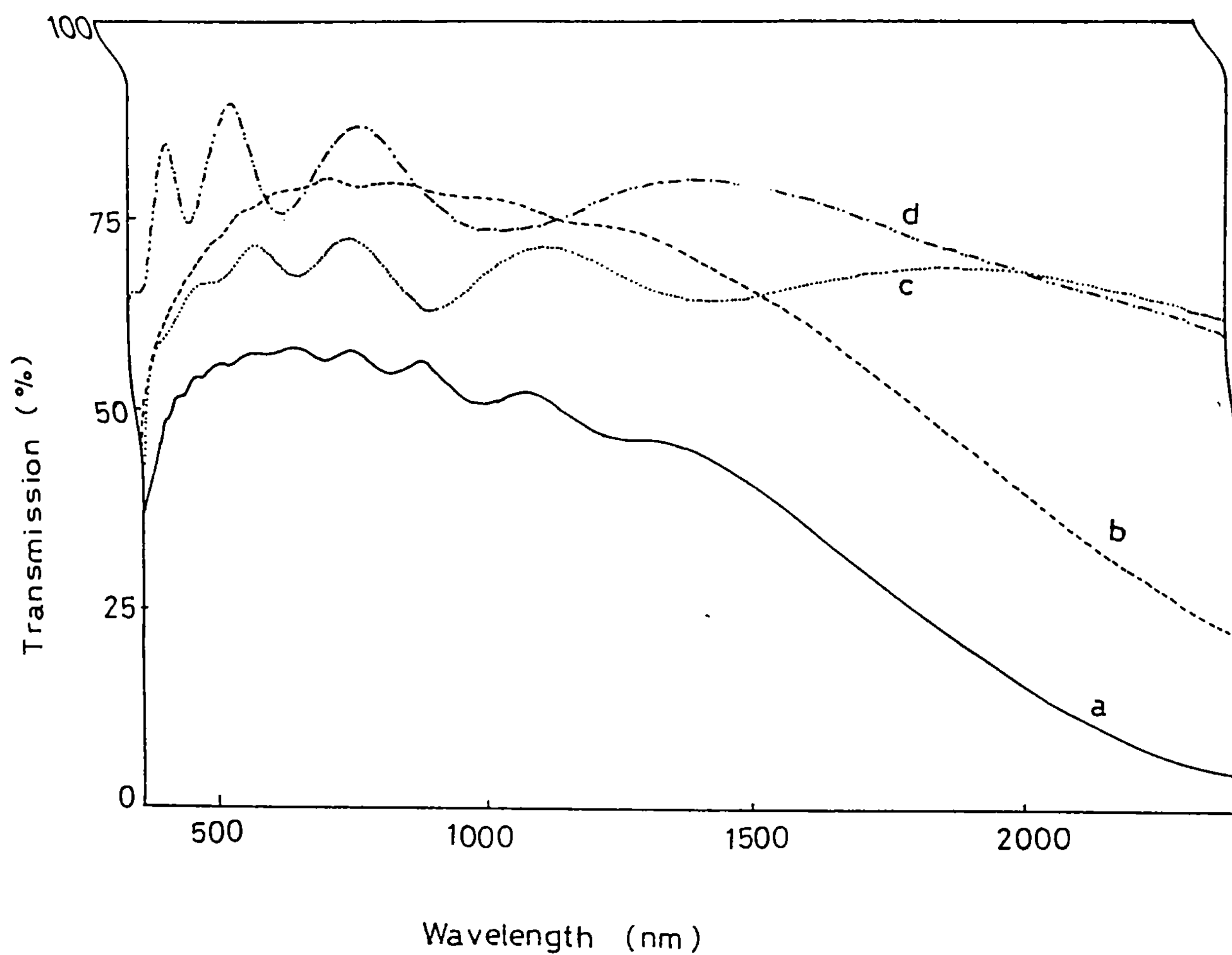

Fig.6.11 Transmission spectrµm of SnO_2 film prepared by spray pyrolysis at different temperature. (a) 500°C (b) 450°C (c) 400°C and (d) 350°C

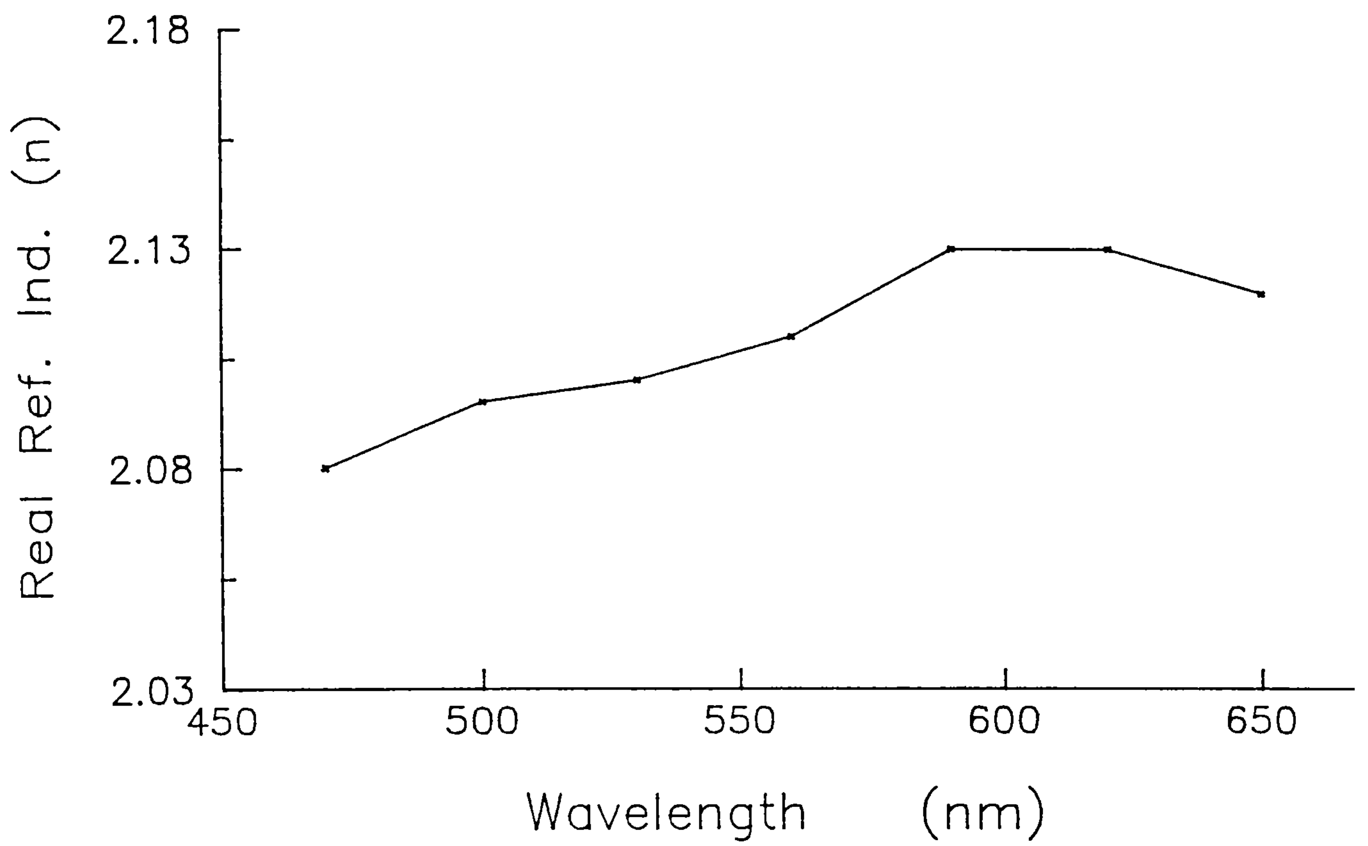

Fig.6.12 Variation of real part (n) of refractive index of SnO_2 thin film prepared by spray pyrolysis technique at 450°C.

refractive index is taken as zero.

The Table 6.12 shows the results of CdS/SnO_2 interlayer anlysis. Ellipsometrically calculated refractive indices of CdS and SnO_2 are used for the analysis. Different optical models are used for the analysis of CdS/SnO_2/glass system. The most important models are given below.

Model (a). air/CdS/SnO_2/glass.

Model (b). air/CdS/($CdS+SnO_2$)/SnO_2/glass.

The ellipsometric data of the bilayer system is used for the analysis of these optical models and best fit of these models were determined using the technique given in section 3.2. At first the model (a) is selected. It is on the assumption that the two layers have sharp boundaries and there is no inter-diffusion. The other model (model (b)) is on the assumption that CdS and SnO_2 do not have sharp boundaries due to the inter-diffusion of CdS into SnO_2 or vice versa. The values of unbiased estimator δ [29] of different optical models derived from VASE analysis are shown in Table 6.12. From this δ value it is clear that the first optical model has the least value for δ compared to the other model. This shows that this model is best suited to the physical system, ie., as prepared CdS/SnO_2 has sharp boundaries and CdS prepared over SnO_2 does not cause any inter-diffusion or chemical reaction.

The thermal stability of the CdS/SnO_2 interface is most important because the fabrication of thin film solar cell involves the thermal treatment [24]. The high temperature annealing is an attempt to simulate a common fabrication technique ie., heat treatment. We have annealed the CdS (400 nm thick)/SnO_2 (450 nm thick) at different temperatures in the range 100- 300°C in air. The results of post annealing VASE measurement are shown in Table 6.12. If CdS reacts with or diffuse into SnO_2, the structure of CdS/SnO_2 bilayer changes from model (a) to model (b). This will cause a

Annealing temperature (°C)	δ Unbiased estimator value of optical models	
	CdS/SnO_2/glass model (a)	$CdS/(CdS+SnO_2)/SnO_2$/glass model (b)
unanne-aled	0.890	2.61
100	0.950	2.72
150	0.910	2.68
200	0.920	2.71
250	0.930	2.67
300	0.980	2.69

Table 6.12 Results of VASE analysis of CdS/SnO_2/glass bilayer thin film system after annealing at different temperatures. This shows that CdS/SnO_2 interface is very stable.

considerable change in δ value of the optical model. But the unbiased estimator δ of different optical models has no considerable change due to annealing, as revealed by values in Table 6.12. This lack of change in δ value with temperature suggests that the CdS/SnO_2 system is highly stable and annealing does not cause any inter-diffusion that results in the degradion of the bilayer thin film system and ultimate failure of cell. Very recently Niles et al [24] have reported almost the same observation using soft x-ray synchrotron radiation photoemission technique. In this study we have used a very simple setup (VASE) for the diffusion study of CdS and SnO_2, this technique can be extented to the *insitu* monitoring of diffusion with temperature.

6.4 Conclusion

The spray pyrolysis technique is again used for the preparations of SnO_2 film. SnO_2 films are optically transparent and good electrical conductors. They are widely used as electrode material in several optoelectronic devices. An alcoholic solution (0.9M) of $SnCl_2.5H_2O$ is used for this purpose. Very low resistivity (30 ohm-cm) films were obtained at a substrate temperature 450°C. It has [illegible] very good optical transmission.

The bilayer structure fabricated using the SnO_2 film is CdS/SnO_2. These bilayer films are prepared by spray pyrolysis. At first SnO_2 film is prepared over glass substrate at 450°C and then CdS film is prepared at 300°C over the SnO_2 film. The ellipsometric studies of CdS/SnO_2 interface using an approximate optical model show that the structure is very stable and has very narrow interface. Since this bilayer is widely used in thin film solar cells the stability of CdS/SnO_2 interface is very important. This interface is stable for thin film system annealed at very high temperature (300°C). A detailed study using correct optical model is required to make final conclusion

Part II.

CdS/$CuInSe_2$ bilayer thin films.

6.5 Introduction.

$CuInSe_2$ has proved to be a very effective absorber material for thin film solar cell [25,26]. Development of highly efficient $CuInSe_2$ based solar cells and modules requires an understanding of the mechanism which controls the photovoltaic performance. Analysis of interlayer diffusion between the films that form the pn junction is also an important study for the characterization of solar cells. Chemically prepared CdS and $CuInSe_2$ films are becoming more and more attractive due to its low cost of production and simplicity of operation. It is important also due to the fact that films having large area can be deposited. Chemical bath deposition (CBD) technique is used for the production of semiconducting thin films like CdS, $CuInSe_2$ etc. This technique (CBD) was first used in 1946 to prepare PbS films [30]. A large number of groups have reported the preparation of CdS by CBD [31-38]. The resistivity of these films is very high [36,37]. Basol et al have reported that this is due to the near stoichiometric nature of the film prepared by CBD [37]. It is also reported that CdS film prepared by CBD techniques is intrinsic in nature [36].

$CuInSe_2$ films is prepared by different techniques [39-42]. Recently CBD is used for the $CuInSe_2$ film preparation [43-46]. Minimum lattice mismatch between CdS and $CuInSe_2$ (only 1.6%) and favourable electron affinity difference (0.1eV) [23] are the attractive aspects of these materials. The p-type $CuInSe_2$ film forms pn junction with n-type CdS film and latter acts as a window layer [25,26]. $CuInSe_2$ based single junction thin film solar cells have shown efficiency as

high as 15% [25]. In this work we have fabricated a bilayer $CdS/CuInSe_2$ structure over glass substrate by CBD and interlayer diffusion taking place in the bilayer structure due to heating is studied using VASE.

6.6 Chemical bath deposition.

CBD is growth from liquid by ion-by-ion condensation of different ions of the compound on the substrate from an aqueous basic medium. According to the solubility product (SP) principle, in a saturated solution of weakly soluble compound the product of the molar concentration of its ions called ionic product (IP) is a constant at a given temperature. If IP exceeds SP precipitation occurs. Spontaneous precipitation is to be eliminated to form a thin film by controlled ion-by-ion reaction. This can be achieved by using a fairly stable complex of the metal ions. The concentration of metal ions are controlled by adding appropriate complexing agents in correct concentration [27].

6.61 CdS Thin Film.

CBD deposition of CdS films was initiated by Mokrushin and Tkachev in 1961 [35]. In this technique triethanolamine (TEA) is used as the complexing agent as reported by Mondel et al [38]. Detailed description of present technique is given in [31,33]. The attraction of work based on TEA is that good quality film is obtained at room temperature. The Cd^{2+} ions are present in the form of a complex species $[Cd(TEA)]^{2+}$ in solution, the dissociation of which causes the release of Cd^{2+} ions and the formation of film by reaction with S^{2-} ions from thiourea in a basic media with pH > 10 [33]. The relevant chemical equation is

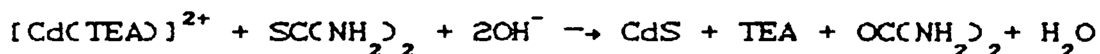

$$[Cd(TEA)]^{2+} + SC(NH_2)_2 + 2OH^- \rightarrow CdS + TEA + OC(NH_2)_2 + H_2O$$

Measured quantity of $CdCl_2$ solution (1N) was mixed

with TEA, followed by the addition of ammonia solution. pH of the solution is maintained above 10 and measured quantity of thiourea is added to the mixture. Substrates were kept vertically in the solution for CdS deposition. About 1500 nm thick CdS film is deposited on glass substrate and 50 nm thick CdS is deposited over $CuInSe_2$ film by CBD.

6.612 $CuInSe_2$ Thin Film.

$CuInSe_2$ thin film is prepared by CBD along with various other techniques [39-42]. In the earlier CBD process TEA was used for complexing copper ions [43-45]. In this case the reaction mixture was maintained at elevated temperature and the pH of the solution is ~10. In the present technique citrate is used as the common complexing agent for Cu and In ions and deposition is made possible at room temperature by controlling the pH of the solution, as reported by Vidyadharan et al [46].

Thin films of $CuInSe_2$ were prepared by CBD from a deposition mixture containing aqueous solutions of copper sulfate, trisodium citrate, sodium selenosulphate and $InCl_3$. Sodium selenosulphate was prepared by dissolving elemental selenium in an aqueous solution of sodium sulfite maintained at a temperature of 90°C and pH>9. The solution was then cooled and filtered. A known quantity of copper sulfate solution (0.2M) mixed with trisodium citrate (0.1M) was added to known quantity of selenosulphate (.1M). $InCl_3$ was dissolved in citric acid and this was added to the above mentioned mixture drop by drop. The solution was thoroughly mixed and taken in a 50 ml beaker. The pH value of the solution was adjusted to be ~8. Ion-by-ion condensation on the clean glass substrate takes place slowly due to the homogeneous precipitation of ions. Uniform film of thickness 80 nm was obtained in a single dipping. Films of any desired thickness can be obtained by repeated dipping [46].

6.7 Measurement.

The CdS/$CuInSe_2$ bilayer thin films were annealed at different temperatures in the range 100-300°C as described in earlier sections. VASE is used for the measurement of $CuInSe_2$ thin film and CdS/$CuInSe_2$ bilayer thin films and also for the study of effect of annealing (details of VASE analysis is given in chapters 2 and 3). The ellipsometric calculation of $CuInSe_2$ films were done in the wavelength range 470-650 nm. The VASE analysis of bilayer thin films was done in the sensitive region wavelength and angle of incidence as given in the section 3.43.

6.8 Results and discussion.

The Figs.6.21 and 6.22 give the refractive index of $CuInSe_2$ films calculated using ellipsometry in the range of wavelength 470 to 650 nm. The calculated values of n and k are used for further analysis of CdS/$CuInSe_2$ bilayer thin film. The thickness of 'thin' $CuInSe_2$ film is measured by ellipsometry and it is ~85 nm for single dip. A second dip of this film into a fresh solution makes the thickness ~180 nm. Gravimetric technique using microbalance is also used for verifying this thickness measurement.

CBD deposition of CdS on glass substrate gives a very thick (~1.5μ) film even at single dip. But the CdS film deposited on $CuInSe_2$ by the same technique has a thickness of ~ 50 nm. This shows that initial growth rate of CdS on $CuInSe_2$ is very slow. In the present study a bilayer film system with $CuInSe_2$ film of thickness ~250 nm and CdS film with thickness ~50 nm is used. For the ellipsometric analysis of CdS/$CuInSe_2$/glass system different optical models were applied. Glass is eliminated from all models, becouse the high absorption of $CuInSe_2$ hides glass from probe beam. Therefore $CuInSe_2$ is treated as substrate material. The results of

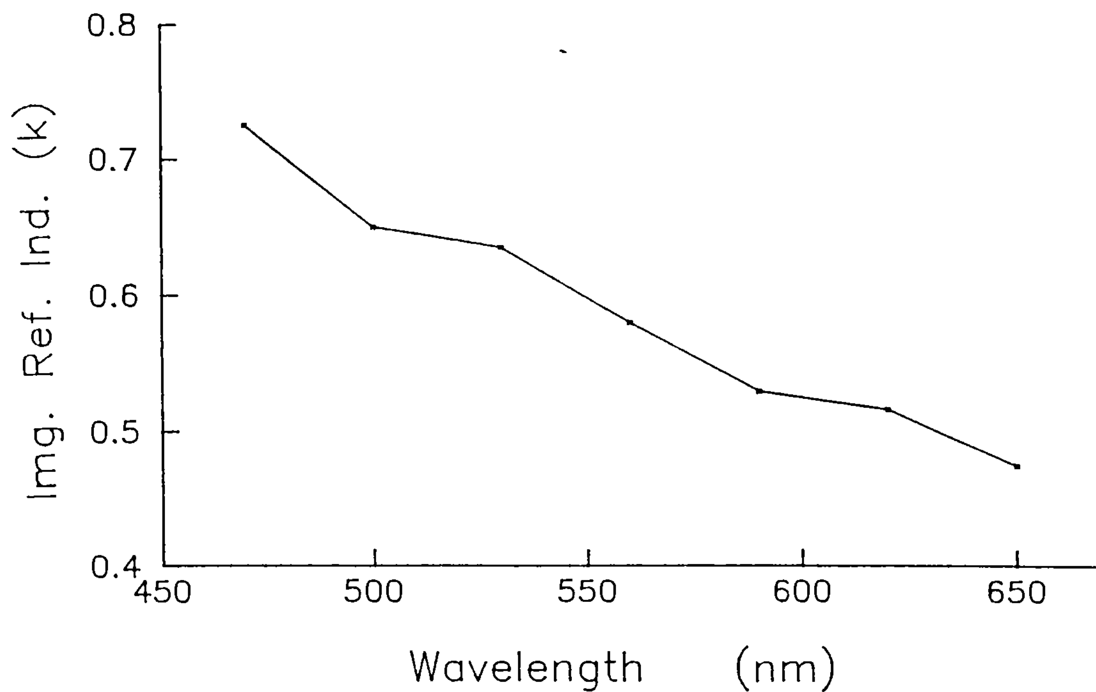

Fig.6.21 Variation of Img. part (k) of refractive index of $CuInse_2$ thin film prepared by CBD technique.

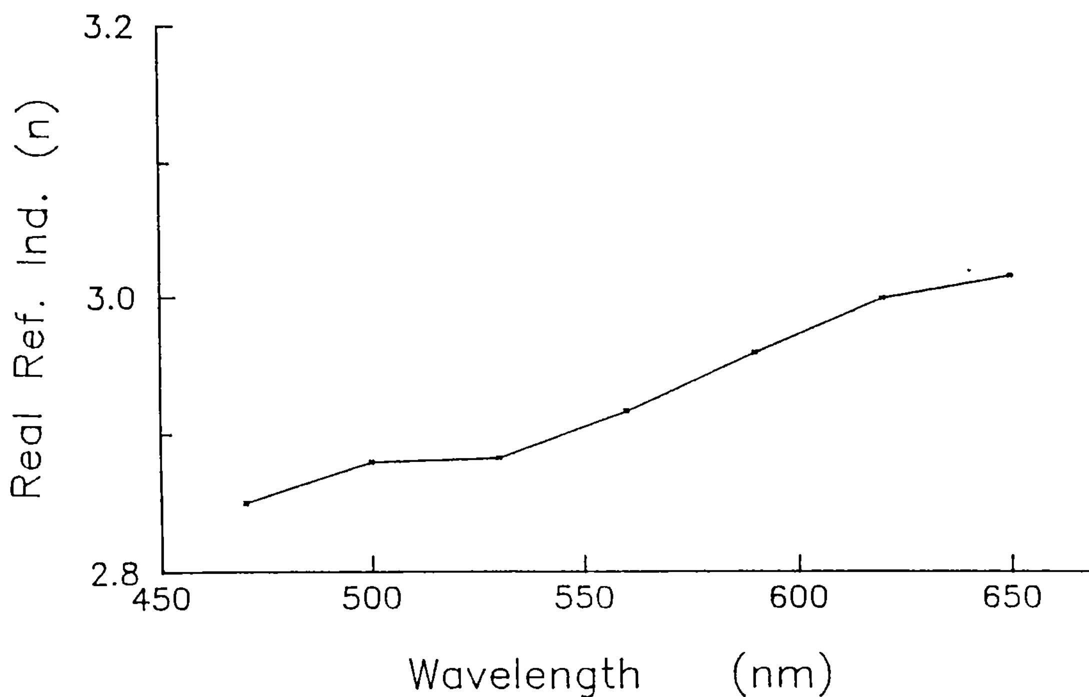

Fig.6.22 Variation of real part (n) of refractive index of $CuInse_2$ thin film prepared by CBD technique.

$CdS/CuInSe_2$ system is given in Table 6.21, which contain VASE analysis of two optical models viz.,

Model (a). air/$CdS/CuInSe_2$.

Model (b). air/$CdS/(CdS+CuInSe_2)/CuInSe_2$.

The VASE studies reveal that as prepared $CdS/CuInSe_2$ system has sharp boundaries between the two layers.

The heat treatment of $CdS/CuInSe_2$ solar cell is useful not only for the post fabrication device optimization but also for the information about the temperature stability of the cell [23]. The stability of this bilayer thin film, which forms the pn junction, is studied in the present work by annealing the $CdS/CuInSe_2$ film system at different temperatures in the range 100-300°C. The VASE studies show that the annealing at low temperature (100°C) does not affect the interface of $CdS/CuInSe_2$. But high temperature annealing (above 200°C) causes the degradation of the interface. Kazmerski et al also reported that the low temperature (60°C) annealing of $CdS/CuInSe_2$ cell does not affect the performance of the cell [23] as in the case of our studies.

In the case of high temperature annealed samples, the model (b) is found to be more suitable. This is due the the diffusion of the materials from one layer into the other. The thickness of the interlayer at 200°C is ~17 nm and the volume fraction of CdS in this interlayer is 0.08 (8%). The annealing at 300°C causes further degradation of the bilayer ie., the thickness of the interlayer increases to ~25 nm while the volume fraction of CdS increased to 0.12 (12%). This shows that the $CdS/CuInSe_2$ layer that forms pn junction is degraded due to high temperature treatment unless some precautionary measures are taken before forming the pn junction. Kazmerski et al have reported that the annealing of $CdS/CuInSe_2$ cell at 220°C causes 38% degradation in its efficiency [23]. This is due to the some physical changes in junction region. The AES studies also confirm the degradation of the cell due to

Annealing temperature (°C)	δ Unbiased estimator value of optical models		Vol. fraction of CdS in mixed layer and its thickness (nm)
	CdS/CIS model a	CdS/(CdS+CIS)/CIS model b	
unanne-aled	0.0750	0.1321	------
100	0.0857	0.1266	------
200	0.1050	0.0974	0.06 (15 nm)
300	0.1150	0.0816	0.12 (23 nm)

Table 6.21 Results of VASE analysis of CdS/$CuInSe_2$/glass bilayer thin film system after annealing at different temperatures. The degradation of CdS/$CuInSe_2$ bilayer starts at 200°C.

annealing at 220°C and above. AES results also show that at 220°C S from CdS and Se from $CuInSe_2$ diffuse into the other layer and hence cause interlayer widening. Also at 400°C Cd diffuses into $CuInSe_2$ layer and this results in fatal failure of the cell [23]. These results are corroborating our observations on $CdS/CuInSe_2$ using a simple non-destructive technique.

6.7 conclusion.

CBD is also used for the preparation of CdS. $CdCl_2$ and thiourea solution complexed with triethanolamine (TEA) is used for the preparation of CdS film at room temperature. Ammonia solution is used to adjust the pH value above 10.

CBD technique is used for the preparation of $CuInSe_2$ films. Thin films of $CuInSe_2$ were prepared by CBD from a deposition solution containing aqueous solution of copper sulfate, trisodium citrate, sodium selenosulphate and indium chloride. The pH of the solution is adjusted to ~8 and the deposition takes place at room temperature itself.

The $CdS/CuInSe_2$ bilayer thin film is prepared by CBD technique. $CuInSe_2$ film is prepared over glass substrate by CBD as mentioned earlier. Next this $CuInSe_2$/glass structure is used for the preparation of $CdS/CuInSe_2$ bilayer films by the same technique CBD.

VASE results indicates that the as prepared samples have no interlayer between CdS and $CuInSe_2$. Again the VASE studies on annealed samples give a clue that annealing upto 100°C does not affect the interface. Annealing at temperature 200°C causes the formation of a thin interlayer of CdS and $CuInSe_2$ and at high temperature more and more material mix together and the thickness of interlayer is very high.

References.

1. J.C.Manifacier. *Thin Solid Films.* 90 (1982) 297.
2. K.L.Chopra, S.Major and D.K.Pandya. *Thin Solid Films.* **102** (1983) 1.
3. I.Hamberg and C.G.Granqvist. *J. Appl. Phys.* **60** (1986) R123.
4. A.L.Dawar and J.C.Joshi. *J. Mater. Sci.* **19** (1984) 1.
5. J.L.Vossen. *Phys of Thin Films.* Vol 9 (G Hass, M H Francombe and R W Hoffman Eds.) Academic Press, New York (1971) 1.
6. M.Watanabe. *Jpn. J. Appl. Phys.* 9 (1970) 1551.
7. W.Spence. *J. Appl. Phys.* **38** (1967) 3767.
8. M.Mizuhashi. *Thin Solid Films.* **70** (1980) 91.
9. E.Leja, A.Kolodziej, T.Pisarkiewicz and T.Stapinski. *Thin Solid Films.* **76** (1981) 283.
10. K.Adachi and M.Mizuhashi. *Proc. 10th Int. Conf. Chemcal Vapor Deposition.* Honolulu, HI, (1987) p 999.
11. Takao Nagatomo, Yukihiro Maruta and Osamu Omoto. *Thin Solid Films.* **192** (1990) 17.
12. E.Shanti, A.Banerjee, V.Dutta and K.L.Chopra . *J. Appl. Phys.* 53 (1986) 1615.
13. V.Vasu and A.Subrahmanyam. *Thin Solid Films.* **202** (1991) 283.
14. K.H.Yoon and J.S.Song. *Thin Solid Films.* **224** (1993) 203.
15. J.C.Manifacier, L.Szepessy, J.F.Bresse, M.Perotin and R.Stuck. *Mater. Res. Bull.* **14** (1979) 109.
16. H.Iida, T.Mishuku, A.Ito, K.Kato, M.Yamanaka and Y.Hayashi. *Solar Energy Mater.* **17** (1988) 407.
17. D.Raviendra and J.K.Sharma. *J. Phys. Chem. Solids.* **46** (1985) 945.
18. F.J.Gracia, J.Muci and M.S.Tomas. *Thin Solid Films.* **97** (1982) 47.
19. K.Kulaszewicz, W.Jarmoc and K.Turowska. *Thin Solid Films.*

112 (1984) 313.

20. R.Hill and J.D.Meakin. " *Current topics in photovoltaic devices*", (Eds. T.J.Coutts and J.D.Meakin), Academic press, New York, (1985) p 223.
21. M.Savelli and J.Baugnot "*Topics in applied physics*", (Ed. B.O.Seraphin) Vol.**31**, Springer-Verlag, Berlin, Heidelberg, (1979) p 213.
22. K.L.Chopra and S.R.Das. "*Thin Film Solar Cells*", Plenum Press, New York. (1983) Chapter 7.
23. L.L.Kazmerski. "*Current Trends in Photovoltaic devices*" Academic press, New york, 1985 p 41.
24. David W.Niles, Dennis Rioux and Hartmut Hochst. *J. Appl. Phys.* **73** (1993) 4586.
25. Lars Stolt, Jonas Hedstrom, John Kesler, Martin Ruckh, Karl Otto Velthaus and Han S-Werner Schock. *Appl. Phys. Lett.* **62** (1993) 597.
26. Bulent M.Basol, Vijay K.Kapur, Aravind Halani and Craig Leidholom. *Solar Energy Mater.* **29** (1993) 163.
27. K.L.Chopra and S.R.Das. "*Thin Film Solar Cells*", Plenum Press, New York. (1983) Chapter 5.
28. K.P.Vijayakumar. *Bull. Mater. Sci.* **16** (1993) 55.
29. K.Vedam, P.J.Mc Marr and J.Narayan. *Appl. Phys. Lett.* **47** (1985) 339.
30. R.J.Cashman. *J. Opt. Soc. Am.* **36** (1946) 356.
31. P.K.Nair, M.T.S.Nair, J.Campos and L.E.Sansores. *Solar Cells.* **22** (1987) 211.
32. I.Kaur, D.K.Pandya and K.L.Chopra. *J. Electrochem. Soc.* **127** (1980) 943.
33. P.K.Nair, M.T.S.Nair, and J.Campos. *Solar Energy Mater.* **15** (1987) 441.
34. Hiroshi Uda, Seji Ikegami and Hajimu Sonomura. *Jpn. J. Appl. Phys.* **29** (1990) 30.
35. S.G.Mokrushin and Yu D.Tkachev. *Colloid J. USSR* **23** (1961) 366.

36. K.Rajeev Kumar. *Ph.D Thesis*, Cochin University of Science and Technology. (1989).

37. Bulent M.Basol, Vijay K.Kapur and Aravind Halani. *Proc. 22nd IEEE Photovoltaic Specialist Conf.* (IEEE, New York 1991) p 893.

38. A.Mondal, T.K.Chaudhuri and P.Pramanik. *Solar Energy Mater.* **7** (1983) 431.

39. K.Kavcar, M.J.Carter and R.Hill. *Solar Energy Mater and Solar Cells.* **27** (1992) 13.

40. Toshiyuki Tamaguchi, Jiro Malsufusa and Akira Yoshida. *Solar Energy Mater Solar Cells.* **27** (1992) 25.

41. C.Guillen and J.Hesraro. *J. Appl. Phys.* **71** (1992) 5479.

42. K.Subbaramaiah and V.S.Rajah. *J. Mater. Sci. Lett.* **10** (1991) 1344.

43. J.C.Garg, R.P.Sharma and K.C.Sharma. *Thin Solid Films.* **164** (1988) 269.

44. K.R.Murali. *Thin Solid Films.* **167** (1988) 269.

45. G.K.Padam. *Mater. Res. Bull.* **22** (1987) 789.

46. P.K.Vidydharan Pillai and K.P.Vijayakumar. *Proc. 36th Sold State Symp.* 36-C (1993) 230.

47. L.L.Kazmershi, O.Jamjoum and P.J.Ireland. *J. Vac. Sci. Technol.* **21** (1982) 486.

Chapter 7

Conclusion of results

The present work is mainly concentrated on the studies of semiconducting thin films useful for solar cell fabrication. Variable Angle Spectroscopic Ellipsometer (VASE) was fabricated and this is used for the analysis of semiconductor thin films. The optical, surface and interface properties of the films are studied in this work. Thin films of materials like CdS, $CuInSe_2$ and SnO_2 were selected for this study. Other techniques like XRD, SEM, XPS, spectrophotometer were also used for corroborating VASE results. The work presented in this thesis can be divided into three parts as shown below.

1. Fabrication of VASE and development of computer software for the analysis of ellipsometric data.

2. Preparation of single layer thin films (CdS, SnO_2 and $CuInSe_2$) and bilayer thin films system (Cu/CdS, CdS/SnO_2 and CdS/$CuInSe_2$). Spray pyrolysis, Chemical Bath Deposition (CBD) and vacuum evaporation techniques were employed for the deposition of thin films.

3. Studies of these thin films using the fabricated VASE and verification of ellipsometric results using other techniques mentioned at the beginning.

Ellipsometric techniques.

An experimental setup for ellipsometric measurements (VASE) was fabricated with facilities to vary the wavelength and angle of incidence. An ordinary spectrometer was modified for this purpose. The collimator and telescope arms were converted into polariser and analyser arms respectively. The accuracy of measurement of azimuth angle of the polariser and the analyser is 1' and that of angle of incidence is 30". The

angle of incidence in this system can be varied between 20 and 80°. A 20 cm monochromator is used for the wavelength selection and it can scan between 400 nm and 750 nm. High power tungsten halogen lamp is used as the light source and this enables the measurement on surfaces with very low reflectivity. A photomultiplier tube is used for the detection of the reflected light signals. The chopper and tuned amplifier arrangement eliminates noise from the system. The use of long focal length lens eliminate the path deviation due to the rotation of polariser.

The ellipsometer is used in the two different modes,

1. Multiple Angle Incidence (MAI) ellipsometer
2. Variable Angle Spectroscopic Ellipsometer (VASE)

The MAI mode is used for the calculation of refractive index of thin films. In all other calculations the VASE mode is used. In both the techniques measurements were taken for different azimuth angles of the analyser. The minimum number of azimuth angle required for the determination of ψ and Δ is three. Different FORTRAN computer programmes are used for the MAI and VASE calculations. Using these programmes, the most suitable optical model is selected by minimizing the error function and the parameters of this best-fit optical model is taken as the physical parameters of the thin film system. Along with refractive index and thickness calculations ellipsometry is also used for the surface and interface analysis of single and multilayer thin film systems. The surface roughness and interface thickness are determined using present setup. Bruggeman's effective medium theory is also included for the determination of volume fraction of inclusion in a mixed medium.

A clean glass plate is used for the standardization of the system. The calculated ψ and Δ values are used for the determination of Brewster angle of glass plate and it is found to be in agreement with standard values. This analysis also

reveals that the glass surface has a roughness of the order of 40 nm.

In the study of multilayer structures, the sensitivity of the ellipsometric measurement is very important. In the present study the sensitivity of the multilayer system is enhanced by the technique suggested by Woollam. The sensitivity analysis of three thin film systems was done by this technique and they are CdS/glass, CdS/SnO_2/glass and CdS/$CuInSe_2$/glass. The further ellipsometric measurements were taken at the sensitive region of angle of incidence and wavelength.

Thin film preparation.

In this thesis we have reported single and bilayer thin film preparation by various techniques like spray pyrolysis, vacuum evaporation and chemical bath deposition. In this the spray pyrolysed CdS films were prepared from aqueous solution of 0.01M $CdCl_2$ and 0.01M thiourea. The geometry of the nozzle used for the spray largely determine the quality of the film prepared by this technique. A fine capillary tube is used for carrying the solution and another tube with comparatively larger diameter is used for carrying the 'carrier gas' and both tubes were made to intercept at an angle of 80° which gave better results. The best substrate temperature for the film preparation was in the range 280 $-300^{\circ}C$. CBD is also used for the preparation of CdS. $CdCl_2$ and thiourea solution complexed with triethanolamine (TEA) is used for the preparation of CdS film at room temperature using CBD. Ammonia solution is used to adjust the pH value above 10.

The spray pyrolysis technique was used for the preparations of SnO_2 film. This film is optically transparent and good electrical conductor. They are widely used as electrode material in several optoelectronic devices. An alcoholic solution (0.9M) of $SnCl_2.5H_2O$ was used for this

purpose. Film having very low resistivity (30 ohm-cm) were obtained at a substrate temperature 450°C.

CBD technique is used for the preparation of $CuInSe_2$ films. Thin films of $CuInSe_2$ were prepared by CBD from a deposition solution containing aqueous solution of copper sulfate, trisodium citrate, sodium selenosulphate and indium chloride. The pH of the solution is adjusted to be ~8 and the deposition was obtained at room temperature.

Vacuum evaporation was also used for the deposition of metallic copper film and CdS films.

Cu/CdS bilayer thin films were prepared by vacuum evaporation of copper films on spray pyrolysed CdS thin films. The copper deposition was done on CdS samples kept at room temperature. The next bilayer structure fabricated was CdS/SnO_2. This bilayer films were prepared by spray pyrolysis. At first SnO_2 film was prepared over glass substrate at 450°C and then CdS film was deposited at 300°C over the SnO_2 film. The $CdS/CuInSe_2$ bilayer thin film was prepared by CBD technique. $CuInSe_2$ film was prepared over glass substrate by CBD as mentioned earlier. Next this $CuInSe_2$/glass structure is used for the preparation of $CdS/CuInSe_2$ bilayer films by the same technique CBD.

Ellipsometric and Other studies.

Composition analysis of CdS samples prepared by using spray pyrolysis at temperature 300°C was done using XPS and this showed that the film contained impurities like Cl, C, and O_2. The band gap of the CdS film was 2.4 eV. The preparation temperature influenced the film structure and morphology of the film. Ellipsometry was used for optimising the preparation temperature of the CdS film and later it was verified using other techniques like XRD and SEM. The ellipsometric studies indicated that the film prepared by this techniques had rough surface. The roughness had very high

value (65nm) for films prepared at low temperature and become minimum (27nm) for films prepared at 280-300°C. Above this temperature, surface roughness again increased. These results from VASE were verified using SEM. The annealing of the films prepared at 300°C showed that the surface roughness increases with annealing temperatures at first and then decreases. Annealing at the preparation temperature, made the film surface very smooth. The XRD and VASE analysis showed that the crystalline quality of the film increased with increase in substrate temperature. It was observed that at low temperature, the deposition rate of the CdS film was very high and this slowly decreases with increase in substrate temperature. When the substrate temperature was above 300°C it decreased drastically. Electrical and optical transmission studies showed that the films prepared above 280-300°C had comparatively low resistivity and good optical transmission. All these studies gave an indication that the films prepared at 300°C had good quality and can be used for the fabrication of thin film solar cells. Using ellipsometer the real (n) and imaginary (k) part of complex refractive index of CdS film in the visible region (400-740nm) were also calculated after eliminating the effect of surface roughness of these film by appropriate optical modelling.

The n-type CdS film was converted into p-type by doping with copper. VASE technique was used for the study of Cu/CdS bilayer thin films; it showed that the copper easily diffused into as-prepared CdS films and diffusion depth increased with annealing temperatures. Copper diffusion into pre-annealed CdS film was less than that of the as-prepared CdS and the diffusion further decreases with increase in pre-annealing temperature. The hot probe and other electrical measurements made it clear that the "Cu-diffused-CdS" film had p type conductivity when the quantity of copper was larger. From the electrical resistivity measurements it could

be inferred that low Cu/Cd atomic percentage caused intrinsic CdS film. The XRD, XPS and absorption studies confirmed that the p type conductivity was due to the presence of copper acceptor in CdS film. All these studies ruled out the chance for the formation of p-type Cu_xS film.

The ellipsometric studies of CdS/SnO_2 interface gave the information that the structure was very stable and had very sharp interface. Since this bilayer is widely used in thin film solar cells the stability of CdS/SnO_2 interface is very important. This interface was found to be stable for the bilayer film even after annealing at very high temperature(300°C). Another bilayer system studied using ellipsometer was $CdS/CuInSe_2$ film. VASE results showed that as prepared samples had no interlayer between CdS and $CuInSe_2$. The low temperature annealing (ie., upto 100°C) do not affect the interface. But annealing at 200°C caused the formation of a thin interlayer of CdS and $CuInSe_2$ and at high temperature more and more material mixed together and the thickness of interlayer become very large.

Suggestions for further studies.

The measurements using a manual VASE is very tedious and time consuming work. In this case for taking measurements, one has to scan entire wavelength region for each angle of incidence. The azimuth angle of analyser is also to be changed for each wavelength and angle of incidence. In order to get maximum output from VASE it should be easy to take measurements and should not be time consuming, which means that the system must be an automated one. For the automation of the system the angle of incidence measurement must be replaced with a reflectivity scanner using microprocessor controlled stepper motor. The analyser and polariser can also be attached to another stepper motor, controlled by the microprocessor. The output of the PMT can be converted into

digital form by using an A to D converter so that the data acquisition using a digital computer is possible. In addition to this, the computer can be used to control all movements like angle of incidence, wavelength scanning and azimuth angle of analyser as well as to calculate ψ and Δ from the light intensity values. All these developments will make the system very useful for the study of multilayer thin film systems.

One of the important outcome of the present work is that the n-CdS can be converted into p-CdS by suitably doping it with copper by a simple process. This process can be extended into the fabrication of a pn homojunction thin film solar cells. Of course the efficiency of this cell may not be very high, but this process can be extended into the fabrication of high efficient multi-junction (tandem) solar cells. The other important bilayer system studied which is useful for the fabrication of heterojunction solar cell is $CdS/CuInSe_2$. The studies on as-prepared $CdS/CuInSe_2$ bilayer thin film system shows that it is not stable with temperature. Annealing of $CdS/CuInSe_2$ cause the inter layer diffusion. Hence further studies are required to optimise the process which will ultimately lead to highly stable bilayer thin film system useful for the fabrication of photovoltaic devices.

G5645